



HAL
open science

Thiol-para-fluoro modified PPFS as building blocks for the design of silica-based nanocomposite and layer by layer self-assembled thin films

Quanyi Yin

► **To cite this version:**

Quanyi Yin. Thiol-para-fluoro modified PPFS as building blocks for the design of silica-based nanocomposite and layer by layer self-assembled thin films. Materials. Université de Lyon, 2018. English. NNT : 2018LYSEI025 . tel-02000999

HAL Id: tel-02000999

<https://theses.hal.science/tel-02000999>

Submitted on 1 Feb 2019

HAL is a multi-disciplinary open access archive for the deposit and dissemination of scientific research documents, whether they are published or not. The documents may come from teaching and research institutions in France or abroad, or from public or private research centers.

L'archive ouverte pluridisciplinaire **HAL**, est destinée au dépôt et à la diffusion de documents scientifiques de niveau recherche, publiés ou non, émanant des établissements d'enseignement et de recherche français ou étrangers, des laboratoires publics ou privés.



N°d'ordre NNT : 2018LYSEI025

THESE de DOCTORAT DE L'UNIVERSITE DE LYON

opérée au sein de

Institut National des Sciences Appliquées de Lyon

(INSA de Lyon)

Ecole Doctorale N° ED34

Matériaux de Lyon

Spécialité de doctorat : Matériaux

Soutenue publiquement le 30/03/2018, par:

Quanyi YIN

**Thiol-*para*-fluoro modified PPFs as building blocks for the
design of silica-based nanocomposite and layer by layer
self-assembled thin films**

Devant le jury composé de :

DELAITE	Christelle	Professeur (Université Haute-Alsace)	Rapporteuse
GROHENS	Yves	Professeur (Université Bretagne-Sud)	Rapporteur
DUCHET-RUMEAU	Jannick	Professeur (INSA de LYON)	Examinatrice
RIEGER	Jutta	Chargé de Recherche CNRS (Université Paris 6)	Examinatrice
COLOMBANI	Olivier	Maître de Conférences (Le Mans Université)	Examineur
BEYOU	Emmanuel	Professeur (Université Lyon 1)	Directeur de thèse
CHARLOT	Aurélia	Maître de Conférences (INSA de LYON)	Co-Directrice de thèse
PORTINHA	Daniel	Maître de Conférences (INSA de LYON)	Co-Directeur de thèse

Département FEDORA – INSA Lyon - Ecoles Doctorales – Quinquennal 2016-2020

SIGLE	ECOLE DOCTORALE	NOM ET COORDONNEES DU RESPONSABLE
CHIMIE	CHIMIE DE LYON http://www.edchimie-lyon.fr Sec. : Renée EL MELHEM Bât. Blaise PASCAL, 3e étage secretariat@edchimie-lyon.fr INSA : R. GOURDON	M. Stéphane DANIELE Institut de recherches sur la catalyse et l'environnement de Lyon IRCELYON-UMR 5256 Equipe CDFA 2 Avenue Albert EINSTEIN 69 626 Villeurbanne CEDEX directeur@edchimie-lyon.fr
E.E.A.	ÉLECTRONIQUE, ELECTROTECHNIQUE, AUTOMATIQUE http://edeea.ec-lyon.fr Sec. : M.C. HAVGOUDOUKIAN ecole-doctorale.eea@ec-lyon.fr	M. Gérard SCORLETTI Ecole Centrale de Lyon 36 Avenue Guy DE COLLONGUE 69 134 Ecully Tél : 04.72.18.60.97 Fax 04.78.43.37.17 gerard.scorletti@ec-lyon.fr
e2m2	ÉVOLUTION ÉCOSYSTÈME, MICROBIOLOGIE, MODELISATION http://e2m2.universite-lyon.fr Sec. : Sylvie ROBERJOT Bât. Atrium, UCB Lyon 1 Tél : 04.72.44.83.62 INSA : H. CHARLES secretariat.e2m2@univ-lyon1.fr	M. Philippe NORMAND UMR 5557 Lab. d'Ecologie Microbienne Université Claude Bernard Lyon 1 Bâtiment Mendel 43, boulevard du 11 Novembre 1918 69 622 Villeurbanne CEDEX philippe.normand@univ-lyon1.fr
EDISS	INTERDISCIPLINAIRE SCIENCES-SANTÉ http://www.ediss-lyon.fr Sec. : Sylvie ROBERJOT Bât. Atrium, UCB Lyon 1 Tél : 04.72.44.83.62 INSA : M. LAGARDE secretariat.ediss@univ-lyon1.fr	Mme Emmamelle CANET-SOULAS INSERM U1060, CarMeN lab, Univ. Lyon 1 Bâtiment IMBL 11 Avenue Jean CAPELLE INSA de Lyon 69 621 Villeurbanne Tél : 04.72.68.49.09 Fax : 04.72.68.49.16 emmanuelle.canet@univ-lyon1.fr
INFOMATHS	INFORMATIQUE ET MATHÉMATIQUES http://edinfomaths.universite-lyon.fr Sec. : Renée EL MELHEM Bât. Blaise PASCAL, 3e étage Tél : 04.72.43.80.46 Fax : 04.72.43.16.87 infomaths@univ-lyon1.fr	M. Luca ZAMBONI Bât. Braconnier 43 Boulevard du 11 novembre 1918 69 622 Villeurbanne CEDEX Tél : 04.26.23.45.52 zamboni@maths.univ-lyon1.fr
Matériaux	MATÉRIAUX DE LYON http://ed34.universite-lyon.fr Sec. : Marion COMBE Tél : 04.72.43.71.70 Fax : 04.72.43.87.12 Bât. Direction ed.materiaux@insa-lyon.fr	M. Jean-Yves BUFFIÈRE INSA de Lyon MATEIS - Bât. Saint-Exupéry 7 Avenue Jean CAPELLE 69 621 Villeurbanne CEDEX Tél : 04.72.43.71.70 Fax : 04.72.43.85.28 jean-yves.buffiere@insa-lyon.fr
MEGA	MÉCANIQUE, ÉNERGÉTIQUE, GENIE CIVIL, ACOUSTIQUE http://edmega.universite-lyon.fr Sec. : Marion COMBE Tél : 04.72.43.71.70 Fax : 04.72.43.87.12 Bât. Direction mega@insa-lyon.fr	M. Jocelyn BONJOUR INSA de Lyon Laboratoire CETHIL Bâtiment Sadi-Carnot 9, rue de la Physique 69 621 Villeurbanne CEDEX jocelyn.bonjour@insa-lyon.fr
ScSo	ScSo* http://ed483.univ-lyon2.fr Sec. : Viviane POLSINELLI Brigitte DUBOIS INSA : J.Y. TOUSSAINT Tél : 04.78.69.72.76 viviane.polsinelli@univ-lyon2.fr	M. Christian MONTES Université Lyon 2 86 Rue Pasteur 69 365 Lyon CEDEX 07 christian.montes@univ-lyon2.fr

*ScSo : Histoire, Géographie, Aménagement, Urbanisme, Archéologie, Science politique, Sociologie, Anthropologie

Abstract

This work describes the preparation of two kinds of thin polymer films : i) self-cleaning silica-based (nano)composites films and ii) LbL self-assembling films, both including poly(2,3,4,5,6-pentafluorostyrene) (PPFS) derivatives, as building blocks. The cornerstone of the approach is to exploit the thiol-*para* fluoro substitution reaction to PPFS chains in order to generate derivatives with tailored properties. In this frame, PPFS chains were anchored onto the surface of vinyl-functionalized fumed silica nanoparticles by nitroxide-mediated polymerization (NMP) in presence of PS-DEPN as macro-initiator via a “grafting through” strategy. The kinetics of NMP of PFS were investigated in presence and without silica in various solvents and well-characterized hybrid silica particles containing different polymer grafting weight were declined. Then, perfluorodecanethiol (PFDT) was employed to modify PPFS, considered as the host polymer matrix, and to functionalize PPFS chains tethered to silica particles. A large panel of (nano)composite films from the different possible host matrix/silica particles combinations was prepared. The wettability and the surface morphology of each film were discussed, as a function of the host structure (PPFS or PPFS-PFDT with different DS) and silica (modified with PPFS or PPFS-PFDT), as well as the silica content. It results that superhydrophobic features can be reached.

Subsequently, PPFS was modified by using carboxylic acid mercapto modifier via the thiol-*para* fluoro coupling. Various carboxylated PPFS derivatives differing in the degree of substitution (DS) were prepared and their ability to develop H-bonds in solution with a model strong H-bond acceptor partner (poly(4-vinyl pyridine) (P4VP)) was investigated. Dependently on the nature of the solvent, a miscible blend or interpolymer complexes (IPC) were achieved. IPC-containing solutions were used to successfully fabricate spin-assisted films. Furthermore, H-bonds mediated LbL self-assembly multilayer films involving carboxylated PPFS and P4VP were prepared and it was evidenced that the nature of the deposition solvent as well as the extent of the modification (quantified by the DS), impact the growth mechanism, the thickness and the surface features, in terms of topology and wettability.

Keywords: poly(2,3,4,5,6-pentafluorostyrene); *para*-fluoro substitution reaction; nanocomposite, fumed silica, superhydrophobic surface; H-bonds; miscibility; layer by layer self-assembly, multilayer films

Résumé

Ce travail de thèse décrit la préparation de deux types de films de polymères : i) des films nanocomposites à base de silice pyrogénée aux propriétés superhydrophobes et ii) des films LbL auto-assemblés, incluant tous deux des dérivés de poly(2,3,4,5,6-pentafluorostyrene) (PPFS), utilisés comme briques élémentaires. La stratégie utilisée ici consiste à exploiter les nombreux avantages que présente la réaction de substitution du fluor en position para du PPFS avec un thiol, pour générer de nouveaux dérivés aux propriétés ajustables. Ainsi, le premier volet de la thèse a consisté à introduire des chaînes de PPFS de façon covalente à la surface de silice pyrogénée par une stratégie dite de «grafting through» en utilisant la polymérisation radicalaire contrôlée par le voir nitroxydes, en présence de PS-DEPN comme macroamorceur. La cinétique de polymérisation du PFS avec et sans particules silice a été étudiée dans divers solvants, différentes particules hybrides de silices modifiées en surface par une couronne de PPFS ont été préparé. Ensuite, un thiol perfluoré (perfluorodecanethiol:PFDT) a été utilisé pour modifier le PPFS, considéré dans ce cadre comme matrice hôte pour la préparation des nanocomposites et pour modifier le PPFS présent à la surface des particules de silice. A partir de là, un large panel de films nanocomposite a été préparé à partir des différentes combinaisons possibles de polymère hôte (PPFS ou PPFS-PFDT) et de charges inorganiques de silice (modifiées par le PPFS ou par le PPFS-PFDT). Les propriétés de mouillabilité ainsi que la morphologie de surface de chaque film ont été analysées et il en résulte que certains films présentent un caractère superhydrophobe.

Le deuxième volet de la thèse a porté sur la modification du PPFS par des thiols porteurs de fonctions acide carboxylique, toujours par la réaction de substitution décrite précédemment. Différents dérivés de PPFS carboxylés de DS variés ont été synthétisés. Leur habilité à développer des liaisons hydrogène avec un polymère modèle accepteur de liaison H (la poly(4-vinyl pyridine) (P4VP)) a été étudiée. Il en ressort que dépendamment de la nature du solvant, des mélanges miscibles ou des complexes interpolymères ont ensuite été formés. Des solutions de complexes préformés ont été successivement déposées par spin-coating pour construire des films. De plus, des films multicouches LbL stabilisés par des liaisons H entre le PPFS carboxylé et la P4VP ont été élaborés and il a été démontré que la nature du solvant de dépôt, ainsi que le taux de modification du PPFS, impactent fortement le mécanisme de croissance, l'épaisseur du film et les caractéristiques de surface, en termes de topologie et de mouillabilité.

Mots clés: poly(2,3,4,5,6-pentafluorostyrene), substitution nucléophile avec un thiol, film nanocomposite, silice pyrogénée, surface superhydrophobe, interactions hydrogène miscibilité, auto-assemblage en couche par couche, films multicouches

Acknowledgments

This work would not have been possible without the mentorship of my advisors, Prof. Emmanuel BEYOU, Dr. Aurelia CHARLOT and Dr. Daniel PORTINHA. I thank them for their extensive support and guidance, invaluable suggestions and profound discussions throughout the period of this thesis. Thanks everything that they did for improving my ability in academic researching and especially the attitude that they showed me to solve problems which will be values for my whole life.

I would like to thank my dissertation committee, Prof. Jannick DUCHET, Prof. Yves GROHENS, Prof. Christelle DELAITE, Dr. Jutta RIEGER and Dr. Olivier COLOMBANI, for their comments, suggestions and challenges that helped drive me to make advances in my research.

Thank China Scholarship Council (CSC) for the final support through the CSC/INSA program.

I would also like to thank the staff at IMP@ Lyon1 and INSA de Lyon, for providing the facilities and business logistics that helped make conducting research and graduating possible, including: Agnes CREPET, Ali HADDANE, Pierre ALCOUFFE, Olivier GAIN, Sylvie NOVAT, Nathalie SINTES, Guillaume SUDRE; Thierry TAMET, Isabelle POLO, Sebastien PRUVOST, Marion COLLELA, Patrick GOETINCK.

I would like to acknowledge my colleagues at Lab IMP, especially for the members of Bureau 326, Marine FALLETTA, Melanie DOMONT, Afef HOOACHTIA, Yann GABET, Soline PEERS, Michael ROBERT, Florian VANNESTE, for their guidance in using various instruments as well as for great friendship that spanned my entire graduate career. I would like to thank my Chinese fellows including: Dr. Xibo YAN, Dr. Biao ZHANG, Dr. Jing YANG, Dr. Bo LU and Luxiao CHAI, for their kindness help.

I want to thank my family for their continuing love and support. My parents always put my education and well-being before all else. I would not have been able to go on an academic tour without their unwavering encouragement and sacrifices throughout my life. I want to thank my sisters for all of their love.

Finally, thank you to my fiancée and future wife Kunyun HE for going on this incredible journey with me in the past 10 years. I am excited for it to continue for the next 50+ years.

List of Abbreviations and Symbols

A	alcohol
AFM	atomic force microscopy
APDMES	3-aminopropyl dimethylethoxysilane
APTMS	(acryloxypropyl)trimethoxysilane
3-APS	3-aminopropyltriethoxysilane
ATR FTIR	attenuated total reflection fourier transform infrared
ATRP	atom transfer radical polymerization
BT	1,4-butanedithiol
Cryo-SEM	cryo-Scanning Electron Microscope
CVD	chemical vapor deposition
CNT	carbon nanotube
CRP	controlled free radical polymerization
DBU	1,8-diazabicyclo[5.4.0]undec-7-ene
DEPN	N-tert-butyl-N-(1-diethylphosphono-2, 2-dimethyl) propyl nitroxide
DFMA	dodecafluoroheptyl methacrylate
DFT	density functional theory
DIPEA	N,N-diisopropylethylamine
DMAc	dimethyl sulfoxide
DMAEMA	2-(dimethylamino) ethyl methacrylate
DMAP	N,N-dimethylpyridin-4-amine
DMF	N,N-dimethylformamide
DNA	deoxyribonucleic acid
DS	degree of substitution
DSC	differential scanning calorimetry
DMSO	dimethyl sulfoxide
DODT	3,6-dioxa-1,8-octanedithiol
DTT	dithiothreitol
EtAc	ethyl acetate
EDX	energy dispersive X-ray analysis
ETFE	tetrafluoroethylene
GMA	glycidyl methacrylate
HBFP	hyperbranched fluorinated polymers
HFS	hydrophobic fumed silica
IPC	interpolymer complex
LbL	layer-by-layer
MEK	methyl ethyl ketone
MMA	methyl methacrylate
M_n	number-average molecular weight
MP	N-methylpyrrolidone
MPD	3-mercapto-1,2-propanediol
MWCNT	multi wall carbon nanotube
N	amine
NMP	nitroxide mediated polymerization
NMR	nuclear magnetic resonances pectroscopy
OEGMA	oligo(ethyleneglycol) methacrylate

LIST OF ABBREVIATIONS AND SYMBOLS

PAA	poly(acrylic acid)
PAAM	poly(acrylamide)
PAH	poly(allylamine hydrochloride)
PANI	polyaniline
PBA	poly(butyl acrylate)
PCL	poly(3-caprolactone)
PCzEMA	poly[2-(9-carbazolyl)ethyl methacrylate]
PDADMAC	poly(diallyldimethylammonium chloride)
PDFHM	poly(dodecafluoroheptyl methacrylate)
PDI	polydispersity index
PDMS	poly(dimethylsiloxane)
PDNBAM	poly[2-[(3,5-dinitrobenzoyl)oxy]ethyl methacrylate]
PDT	1,4-phenylenedimethanethiol
PE	poly(ethylene)
PEI	poly(ethyleneimine)
PEG	poly(ethylene glycol)
PEO	poly(ethylene oxide)
PET	poly(ethylene terephthalate)
PEtOX	poly(2-ethyl-2-oxazoline)
PETPTA	poly(trimethylolpropane ethoxylate triacrylate)
PFBi	2,3,4,5,6-pentafluorobiphenyl
PFDT	1H,1H,2H,2H-Perfluorodecanethiol
PFP	pentafluorophenyl
PFS	2,3,4,5,6-pentafluorostyrene
PFSR	<i>para</i> -fluoro substitution reaction
PFPMA	pentafluorophenylmethacrylate
PFTR	<i>para</i> -fluoro thiol reaction
P3HT	poly(3-alkyl thiophene)
PHMPA	poly(N,N-dimethyl-N',N'',N''',N'''-tetramethylenephosphoramidate)
PI	poly(imide)
PLA	poly(lactide)
PMAA	poly(methacrylic acid)
PMMA	poly(methyl methacrylate)
POSS	polyhedral oligomeric silsesquioxanes
P3OT	poly(3-octyl)thiophene
PP-PMMA	poly(propylene)-poly(methyl methacrylate)
pPFBMA	poly(2,3,4,5,6-pentafluorobenzyl methacrylate)
PrS	1,3-propane sultone
PS	poly(styrene)
PSS	poly(sodium styrene sulfonate)
PSU	poly(sulfone)
PTFE	poly(tetrafluoroethylene)
PTFSPA	poly(2,3,5,6-tetrafluorostyrene-4-phosphonic acid)
PTFMS	poly(2,3,5,6-tetrafluoro-4-methoxy-styrene)
PU	poly(urethaneurea)
PVA	poly(vinyl alcohol)

LIST OF ABBREVIATIONS AND SYMBOLS

PVDF	poly(vinylidene fluoride)
PVDF-PHFP	poly(vinylidene fluoride-co-hexafluoropropylene)
P4VP	poly(4-vinyl pyridine)
PVPON	poly(N-vinyl pyrrolidone)
PVPh	poly(vinylphenol)
PVS	poly(vinyl sulfonate)
QCM	quartz crystal microbalance
RAFT	reversible addition–fragmentation chain-transfer polymerization
ROP	ring-opening polymerization
R _q	root-mean-square roughness
S	substrates
SEC	size exclusion chromatography
SEM	scanning electron microscopy
SNAr	nucleophilic aromatic substitution
T	thiol and sulfur-based nucleophile
TEA	triethylamine
TEM	transmission electron microscope
TFS	2,3,5,6-tetrafluorostyrene
TFSOH	<i>para</i> -hydroxy-tetrafluorostyrene derivative
TFSSNa	sulfopropylated tetrafluoro derivative of styrene
TFSOBu	<i>p-t</i> -Butoxy-tetrafluorostyrene
T _g	glass transition temperature
TGA	thermo gravimetric analysis
THF	tetrahydrofuran
TrEG	tri(ethylene glycol)
TSP	tris(trimethylsilyl) phosphite
UV-vis	ultraviolet–visible spectroscopy
WCA	water contact angle
XPS	X-ray photoelectron spectroscopy
θ	contact angle
Δθ	contact angle hysteresis
θ _A	advancing contact angle
θ _R	receding contact angle
η	intrinsic viscosity

TABLE OF CONTENTS

GENERAL INTRODUCTION	1
CHAPTER 1: BIBLIOGRAPHY	7
1.1 <i>PARA</i> -FLUORO CHEMISTRY OF PENTAFLUOROPHENYL GROUP CONTAINING POLYMER MATERIALS	7
1.1.1 <i>Mechanism</i>	8
1.1.2 <i>Substrates</i>	9
1.1.3 <i>Nucleophiles</i>	11
1.1.3.1 Alcohols as nucleophiles	11
1.1.3.2 Amines as nucleophiles	14
1.1.3.3 Thiols and sulfur-based nucleophiles	17
1.1.3.4 Other nucleophiles	21
1.1.4 <i>Influence of the experimental conditions on the PFSR</i>	22
1.1.4.1 Base	23
1.1.4.2 Solvent	25
1.1.4.3 Temperature	27
1.1.5 <i>Chemical strategies involved para-fluoro substitution reaction (PFSR)</i>	28
1.1.5.1 Pre-polymerization modification	28
1.1.5.2 Post-polymerization modification	33
1.1.5.2.1 Polymers with PFP groups along the backbone	34
1.1.5.2.2 Polymers with PFP groups at chain-ends	40
1.1.5.3 Polymerization through PFSR	42
1.1.5.4 Surface modification by PFSR	45
1.1.5.4.1 Polymeric microparticles	46
1.1.5.4.2 Membranes or dense polymer materials	46
1.1.5.4.3 Films	48
1.1.5.4.4 Inorganic particles	50
1.1.6 <i>Conclusion</i>	50
1.2 FLUORINATED POLYMERS IN NANOCOMPOSITE FILMS WITH SUPERHYDROPHOBIC PROPERTIES	51
1.2.1 <i>Definition of superhydrophobic surfaces</i>	52
1.2.1.1 Wenzel model	54
1.2.1.2 Cassie-Baxter model	55
1.2.2 <i>Polymer-based superhydrophobic surfaces</i>	55
1.2.2.1 The main approaches involving polymers	56
1.2.2.2 Superhydrophobic nanocomposite films composed of fluorinated polymers and fillers	63
1.2.3 <i>Conclusion</i>	76
1.3 PREPARATION OF MULTILAYER FILMS THROUGH LAYER-BY-LAYER (LbL) APPROACH	76
1.3.1 <i>General introduction of the LbL</i>	76
1.3.2 <i>Presentation of the different types of non-covalent interactions used for the LbL film construction</i>	79

1.3.2.1 Exploitation of conventional electrostatic interactions	79
1.3.2.2 Exploitation of H-bonds.....	80
1.3.2.3 Other kinds of physical interactions.....	83
1.3.3 H-bonds mediated LbL films involving -COOH containing polymers	87
1.3.4 Conclusion	100
1.4 REFERENCES	101
CHAPTER 2: POLY(2,3,4,5,6-PENTAFLUOROSTYRENE) MODIFIED FUMED SILICA AND ITS APPLICATION IN PREPARING SELF-CLEANING NANOCOMPOSITE FILMS.....	121
2.1 GENERAL INTRODUCTION	121
2.2 NITROXIDE-MEDIATED POLYMERIZATION OF PENTAFLUOROSTYRENE INITIATED BY PS-DEPN THROUGH THE SURFACE OF APTMS MODIFIED FUMED SILICA: TOWARDS FUNCTIONAL NANOHYBRIDS	124
2.2.1 Abstract.....	124
2.2.2 Introduction.....	124
2.2.3 Experimental section.....	126
2.2.3.1 Materials.....	126
2.2.3.2 Analytical technique.....	126
2.2.3.3 Preparation of macroinitiator (PS-DEPN).....	127
2.2.3.4 Polymerization of PFS using PS-DEPN as macroinitiator.....	128
2.2.3.5 Synthesis of APTMS-modified silica (SiO ₂ -APTMS)	128
2.2.3.6 Polymerization of PFS in presence of APTMS modified silica and PS-DEPN by “grafting through” approach	129
2.2.3.7 Deposition of the hybrid modified silica onto silicon wafer	130
2.2.4 Results and discussion.....	130
2.2.4.1 Kinetic of the nitroxide mediated polymerization of PFS in presence of PS-DEPN and without silica	132
2.2.4.2 Synthesis of the PS-b-PPFS-grafted silica	135
2.2.5 Conclusions.....	142
2.2.6 References	143
2.2.7 Supporting information	148
2.3 CONTROLLED PERFLUORINATION OF FLUORINATED POLYMER AND FUNCTIONALIZED FUMED SILICA: TOWARDS THE DESIGN OF SELF-CLEANING (NANO)COMPOSITE FILMS.....	151
2.3.1 Abstract.....	151
2.3.2 Introduction.....	152
2.3.3 Experimental part	155
2.3.3.1 Materials.....	155
2.3.3.2 Polymerization of 2,3,4,5,6-pentafluorostyrene (PFS).....	156
2.3.3.3 Modification of PPFS by thiol- <i>para</i> -fluoro substitution reaction	156
2.3.3.4 Film preparation.....	157
2.3.3.5 Characterization Methods	157
2.3.4 Results and discussion.....	160
2.3.4.1 Synthesis of polymer matrices: PPFS and PPFS-PFDT samples	160
2.3.4.2 Synthesis of nanohybrids: SiO ₂ -PS-PPFS-PFDT samples	167

2.3.4.3 Preparation of (nano)composite films	168
2.3.5 Conclusion	174
2.3.6 References	175
2.3.7 Supporting information	181
CHAPTER 3: NOVEL CARBOXYLIC ACID MODIFIED POLY(2,3,4,5,6-PENTAFLUOROSTYRENE) AND THEIR APPLICATION IN PREPARING H-BONDS DRIVEN MULTILAYER THIN FILMS	186
3.1 GENERAL INTRODUCTION	186
3.2 EXPERIMENTAL PART	188
3.2.1 Materials and characterization methods.....	188
3.2.2 Modification of PPFS by thiol-para-fluoro substitution reaction	190
3.2.3 Preparation of P4VP/PPFS-MPA blends	191
3.2.4 Spin-assisted film buildup of preformed H-bonded interpolymer complexes.....	191
3.2.5 Preparation of H-bonded multilayer films	192
3.3 SYNTHESIS OF CARBOXYLATED PPFS DERIVATIVES BY THIOL-PARA-FLUORO SUBSTITUTION REACTION	192
3.3.1 Chemoselective modification of PPFS.....	193
3.3.2 Kinetics of modification	195
3.3.3 Thermal properties of PPFS-MPA	198
3.3.4 Wettability properties of PPFS-MPA.....	199
3.3.5 Conclusion	200
3.4 STUDY OF THE PPFS-MPA/P4VP BLENDS.....	200
3.4.1 Intrinsic viscosity measurements.....	201
3.4.2 Influence of the DS of PPFS-MPA and the solvent on miscibility of PPFS-MPA with P4VP	202
3.4.3 Evidence of the formation of H-bonds.....	205
3.4.4 Study of the interactions through the thermal properties.....	208
3.4.5 Conclusion	209
3.5 CONSTRUCTION OF PPFS-MPA AND P4VP BASED THIN FILMS	210
3.5.1 Successive deposition of PPFS-MPA/P4VP interpolymer complexes	210
3.5.2 Construction of (P4VP/PPFS-MPA) <i>n</i> multilayer films through the LbL self-assembly approach	216
3.5.2.1 Evidence of the film feasibility	217
3.5.2.2 Influence of the nature of the deposition solvent	219
3.5.2.2.1 General characterization of the depositions	220
3.5.2.2.2 Study of the growth mechanism.....	224
3.5.2.2.3 Study of the surface features by AFM.....	229
3.5.2.2.4 Study of the surface features by wettability measurements	234
3.5.2.3 Influence of DS of PPFS-MPA by using CHCl ₃ for P4VP and MEK for PPFS-MPA	236
3.5.2.3.1 Study of the growth mechanism.....	239
3.5.2.3.2 Study of the surface features by AFM.....	240
3.5.2.3.3 Study of surface features by the wettability measurements	242
3.5.2.4 Other attempts by using CHCl ₃ /MEK mixture	243

TABLE OF CONTENTS

3.5.2.4.1 Influence of the DS of PPFS-MPA.....	244
3.5.2.4.2 Influence of the concentration of the deposition solution	245
3.5.2.5 Conclusion	247
3.6 GENERAL CONCLUSION	248
3.7 REFERENCES	250
3.8 APPENDIX DATA.....	256
GENERAL CONCLUSIONS AND PERSPECTIVES	260

General Introduction

Multi-functional polymer (nano)materials have attracted tremendous attention for applications in optical, electrical, biological and chemical fields. The macromolecular engineering, especially the techniques of controlled radical polymerization (CRP) allows for the design of perfectly defined polymers, which structural aspects can be finely controlled and tuned. Also, chemical post-polymerization functionalization of preformed macromolecular chains with judiciously chosen reactive molecules affords to access to functional (co)polymers, which can be employed as building blocks to develop novel materials or thin polymer films. In particular, a chemical derivatization of polymers involving an efficient and adjustable coupling appears as a powerful way to adjust the properties of the (co)polymers and then allows for preparing well-tailored materials. In the polymer material science field, a great attention has been dedicated to thin polymer films. The interest is twofold: such thin films and their formation are very relevant from fundamental aspect together with a high potential to confer peculiar properties to a given substrate. In this respect, (nano)composite thin polymer films combining both the benefits of polymer matrix and inorganic fillers are particularly attractive. The key parameter is to well choose the suited polymer/inorganic particles couple and to enhance the interfacial adhesion. We can cite also thin polymer films built up *via* the Layer by Layer (LbL) approach involving polymers able to develop specific interactions. It has emerged as a powerful bottom-up approach for the construction of multilayer thin polymer films with a precise control of the thickness, the architecture and the composition at the nanoscale. For these two kinds of polymer films, the cornerstone is to use building blocks, of which the structural aspects are well defined and easily adjustable. To respond to these requirements, poly(2,3,4,5,6-pentafluorostyrene) (PPFS) is an ideal candidate, since i) it can be synthesized by CRP techniques and ii) it is a versatile functionalizable platform since the fluorine atom in *para* position can be selectively substituted by nucleophiles, such

as amines, alcohols, or thiols. For several years now, the laboratory (IMP, Ingénierie des Matériaux Polymères) has been interested in the modification of PPFS with various mercapto- derivatives in view of preparing peculiar assembly in solution and/or LbL polymer films, of which properties/functionalities can be tuned by the chemical nature of the thiol involved in the substitution reaction.

This basic research thesis, funded by the China Scholarship Council (CSC) program, is inscribed in this frame. In the continuing challenge to develop new thin films, we exploited many of the benefits of PPFS, by following different strategies and methodologies. Indeed, the first part of this PhD work concerns the preparation of thin polymers films exhibiting superhydrophobic surface features and the second part deals with the generation of novel H-bonded LbL self-assembly films. For that, the use of PPFS was declined according to different routes.

The strategy that we developed to access to polymer films with super water-repellent properties, relies in the attributes offered by (nano)composite coatings constituted of i) hydrophobic PPFS (chemically modified or not) as polymer host matrix and ii) embedded fumed silica (SiO_2) particles (chemically modified), which are expected to migrate at the film surface. Indeed, it is well known that a surface with an apolar character combined to a well-suited dual-size hierarchically textured surface is a key prerequisite to achieve superhydrophobic properties. PPFS was chemically modified with perfluorodecanethiol (PFDT) in order to introduce perfluoroalkyl groups onto PPFS backbone to give PPFS-PFDT derivatives with enhanced hydrophobicity. Concomitantly, silica fillers were functionalized by PPFS segments by nitroxide-mediated polymerization (NMP) and by using a “grafting through” strategy. By playing on the structural aspect of the PPFS-based host matrix (modified or not, extent of the perfluoro modification), on the surface chemistry of fumed silica (modified or not) and on the amount of incorporated silica fillers, different water wettability properties can be faced (less or more hydrophilic, hydrophobic and superhydrophobic).

Regarding the second objective of the PhD work, the strategy that we considered to access novel H-bond donor polymers is also based on the chemoselective

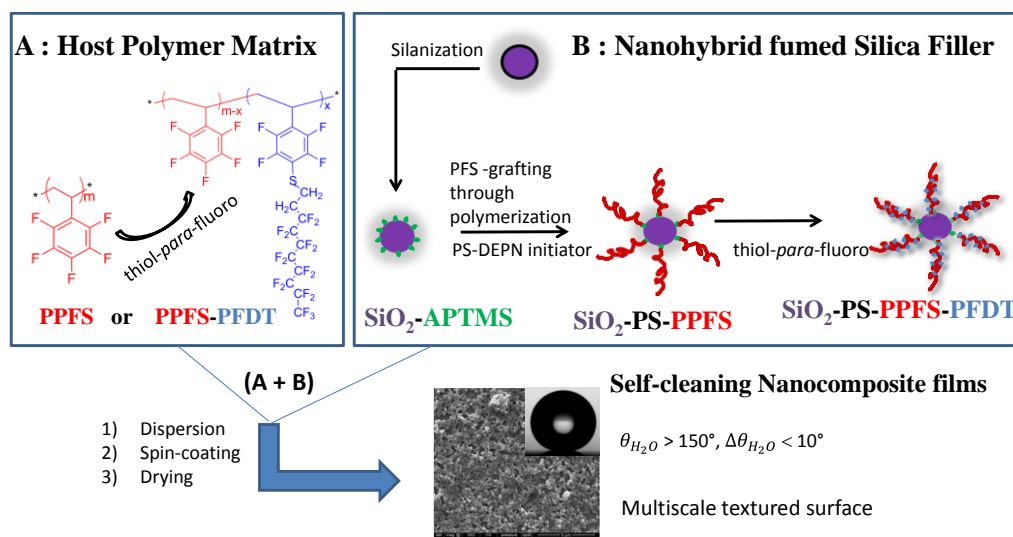
post-modification of PPFS with carboxylic acid containing-thiols. The control of the extent of modification allows for tuning the H-bond donation capability. Herein, we choose poly(4-vinyl pyridine) (P4VP) as a model strong H-bond acceptor polymer. The propensity of PPFS derivatives to undergo H-bonds with P4VP in organic solvents was undertaken. As a function of the extent of the PPFS modification by carboxylated modifiers and dependently on the solvent used for the blend preparation, the formation and the strength of H-bonds can be tuned. From the investigation in solution, various multilayered films were targeted.

Thus, this thesis manuscript is organized into three different main chapters.

The first bibliographic chapter aims at defining the context of the thesis project. Hence, the chapter is divided into three distinct parts. The first section is dedicated to a presentation of the *para*-fluoro substitution reaction (PFSR) of pentafluorophenyl containing-polymers according two directions: - one deals with the mechanism, substrates, nucleophiles and reaction conditions of PFSR, and - the second covers the chemical strategies involving PFSR such as pre-polymerization modification, post-polymerization modification, polymerization through PFSR as well as surface modification. The second section is focused on the definition of superhydrophobic surfaces and on the main approaches involving polymers to access such surface features. In particular, in order to do the link with the objectives of the thesis, a peculiar attention is allocated to super water-repellent (nano)composite films containing fillers embedded in fluorinated (co)polymers. The third and last section is devoted to LbL multilayer films. After a summary of the main assets of this surface functionalization technique, an overview of the different kinds of non-covalent forces used for LbL self-assembly is presented. Finally, an overview covering multilayer H-bonded films constructed from carboxylic acid-containing (co)polymers is in-depth described and discussed.

The second chapter is devoted to the preparation of superhydrophobic (nano)composite films involving PPFS or PPFS derivatives as the polymer matrix and surface modifier of the filler. To better settle the objectives of the thesis, an introduction describes the envisaged chemical strategy to generate fumed silica

functionalized by PPFS chains, and to synthesis the different host PPFS-based polymer matrices, either constituted of PPFS or PPFS chains bearing perfluoroalkyl segments, covalently introduced by the thiol-*para*-fluoro substitution reaction (PFSR) (Scheme G1).



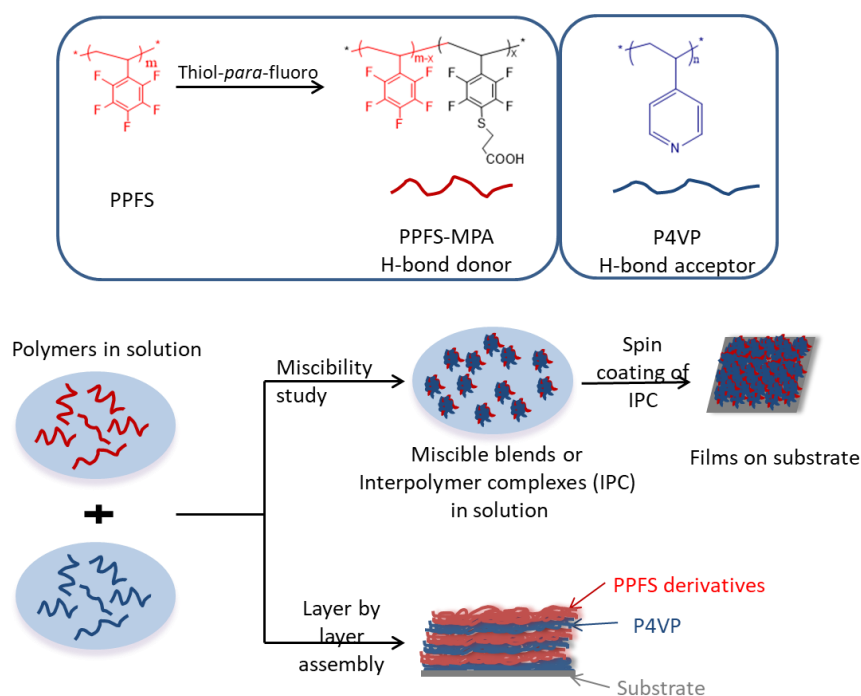
Scheme G1 General strategy for the preparation of self-cleaning nanocomposite films envisaged with PPFS-based components.

This chapter relies on two complementary publications.

The first article particularly deals with organic/inorganic hybrid particles. Firstly, NMP of PFS is discussed, with notably the effect of the solvent on kinetics. The introduction of PPFS onto the silica surface is described and relies in NMP of PFS with PS-DEPN as macroinitiator and by using a “grafting through” strategy from (acryloxypropyl)trimethoxysilane (APTMS) modified silica. The chemically modified silica was fully characterized and the corresponding surface properties of hybrid particles in terms of water wettability were evaluated. The second part of this chapter (a manuscript that has been submitted for publication at the time this PhD manuscript was submitted) concerns the generation of (nano)composite films, which exhibits superhydrophobic properties. The films are composed of PPFS-based polymers with hybrid silica particles (synthesis described in the first article). PPFS was perfluorinated through thiol-PFSR by using *1H,1H,2H,2H*-perfluorodecanethiol (PFDT) as modifier. The substitution reaction was investigated and optimized as a

function of the experimental conditions and the resulting apolar character was emphasized. The preparation of a large panel of (nano)composites films from the different possible host matrix/silica particles combinations was achieved. The wettability properties and the surface morphology of each (nano)composite were discussed, as a function of the structure of both host matrix (PPFS or PPFS-PFDT with different degree of substitution) and silica (modified with a silane, with PPFS or with PPFS-PFDT) as well as the amount of introduced silica particles.

The third chapter describes the preparation and the characterization of multilayer films mediated by H-bonds by using carboxylated PPFS derivative as H-bond donor polymer, and poly(4-vinyl pyridine) as H-bond acceptor (Scheme G2).



Scheme G2 General strategy for the preparation of polymer thin films.

For this aim, the first section is devoted to the synthesis of PPFS bearing carboxylic acid moieties through thiol-PFSR with different carboxylic acid-containing thiols. The extent of the nucleophilic substitution, defined as the degree of substitution (DS), can be successfully adjusted by the experimental conditions. Their ability to interact with P4VP in solution was evaluated by various techniques. We demonstrated

that the strength and the extent of interactions (H-bonds) between the two partners can be tuned not only by the structural aspects, but also by the solvent used when blending the two polymers. Interpolymer complexes (IPC) or miscible blends can be obtained. From these statements, various thin films were successfully prepared using the PPFS derivatives modified with mercaptopropionic acid (MPA). Firstly, PPFS-MPA/P4VP interpolymer complexes (IPC), spontaneously formed in solution, were successively deposited onto a plane substrate. Secondly, large efforts were dedicated to the elaboration of LbL self-assembly films. The feasibility to construct such a film was proved and the influence of various parameter, such as the solvent, the DS, and the polymer concentration were investigated in terms of *i*) growth mechanism, *ii*) internal organization and *iii*) surface features of the resulting self-assembly multilayer films.

Chapter 1: Bibliography

The objective of this work is to prepare superhydrophobic silica-based (nano)composite films and to generate novel H-bonded layer by layer (LbL) self-assembly thin films by using the perfluoroalkyl or carboxylic acid containing thiol modified poly(2,3,4,5,6-pentafluorostyrene) (PPFS) as building blocks. Thus, it is required to expose the state of art linked to these scopes by giving a bibliographic overview dealing with: a) the development of *para*-fluoro substitution reaction of pentafluorophenyl containing polymers; b) the definition of superhydrophobic surfaces and the main approaches based on the use of polymers to access to such surface features, in particular for the super water-repellent (nano)composite films containing fillers embedded in fluorinated (co)polymers and c) the main assets of the LbL self-assembly technique and different kinds of non-covalent forces used for the construction of thin films in LbL, especially for the H-bonds driven multilayer films constructed from carboxylic acid-containing (co)polymers.

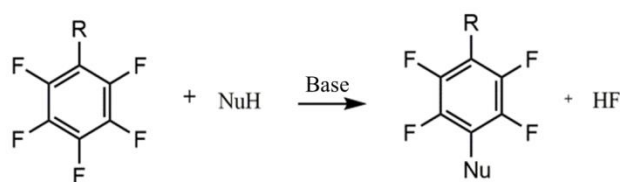
1.1 *Para*-fluoro chemistry of pentafluorophenyl group containing polymer materials

The fluorine atom has low polarizability, strong electronegativity and small van der Waals radius (1.32 Å) and the corresponding fluorinated organic molecules or polymers display a strong C-F bond (485 kJ/mol). The replacement of five hydrogen atoms on phenyl groups by five electron-withdrawing fluorine atoms leads to pentafluorophenyl (PFP) aromatic groups. In presence of nucleophiles, the highly positive *para*-carbon atom of PFP is attacked, forming 2,3,5,6-terafluorophenyl derivatives, named *para*-fluoro substitution reaction (PFSR). With this strategy, PFP groups containing polymer materials become versatile candidates for further functionalities and applications in the field of electronics and optics, biomaterials, and chemical coatings.

Currently, much effort is being devoted to explore the versatility of PFSR of fluorinated polymers in terms of low surface energy properties and good chemical resistance in the recent years. As an alternative class of highly efficient reactions, PFSR has also received great attention in chemical transformation of nonfluorinated polymers with providing unique access to functional materials and enable the study of structure-property relationships in series of functional polymers. This review initially summarizes the features of PFSR involving polymers in two parts. One dealing with the mechanism, substrates, nucleophiles and reaction conditions of PFSR; the other one focusing on the strategies including pre-polymerization modification, post-polymerization modification, polymerization through PFSR as well as surface modification involved into PFSR.

1.1.1 Mechanism

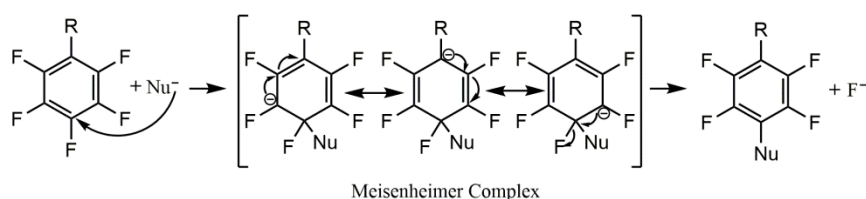
PFSR as one kind of nucleophilic aromatic substitution (S_NAr) involves the replacement of a fluorine atom in the *para* position on an aromatic ring by a nucleophile (Scheme 1-1).



Scheme 1-1 General *para*-fluoro substitution reaction (PFSR).

One of the earliest studies regarding the PFSR involved tetra-pentafluoro of meso-tetra-(pentafluorophenyl)porphyrin (or its Zn(II) and Fe(III) complexes) was reported by Battioni and coworkers in 1991,¹ who described the reaction of various nucleophiles and studied the selectivity of the fluorine replacement in the PFP group. By using nucleophiles such as amines, alcohols or thiols with electron-donating substituents, the regioselectivity in *para*-position was observed. On the contrary, the substitution in a given PFP group by using such electro-withdrawing nucleophiles as

CN^- leads to multiple mixtures. Kvičala *et al.*² modified 2,3,4,5,6-pentafluorobiphenyl (PFBi) by using a series of O-, S- and N-nucleophiles and all the substitutions took place exclusively at the *para* position of the phenyl group. Based on the computational analysis with density functional theory (DFT) calculation, the authors demonstrated that the regioselectivity can be attributed to higher polarizability of the system during the C-4 attack and improved stability of the corresponding dearomatized transition states, which corresponds well with their lower HOMO orbital energy. In addition, Baker and coworkers^{3,4} predicted the primary substitution site in aromatic perfluorocarbons, $\text{C}_6\text{F}_5\text{X}$, where X are: -H; - CH_3 ; - CF_3 ; -CHO; - NO_2 ; - $\text{NH}(\text{CH}_3)$, - $\text{N}(\text{CH}_3)_2$; - $\text{CH}=\text{CH}_2$; - CH_2OH and - SCH_3 by designing computational models which were based on the standard two-stage description of nucleophilic substitution involving the formation of a negatively charged intermediate, known as a Meisenheimer complex (Scheme 1-2).



Scheme 1-2 The mechanism of *para*-fluoro substitution reaction (PFSR).⁴

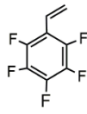
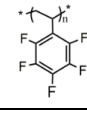
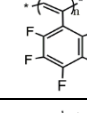
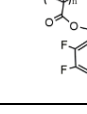
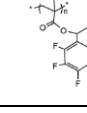
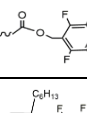
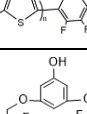
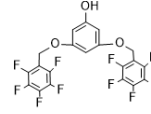
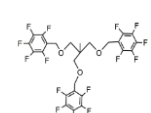
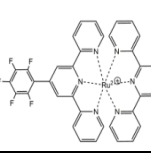
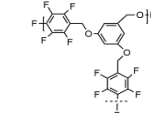
The relative energy of Meisenheimer complex that involve *para*-fluoro substitution is the lowest one compared to other possible intermediates, leading to a highly stable intermediate and a more stable product.

1.1.2 Substrates

As an efficient reaction, PFSR has drawn great attention in designing new polymer materials over the past decades. The pentafluorophenyl (PFP) groups may be introduced by using various paths in the polymer backbone. As shown in Table 1-1, the substrates can be sorted into two categories in terms of modification/functionalization of monomer, side group or end group of polymer, and

polymerization involving the PFSR. From the number of reference, more than 90% work on PFSR has focused on the modification/functionalization of monomer and polymers, mainly based on 2,3,4,5,6-pentafluorostyrene (PFS) (Table 1-1, S1).

Table 1-1 Various substrates with PFP groups in polymer materials.

Purpose	Strategy	Type	Substrate (S)	Abbreviation (S)	Ref	
Modification/functionalization	Pre-polymerization	Monomer		S1	2, 5–16	
		polymer		S2	17–34	
			S3	35		
	side group			S4	36	
			S5	37		
	end group		S6	38		
			S7	39,40		
	Polymerization	Monomer	AB ₂		S8	41
			A ₃		S9	42
			A ₂		S10	43
Macro monomer		AB ₂		S11	5,44,45	

In particular, various architectures contain homo, block and random copolymers have been developed (Table 1-1, S2). As an expand work, PFSR was also applied in conjugated (co)polymers (Table 1-1, S3). Differing from PPFS and its derivatives, other vinyl containing monomers such as methacrylates possessing a PFP group in the ester group (Table 1-1, S4 and S5), while still keep the activity of *para*-fluorine of PFP after polymerization. In addition to side group, PFP as end group (Table 1-1, S6 and S7) to functionalize polymer chains were also reported.^{38,39,44}

With the aim of polymerization, AB₂ type monomers with two PFP groups (A) and one hydroxyl group (B) have been prepared as monomer (Table 1-1, S8)⁴¹ and macromonomer (Table 1-1, S11)^{44,45}. Another A₃ type monomer with three PFP groups (Table 1-1, S9) has recently been prepared.⁴² What's more, A₂ type monomer (Table 1-1, S10) with two PFP groups was reported by Wild and coworkers in preparing linear metallopolymers.⁴³

1.1.3 Nucleophiles

The type of specific nucleophiles have a notably influence on the reactivity of the *para*-fluorine of the PFP moiety, where softer nucleophiles are more reactive than harder nucleophiles in the order of HS-CH₂R > H₂N-CH₂R >> HO-CH₂R.⁴¹ Using nucleophiles to modify PFP groups in PFSR allow for the preparation of various derivatives with specific properties, and has become a popular way for polymer functionalization. Advances in searching for nucleophiles, ranging from weak to strong nucleophilic and better ways to control the process of reactions, permit to give us an overview of the PFSR in the last decade.

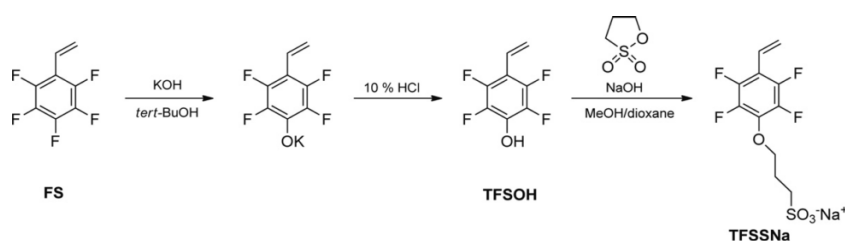
1.1.3.1 Alcohols as nucleophiles

Alcohols (A) react very slowly and thus the corresponding alkoxides are the active species in PFSR. Herein, four basic types of alcohols have been selected for discussion (Table 1-2): alkyl alcohols (A1, A2, A3), semifluorinated alkyl alcohols (A4-A9), perfluoropolyether alcohol (A10) and multi-functional alcohols (A11-A18).

Table 1-2 Alcohols as nucleophiles.

Alcohols	Abbreviation (A)	Nucleophiles	ref
Alkyl Alcohol	A1		5,7
	A2		10,46
	A3		39
Semifluorinated alkyl alcohol	A4		8
	A5		5
	A6		8,33,34
	A7		34
	A8		11
	A9		12
Perfluoro polyether alcohol	A10		11
Multi-functional alcohol	A11		6,14,16
	A12		15
	A13		13
	A14		13
	A15		5
	A16		9
	A17		9
	A18		9

The aliphatic alcohol, methanol (Table 1-2, A1) and tert-butanol (Table 1-2, A2) as well as pentanol (Table 1-2, A3), bring electron-donating alkoxy groups onto *para*-position of PFS monomer. For example, PFS was converted into 2,3,5,6-tetrafluoro-4-methoxystyrene with a yield of 86% by using a solution of sodium in methanol and then transformed to a *para*-hydroxy-tetrafluorostyrene derivative (TFSOH) by demethylation with boron tribromide in a complete separate procedure.⁵ TFSOH was also synthesized by using PFS with potassium hydroxide in tert-BuOH followed by acidification (Scheme 1-3).¹⁰



Scheme 1-3 Synthesis of TFSOH and TFSSNa fluorinated monomer.¹⁰

After further activation in alkaline MeOH/dioxane, TFSOH was used for the ring-opening of 1,3-propane sultone (PrS), leading to sulfopropylated tetrafluoro derivative of styrene (TFSSNa) that can be polymerized for the preparation of conductive polymers.

On the contrary, semifluorinated alcohols, $\text{CF}_3(\text{CF}_2)_n(\text{CH}_2)_m\text{OH}$ ($n = 0-10$, $m = 1$ or 2) (Table 1-2, A4 - A9), and perfluoropolyether alcohol (Table 1-2, A10) bring electron-withdrawing fluorine rich alkoxy groups onto *para*-position of PFP groups. Hvilstedt *et al.*⁸ introduced fluorine rich alkoxy chains (Table 1-2, A4 and A6) to monomer PFS by using sodium alcoholates of the relevant fluorinated alcohols with high yield (80%). Pitois *et al.*⁵ took A5 (Table 1-2) to modify hyper branched fluoropolymers. Zhu and coworkers¹¹ modified PFS by using short fluoroalkyl alcohol (Table 1-2, A8) and perfluoro polyether (Table 1-2, A10) with NaH as base in THF for 19h with a yield of 67%. Valtola *et al.*¹² used A9 (Table 1-2) for the preparation of perfluorinated PFS monomer in 50% aqueous NaOH solution at 40 °C with a yield of 50% after 24 h. The authors also modified PPFS by using the Na salt of 1H, 1H-perfluorododecanol (Table 1-2, A7) at 65 °C in THF to improve the

fluorophilicity of the PPFS block.³⁴ The effect of electron-donating and electron-withdrawing groups on PFS derivatives are reflected by the further polymerization rate and the physical properties (solubility, Tg) of the corresponding polymers.⁴⁷

Tri(ethylene glycol) (TrEG, Table 1-2, A11) as bifunctional alcohols underwent one successful PFSR and still keep the reactivity of the other hydroxyl groups to prepare ATRP initiator for further polymerization.¹⁹ α -CH₃ TrEG with one hydroxyl end group was introduced to PFS monomer via PFSR for the fabrication of surface-activate copolymers.¹⁴ Vinyl contained alcohol (Table 1-2, A12) was used for the modification of PPFS (Table 1-1, S2) in the presence of NaH heated in THF and reached to a full conversion after 3 h. With the same experimental conditions, other vinyl alcohols, such as cyclohex-3-enylmethanol (Table 1-2, A13) and 6-methylcyclohex-3-enylmethanol (Table 1-2, A14) were used to modify PFS (Table 1-1, S1) with yields of 84% and 85%, respectively. The A15 (Table 1-2) bearing *para*-hydroxyl was employed to modify hyperbranched fluorinated polymers, allowing for reducing the refractive index of the resulting polymers.⁵

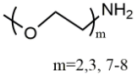
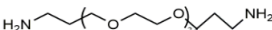
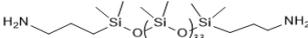
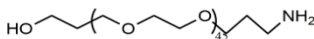
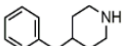
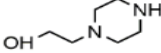
A series of hexanol-substituted azobenzenes differing by the substituent on the azobenzene being fluoro, trifluoromethyl or nitrile azobenzene (Table 1-2, A16, A17, A18) are selected to modify S1 (Table 1-1) with great potential for high-capacity holographic information storage (volume holography) in mind.

1.1.3.2 Amines as nucleophiles

The other important class of nucleophiles is amines (N) regarding the PFSR. These amines can be categorized into primary amines, diprimary amines, functional amines and secondary amines (Table 1-3).

Boufflet *et al.*³⁹ selected a long chain length amine, N-octylamine (Table 1-3, N3), to modify PFP end-capped polythiophene derivatives in the presence of K₂CO₃ at 70 °C in THF and a full conversion was obtained after 48 h. Another primary amine

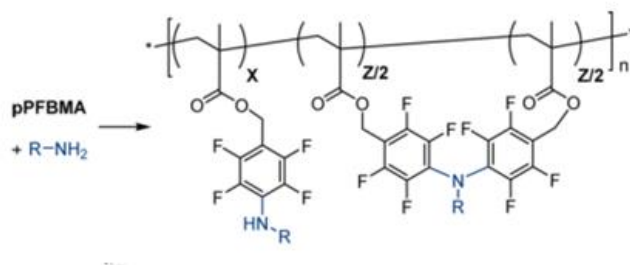
Table 1-3 Amines as nucleophiles.

Amines	Abbreviation (N)	Nucleophiles	ref
Primary amine	N1		36
	N2		36
	N3		39
	N4		36
	N5		18
	N6		36
	N7		36
Diprimary amine	N8		44
	N9		48
Functional primary amine	N10		17
	N11		17
Secondary amine	N12		36
	N13		36
	N14		36

aminopropylisobutyl POSS (Table 1-3, N5) bearing hydrophobic group of POSS was used to modify the PPFS block of PEG-*b*-PPFS diblock copolymers with DIPEA as catalyst at 80 °C for 12 h in THF. However, this reaction shows a low efficiency as some N5 (Table 1-3) remain unreacted even after very long reaction times (20 h).¹⁸

Lu *et al.*⁴⁸ and Gudipati *et al.*⁴⁴ employed the diprimary amines end-capped macromolecules of PEG (Table 1-3, N8) or/and PDMS (Table 1-3, N9) to cross-link hyperbranched polymers under refluxing in THF by using DIPEA as base. Hydroxyl containing aliphatic or polymeric amines (Table 1-3, N10, N11) were involved in PFSR under microwave irradiation, leading to 10% of PFP groups were modified.¹⁷

Most recently, Noy *et al.*³⁶ reported on the modification of poly(2,3,4,5,6-pentafluorobenzyl methacrylate) (pPFBMA) homopolymers by using aliphatic primary amines, including n-butylamine (Table 1-3, N1), n-pentylamine (Table 1-3, N2), 3-(dimethylamino)propylamine (Table 1-3, N4), oligo(ethylene glycol)-based amines (Table 1-3, N6) and cyclohexylamine (Table 1-3, N7), which exhibit various pKa and different steric hindrance. The reactions were conducted in DMF at 50-60 °C overnight, resulted in complete substitution without any ester cleavage reactions. Interestingly, the authors observed double substitution reactions yielding tertiary $(-C_6F_4)_2NR$ amine bridges (Scheme 1-4).



Scheme 1-4 PFSR of pPFBMA with primary amines (RNH₂ = N1, N2, N4, N6, N7, Table 1-3): Formation of copolymers comprising the expected N-functional tetrafluoroaniline side groups (X) as well as N,N-bis(tetrafluoroaniline) side groups (Z).³⁶

The authors concluded that such bridges mainly occurs along one chain and do not lead to crosslinked polymer materials which was confirmed by ¹⁹F-NMR with the appearance of signals associated with N,N-dialkyl tetrafluoroaniline side groups. The amount of disubstituted aromatic rings ranged from 6 to 9 mol % for the set of smaller primary amines to 26-28 mol% for the oligo(ethylene glycol) methyl ether amine-modified samples. The higher reactivity of the secondary amine intermediate was attributed to a higher N-H acidity caused by the fluorinated substituent. Then, the

reactivity of secondary amine reagents (Table 1-3, N12, N13, N14) was examined. It was found that the modification of pPFBMA with the secondary amine piperidine proceed without side reactions as the ^{19}F -NMR analysis showed only the expected tertiary amine functionality.

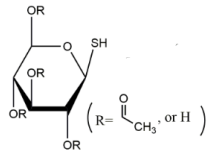
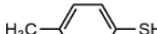
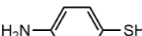
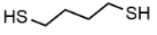
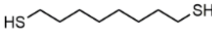
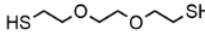
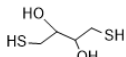
Besides, aromatic amines have been employed to react with PFP groups while these amines typically show lower reactivity in PFSR because of their lower nucleophilicity. For example, Noy *et al.*³⁶ reported that no reaction occurred when aniline was used to modify pFBMA while aliphatic amines under the same investigated experimental conditions reached a full substitution. The same conclusion was done by Boufflet³⁹ using another aromatic amines (2,5-dimethyl aniline) to modify PFP groups of polythiophenes.³⁹

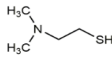
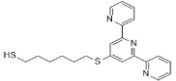
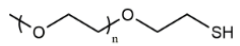
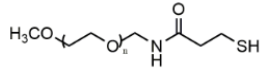
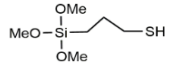
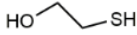
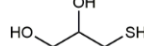
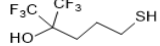
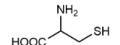
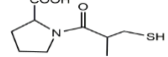
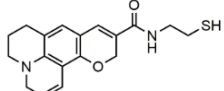
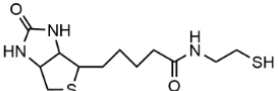
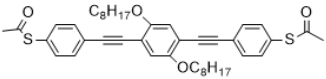
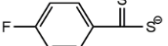
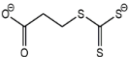
1.1.3.3 Thiols and sulfur-based nucleophiles

Thiols and sulfur-based nucleophiles as soft nucleophiles have been extensively studied in PFSR by many researchers due to their strong nucleophilicity. Table 1-4 shows that around 40 different thiols and sulfur-based nucleophiles have been reported in PFSR, making them the most often used nucleophiles for such reaction.

The first category contains various aliphatic thiols, $\text{C}_n\text{H}_{2n}\text{SH}$, with chain length varying from $n = 3$ to $n = 12$ (Table 1-4). T1 ($n = 3$, Table 1-4) was used for the modification of PFP groups end-capped star polymers in which a full conversion was obtained in DMF when catalyzed by TEA after 4 h.³⁸ The PFSR between T3 ($n = 5$, Table 1-4) and conjugated PPFS polymers needs 67 h in DMF with DBU at 40 °C to achieve a full conversion.³⁵ T6 ($n = 12$, Table 1-4) was used to modify α -PFP of S7 (Table 1-1) in THF with K_2CO_3 at 70 °C for 12 h to reach a complete conversion³⁹ and it was also used as a linker to polymerize the macromonomer (Table 1-1, S9) with DBU in THF.⁴²

Table 1-4 Thiols and sulfur-based nucleophiles.

Thiols and sulfur based nucleophiles	Abbreviation (T)	Nucleophiles	ref
Aliphatic thiol	T1		38
	T2		36
	T3		35
	T4		24,37,49
	T5		36
	T6		39,42
	T7		37
	T8		37
	T9		37
Thiolglucose	T10		20– 22,25,27– 31,35,37
Aromatic thiol	T11		19,36,37
	T12		39
	T13		35
Dithiol	T14		39,42
	T15		39
	T16		42
	T17		42
	T18		42

Functional thiol	T19		35,36
	T20		43
	T21		39
	T22		26
	T23		32,39
	T24		23,24,50
	T25		23,35,51
	T26		52
	T27		25
	T28		39
	T29		36,37
	T30		39
	T31		39
	Sulfur based nucleophiles	T32	NaSH
T33			36
T34			43
T35			36
T36			36

Noy *et al.*^{36,37} used C₄H₈SH (Table 1-4, T2), C₈H₁₇SH (Table 1-4, T4) and C₁₀H₂₀SH (Table 1-4, T5) for complete modification of pPFBMA homopolymers with DBU in DMF at room temperature in 40 min. Then, the authors expanded the versatility of PFSR to secondary (Table 1-4, T7, T8) and tertiary thiols (Table 1-4, T9) which are expected to be even less acidic than primary thiols, leading to efficient couple reaction with PFP groups in less than 45 min.³⁷

Dithiols (T14 to T18) are listed in Table 1-4. Cavalli *et al.*⁴² introduced the regioselective PFSR for network formation by using dithiols (T14 and T16), aromatic dithiols (T18) and functional dithiols (T17) with DBU at room temperature in a very short time (20 min). Boufflet *et al.*³⁹ generated a thiol-terminated polythiophene by reacting S7 (Table 1-1) with a large excess of T15 (10 eq.) with K₂CO₃ in THF for 12 h at 40 °C under argon. This fact provides an alternative way to prepare reversible crosslinking and self-healing materials by using disulfide bond formation.

Noy *et al.*^{36,37} successfully performed PFSR in PFP-functional homo- and copolymers with a range of functional thiols, such as thiophenol (T11), mercaptopropionic acid (T27), the amino acid L-cysteine (T28) and the enzyme inhibiting drug captopril (T29). In the modification of pPFBMA (Table 1-1, S4) with T19 in DMF with DBU as base, a full conversion was reached after 90 min at room temperature,³⁶ Bhebhe *et al.*³⁵ reported on the modification of conjugated polymers (Table 1-1, S3) with T19 (Table 1-4) in the same experimental conditions, while a full conversion was reached after 67 h even at 40 °C.

Other functional thiols, for example alkoxy silane containing thiol, 3-mercaptopropyl-(trimethoxysilane) (3-MPTS, Table 1-4, T23), was used to modify PFP groups along the polymer backbone of PPFS and further condensed on a silica substrate to achieve high-performance electrically stable organic field-effect transistors.³² A same strategy was used to modify α -PFP polythiophene and the resulting polymer can be easily used to functionalize glass substrates with potential applications in organic electronic devices.⁶ Chen *et al.*²³ used hydroxyl containing thiols (Table 1-4, T24, T25 and T26) by using TEA as base in different solvents to introduce hydrogen bond donor groups into PPFS; carboxylic acid contained thiols

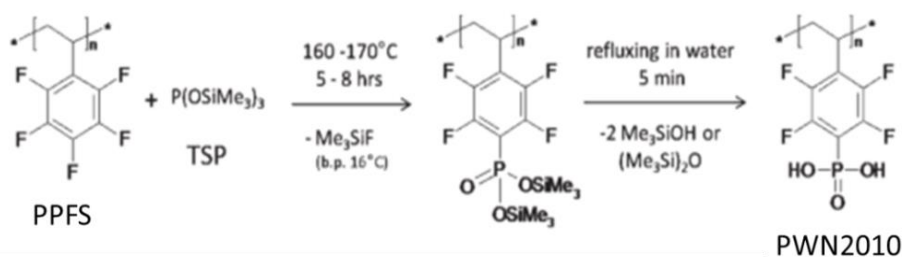
(Table 1-4, T27, T28 and T29) were involved in PFSR by using TEA²⁵ or K₂CO₃³⁹ or DBU³⁷ in DMF at room temperature. Sensitive functional molecules such as the Coumarin 343 derivative (Table 1-4, T30 and T31) can be tethered to α -PFP polythiophene in quantitative yield after reaction for 48 h at room temperature.³⁹

In addition to the results obtained with thiols, Noy *et al.*³⁶ have reported other sulfur-based nucleophiles in PFSR with the aim of preparing tetrafluorophenylthiol. It was demonstrated that the PFSR with sodium hydrogen sulfide (NaSH, Table 1-4, T32) occurred without any base, with a full conversion in 30 min at room temperature. The potassium thioacetate (Table 1-4, T33) showed reasonably high reactivity in the absence of base and the expected tetrafluorophenyl thioacetate product was too reactive to be isolated with products containing about 30 mol % of thiols. On the other hand, bis(triethylammonium) salt of S-carboxypropyl trithiocarbonic acid (Table 1-4, T35), was less reactive and gave 90% *para*-fluoro substitution after heating to 65 °C for 6 days. It was also found that the triethylammonium 4-fluorodithiobenzoate (Table 1-4, T36) enabled full conversion to the tetrafluorophenyl benzenedithioate derivative within 24 h at 65 °C.

Besides, Wild *et al.*⁴³ used a conjugated monomer, bearing two acetate-protected thiol groups (Table 1-4, T34), to polymerize with S10 (Table 1-1) in DMF in the presence of a very strong nonnucleophilic phosphacene base at room temperature. The fluorescence of the conjugated spacer was completely quenched, indicating a full conversion.

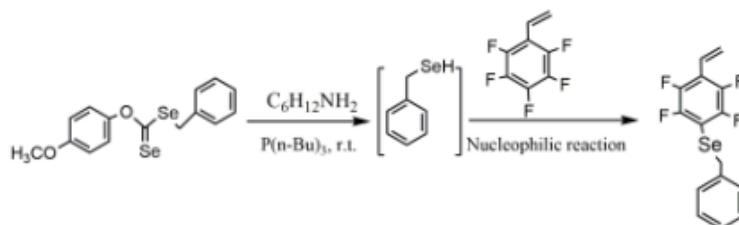
1.1.3.4 Other nucleophiles

Giannopoulos *et al.*⁴⁰ reported the modification of TiO₂ nanoparticles by using regioregular poly(3-alkyl thiophene) (P3HT) polymeric chains via PFSR between its surface Ti-OH and α -PFP group of P3HT. Atanasov *et al.*⁵³ reported the selective and complete phosphonation of the PFS blocks in two steps (Scheme 1-5).

Scheme 1-5 Post-phosphonation of PPFS.⁵³

PPFS was firstly reacted with tris(trimethylsilyl) phosphite (TSP) at $T = 170\text{ }^{\circ}\text{C}$ for 5-8 h to ensure a full conversion; then, the resulted products were hydrolyzed by refluxing in water for 5 min leading to phosphonic acid derivative (PWN2010) with a yield of 98%. With the aim of improving proton conductivity, they employed Na_2S to modify PPFS in DMAc together with $\text{H}_2\text{O}_2/\text{HCOOH}$ for preparing sulfonated PPFS. The enhanced higher acidity of sulfonated PPFS leads to a higher conductivity compared with phosphonated PPFS.^{54,55}

In addition, the nucleophilic reaction of an in situ generated selenol was explored by Lu and coworkers (Scheme 1-6).⁴⁸

Scheme 1-6 Selenol-*para*-fluoro substitution reaction.⁴⁸

Selenols are more reactive compared to thiols and were prepared from aminolysis of a selenium-based RAFT agent by *n*-hexylamine with tributylphosphine as reducing agent. The following PFSR reaction was processed to 90% conversion after 12 h at room temperature. With the same method, the diselenocarbonate end-capped polystyrene (PS-Se) was synthesized and used to modify PFS via selenol-*para*-fluoro substitution reaction.

1.1.4 Influence of the experimental conditions on the PFSR

1.1.4.1 Base

The types of base used in PFSR with the corresponding nucleophiles are presented in Table 1-5.

Table 1-5 Summary of base used in PFSR.

Base	Nucleophiles		
	Alcohols	Amines	Thiols and sulfur based nucleophiles
NaH	A5, A8, A10, A11, A12, A13, A14, A15		
NaOH (or KOH)	A1, A2, A3, A4, A6, A7, A9, A16, A17, A18		T10
K ₂ CO ₃		N3	T6, T21, T12, T15, T23, T28, T30, T31
TEA			T1, T4, T20, T22, T10, T11, T13, T23, T25, T26, T27, T35, T36
DBU			T2, T3, T4, T5, T6, T7, T8, T9, T19, T10, T14, T16, T17, T18, T24, T25, T27, T28, T29
P1-t-Bu*			T34
DiPEA		N5, N8, N9	
Sec- or tert -BuLi	A2, A6		
No Base		N1, N2, N4, N6, N7, N12, N13, N14, N10 [#] , N11 [#]	T32, T11, T33
*tert -butylimino-tris (dimethylamino)phosphorane; # with microwave irradiation			

Generally, the weak nucleophilicity of alcohols requires the use of strong bases, such as NaH, NaOH (or KOH) and sec- or tert-Butyllithium to form alkoxides; long reaction times from few hours to few days and high temperatures are needed.^{2, 5-16}

Amines used as modifier may also act as a base, meaning that the addition of a base catalyst (mandatory for alcohols) is not necessary. There are some examples of using microwave-assisted technology to initiate the PFSR but the conversion was low. For example, Schubert *et al.*¹⁷ investigated the PFSR with α -amino- ω -hydroxy-PEG (Table 1-3, N11), in a capped microwave vial with N-methylpyrrolidone as solvent for 20 min at 95 °C. The number of attached PEG chains was determined by ¹H-NMR spectroscopy, revealing that 10 grafted side chains per PFS backbone. The scope of this synthetic concept was extended by reacting PPFS with 5-aminopentanol (Table 1-3, N10) under microwave irradiation, which leads to the introduction of several hydroxyl groups on the side chains. K₂CO₃ was scarcely used as a strong base for PFSR.³⁹ A stronger base such as DIPEA was used when chemical linking was envisaged using diamine (Table 1-3, N8, N9).^{44,48}

With thiols or sulfur based nucleophiles, three bases have been mainly used, namely, TEA, K₂CO₃ and DBU. Schubert and coworkers^{19,20} demonstrated that the versatility and efficiency of thiol substitution of the *para*-fluoro group of PPFS with TEA as base in introducing carbohydrate groups onto PPFS polymer backbone, forming glycopolymers or glycosylated materials. The impact of various base on reaction rate when thiols are used as nucleophiles in DMF without or with base (TEA, DBU) are shown in Table 1-6.

Table 1-6 Various experimental conditions for the PFSR of thiophenol (T11) or octanthiol (T4) with PFP groups containing pPFBMA (S5)

Nucleophiles	Base	Temperature	Reaction time	Conversion	Ref
T11	No base	45°C	22 h	35%	37
T11	TEA	45°C	69 min	99%	37
T4	TEA	45°C	24.5h	28%	37
T4	DBU	R.T.	3min	100%	37

Without base, thiophenol (Table 1-4, T11) was used for the modification of S5 (Table 1-1) at 45 °C and resulted a conversion of 35% after 22h. However, in the presence of 1 equiv. of TEA, the reaction was faster and proceeded to 99% conversion

after 69 min.³⁷ Moreover, the reaction with 1-octanethiol (Table 1-4, T4) with TEA at 45 °C allowed a conversion of only 28% after 24.5 h, while the use of a stronger base (DBU) permitted a conversion higher than 99% within 3 minutes at room temperature.³⁷ The addition of base promoted the PFSR; the stronger the base is, the faster reaction is.

1.1.4.2 Solvent

The solvent used for PFSR are listed in Table 1-7.

Table 1-7 Summary of solvents used in PFSR.

Solvent	Nucleophiles		
	Alcohols	Amines	Thiols and sulfur based nucleophiles
THF	A3, A4, A6, A7, A8, A10, A11, A12, A13, A14, A16, A17, A18	N3, N5, N8, N9	T6, T22, T12, T14, T15, T16, T17, T18, T23, T24, T25, T26, T30, T31
DMF		N1, N2, N4, N6, N7, N12, N13, N14	T1, T2, T3, T4, T5, T7, T8, T9, T19, T20, T21, T10, T11, T13, T24, T27, T28, T29, T32, T33, T34, T35, T36
NMP		N10, N11	
MEK			T24, T25,
EtAc			T24, T25,
MeOH	A1		
Tert-BuOH	A2		
Acetone			T13
DMSO			T10
CH ₂ Cl ₂	A9		
DMAc	A5, A15		
H ₂ O/DMF			T28
H ₂ O(pH=11-13)			T24

It can be seen that PFSR often performed in polar aprotic solvents (Table 1-7).^{5,17,29,30,35,56} such as acetone was used in the modification of conjugated polymers;³⁵ N-Methylpyrrolidone (NMP) as a high boiling point solvent was used in the microwave-assisted systems in high temperature;¹⁷ dimethyl sulfoxide (DMSO) was used when thioglucose acts as nucleophiles;^{29,30} dimethylacetamide (DMAc) was used in the modification of fluorinated hyperbranched polymers;⁵ dichloromethane (CH₂Cl₂) as solvent happened in perfluorinated nucleophiles modify PFS;⁵⁶ the most often ones being tetrahydrofuran (THF)⁷ and N,N-dimethylformamide (DMF)³⁸, as reflected by the number of nucleophiles. In addition, Chen *et al.*²³ have studied the kinetics of *para*-fluoro thiol reaction with hydroxyl containing thiols in different aprotic solvents (Table 1-8).

Table 1-8 Effect of solvent on reaction rate of PFSR of 2-mercaptoethanol (T24) with PPFS (S2).

Nucleophiles	Solvent	Reaction time	Conversion	Ref
T24	EtAc	4 days	50%	23
	THF	4 days	60%	
	MEK	4h	50%	
		2 days	95%	

The authors selected various solvents, including ethyl acetate (EtAc), THF and methyl ethyl ketone (MEK), and employed 2-mercaptoethanol (Table 1-4, T24) to modify PPFS with TEA as base. It was demonstrated that the reaction rate increased by increasing the polarity of solvent: EtAc ($\epsilon=6.0$) < THF ($\epsilon=7.1$) < MEK ($\epsilon=18.4$).

In polar protic solvents such as methanol and tert-BuOH, only PFS monomer was tolerating PFSR due to the poor solubility of most of the fluorinated polymers. Moreover, few work reported on the PFSR performed in water containing solution, such as Boufflet *et al.*³⁹ investigated the PFSR between T28 (Table 1-4) and PFP end-capped polythiophenes by using DMF/water mixture. Turgut *et al.*⁵⁰ demonstrated the feasibility of PFSR in basic water by using a random copolymer of poly(N,N-dimethylacrylamine-stat-pentafluorostyrene) poly(DMAAm-stat-PFS) with

5% PFS.

1.1.4.3 Temperature

The temperature employed in PFSR is shown in Table 1-9.

Table 1-9 Temperature used in PFSR.

Temperature	Nucleophiles		
	Alcohols	Amines	Thiols and sulfur based nucleophiles
-20°C			T20
25 °C			T1, T2, T4, T5, T6, T7, T8, T9, T19, T21, T22, T10, T11, T14, T16, T17, T18, T24, T25, T27, T28, T29, T30, T32, T33, T34
40-65 °C	A1, A2, A3, A4, A6, A7, A8, A9, A10, A11, A12, A13, A14, A16, A17, A18	N1, N2, N4, N6, N7 , N12, N13, N14	T3, T4, T6, T19, T10, T11, T13, T15, T23, T24, T25, T26, T35, T36
70-80 °C		N3, N5, N8, N9	T12, T23, T31
90-100 °C		N10, N11	
150 °C	A5, A15		

With using alcohols as nucleophiles, it is generally needed to heat the reaction medium to reflux (Table 1-9).

When using amines as nucleophiles in the absence of any other base, high temperatures (40-65 °C) are required. Even in presence of a base, for example K_2CO_3 for N3 (Table 1-3)³⁹ or DiPEA for N5 (Table 1-3)¹⁸, the solvent still need to be heated at 70-80 °C. Very high temperature (90-100 °C) was used when performing PFSR with

microwave irradiation (Table 1-3, N10, N11)¹⁷. The strong nucleophilicity of thiols makes it possible to perform PFSR at room temperature. More than 70% of thiols react with PFP at room temperature in presence of TEA or DBU as base. Boufflet *et al.*³⁹ used 10 eq. weaker thiol nucleophile p-thiocresol (Table 1-4, T10) and 15 eq. of K₂CO₃ to modify PFP group in THF. The reaction showed no conversion after 24 h at room temperature, while obtained complete conversion with heating to 70 °C after 12 h.

1.1.5 Chemical strategies involved *para*-fluoro substitution reaction (PFSR)

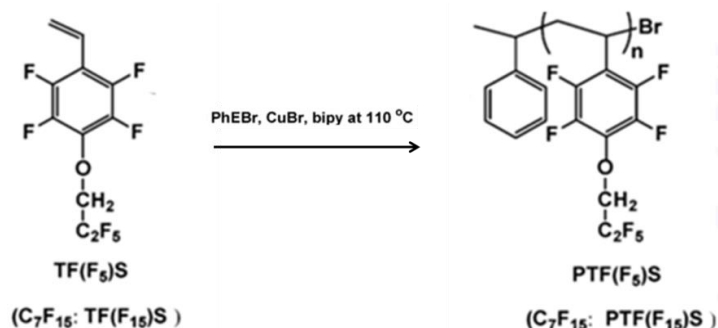
The preparation of novel PFP groups based polymers or hybrid materials have been highly significant in the material fields. In this context, various strategies to prepare new materials involving PFSR are discussed and classified.

1.1.5.1 Pre-polymerization modification

The pre-polymerization route includes the popular monomer based on 2,3,5,6-tetrafluorostyrene (TFS) with functional pendant groups which has mainly been achieved with using alcohols as nucleophiles. Then, these novel monomers were involved in various controlled polymerization methods including atom transfer radical polymerization (ATRP),⁸ reversible addition-fragmentation transfer (RAFT) polymerization,¹³ nitroxide mediated polymerization (NMP)⁵⁷ or/and free radical polymerization.¹¹ Furthermore, TFS derivatives have been much exploited to produce block copolymers with various monomers in the formation of a multitude of shapes and novel functional materials.

Fluorinated alkyl moieties such as -CF₂-, -CF₂H, and -CF₃ are quite effective for lowering surface free energy and combining water repellency with an outstanding chemical stability. To reach this target, the homo- and co-polymerization of pre-formed fluorinated alcohol modified PFS monomers have been reported.^{8,10,11,12, 47} In particular, Hvislted *et al.*^{8,10,47} reported the versatility of ATRP of PFS and its derivatives comprehensively. PFS was modified by fluorinated alcohols (Table 1-2,

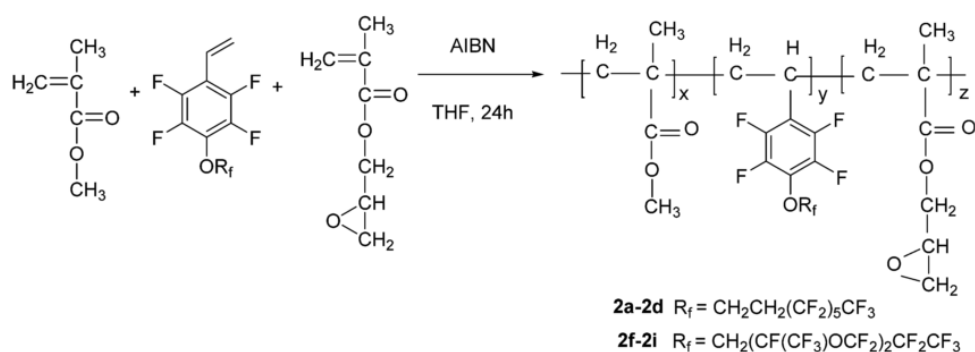
A4 or A6), and the corresponding derivatives were subjected to ATRP to prepare homopolymers (Scheme 1-7).



Scheme 1-7 ATRP of fluorinated PFS with fluoroalkyl.⁸

The fluorinated homopolymers were used as macroinitiator to initiate styrene for preparing block copolymers. After modification, the advancing water contact angle increased from 108 ° to 117 ° for PTF(F5)S and 122 ° for PTF(F15)S. The fluorination of the phenyl ring lower the surface energy and increases the hydrophobicity of the material surface as argued from the increase in water contact angle. Hydrophobicity of the surfaces can be further enhanced by electrospinning of the fluorinated diblock polymer based on polystyrene (PS) macroinitiators and perfluoroalcohol (Table 1-2, A9) modified PFS monomers. Superhydrophobic surfaces with water contact angle of 160° was yielded thanks to the presence of -CF₂ and -CF₃ groups.¹²

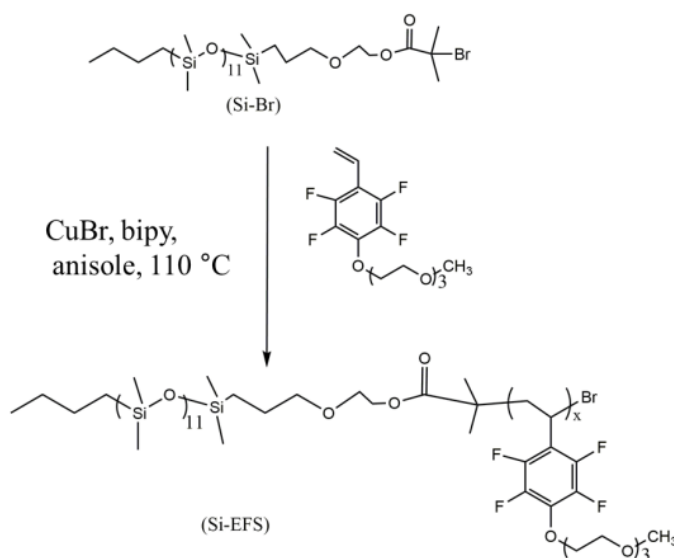
In addition, random copolymers can be easily prepared through free radical polymerization. In particular, Zhu *et al.*¹¹ reported the modification of PFS with A9 or A10 (Table 1-2), and the obtained functionalized monomer was copolymerized with methyl methacrylate (MMA) and glycidyl methacrylate (GMA) via radical polymerization with AIBN as initiator (Scheme 1-8).



Scheme 1-8 Copolymerization of fluorinated PFS with MMA and GMA via free radical polymerization.¹¹

The hydrophobicity of the obtained random copolymer coatings was increased with the increase of fluorinated monomer content and exhibited excellent antibacterial activity.

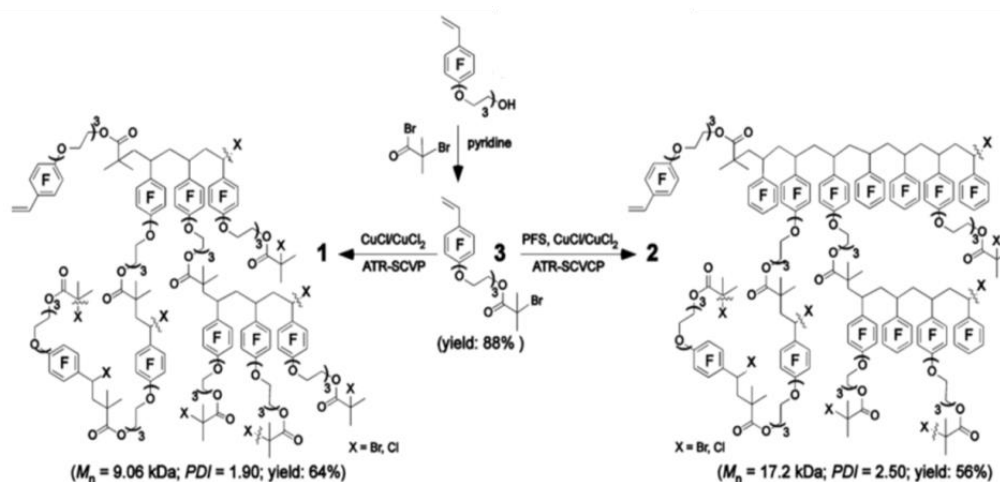
Some works have combined the hydrophobicity of fluoropolymers and the ability of PEGs in resistance to protein adsorption in order to prepare well defined anti-fouling surface. For example, Elisa Martinelli *et al.*⁵⁸ prepared an antifouling amphiphilic block copolymer, poly(dimethyl siloxane) (Si)-b-poly(4-(triethyleneglycol monomethyl ether)-2,3,5,6-tetrafluorostyrene) (EFS) through ATRP (Scheme 1-9).



Scheme 1-9 ATRP of diblock copolymers poly(dimethyl siloxane)-b-poly(4-(triethyleneglycol monomethyl ether)-2,3,5,6-tetrafluorostyrene) (Si-EFS).⁵⁸

First, PFS monomer was modified in order to incorporate 4-(triethyleneglycol monomethyl ether) group and then, it was polymerized with a bromo-terminated Si macroinitiator. The authors found that the Si block is concentrated at the polymer-air interface while the EFS block is located in the layers underneath in the dry state. Moreover, this polymer films underwent a significant surface reconstruction after immersion in water for 7 days, which results in the exposure of the hydrophilic oxyethylene chains to the surface. It was concluded that the ability of the block copolymers respond to the external environment which can be exploited to prepare atoxic, nonbiocidal coatings for marine applications. The resulted dynamical changes of a (nano)heterogeneous chemical surface can deter the settlement and adhesion of fouling organisms.

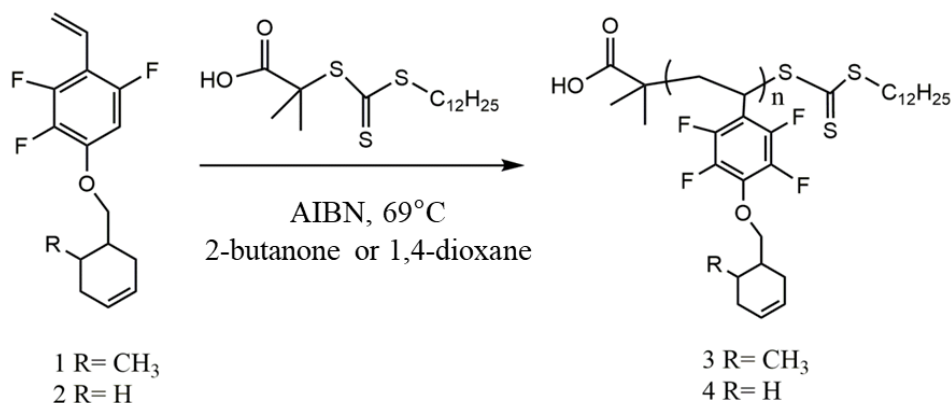
Similarly, Imbesi *et al.*⁶ reported the PEG containing antifouling hyperbranched HBFP-PEG networks by ATRP of the oligo PEG modified PFS followed by cross linking with α , ω -diamino terminated PEG. To improve the antibiofouling characteristics by increasing the PEG content while retaining nanoscale surface heterogeneities, Powell *et al.*¹⁶ developed another type of antifouling amphiphilic HBFP through atom transfer radical self-condensing vinyl homopolymerization of the tri(ethylene glycol)-functionalized amphiphilic fluorinated inimer, and its copolymerization with PFS (inimer/monomer = 1/3) (Scheme 1-10).



Scheme 1-10 Synthesis of hyperbranched fluorohomopolymer 1 and fluorocopolymer 2 by atom transfer radical vinyl self-condensing vinyl(co)polymerization.¹⁶

The homo- and co-polymers had thermal stability up to 175 and 210 °C, respectively. Both polymers showed good solubility in a broad range of organic solvents, and also in water as the presence of tri(ethylene glycol) units resulted in the formation of water-dispersible micelles. These materials are expected to exhibit increased surface wettability and anti-biofouling ability.

The pre-polymerization modified monomers with various pendant groups have shown other interests. For example, Wooley *et al.*¹³ reported the preparation of well-defined polymers bearing cycloalkenyl side groups via selective RAFT polymerization of cycloalkene-functionalized asymmetrical divinyl monomers prepared by PFSR (Scheme 1-11).

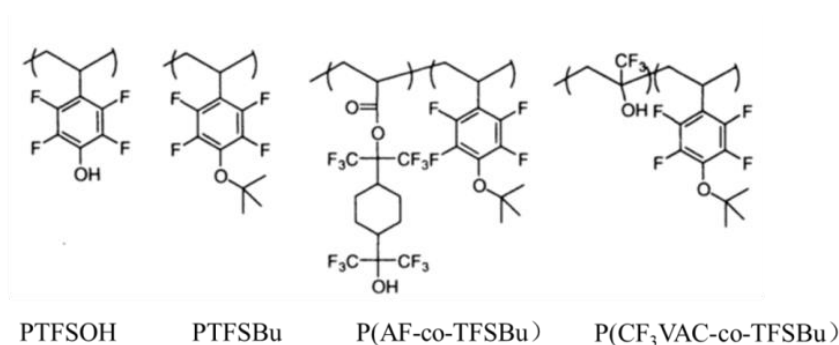


Scheme 1-11 Selective RAFT polymerizations of asymmetrical divinyl monomers bearing a pendent cyclohexene group.¹³

This polymerization shows great selectivity toward the substituted styrenyl vinylic unit relative to the cyclohexenyl unit. The resulting polymers retained quantitative cyclohexenyl groups, which can be further used as precursors for preparing functional polymers.

The pre-synthesized monomers can also be subjected to homo- or co-polymerization with other fluorinated monomers to prepare photoresist materials. For example, Conley and coworkers⁴⁶ prepared the homopolymers of p-hydroxy-tetrafluorostyrene (TFSOH), p-t-Butoxy-tetrafluorostyrene (TFSOBu); and the random copolymers of TFSOBu with 2-[4-(2-hydroxyhexafluoroisopropyl)cyclohexane]hexafluoroisopropyl acrylate (AF) or trifluoromethyl

vinylacetate (CF_3VAc) via free radical polymerization. Their structures are shown in Scheme 1-12. These unique polymers are highly transparent at 157 nm and can be applied to 157 nm photolithography.



Scheme 1-12 Structure of homopolymer PTFSOH, PTFSBu and random copolymers of P(AF-co-TFSBu) and P(CF_3VAC -co-TFSBu).⁴⁶

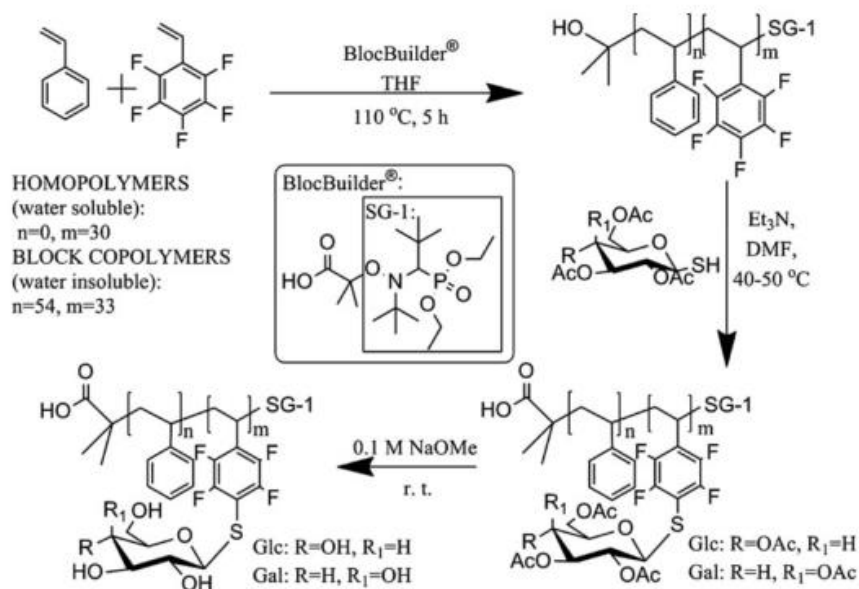
The synthesized fluorinated polymers with sulfonate side groups might be used as building blocks for numerous bio-related applications as well as for polymer electrolytes in fuel cells.¹⁰ Sugar-modified polymers were obtained by a direct polymerization of glucosylated monomers and then used in the modification of magnetic nanoparticles to prepare biocompatible coating.⁵⁷ Poly(2,3,5,6-tetrafluoro-4-methoxy-styrene) (PTFMS) was demethylated and the resulting hydroxyl sites further alkylated with different azobenzene side chains. Additionally, the azobenzene derivatized polymer has been copolymerized with styrene. Both homo- and block copolymers with azobenzene side chains formed materials exhibiting liquid crystal-type behavior.⁷

1.1.5.2 Post-polymerization modification

Differing from the direct polymerization of monomers with desirable properties, new polymeric materials with specific properties can be prepared by the post-polymerization modification of polymers. During the process of post-polymerization, only the functionality (degree or nature) may vary without altering the polymer backbone specifications (e.g., degree of polymerization, dispersity).⁵⁹

1.1.5.2.1 Polymers with PFP groups along the backbone

Poly(pentafluorostyrene) (PPFS) as the most widely used conventional fluorinated polymers have drawn great attention in the post-polymerization modification process with PFSR. Schubert *et al.*²⁷ reported on the post-polymerization modification of polymeric backbones with thioglucose. The authors prepared PFS containing homopolymers and random copolymers in combination with styrene by using BlocBuilder as alkoxyamine initiator via NMP. Furthermore, they examined the kinetics for the PFSR of the PFP units with thiol-glucose and obtained well-defined glycopolymers (Scheme 1-13).^{20,28}

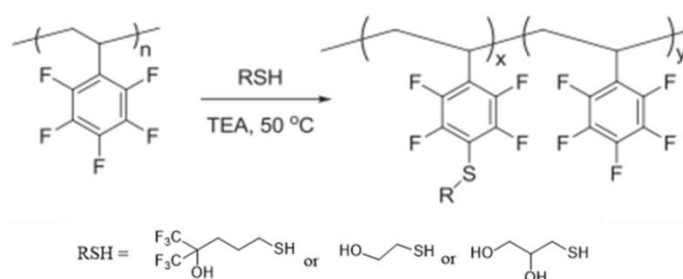


Scheme 1-13 Synthesis of the glucosylated and galactosylated based homo- and block-copolymers.²⁸

The glucosylated (hGlc) based and galactosylated (hGal) based homopolymers as well as the respective polystyrene block copolymers, bGlc and bGal, were obtained by using the PFSR to graft acetylated 1-thio-β-D-glucopyranose and 1-thio-β-D-galactopyranose onto the appropriate backbone. Subsequently, the deprotection of the carbohydrate moieties yield well defined glucose or galactose-modified polymers. The authors illustrated the well cellular recognition of carbohydrates in the water soluble homopolymers as well as nanoprecipitated PS

block copolymers, carrying β -D-thioglucose or β -D-thiogalactose moieties. In a different work, they reported the synthesis of thermo-responsive random copolymers of oligo(ethyleneglycol) methacrylate (OEGMA) or 2-(dimethylamino) ethyl methacrylate (DMAEMA) with PFS via NMP.¹⁹ The obtained copolymers have cloud points between 87 °C and 33.1 °C. Two ways were developed to tune the cloud points of well-defined copolymers: one by controlling the incorporation of more hydrophobic units during the polymerization and the other one by controlling the PFSR involving thiophenol to introduce hydrophobic phenyl groups.

Recently, some researchers have developed the substitution process with the aim of introducing functional groups. Chen *et al.*²³ prepared PPFS homopolymers via ATRP and then, they designed H-bond donor copolymers by introducing unprotected mercaptoalcohols onto PPFS via PFSR (Scheme 1-14).

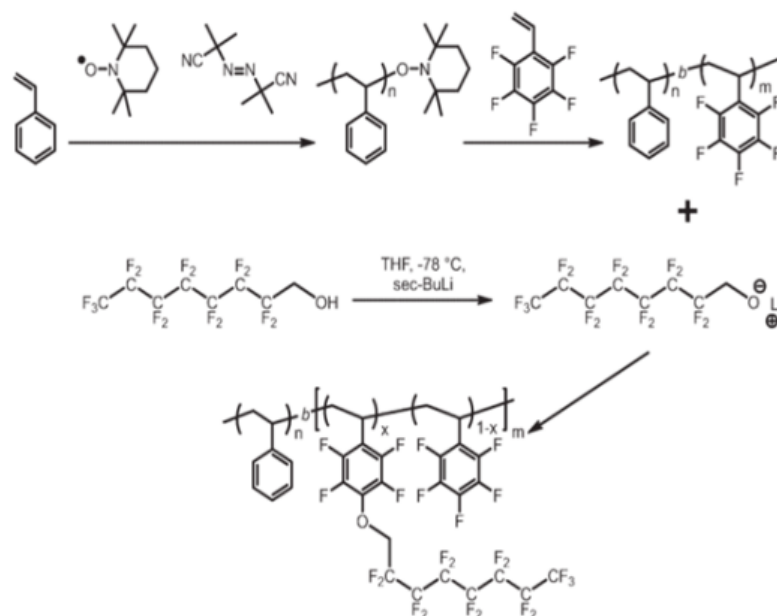


Scheme 1-14 Post-modification of PPFS by RSH.²³

Three kinds of thiols with various structures (either one or two hydrogenated hydroxyl groups or a polyfluorinated hydroxyl) were used as nucleophiles. The authors demonstrated the influence of the hydrogen bond donor type of hydroxylated PPFS with three different hydrogen bond acceptor, poly(4-vinyl pyridine (P4VP), poly(ethylene oxide) (PEO) and poly(butyl acrylate) (PBA).⁶⁰ Then, the H-bonded LbL multilayer films between P4VP and hydroxylated PPFS derivatives were investigated.⁵²

Müllen *et al.*³³ prepared PS-*b*-PPFS block copolymers via NMP and modified the PPFS block by using perfluorinated alcohols (Table 1-2, A6) via PFSR. The obtained amphiphilic block copolymers with a lipophilic and a fluorophilic block were used as

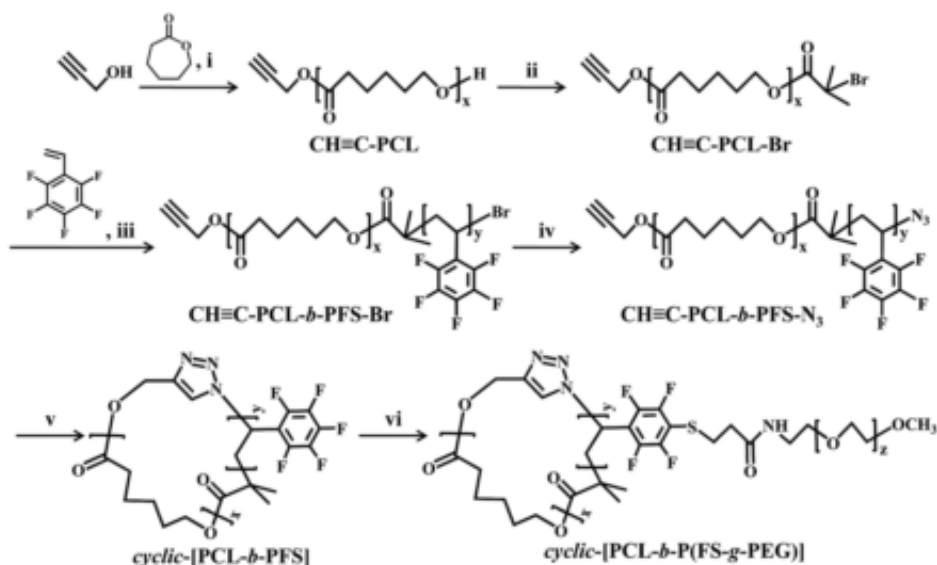
emulsifier to control the polymerization, the morphology, the size, and the shape of the obtained polyolefins based particles (Scheme 1-15).



Scheme 1-15 Synthesis of PS-PPFS functionalized emulsifier.³³

Liquid propene was used directly as a dispersed phase in a perfluorinated miniemulsion. As the fluorine content was significantly increased, an improved stabilization effect on the perfluoroalkane/alkane interface was obtained, providing a better control over the emulsion properties. With the same strategy, they developed another emulsifier, poly(isobutylene)-*b*-poly(pentafluorostyrene) in which the PPFS block was modified by using A6 or A7 (Table 1-2), for the polymerization of isobutylene.³⁴

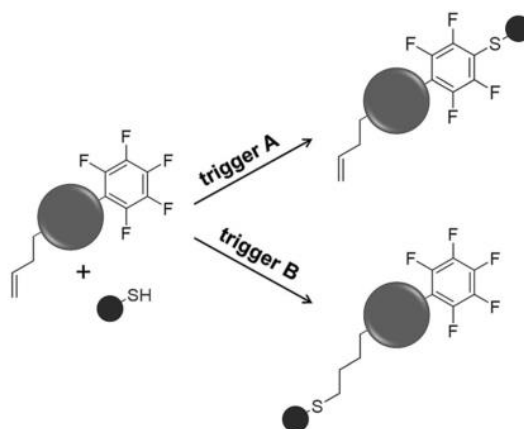
Cai *et al.*²⁶ prepared jellyfish-shaped amphiphilic block-graft copolymers with a hydrophobic ring of controllable dimensions, consisting of tailored length and number of 3-caprolactone (CL) and PFS units, and hydrophilic poly(ethylene glycol) (PEG) grafts (Scheme 1-16).



Scheme 1-16 Synthetic route of cyclic-[PCL-*b*-P(FS-*g*-PEG)] copolymers.²⁶

The authors combined the ring-opening polymerization (ROP) of CL, then the ATRP of PFS; followed with alkyne-azide click reaction result in the formation of cyclic block copolymer PCL-PPFS; the PPFS block was then subjected to PFSR to introduce hydrophilic PEG grafts. These polymers formed micelles with a diameter in the range of 50–60 nm. It was suggested that the driving force for the micelle formation from the amphiphilic copolymer involves strong repulsion between the highly hydrophobic cyclic-[PCL-*b*-PFS] ring and hydrophilic PEG tails. The PFP groups allow the design and preparation of a broad range of cyclic block copolymers with tailored ring morphology and functionalities via PFSR.

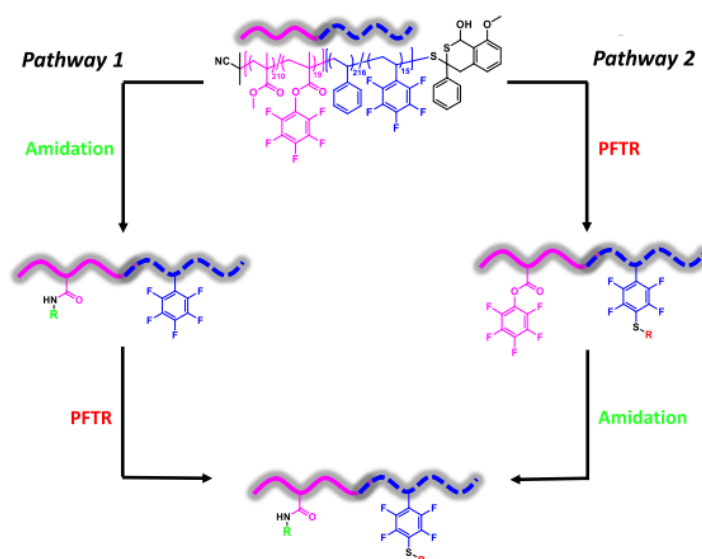
Thiols, as the strongest nucleophiles, can undergo thiol-ene and thiol-yne radical additions, Michael addition beyond *para*-fluoro thiol reaction. The chemoselectivity and orthogonality of *para*-fluoro thiol reaction have been studied by some researchers.^{24,49} In particular, Turgut *et al.*⁴⁹ assessed the chemoselectivity of two thiol-based modular ligations operating under mild conditions in terms of thiol-ene addition and *para*-fluoro thiol reaction (Scheme 1-17).



Scheme 1-17 Competition between thiol-ene addition and PFSR.⁴⁹

The authors developed a one-pot procedure to modify the scaffolds with two distinct thiols by tuning the amount of thiol that used in the thiol-ene step and delayed addition of a base to trigger the PFSR in the second step.

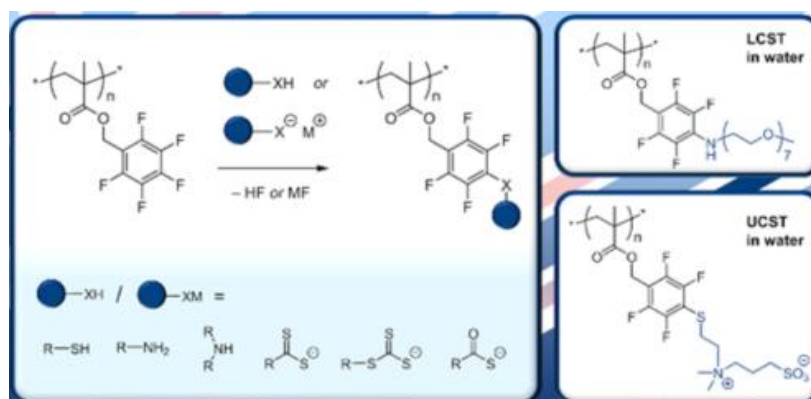
Delaittre *et al.*²⁴ prepared a dual reactive block copolymer poly(methyl methacrylate-co-pentafluorophenylmethacrylate)-b-poly(styrene-co-pentafluorostyrene)(P(MMA-r-PFPMA)-b-P(S-r-PFS)) by RAFT polymerization. The authors established experimental conditions to perform orthogonal amidation on the pentafluorophenyl ester and *para*-fluoro thiol reaction (PFTR) on the PFS, respectively (Scheme 1-18).



Scheme 1-18 Orthogonal amidation and PFTR between two different functional PFP-based groups on the same block copolymer.²⁴

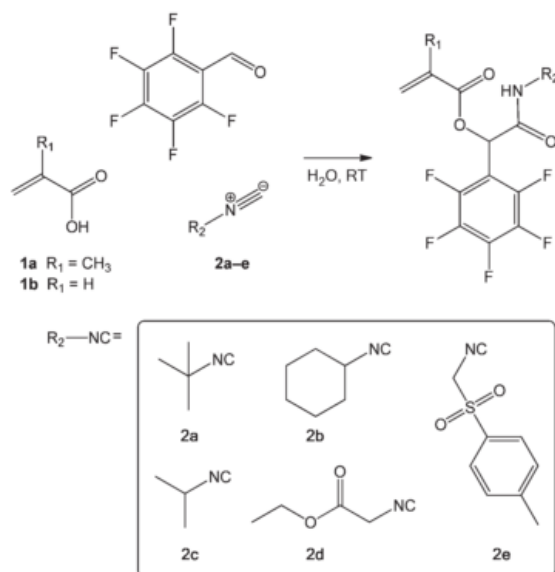
To prove the versatility of both reactions, amidation and PFTR were performed with functional amines and thiols, respectively. Pathway 1, where amidation was performed on PFPMA units followed by PFTR on PFS units, proved to be a successful route, while Pathway 2 (PFTR, then amidation) cannot be achieved owing to the reactivity of multiple fluorine atoms of the PFPMA motif towards thiols (Scheme 1-18).

Some unconventional polymers with PFP group as side groups have appeared in the form of poly(2,3,4,5,6-pentafluorobenzyl methacrylate) (pPFBMA) which reactivity towards FSR were reported by Noy and coworkers.^{36,37} They synthesized pPFBMA homopolymers with degrees of polymerization from 28 to 132 and $\bar{D} \leq 1.29$ by the RAFT process and systemically studied the post-polymerization modification of pPFBMA with amines, thiols and sulfur based nucleophiles (Scheme 1-19).³⁶



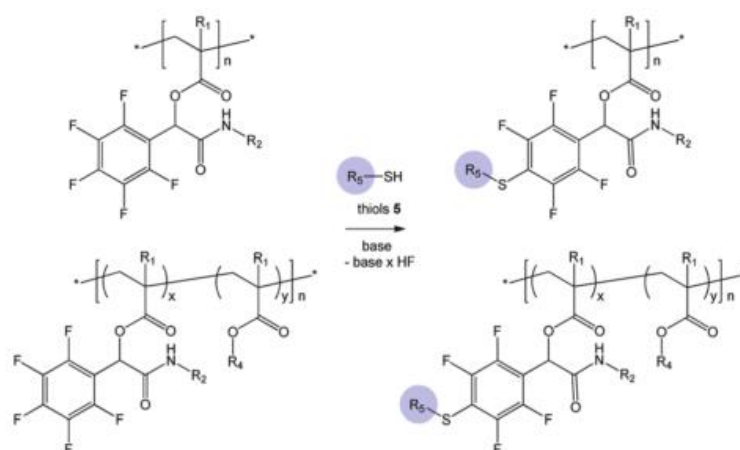
Scheme 1-19 PFSR of pPFBMA with the thiols, amines and sulfur-based nucleophiles.³⁶

PFSR with different (thio)-carbonylthio reagents were achieved and allowed for subsequent one-pot cleavage of dithioester pendent groups with concurrent thio-Michael side group modification. It was demonstrated the versatility of this reactive platform through the synthesis of a pH-responsive polymers and novel thermoresponsive polymers. The authors expanded the scope of Passerini-made PFP-functional monomers to a total of six (meth)acrylate monomers prepared from (meth)acrylic acid, 2,3,4,5,6-pentafluorobenzaldehyde, and different isocyanides in a single step (Scheme 1-20).³⁷



Scheme 1-20 Multicomponent monomer synthesis in presence of employed isocyanide reagents.³⁷

The well-defined homo- and copolymers of these monomers were achieved by RAFT polymerization and then, the extremely efficient and quantitative post-modification (reaching completion in > 3–80 min) with a range of aromatic, glycosidic, and primary, secondary, and tertiary aliphatic thiols and in the absence of any observable side reactions, were highlighted (Scheme 1-21).

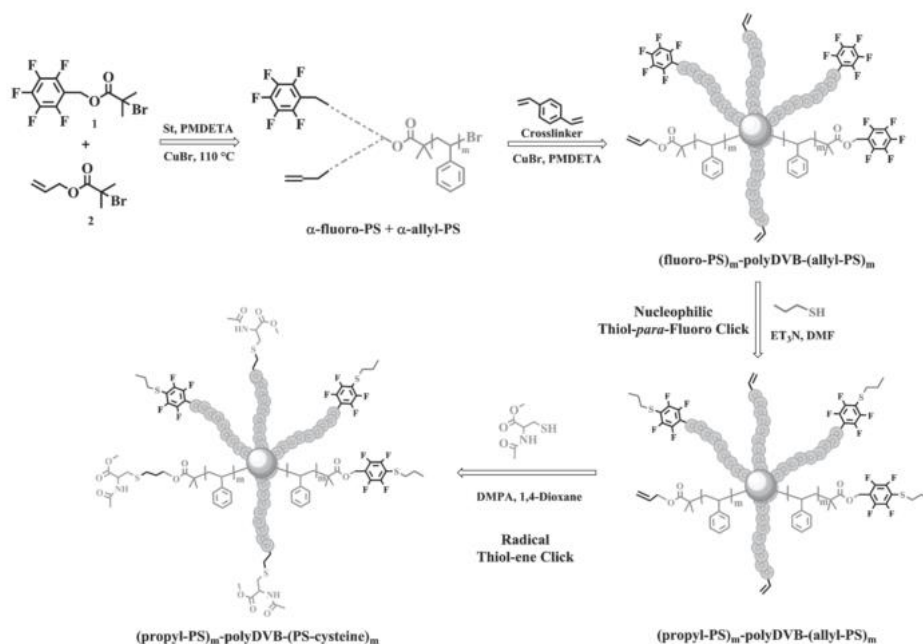


Scheme 1-21 PFSR on PFP-functional homo- and copolymers.³⁷

1.1.5.2.2 Polymers with PFP groups at chain-ends

A few examples have dealt with the end-group functionalization of polymer chains by using PFSR.^{38,39} For example, Cakir *et al.*³⁸ described the post

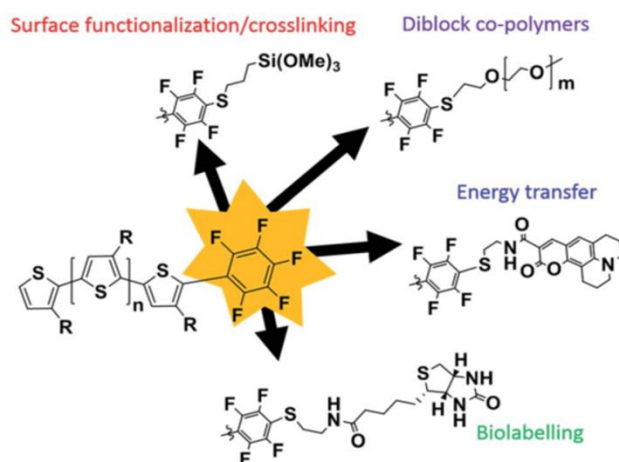
functionalization of multiarm polystyrene (PS) with PFP and allyl moieties at the periphery (Scheme 1-22).



Scheme 1-22 General synthetic strategy to heterofunctionalized multiarm polymers.³⁸

First, α -fluoro and α -allyl functionalized PS (α -fluoro-PS and α -allyl-PS) were in situ prepared by ATRP of styrene and then, the obtained polymers were crosslinked by using divinyl benzene (DVB) yielding $(\text{fluoro-PS})_m\text{-polyDVB-(allyl-PS)}_m$ multiarm star polymers. The end groups of the obtained polymers were modified by employing the thiol-*para*-fluoro and thiol-ene “click” reactions with 1-propanethiol and N-acetyl-L-cysteine methyl ester, respectively. Heterofunctionalized multiarm star polymers with higher molecular weight and narrow molecular weight distribution were obtained.

Polythiophenes have found many applications in organic electronics and their end-group functionalization allow for the integration of a wide variety of functional groups onto the polythiophene chains. Bouffle *et al.*³⁹ incorporated the PFP as a single end-group in poly(3-octyl)thiophene (P3OT) polymer chains by an optimized in situ quenching procedure. PFSR can occur on the PFP-end-capped P3OT with common nucleophiles such as thiols, amines, and alcohols, all under mild conditions and quantitative yield. To further highlight the utility of this approach, several sensitive functional groups were incorporated onto the polymer end-group (Scheme 1-23).



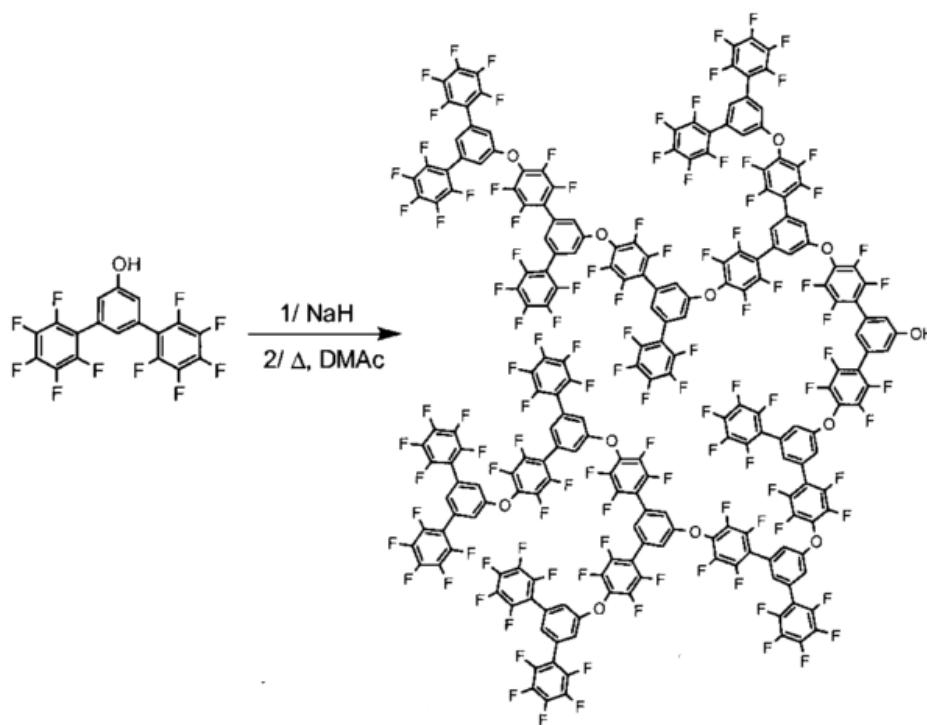
Scheme 1-23 Post-modification of PFP encapped P3OT. ³⁹

For example, biotin was tethered to the mono-functionalized polymer via a thiol linker provide one way for further biomarkers. Polythiophenes can also find application in energy transfer after incorporated thiol-functionalized dye; or surface modification after modified by 3-MPTS; or prepare block copolymers with thiol-end capped PEG macromolecular.

1.1.5.3 Polymerization through PFSR

With high efficiency and technical simplicity of PFSR, several kinds of monomer or macromonomers were introduced into hyperbranched or cross-linked fluorinated polymers via PFSR.

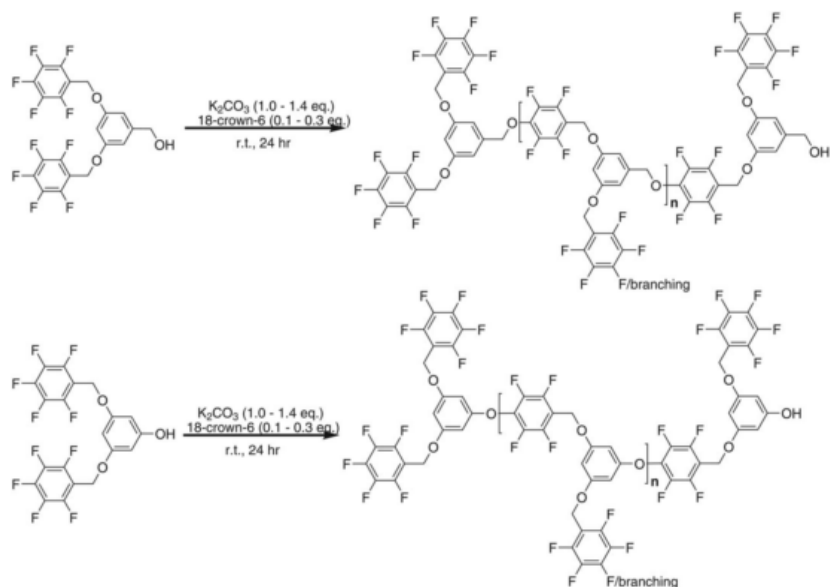
Pitois *et al.*⁵ described the application of hyperbranched fluorinated polymers (HBFP) in the field of optical waveguide. These HBFP were obtained by a one-step polymerization of the AB₂ monomer, 3,5-dipentafluorophenyl-1-(hydroxyl)benzene (Table 1-1, S8) in DMAc with NaH as base (Scheme 1-24).



Scheme 1-24 Polymerization of AB₂ monomer to prepare HBFP.⁵

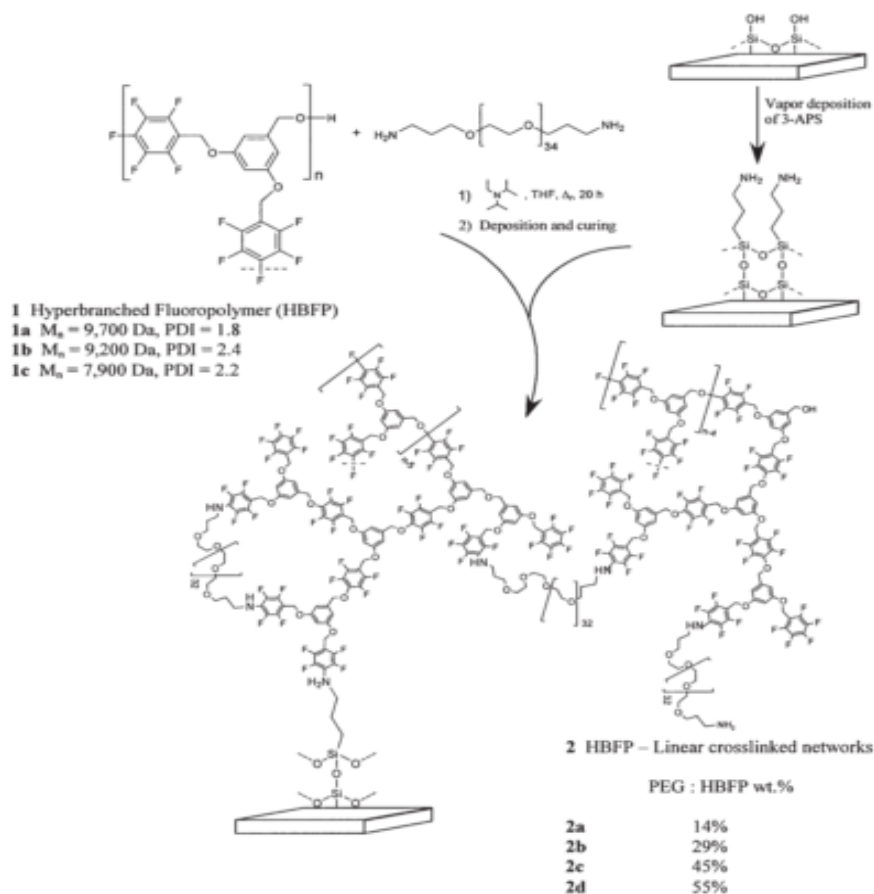
The obtained polymer exhibits a molecular weight of 25100 g/mol with a glass transition temperature of 140 °C. For ease of processing and good long-term mechanical properties, the HBFP was functionalized with 2,3,5,6-tetrafluoro-4-hydroxystyrene (TFSOH, Table 1-2, A15) via PFSR and crosslinked by a photolithographic procedure. Aliphatic fluorinated groups (Table 1-2, A5) was tailored by modifying the functional end PFP groups at the periphery to decrease the refractive index of HBFP. With the same strategy, Quast *et al.*⁴¹ prepared HBFP from the polycondensation of AB₂ monomers, 3,5-bis[(pentafluorobenzyl)oxy]benzyl alcohol and 3,5-bis[(pentafluorobenzyl)-oxy]phenol in presence of potassium carbonate as base, and a 18-crown-6 phase transfer agent (Scheme 1-25).

The authors optimized the regioselectivity of the polymerization and found that the reaction was temperature dependent. The resulting optimization was used to control substitution of oxygen-bearing nucleophiles along nonactivated fluoroaryl system in high yield with the formation of crosslinked tetrafluorinated aryl ethers.



Scheme 1-25 Synthesis of HBFP-bearing benzyl alcohol and phenol nucleophiles.⁴¹

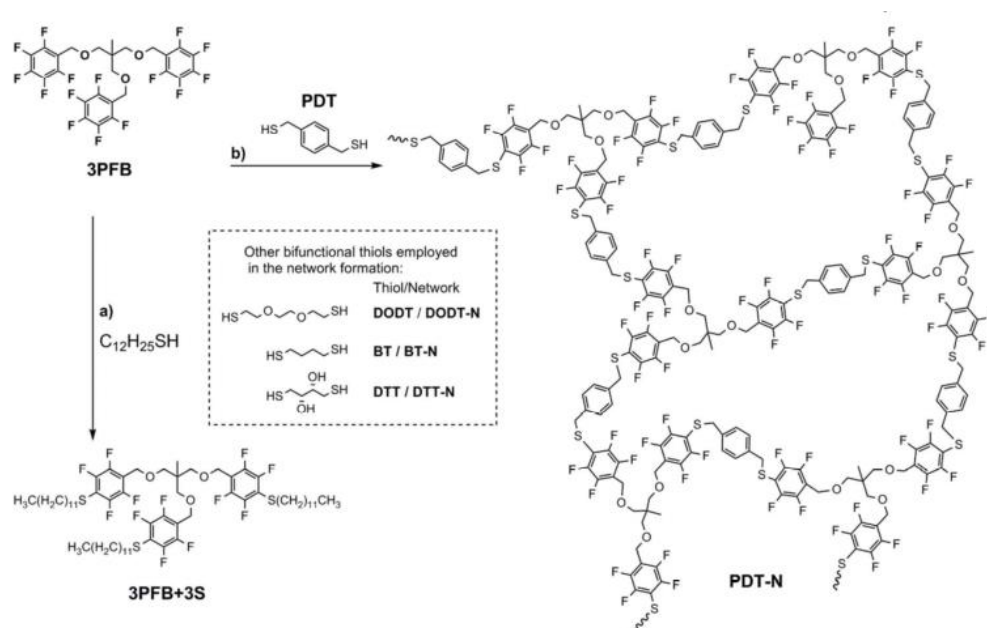
Gudipati *et al.*⁴⁴ synthesized HBFP with 3,5-bis[(pentafluorobenzyl)oxy]benzyl alcohol (Scheme 1-26).



Scheme 1-26 Preparation of the crosslinked HBFP-PEG networks and the covalent attachment of the coatings to 3-APS-functionalized glass microscope slide.⁴⁴

Glass substrates functionalized with 3-aminopropyltriethoxysilane (3-APS) were reacted with PFP end groups of the HBFP (Scheme 1-26). The intramolecular or intermolecular crosslinking of the HBFP occurred via the PFSR with a α,ω -diamino-terminated poly(ethylene glycol) (PEG) amine. The degree of crosslinking, compositions, topographies, and morphologies were changed by varying the PEG/HBFP stoichiometry, leading to polymer coatings with different features of differing hydrophilicity, mobility, and topography.

In addition, Cavalli *et al.*⁴² selected few model compounds, including 1,4-butanedithiol (BT), 3,6-dioxa-1,8-octanedithiol (DODT), dithiothreitol (DTT) and 1,4-phenylenedimethanethiol (PDT) to react with a stable fluorinated linker A₃ monomer (3PFB) (Scheme 1-27).



Scheme 1-27 Representation of the A₃ monomer 3PFB linker, (a) investigation of the regioselective behavior of PFSR employing dodecanthiol, (b) network formation using PDT. In the box, the other bifunctional thiols employed for network formation are depicted.⁴²

T_g of the analyzed networks varied in the order of PDT-N (54.7 °C) > DTT-N (50.2 °C) > DODT-N (40.2 °C) > BT-N (38.0 °C).

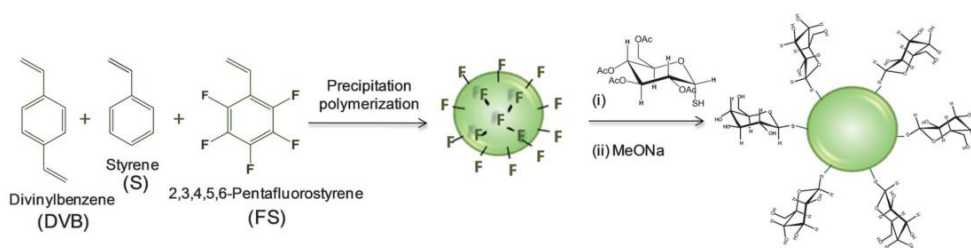
1.1.5.4 Surface modification by PFSR

Fluorinated polymers have attracted wide interest in modification and

functionalization of surfaces due to their low surface energy, low wettability and the possibility to incorporate different kinds of functional groups in the PFP groups via PFSR. The substrates involved in PFSR include polymeric microparticles, membranes, films as well as inorganic particles.

1.1.5.4.1 Polymeric microparticles

One of the interests in designing and preparing cross-linked microparticles is the control of the surface functionalization that dictates the interactions between the substrate and the environment. Alvarez-Paino *et al.*²¹ described the preparation of cross-linked polymeric micrometer sized particles of styrene and pentafluorostyrene functionalized with carbohydrate moieties (Scheme 1-28).



Scheme 1-28 Surface modification of glycosylated cross-linked microparticles by PFSR.²¹

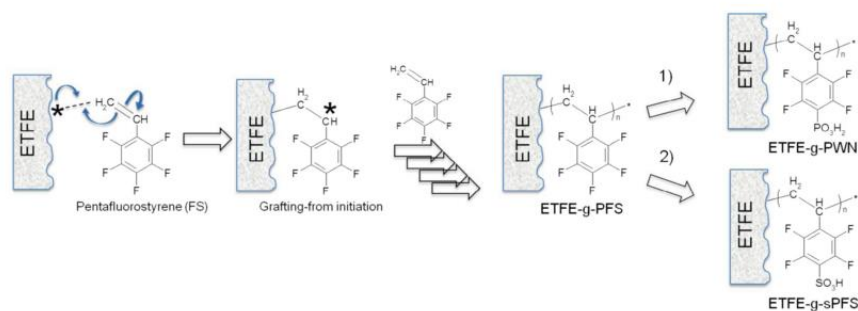
The particles were synthesized via precipitation polymerization consisting in the radical copolymerization of pentafluorostyrene, styrene and divinylbenzene. Then, the acetate-protected carbohydrate moieties were attached to the particles based on the PFSR of acetylated β -D-thioglucopyranose onto PPFS block, followed by the deprotection of the acetate-protected thioglucose. These microparticles were able to retain specifically Concanavalin due to the presence of carbohydrates glycopolymers that can induce strong interactions with lectins by the multivalent effect of densely packed carbohydrates on the polymer chains, termed as “glycocluster effect”.^{61,22}

1.1.5.4.2 Membranes or dense polymer materials

The fluorinated polymers have low surface energy leads to the corresponding materials are more suitable for manufacturing membranes or thin films. The design

and preparation of polymer membranes based on PFSR reaction with desired properties have drawn great attention in particular for the preparation of polyelectrolyte membranes.^{62,63,64,65}

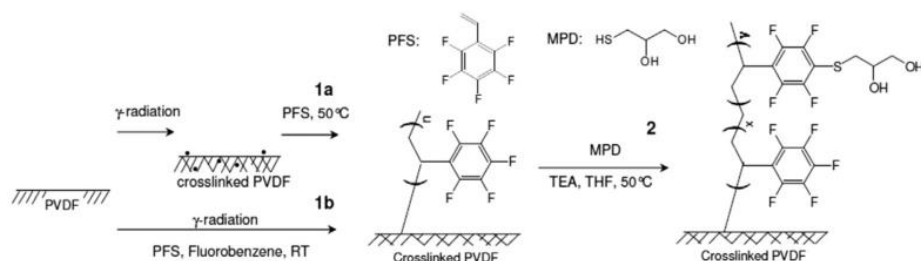
Atanasov *et al.*⁵⁴ reported on the preparation of polyelectrolyte membranes with enhanced proton conductivity in two steps (Scheme 1-29).



Scheme 1-29 Grafting of PPFS from irradiated ETFE film and post-sulfonation and phosphonation of PPFS.⁵⁴

PPFS chains were grafted from an irradiated ethylene tetrafluoroethylene (ETFE) films, followed by post-functionalization to introduce sulfonic groups or phosphoric groups. The degree of substitution was 44 % for the sulfonation and 62 % for the phosphonation. The sulfonated film showed a higher conductivity than the phosphated film due to a higher acidity. Inspired from this work, Dimitrov *et al.*^{62,63} developed a new polyelectrolyte membranes based on polysulfone (PSU) grafted with phosphonated poly(pentafluorostyrene) (PPFS). Shao *et al.*⁶⁴ prepared an ionic ABA triblock copolymers which have a central PSU block and poly(2,3,5,6,-tetrafluorostyrene-4-phosphonic acid) (PTFSPA) outer blocks with different lengths. These routes open the possibility to tune copolymers' hydrophilic–hydrophobic balance to obtain membranes with an optimal balance between proton conductivity and mechanical properties for potential fuel cell applications.

Dumas *et al.*⁵¹ described a strategy combining PFS grafting and PFSR to tune the surface wettability of bulky poly(vinylidene fluoride) (PVDF). First, PFS was radiation-induced grafted on the surface of PVDF using γ -rays as the radiation source in two ways (Scheme 1-30, 1a and 1b).

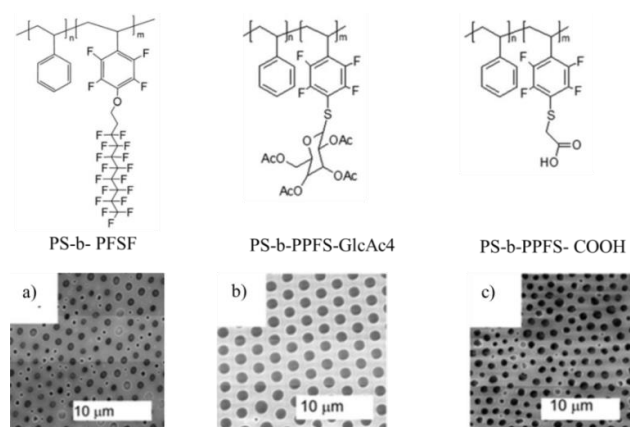


Scheme 1-30 Radiation-induced grafting of PFS onto PVDF (1) and subsequent modification of the grafted PPFS (2).⁵¹

Subsequent PFSR was undertaken using 3-mercaptopropanediol (MPD). The chemoselective functionalization was qualitatively and semi-quantitatively evidenced by FT-IR in ATR mode and led to PVDF-g-PPFS decorated with hydroxyl groups. The corresponding surfaces exhibited an enhanced affinity with polar probes such as water or acetonitrile as reflected by wettability measurements.

1.1.5.4.3 Films

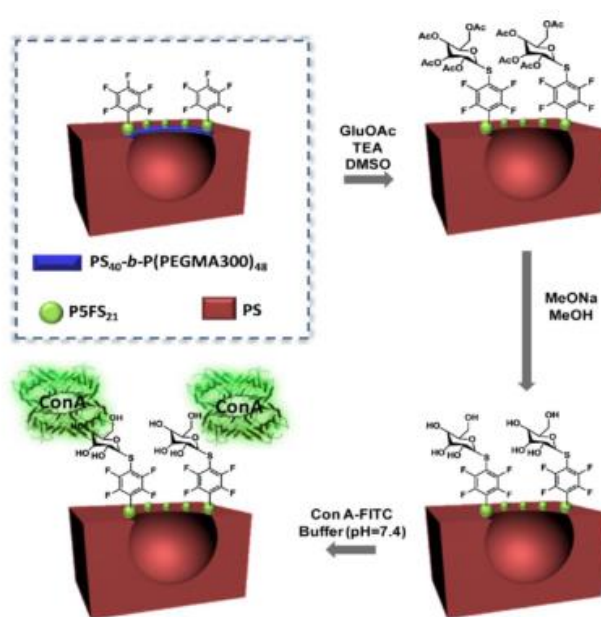
Semifluorinated polymer films often exhibit low surface energy due to the surface enrichment of fluorinated units and thus exhibit hydrophobicity and oleophobicity.¹⁴ This behavior can be enhanced by increasing the surface roughness, for example by introducing pores on the film surface. Valtola *et al.*²⁵ prepared breath figure (BF) films based on semifluorinated diblock copolymers (PS-*b*-PPFS) (Scheme 1-31).



Scheme 1-31 Semifluorinated polymers and the morphology of BF films, a) PS-*b*-PPFS; b) PS-*b*-PPFS-GlcAc4; c) PS-*b*-PPFS-COOH.²⁵

The modification of the PPFS block was performed with fluorinated alkyl alcohol (a), 2,3,4,6-tetra-O-acetyl-1-thio- β -D-glucopyranose (SH-GlcAc4) (b) and thioglycolic acid (c) via PFSR. The structure of the polymer alters the obtained porous morphology of the films. By measuring water contact angles, it was found that porous BF films are hydrophobic and the hydrophobicity was enhanced compared to solvent cast films, as expected. The contact angle of dodecane in the hydrophobic porous films has also increased significantly. For the deprotected glucose-modified film, the surface becomes hydrophilic with a water contact angle below 90° .

Rodríguez-Hernández *et al.*^{29,30} combined breath figures method with phase separation process to prepare multifunctional micropatterned films which is composed of PS and PS-*b*-PPFS (Scheme 1-32).



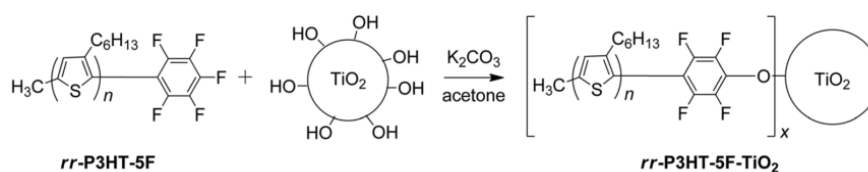
Scheme 1-32 The approach employed to incorporate glucose moieties and subsequently, Con A onto the micro structured films.³⁰

It was demonstrated that the diblock copolymers are homogeneously distributed along the whole surface of the films due to the reorientation towards the solution/air interface. The obtained porous films have a wetting behavior that can be described by the Cassie state equations.²⁹ Thiolated glucose molecules were specifically attached to the PPFS domains via PFSR. Subsequently, the specific lectin (Concanavalin A, *Canavalia ensiformis*) was attached to the surface by conjugation with the glucose

moieties.

1.1.5.4.4 Inorganic particles

PFSR was also found applications in the modification of inorganic particles to prepare organic-inorganic hybrid particles. In order to sensitization of TiO₂ nanoparticles and electrodes with organic semiconducting dyes polymeric chains, the desired organic dye moieties were grafted onto the surface of TiO₂ via PFSR (Scheme 1-33).⁴⁰



Scheme 1-33 Surface modification of TiO₂ NPs via PFSR.⁴⁰

A conjugated polymers, 2-perfluorophenyl terminated regioregular poly(3-hexylthiophene) (P3HT-5F), was synthesized firstly and then, it was reacted with hydroxyl groups of TiO₂ via PFSR. From the TGA diagrams, a 13% functionalization of TiO₂ nanoparticles with P3HT-5F was calculated. The formation of non-hydrolysable Ti-O-C bond is more stable than the ester bonds formed after typical reactions with carboxylic end-group molecules, leading to the obtained poly(thiophene)-sensitized TiO₂ photoanodes exhibit good stability after water and alkaline solution treatment.

1.1.6 Conclusion

One of the targets in the field of polymer chemistry is to develop materials with specific properties and high value applications. As such, the demand for highly efficient, chemo and regioselective of *para*-fluoro substitution reaction (PFSR) that yield high purity, readily accessible products is significant. Here, the development of PFSR between pentafluorophenyl (PFP) groups containing polymers and various nucleophiles in the past decades was reviewed. The substrates involved in PFSR

include monomers, polymers, side groups and end groups. Uniquely and depending specifically on the experimental conditions and methodology employed, the PFP groups are capable of participating in PFSR with a vast range of nucleophiles which mainly include alcohols, amines and thiols. The strategies for employing this reaction in the design and preparation of homo-, co-, hyperbranched- and crosslinked polymers and the functionalization of various substrates were also described.

1.2 Fluorinated polymers in nanocomposite films with superhydrophobic properties

Surface wettability is one of the most important phenomena of solid surface. It not only directly affects the life activities of animal and plant species, but also plays an important role in the daily life of industrial goods and agricultural production. Since the appearance of Young's equation in 1805,⁶⁶ great attention has been allocated on wetting and wettability. In nature, many organisms have gradually developed superior anti-wetting properties to survive in harsh environments. Inspiration from these organisms is a good approach to prepare materials that contain parts with super water repellent materials and provides an alternative way to uncover the mechanisms of their excellent performance.

As the pioneering work dealing with water-repellency, Barthlott and Neinhuis carried out a systematic study in plants and highlighted the water-repellency and self-cleaning behavior of lotus leaf.^{67,68} Figure 1-1 shows both the photography (a) and the SEM image (b) of a lotus leaf.

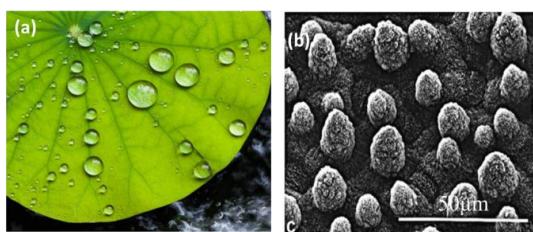
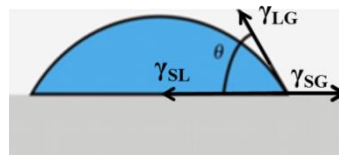


Figure 1-1 (a) Photography and (b) SEM image of lotus leaf.^{67,68}

The SEM image shows that lotus leaf presents a two-scale structure: one around 10 μm (rough structure) and the other one around 100 nm (fine structure). In addition to the hierarchical structure, hydrophobic wax exists on the surface. The super water-repellent property of lotus leaf benefits from both the hierarchical structures and the hydrophobic wax.

1.2.1 Definition of superhydrophobic surfaces

The wettability can be quantified expressed by the water contact angle (WCA) of a droplet deposited onto a solid surface. As shown in Scheme 1-34, WCA is linked to the surface tension of a water droplet on the equilibrium point of solid, liquid and gas phases.



Scheme 1-34 Illustration of a stable water droplet on a hydrophilic surface.

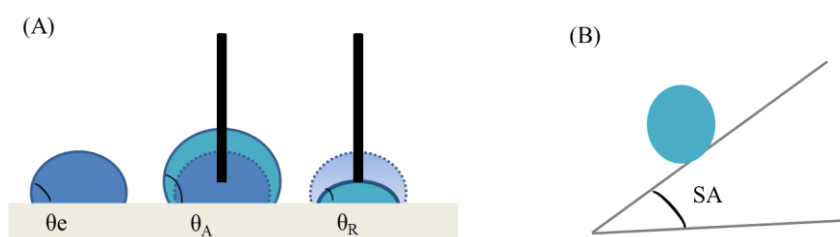
θ represents the contact angle of a drop on an ideal rigid, homogeneous, flat and inert surface. γ_{SG} , γ_{SL} and γ_{LG} refer to the interfacial surface tension between solid and gas, between solid and liquid and between liquid and gas, respectively. It can be determined by using the Youngs' equation (Equation 1-1):⁶⁶

$$\cos \theta = (\gamma_{SG} - \gamma_{SL}) / \gamma_{LG} \quad (\text{Equation 1-1})$$

When water is used as the probe liquid, the surface is totally wet when γ_{SG} is large enough or γ_{LG} is small enough, which gives a WCA of 0° ; when $\gamma_{SG} > \gamma_{SL}$, $0^\circ < \text{WCA} < 90^\circ$, the surface is hydrophilic; when $\gamma_{SG} < \gamma_{SL}$, $\text{WCA} > 90^\circ$, the surface is hydrophobic and the contact area between the solid and the deposited liquid decreases. A surface with a static WCA greater than 150° is called superhydrophobic surface. However, static WCA is not sufficient to reflect the real wetting state of a

droplet on a superhydrophobic surface so that the contact angle hysteresis has to be considered.

The water contact angle hysteresis ($\Delta\theta$) is defined as the difference between the advancing water contact angle (θ_A) and the receding water contact angle (θ_R) ($\Delta\theta = \theta_A - \theta_R$).⁶⁹ As shown in Scheme 1-35-A, a liquid drop at the equilibrium state on the solid surface has a static WCA (θ_e), after adding a small enough amount of liquid in the droplet, the contact line of the droplet will still be pinned, and the contact angle will increase to maximum which is defined as advancing angle (θ_A); when removing a small enough amount of liquid from the droplet, the contact line will still be pinned, and the contact angle will decrease to lead to the receding contact angle (θ_R).



Scheme 1-35 Representation of the measurement of hysteresis contact angle (A) (θ_e : static contact angle; θ_A : advancing contact angle; θ_R : receding contact angle) and sliding angle (SA) (B).⁷⁰

The hysteresis of a droplet on the surface can also be reflected by the sliding angle (SA) (Scheme 1-35-B) which is defined as the critical inclination angle of the droplet placed on the surface when the solid surface is slowly tilted under the action of gravity.⁷¹

The larger the hysteresis is, the more water drops will stick to the surface. For surface having a static WCA greater than 150° combine to a low water hysteresis angle (typically $< 10^\circ$), water droplets will roll off to form a self-cleaning surface, which is called as the “Lotus” effect.⁶⁸ However, it was found that a high WCA ($> 150^\circ$) can coexist with strong adhesion between water and a solid surface with a high water hysteresis angle ($> 10^\circ$) in the case of the so-called “rose petal” effect.⁷² Rough surfaces with hierarchical structure are built of micro- and nanoscale roughness, so that

a composite interface can exist at the microscale, while a homogeneous interface can exist at the nanoscale or vice versa.^{73,74}

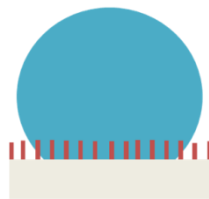
The understanding of the wetting of rough surfaces is important for designing superhydrophobic surfaces with various potential applications. The effect of the surface roughness on the wettability, in particular on the apparent contact angle of a droplet, has been modeled by Wenzel⁷⁵ and Cassie-Baxter.⁷⁶

1.2.1.1 Wenzel model

Young's equation cannot be exploited to explain the real wettability of a droplet on a rough surface with hierarchical structure. Hence, Wenzel⁷⁵ developed a model to reflect the impact of roughness on wettability. In this model, the contact angle of a droplet on rough surface can be calculated by Equation 1-2,

$$\cos \theta^w = r \cdot \cos \theta \quad (\text{Equation 1-2})$$

θ^w and θ stand for the apparent contact angle in Wenzel's state and the static contact angle of a smooth surface, respectively; r represents the roughness factor and is defined as the ratio of the actual contact area over the apparent surface area of the substrate. Scheme 1-36 shows a water droplet in Wenzel state on a rough surface which contains many micro- or (and) nano-asperities.



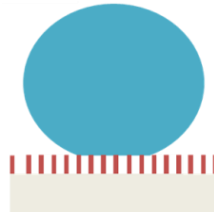
Scheme 1-36 A droplet in “Wenzel” state.

The water droplet can penetrate into the asperities and complete contact with the solid surface. The actual contact area is larger than apparent area, which makes the value of r always larger than 1 ($r > 1$). So that, Wenzel's model predicts that roughness will enhance hydrophobicity if $\theta > 90^\circ$; the roughness will enhance hydrophilicity as well if $\theta < 90^\circ$. The droplet in Wenzel's state has a strong adhesion

and is stick to the solid surface, leading to a high contact angle hysteresis ($> 10^\circ$).

1.2.1.2 Cassie-Baxter model

With the decrease of contact angle hysteresis, the droplet switches from Wenzel to the Cassie-Baxter state because of the increased air fraction between the droplet and the solid surface. As shown in Scheme 1-37, the water droplet is suspended on the top of the asperities of the solid surface, which is described as a composite state.⁷⁷



Scheme 1-37 A droplet in “Cassie-Baxter” state.

Cassie and Baxter⁷⁶ introduced the concept of a phase area fraction (f) in order to quantitatively consider the effect of surface heterogeneity (Equation 1-3):

$$\cos \theta^{CB} = f(1 + \cos \theta) - 1 \quad (\text{Equation 1-3})$$

θ^{CB} is the apparent contact angle of a droplet in Cassie-Baxter state; θ is the static contact angle of a smooth surface; f is the fraction of surface present at the top of the surface protrusions with a value < 1 . For a hydrophobic surface, the smaller the f is, the greater the apparent contact angle (θ^{CB}) is. When f is infinitely close to 1, the droplet is suspended onto the top of protrusions and air is trapped into the protrusions. A droplet in the Cassie-Baxter regime shows significantly lower water hysteresis compared to a droplet in Wenzel regime due to the low resistance from the air pockets in which water droplet can be easily rolled off, leading to a self-cleaning surface.

1.2.2 Polymer-based superhydrophobic surfaces

The super water-repellent ability of various materials has shown many applications such as anti-icing, water-oil separation, water corrosion in electrical industry, water proof textiles, controlled transportation of fluids.⁷⁷⁻⁸⁰ With the

development of fundamental research on basic principle of superhydrophobic surfaces, the fabrication methods have been continually optimized.^{8,9,77,79,82, 83}

1.2.2.1 The main approaches involving polymers

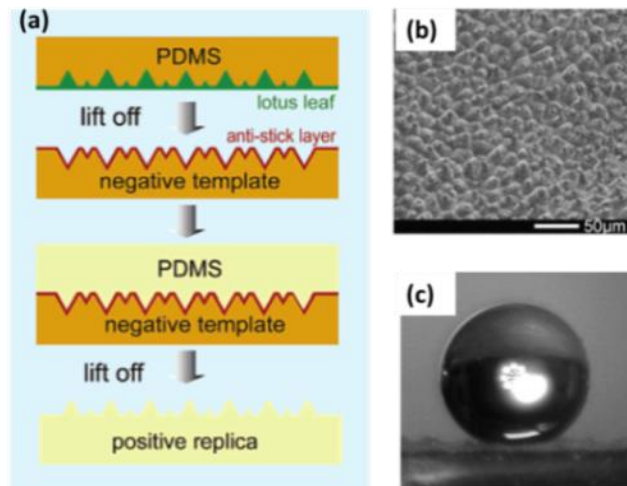
Li *et al.*⁷⁷ classified the strategies according to two directions: top-down and bottom-up approaches. Very recently, Wen *et al.*⁸² comprehensively reported on the recent advances in dealing with the fabrication of superhydrophobic surfaces and they divided the methods in three main groups: the coating method, the deposition method, and the template method. Both of them systematically overviewed various physical and chemical methods and materials from inorganic to organic compounds for the preparation of superhydrophobic surfaces. Herein, we simply summarized the methods that allow for the preparation of superhydrophobic surfaces including hydrophobic polymers. The strategies involve: (1) the introduction of a rough structure onto the surface of hydrophobic polymer materials or (2) the modification of a rough surface by using hydrophobic polymer materials or (3) the combination of a rough structure with hydrophobic polymer materials in the same procedure. Few examples are presented in Table 1-10.

Table 1-10 Examples of superhydrophobic surfaces by using hydrophobic polymers.

Strategy	Method	Material	WCA (°)	$\Delta\theta_{H_2O}$ (°)	ref
Introduce hierarchical structure to hydrophobic polymer film	Templated	PDMS	160	< 2	84
	Colloidal assemblies	PS+CaCO ₃	156	—	85
	Electrospinning	PPFS	170	< 2	87
	Phase separation	PP-PMMA	160	9	86
First, produce hierarchical structure; Second, reduce surface free energy	Plasma treatment + Plasma enhanced chemical vapor deposition	PET	150°	—	88
	Plasma treatment	LDPE	170	< 5	89
	Lithography + chemical modification	PETPTA	150	< 5	90
Combine hierarchical structure and low free energy polymer	Layer by layer	clay+PFPVP	168	13	56
	Spray coating	silica+PDMS	150	—	91
	Spin coating	silica+ PU	170	< 3	93

poly(dimethylsiloxane) (PDMS); polystyrene (PS); poly(pentafluorostyrene) (PPFS); poly(ethylene terephthalate)(PET); Low-density polyethylene (LDPE); poly(trimethylolpropane ethoxylate triacrylate) (PETPTA); polypropylene-poly(methyl methacrylate) (PP-PMMA); polyurethane (PU).

One method to create hierarchical structures on hydrophobic polymer consists in using a template. For example, Sun *et al.*⁸⁴ duplicated a rough surface as negative template from lotus leaf with PDMS which has an intrinsic WCA around 105° (Scheme 1-38).



Scheme 1-38 (a) Creation of a superhydrophobic surface via templated method; (b) and (c) are SEM and WCA images of the positive replica.⁸⁴

The SEM image of the positive replica shows the same surface morphology of papillate hills of the lotus leaf (Scheme 1-38-b). The WCA on the positive replica is 160° (Scheme 1-38-c) with a $\Delta\theta_{H_2O}$ lower than 2° .

With the same idea of introducing multi-scale structures onto hydrophobic polymers, Zhang *et al.*⁸⁵ employed the colloidal assembly method to prepare a superhydrophobic surface with a WCA of 156° . The hydrophilicity difference between silicon wafers and CaCO_3 -loaded hydrogel spheres leads to a selective localization of polystyrene spheres which produced irregular binary structures (Figure 1-2-A).

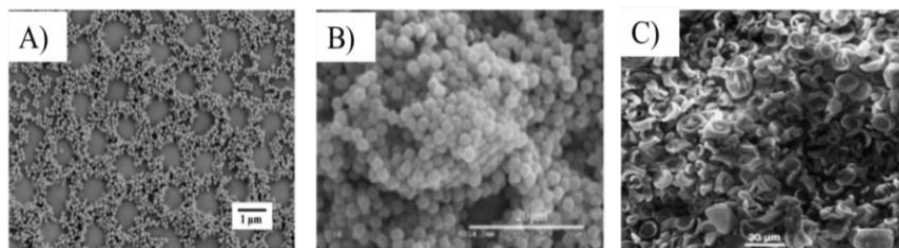
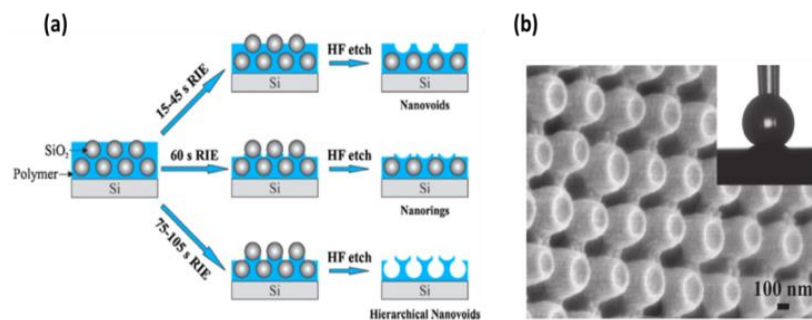


Figure 1-2 SEM images of superhydrophobic surfaces: (A) CaCO_3 -loaded hydrogel sphere with selective localization of PS;⁸⁵ (B) Aggregate spheres of micelles with PP as core and PMMA as shell via phase separation;⁸⁶ (c) electrospinning surface of PPFS.⁸⁷

Xie *et al.*⁸⁶ used the phase separation method to prepare a superhydrophobic surface based on polypropylene-*b*-poly(methyl methacrylate) (PP-*b*-PMMA) block

copolymer. In their study, PP-b-PMMA was dissolved in a selective solvent of DMF to form micelles with an insoluble core of PP chains and a soluble shell of PMMA. After casting this solution onto a glass substrate, the authors obtained a surface composed of aggregated spheres (Figure 1-2-B) formed from phase separation. The resulting WCA is 160° and $\Delta\theta_{H_2O} < 9^\circ$. Moreover, Agarwal *et al.*⁸⁷ reported the electrospinning of fluorinated homopolymers and copolymers of PPFs which produced a superhydrophobic surface (Figure 1-2-C) with a WCA of 170° and $\Delta\theta_{H_2O}$ near 0° .

Another way of preparing superhydrophobic surface is to introduce non-polar groups onto fine structures to reduce the surface free energy. For example, Kothary *et al.*⁸⁸ prepared a superhydrophobic surface of poly(trimethylolpropane ethoxylate triacrylate) (PETPTA) via lithography method (Scheme 1-39).



Scheme 1-39 (a) Illustration of the colloidal templating processes for fabricating periodic arrays of polymer nanovoids, nanorings, and hierarchical nanovoids via lithography; (b) SEM and WCA images of hierarchical nanovoids.⁸⁸

Silica colloidal particles with a volume fraction of 20% were embedded in a PETPTA polymer matrix and self-assembled onto a silicon wafer by a scalable spin-coating technology, followed by RIE (reactive-ion etching) with different durations.⁸⁸ The unusual non-close-packed crystal structure combined with a thin polymer film separating the top and the bottom colloidal layers render great versatility in templating periodic nanostructures, including arrays of nanovoids, nanorings, and hierarchical nanovoids (Scheme 1-39-a). The resulting polymer nanostructures were then modified by fluorosilane (tridecafluoro-1,1,2,2-tetrahydrooctyl)-trichlorosilane

to reduce the surface energy. Superhydrophobic surface with a WCA $> 150^\circ$ and $\Delta\theta_{H_2O} < 5^\circ$ were achieved on hierarchical nanovoid arrays (Scheme 1-39-b).

In addition, Teshima *et al.*⁸⁹ reported on the fabrication of poly(ethylene terephthalate) (PET) substrate with ultra-water repellency via plasma treatment (Figure 1-3).

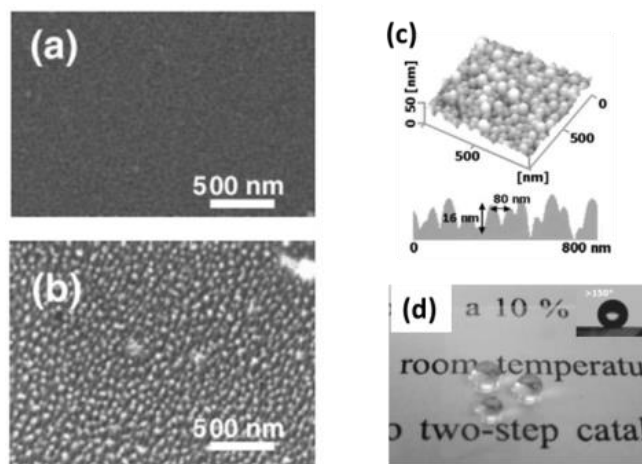


Figure 1-3 SEM images of the PET surfaces: (a) untreated; (b) treated with oxygen plasma; AFM 3D (c) and water droplet images of the PET surfaces treated with oxygen plasma.⁸⁹

First, PET was treated with oxygen plasma to introduce surface roughness. Subsequently, to reduce its surface energy, a hydrophobic layer coating was applied using plasma enhanced chemical vapor deposition (PECVD). The untreated PET surface is completely flat (Figure 1-3-a), while the treated one appears to be rough (Figure 1-3-b). The prominences are formed in an orderly manner on the PET surface. The hydrophobic layer was prepared on the nanotextured PET substrates by PECVD with tetramethylsilane. Protrusions that appeared on the nanotextured PET surface covered with the PECVD layers are smaller in height and much larger in diameter (Figure 1-3-c) than the untreated one.⁸⁹ The resulting surface is highly transparent and gives a WCA above 150° (Figure 1-3-d). Similarly, Fresnais *et al.*⁹⁰ prepared superhydrophobic surface of low-density polyethylene (LDPE) in two steps by using O_2 and CF_4 plasma treatment. The O_2 plasma allows for creating a variable roughness while CF_4 plasma emphasize this roughness and create the apolar layer, resulting in

the formation of a superhydrophobic surface with a WCA of 170° and $\Delta\theta_{H_2O}$ less than 5° .

There are many other methods that combine the roughness and the low free energy to prepare superhydrophobic surfaces. For example, Jisr *et al.*⁵⁶ prepared a superhydrophobic multilayered film by combining fluorinated polyelectrolytes and natural magnesium aluminium silicate clay via layer by layer sequential adsorption method (Figure 1-4).

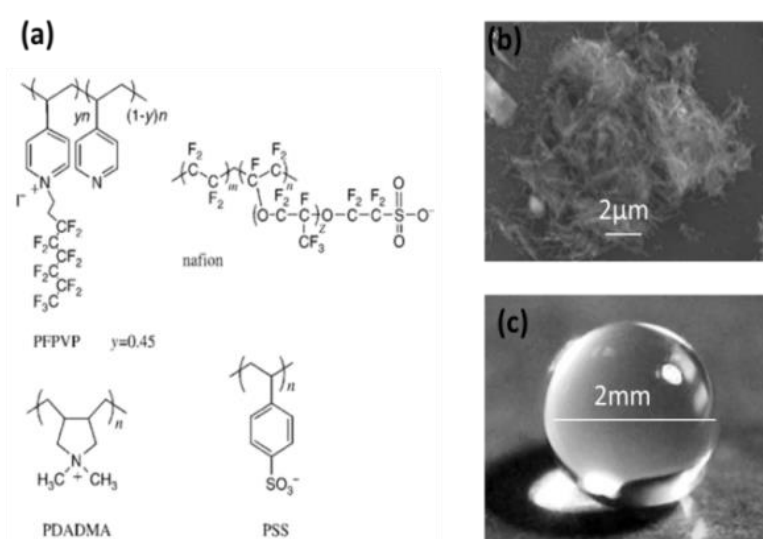


Figure 1-4 (a) Structures of the polyelectrolytes; (b) SEM image of the polyelectrolyte–clay superhydrophobic multilayer (PSS/PDADMA)₃(clay/PDADMA)₃-nafion/PFPVP)₄-PFPVP; (c) photo of a water droplet on its surface.⁵⁶

The structures of the used polyelectrolytes they used is shown in Figure 1-4-a. The SEM image (Figure 1-4-b) of the multilayer films shows that the surfaces have two scale structure, one is at the micrometer scale resulting from the disordered clay particles aggregates, the other one is the intrinsic nanometer dimensions of clay particles. A superhydrophobic surface with a WCA = 168° and $\Delta\theta_{H_2O} = 13^\circ$ was obtained (Figure 1-4-c).

Cao *et al.*⁹¹ studied the water-repellent and the self-cleaning properties of a silicone-based superhydrophobic (SUB) surface which was fabricated via dip-coating of a mixed solution composed of hydrophobic fumed silica (HFS) nanoparticles and

poly(dimethylsiloxane) (PDMS) (Figure 1-5).

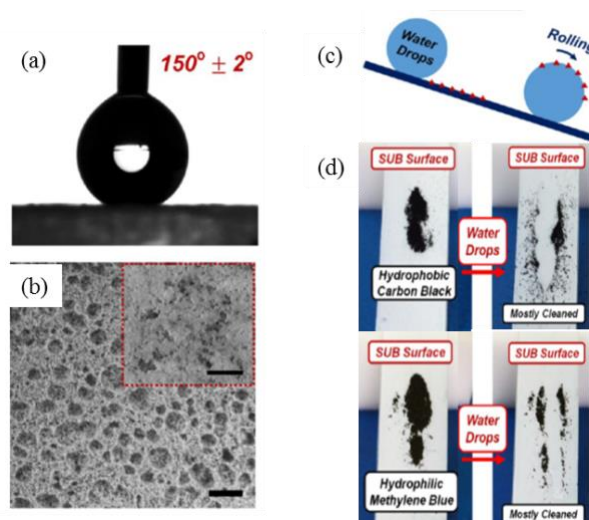


Figure 1-5 (a) Photo of a water droplet on the surface of SUB; (b) SEM image of the surface morphology exhibits the microstructure of the SUB surface. The inset image reveals the nanoscale roughness of the coating layer. (c) Schematic representation of a self-cleaning process. (d) Optical image of removing hydrophobic and hydrophilic dust.⁹¹

The coating layer with a weight ratio of PDMS/HFS = 1/1.25 exhibited a more reliable performance with a WCA of $150 \pm 2^\circ$ (Figure 1-5-a), and micro- and nano-scale structures (Figure 1-5-b). The authors investigated the self-cleaning ability of this superhydrophobic surface by using two kinds of dust compounds, carbon black and methylene blue (Figure 1-5-c). The hydrophobic carbon black dust tended to accumulate at the air/water interface to reduce the surface energy so that the rolling water droplet was able to pick up the hydrophobic dust without influence on its motion; while the hydrophilic methylene blue prone to be dissolved in water and then rolled/slid off the surfaces (Figure 1-5-d).

Moreover, spin- or spray-coating methods are widely used in fabricating superhydrophobic films by using nanofillers containing polymer matrix solution. For example, Basu *et al.*⁹² reported on the preparation of superhydrophobic PDMS/silica nanocomposite film with a WCA of $158\text{--}160^\circ$ via spray-coating method. Yilgor and co-workers⁹³ introduced rough structure into nanocomposite of polyurethane (PU)/silica via spin-coating, resulting in a superhydrophobic surface with a WCA of

170° and $\Delta\theta_{H_2O} < 3^\circ$.

In conclusion, wettability of a solid surface is governed by both the surface morphology and its chemical composition. The surface micro/nanostructuring combined with low surface energy of materials contributes to unexpected anti-wetting properties. People can get inspiration from natural materials to modify the surface morphology with specific structures or functionalize the surface with non-polar group to reduce the surface free energy. The most widely used way is to decrease the surface energy and increase the surface roughness by the same procedure. Among various low surface free energy materials, fluorinated polymers as matrix with associated (nano)fillers to render the surface rough is expected to be efficient for the preparation of superhydrophobic surfaces. This approach will be in detailed discussed in the following part.

1.2.2.2 Superhydrophobic nanocomposite films composed of fluorinated polymers and fillers

Fluorinated polymers, such as poly(tetrafluoroethylene) (PTFE),⁹⁴ PVDF and its copolymers, poly(vinylidene fluoride-co-hexafluoropropylene) (PVDF-co-PHFP)^{95,96} have been reported as excellent hydrophobic polymers thanks to the fluorinated alkyl are good candidates for lowering surface free energy.⁹⁷ In order to take benefit from the low surface free energy provided by such fluorinated polymers, various (nano)fillers, such as carbon nanotube, TiO₂, ZnO, clay, POSS and colloid or fumed silica were used as (nano)fillers to prepare superhydrophobic nanocomposite films. Here, few cases are presented to explain the effect of fillers on the surface structure and on the wettability of fluorinated polymer-based nanocomposites.

Carbon nanotube (CNT)/fluorinated polymer nanocomposites

Wang *et al.*⁹⁸ fabricated stable superhydrophobic coatings by spray-coating of an aqueous solution containing CNT and perfluoroalkoxy resin (Teflon[®] PFA) with various CNT/PFA weight ratios, ranging from 5 wt% to 30 wt%. CNTs were modified

by PAA firstly to disperse and stabilize CNTs in water and make the resulting CNT dispersion compatible with the PFA latex. Both the WCA and sliding angle were tuned simply by changing the CNT loading (Figure 1-6-A).

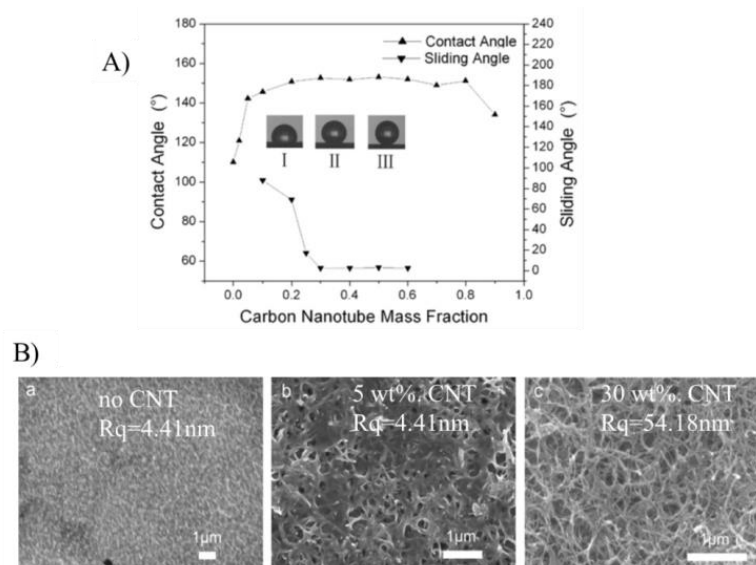


Figure 1-6 A) WCA and sliding angle as a function of CNT loading in nanocomposite films with Teflon® PFA as polymer matrix (I: no CNT loading; II: 5 wt% CNT loading; III: 30 wt% CNT loading). B) SEM images of CNT/PFA nanocomposite film with various CNT loading (a) 0 wt%, (b) 5 wt% and (c) 30 wt%.⁹⁸

The WCA varied from 110.4° to 142.2° and 153.1° by increasing the CNT loading from 0 wt% to 5 wt%, and 30 wt%, respectively. The sliding angle decreased from 90° to less than 5°. SEM image shows that no nanopits for pure PFA coating (Figure 1-6-B-a) while the density of the nanopits significantly grew by increasing the CNT concentration from 5 wt% (Figure 1-6-B-b) to 30 wt% (Figure 1-6-B-c). The roughness of the nanostructure (Rq) increased from 4.41 nm to 22.13 nm and 54.18 nm, respectively, while the microscale roughness remained in the range of 0.55-0.65 μm. It can be concluded that this enhancement of the nanoscale roughness contributes significantly to the increase of WCA.

Similarly, Bayer *et al.*⁹⁹ used an emulsion-based process to fabricate superhydrophobic fluoroacrylic copolymer (Capstone ST-100)/multi wall carbon nanotube (MWCNT) nanocomposite films by adjusting the MWCNT content. They reported two ways to produce superhydrophobic surface. One was thermal curing of

the spray-casted films slightly above the melting point of the fluorinated acrylic latex that transforms them into superhydrophobic films. Alternatively, a thermal treatment by applying flame heating by small diffusion flames for a few seconds, also provide same superhydrophobic features to the film. SEM images of a MWCNT–polymer nanocomposite film containing 14 wt% MWCNTs before and after thermal treatment are shown in Figure 1-7.

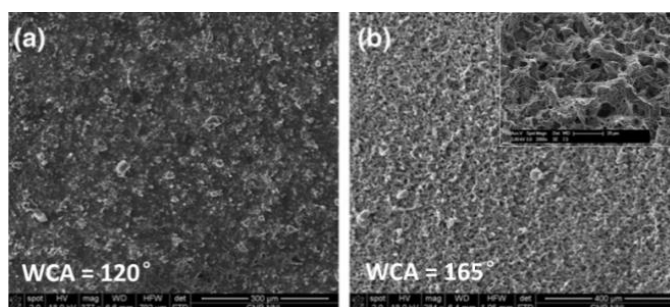


Figure 1-7 SEM images of nanocomposite containing 14 wt% MWCNTs before (a) and after (b) thermal treatment.⁹⁹

It can be easily noticed the change in surface morphology due to the melting of fluoroacrylic copolymer (Figure 1-7-b). A microporous MWCNT–polymer network with hierarchical surface roughness appears after thermal treatment. The detailed surface morphology (insert image in Figure 1-7-b) obtained with higher magnification also indicates the formation of micro-pores. The nanostructuring of the surface is due to the assembly of the MWCNTs over the micro-roughness generated by the spraying of the polymer emulsion. The WCA of the untreated film is 120° and it is increased to 165° with very low droplet roll-off angles (< 5°) after the thermal treatment.

TiO₂/fluorinated polymer nanocomposites

TiO₂ particles have been used in the fabrication of self-cleaning surfaces with photocatalytic properties.^{100,101,102} For example, Kamegawa *et al.*¹⁰² reported on the superhydrophobic TiO₂/polytetrafluoroethylene (PTFE) nanocomposite films with photocatalytic self-cleaning effect by using a radio frequency-magnetron sputtering (RF-MS) deposition on fine structured Ti substrate (Ti). The molar ratio of titanium

and fluorine (Ti/F) of original TiO₂/PTFE is 0.15. The resulting morphology was analyzed by SEM (Figure 1-8).

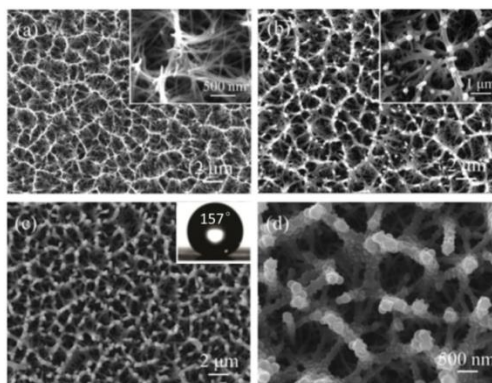


Figure 1-8 SEM images of (a) structured Ti substrate; (b) PTFE deposited on Ti; (c) TiO₂/PTFE deposited on Ti and (d) high magnification image. The inset of (a,b) is also magnified images. The inset of (c) is the droplet image on that surface.¹⁰²

It can be seen that Ti substrate exhibits a needle-like structure with tangled shapes (Figure 1-8-a). The deposited PTFE (Figure 1-8-b) and TiO₂/PTFE (Figure 1-8-c) were uniformly accumulated on structured Ti substrate without any large geometric and dimensional changes. TiO₂/PTFE had similar shape with sea-island structure due to the coexisting roundish TiO₂ and PTFE (Figure 1-8-d). The initial WCA of PTFE (168°) and TiO₂-PTFE (157°) were quite higher than that of TiO₂ (107°), demonstrating the importance of fine structures of coated materials.

ZnO/fluorinated polymer nanocomposites

Among the use of nanosized particles to increase surface roughness of a hydrophobic surface, ZnO nanoparticles have been used by Qing and coworkers.¹⁰³ First, hydrophobic α,ω -bis(hydrogen)-terminated poly(dimethylsiloxane) (PDHS) was modified by dodecafluoroheptyl-propyl-trimethoxysilane (DFTMS) to design a fluorinated PDHS (PFDHS); ZnO was modified by stearic acid to increase the dispersion in polymer matrix of fluorinated polysiloxane (PFDHS). The composites of modified-ZnO/PFDHS with various weight percent of ZnO were fabricated on steel substrates via spray-coating (Figure 1-9-A).

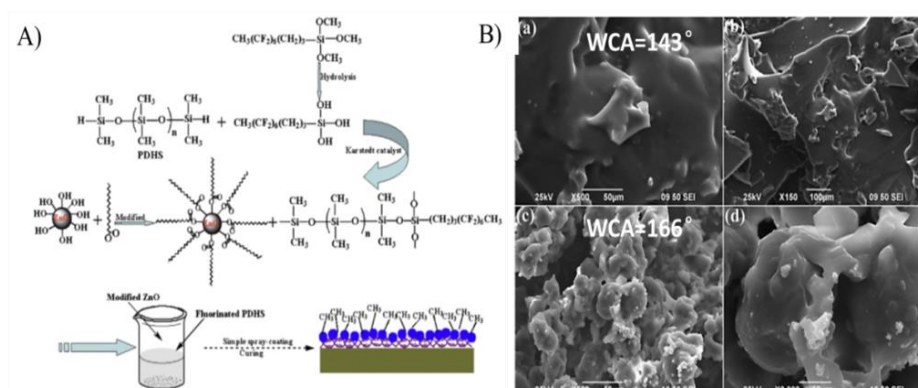


Figure 1-9 SEM images of the different coating on steel substrate: (a) and (b) FPDHS coating; (c) and (d) modified-ZnO/FPDHS coating with 65 wt% of ZnO.¹⁰³

Figure 1-9-B-a, b shows the surface morphology of the deposited FPDHS surface without modified ZnO nanoparticles. This surface is composed of a few large mastoids with an intrinsic WCA of 143° . The SEM images of modified-ZnO/FPDHS (65 wt% of ZnO) are shown in Figure 1-9-B-c and d. It can be seen that the pine-cone-like microclusters consist in numerous irregular petal-like structures with diameter size ranging from dozens to hundreds of nanometers. The hydrophobic FPDHS reduces surface energy and the modified ZnO creates a dual type of roughness on the surface. These two factors contribute to the formation of superhydrophobic surface with a WCA of 166° .

Clay/fluorinated polymer nanocomposites

To prevent the wetting of membrane pore in membrane distillation, electrospun nanofiber membranes constituted of PVDF/clay superhydrophobic nanocomposites were prepared and tested by Prince and co-workers.¹⁰⁴ The clay particles are commercially available one, Cloisite®20A, and were modified by organic modifiers containing dimethyl dehydrogenated tallow quaternary ammonium chloride. The nanocomposite nanofiber membranes (NNMs) of clay/PVDF were prepared by the electrospinning of a solution of DMAC/acetone containing PVDF and clay particles at different concentrations. The morphology of NNMs is shown in Figure 1-10.

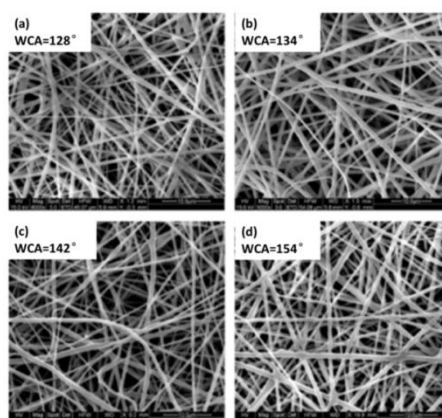


Figure 1-10 SEM images of clay/PVDF nanofiber membranes prepared by the electrospinning of a solution of (a) 12 wt% PVDF, (b) 12 wt% PVDF + 2 wt% clay, (c) 12 wt% PVDF + 4 wt% clay, and (d) 12 wt% PVDF + 8 wt% clay, respectively.¹⁰⁴

The obtained membranes present a rough surface with a pore size around $0.6\ \mu\text{m}$ in all cases. The fiber diameter increased from 417 nm up to 625 nm as the clay concentration varied from 0 wt% to 8 wt%. This might be due to the enhancement in the viscosity of the clay/PVDF solution by increasing the clay concentration, which leads to the rise of electrospun fiber's diameter. The WCA of the neat PVDF membrane is 128° , while the WCA of NNMs increased to 134° and 142° with increasing clay concentration to 2 wt% and 4 wt%, respectively. Superhydrophobic NNMs with a WCA of 154.2° was obtained at the highest clay concentration of 8 wt%.

POSS/fluorinated polymer nanocomposites

Polyhedral oligomeric silsesquioxanes (POSS) molecules can be covalently attached to polymers with organic groups that are covalently anchored at the cage periphery. This fact permits POSS as excellent organic fillers to prepare water-repellent coatings. For example, Genesh *et al.*¹⁰⁵ reported on the fabrication of a transparent, superhydrophobic nanocomposite coating of fluoroPOSS/poly(vinylidene fluoride-co-hexafluoro propylene) (PVDF-HFP) on a glass substrate via electrospinning. FluoroPOSS functionalized with perfluoroalkylthioether corner

groups were used as nanofillers (FPSi8, Figure 1-11-A).

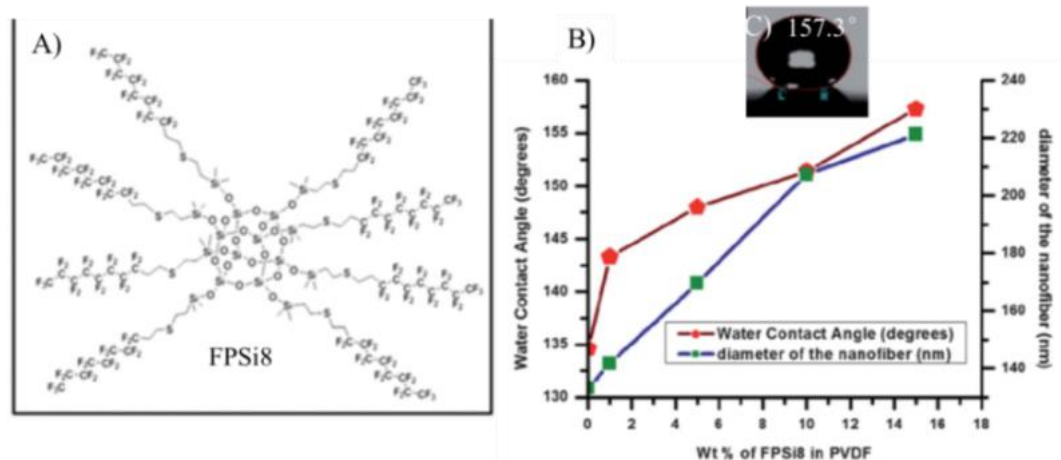
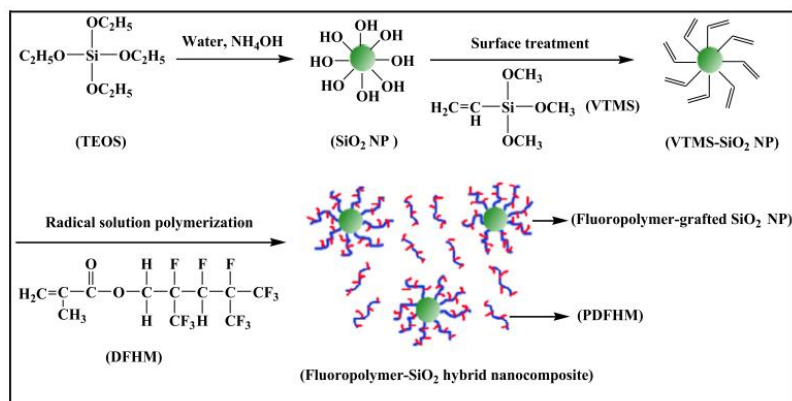


Figure 1-11 A) Structure of fluoroposs FPSi8; B) The impact of wt. % of FPSi8 on WCA and fiber diameter; C) 15 wt. % of FPSi8 in nanocomposite film with a WCA of 157.3° .¹⁰⁵

The solutions of fluoroPOSS/PVDF-HFP with various FPSi8 content in DMA/THF were electrospun on glass slide. Figure 1-11-B shows the impact wt% of FPSi8 on the fiber diameter and the WCA. As the concentration of the FPSi8 in the fluoroPOSS/PVDF-HFP composite mixture increases, the viscosity of the electrospinning solution enhances thereby enlargement the average diameter of the synthesized nanofiber. The WCA increases with rise of FPSi8 content: the 15 wt% FPSi8 exhibited a WCA as high as 157.3° with SA $<5^\circ$.

Colloid or fumed SiO₂ /fluorinated polymer nanocomposites

Wang *et al.*¹⁰⁶ prepared a superhydrophobic fluoropolymer-SiO₂ hybrid nanocomposite composed of a core-corona fluoropolymer-grafted SiO₂ and fluorinated poly(dodecafluoroheptyl methacrylate) (PDFHM). First, core-corona fluoropolymer-grafted colloid SiO₂ nanoparticle (NP) and PDFHM were obtained by free radical polymerization of the vinyl trimethoxy silane (VTMS)-treated SiO₂ NP with dodecafluoroheptyl methacrylate (DFHM) (Scheme 1-40).



Scheme 1-40 Preparation of fluoropolymer–SiO₂ hybrid nanocomposite.¹⁰⁶

The nanocomposite films were obtained by casting the suspensions of fluoropolymer-SiO₂ hybrid nanocomposites. Different dispersants (THF, H₂O/THF = 1/9, H₂O/THF = 1/3) were used to illustrate the effect of water volume on surface morphology and WCA. Figure 1-12-a shows the SEM image of the coating casted from THF suspension. An irregular rough surface made of flat patches (Figure 1-12-b) and also of large clusters is observed giving a low WCA of 118°.

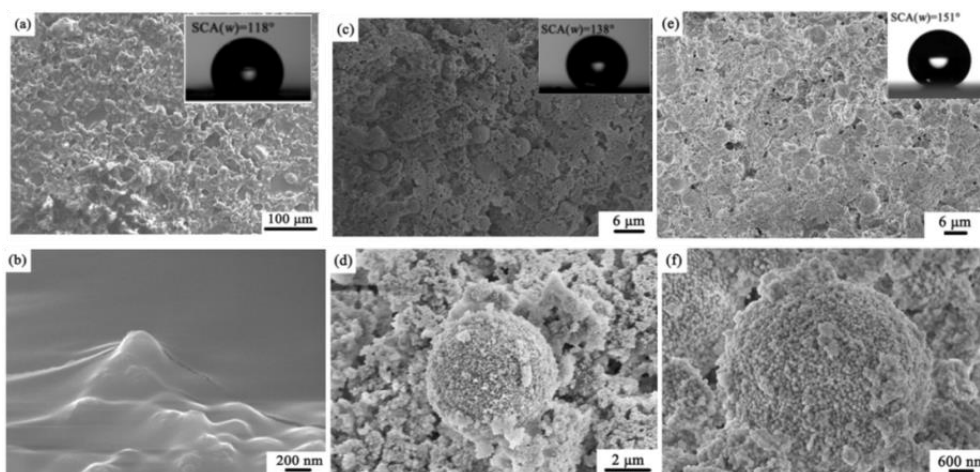


Figure 1-12 SEM images of fluoropolymer–SiO₂ hybrid nanocomposite film from (a) a THF suspension, (c) a H₂O/THF (v/v=1/9) suspension, (e) a H₂O/THF (V/V=1/3) suspension; images (b), (d) and (f) are high magnification images corresponding to (a), (c) and (e), respectively. The insert images in (a), (c) and (e) are WCA of surfaces with the value of 118°, 138° and 151°, respectively.¹⁰⁶

After the addition of a small amount of water (H₂O/THF, v/v = 1/9), the coating casted from the novel suspension displays a few micro-spheres and a large number of flaky aggregations with uneven size in the range of 1-6 μm (Figure 1-12-c). Figure

1-12-d reveals that microspheres and flaky aggregates are both composed of a large number of particles with a uniform diameter of ca. 90 nm. This result indicates that micro–nanoscale binary structure was formed on the surface, but this unevenness still results in a low WCA of 138°. However, by increasing the water content ($\text{H}_2\text{O}/\text{THF}$, $v/v = 1/3$), the number of microspheres was increased (Figure 1-12-e). Moreover, it is found from high magnification image (Figure 1-12-f) that the surface of microsphere has a higher stacking density of particles than that shown in Figure 1-12-d, which results in a high WCA (151°) and water droplet can roll off easily from the surface. Due to the low solubility of fluoropolymer in water, the authors concluded that the addition of H_2O to the THF suspension of fluoropolymer– SiO_2 hybrid nanocomposite induces a transfer of surface morphology of cast film from smooth film, to bare-exposed flaky aggregation and micro-sphere aggregation with enhancing superhydrophobicity. Surface topology and roughness were analyzed by AFM (Figure 1-13).

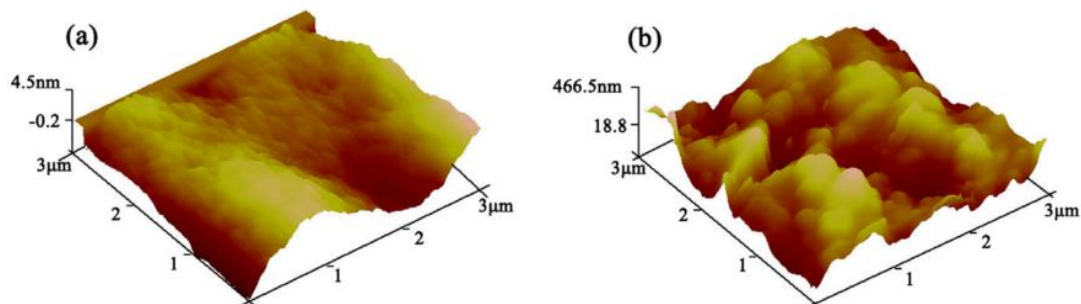


Figure 1-13 AFM images from the surfaces of coating casted from (a) THF suspension and (b) $\text{H}_2\text{O}/\text{THF}$ ($V/V=1/3$) suspension.¹⁰⁶

Coating casted from THF shows a smooth surface (Figure 1-13-a) with a low roughness (1.0 nm). Conversely, the surface of coating casted from $\text{H}_2\text{O}/\text{THF}$ ($V/V=1/3$) suspension (Figure 1-13-b) presents a structure composed of aggregated particles with a higher roughness (102 nm). Therefore, the increase of the number of microspheres results in an roughness enhancement, which promotes the surface hydrophobicity.

Li *et al.*¹⁰⁷ synthesized fluorine-containing acrylate (FAC) and used it as matrix

for the preparation of superhydrophobic composite films with colloidal SiO₂-based fillers. The structure of FACs is shown in Figure 1-14-A. The content of fluorine atoms was adjusted by the mass ratio of monomers of methyl methacrylate (MMA), butyl acrylate (BA) and dodecafluoroheptyl methacrylate (DFMA).

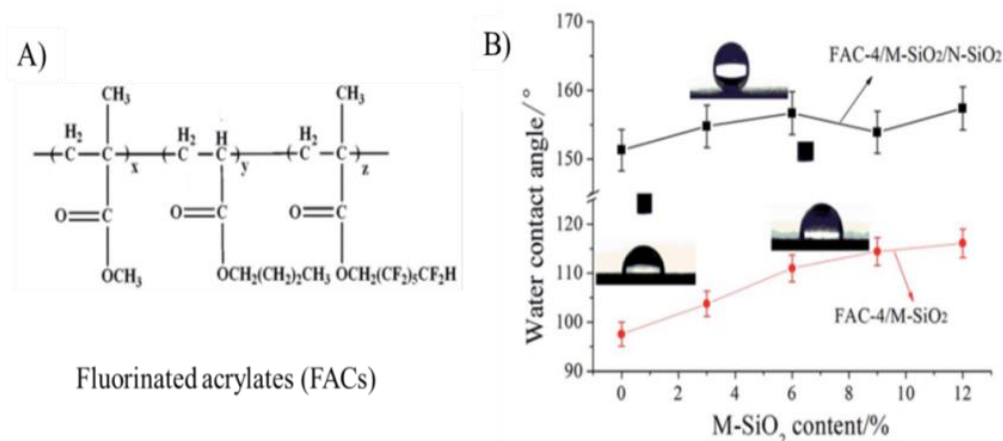


Figure 1-14 A) Structure of fluorinated acrylates (FACs); B) Effects of M-SiO₂ content on the WCA of FAC-4/M-SiO₂ and FAC-4/M-SiO₂/N-SiO₂ composite coating. ¹⁰⁷

FAC-4 was synthesized with a MMA/BA/DFMA mass ratio of 1:4:0.1 and used as polymer matrix. Micro-SiO₂ (M-SiO₂) with a diameter of about 3 μm was used as fillers while nano-SiO₂ (N-SiO₂) with a diameter of 16–20 nm were sprayed on the surface of nanocomposite film as a second top layer. Figure 1-14-B shows the effects of M-SiO₂ content on the WCA of FAC-4/M-SiO₂ and FAC-4/M-SiO₂/N-SiO₂ composite coatings. The surface of the FAC-4 coating is hydrophobic with a WCA of about 97°. With the increase of M-SiO₂ content from 3 to 12 wt%, the WCA on the surface gradually varied from 103° to 115°. Although the addition of M-SiO₂ particles on the surface is suitable to create a roughness and to increase the WCA, the surface is not superhydrophobic because the micro structure roughness is insufficient. After the spraying of N-SiO₂ particles, all of the FAC-4/M-SiO₂/N-SiO₂ composite coatings became superhydrophobic with a WCA higher than 150°. The authors prepared FAC-4/N-SiO₂ composite film by only using nano-SiO₂ which also exhibited superhydrophobicity. The formation of hierarchical micro–nano structures on the surface was confirmed by SEM (Figure 1-15).

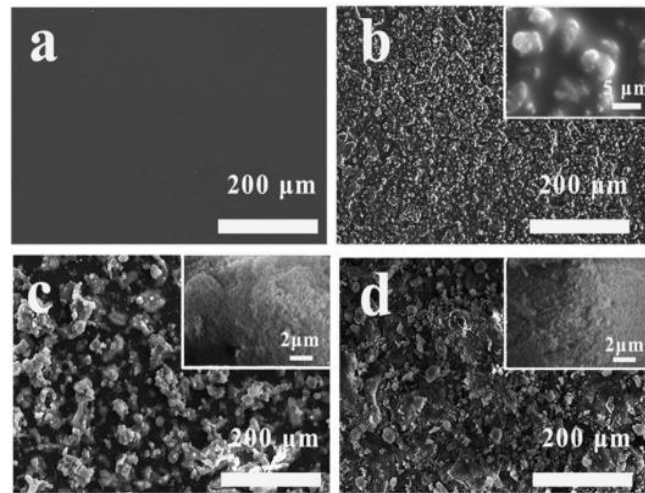
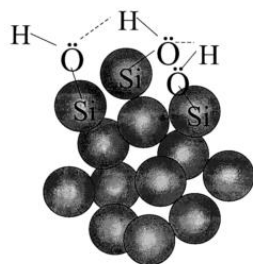


Figure 1-15 SEM images of (a) FAC-4; (b) FAC-4/M-SiO₂ coating (the M-SiO₂ content was 6 wt %); (c) FAC-4/N-SiO₂ coating; (d) FAC-4/M-SiO₂/N-SiO₂ (the M-SiO₂ content was 6 wt %).¹⁰⁷

The surfaces of the FAC-4 coating are rather smooth and no obvious bulges can be observed (Figure 1-15-a). When 6 wt% M-SiO₂ particles are added (Figure 1-15-b), there are many bumps of M-SiO₂ particles in micro sizes of about 3–5 μm on the surface, which induces an increase of the surface roughness and WCA. After coating with N-SiO₂ particles, as shown in Figure 1-15-d, plenty of protrusions in micro sizes appear on the surface and the high resolution image confirms that the protrusions are mainly composed of N-SiO₂ particles, indicating that the N-SiO₂ particles form micro–nano structures on the surface. Figure 1-15-c shows that surface of FAC-4/N-SiO₂ coating exhibits similar morphology in comparison with Figure 1-15-d.

In addition to colloid silica particles, fumed silica particles have also been used for the fabrication of superhydrophobic films or coatings thanks to their intrinsic nanostructure. Individual fumed silica nanoparticles display diameters ranging from 5 to 50 nm and form aggregates with a size of a few hundred nanometers because of the H-bonds between -OH groups, as shown in Scheme 1-41.¹⁰⁸



Scheme 1-41 Aggregates formation between adjacent fumed silica particles through H-bond between the silanol groups.¹⁰⁸

After mixing fumed silica with a hydrophobic polymer matrix, nanocomposite films with hierarchical structures and enhanced hydrophobicity are expected. For example, Basu *et al.*⁹⁵ obtained a superhydrophobic surface by embedding hydrophobically hexamethyldisilazane treated fumed silica (HMFS) particles in PVDF matrix via spray-coating method. The WCA of the PVDF-HMFS hybrid composite coating was influenced by the silica particles amount content. When the silica concentration in PVDF matrix was increased from 33.3 wt% to 71.4 wt%, WCA varied from 117.8 to 168.8° and the sliding angle decreased from 90.8 to < 1.8°. The resulting composite coating with 66.7 wt% of HMFS displays a rough and porous structure (Figure 1-16).

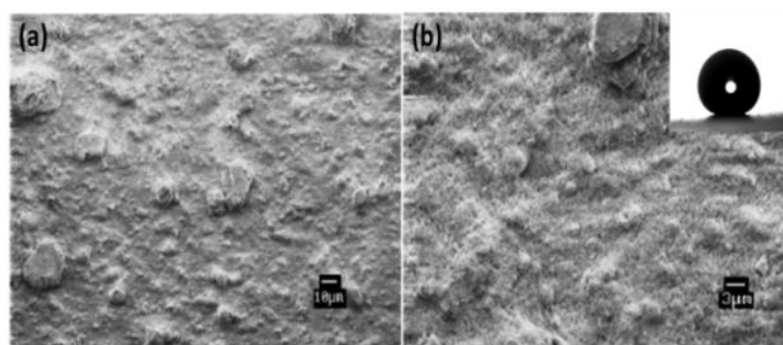


Figure 1-16 SEM images of PVDF-HMFS (66.7 wt%) composite coatings (a) and higher magnification of (b).⁹⁵

Water droplets cannot easily penetrate into micropores on the surface and therefore rough surfaces with a high fraction of micropores were obtained, which led to superhydrophobicity with a WCA of 167° and sliding angle lower than 1°.

Another example was reported by Ozbay and coworkers¹⁰⁹ who employed fumed

silica and fluorinated polymers to prepare superhydrophobic surfaces (Figure 1-17).

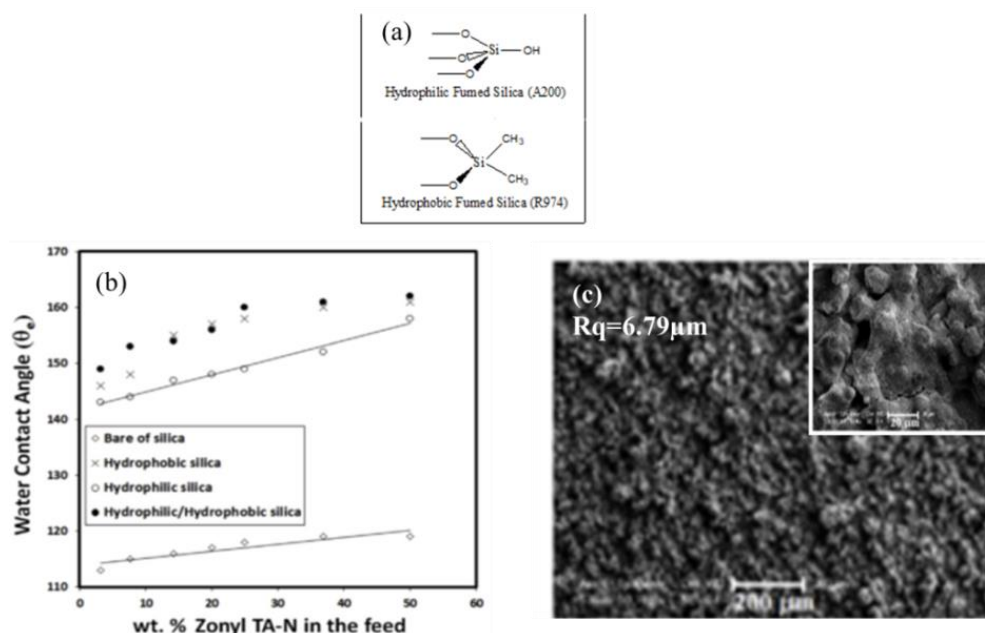


Figure 1-17 (a) Chemical structures of fumed silica particles; (b) Change of WCA values with changing silica type and Zonyl TA-N wt% in the feed composition; SEM images (x 250, c) and (x 1000, insert image of c) of poly(SBR-g-TA-N 50%)/A200-R974 (30 wt%) coating.¹⁰⁹

Perfluoroalkyl ethyl acrylate (Zonyl TA-N) monomer was firstly grafted onto styrene butadiene rubber (SBR-1502) by free radical polymerization using different Zonyl TA-N feed compositions. Then, the synthesized graft fluorocopolymers, poly(SBR-g-Zonyl TA-N), were mixed with various ratios of hydrophilic (A200) and hydrophobic (R974) fumed silica (Figure 1-17-a) powders in toluene solution. Finally, SBR-g-Zonyl TA-N/SiO₂ hybrid coatings were prepared by a spray-coating step onto glass slides. The effect of silica type and weight content of Zonyl TA-N in the copolymer was studied (Figure 1-17-b). The presence of the methylene groups on hydrophobic silica particles appears more efficient to repel water than that of the hydroxyl groups on the hydrophilic silica particles. When the mixture of equal mass of hydrophobic and hydrophilic silica particles was added into the graft copolymer solution, the resultant SBR-g-Zonyl TA-N/SiO₂ hybrid coatings showed the highest surface roughness due to the high agglomeration tendency of hydrophilic silica particles into the graft copolymer. Figure 1-17-c and its insert images are the SEM images of SBR-g-Zonyl TA-N/SiO₂ hybrid coatings in which the total silica

(hydrophilic: hydrophobic = 1:1) content is 30 wt%, and the Zonyl TA-N in poly(SBR-g-Zonyl TA-N) is 50 wt%. The presence of fluoroacrylate pendant groups caused the agglomeration of silica particles, which resulted in high surface roughness with a value of 6.79 μm and a WCA of 162°.

1.2.3 Conclusion

Superhydrophobic surfaces (WCA > 150°) are generally classified according to their affinity to water: low adhesion (lotus effect) and high affinity (rose petal effect). Plenty of methods have been developed to prepare superhydrophobic surfaces displaying pronounced water-repellency property. The basic principles are to combine hierarchical structures with low surface free energy materials, especially fluorinated polymers. Superhydrophobic fluorinated polymers-based nanocomposite films can be obtained by optimizing parameters in terms of filler nature, filler content and host polymer chemical nature. The nanofillers are expected to migrate to the surface which allow for the formation of multiscale structures with desired roughness, combine to the apolar character of the host polymer, leading to superhydrophobicity.

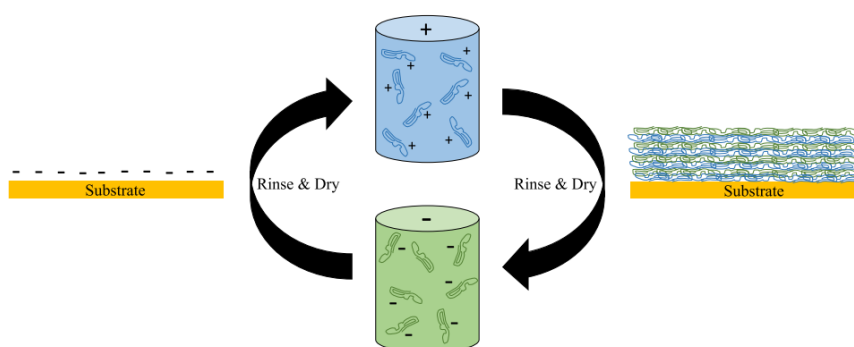
1.3 Preparation of multilayer films through layer-by-layer (LbL) approach

1.3.1 General introduction of the LbL

Multilayer thin films built with supramolecular layer-by-layer (LbL) self-assembly techniques have drawn great attention thanks to the numerous advantages of LbL technique (simple, robust, versatile and reproducible) and the tailored properties of the corresponding films (controlled structures, composition and multifunctionality).^{110,111,112} Two types of driving forces are employed in LbL assembly. One is covalent bonding which is based on the chemical reaction between the building blocks that are alternatively deposited; the other one is based on noncovalent interactions, among which one can cite electrostatic interactions,

H-bonds interaction and other physical forces.¹¹³ In this part, we will focus on non-covalent interactions.

The first work of LbL assembly through non-covalent interactions was reported by Iler *et al.*¹¹⁴ in 1966, who fabricated multilayer films from positively and negatively charged colloidal particles onto solid surfaces. Further exploration of LbL was done by Decher who described the preparation of polyelectrolyte multilayers (PEMS) by using commercially available polyelectrolytes.¹¹⁵ Since then, non-covalent interactions driven LbL assembly have gained tremendous interest in the preparation of functional polymer films. The typical procedure to prepare non-covalent interactions mediated multilayer films, for example through electrostatic interaction, is shown in Scheme 1-42.



Scheme 1-42 Representation of LbL assembly of polyelectrolytes onto a charged surface.¹¹⁶

The LbL deposited films start by appropriately preparing the surface in order to favor the adsorption of the 1st layer. In this example, the surface was negatively charged. The negative substrate is then immersed in positively charged building blocks containing solutions, with tailored affinities to one another, for periods of time ranging from seconds to minutes, followed by rinsing and drying steps to remove any loosely adhered material and yielding a layer deposited on to the surface. The effective surface is reversed to positively charged, subsequently dipped into a polyanion solution. After the same rinsing and drying step, one bilayer film is obtained; and this procedure is repeated to reach the targeted multilayer films.

LbL processes include simply alternating deposition of building blocks with

complementary interactions or structures which allow for fabricating a large variety of multilayer thin films on both planar and non-planar substrates, including silicon wafer,¹¹⁷ gold-coated wafer,¹¹⁸ micro glass,¹¹⁹ quartz,¹²⁰ polymers,¹²¹ fibers,¹²² (nano)particles¹²³ or biomaterials,¹²⁹ etc. The versatility of this process is explained by the large variety of substrate which is possible to use and by the properties of the multilayer films which can be tuned precisely by varying different parameters:

(1) The use specific polymer materials. The nature of the polymers decides the driving force of LbL; and the strength of interaction will be discussed in the following part.

(2) The introduction (or not) of other species than polymers, such as additives (cyclodextrin,¹²⁶ metal ions,¹²⁷ Fe₃O₄ nanoparticles,¹²⁸ graphene,¹²⁹ and carbon nanotube¹³⁰).

(3) The deposition method operated in LbL assembly: spin- and spray-assisted LBL assemblies,^{117,131,132} as well as conventional dip-coating¹¹⁹.

(4) The specific operating conditions. For instance, the temperature of adsorption,¹³³ the solvent polarity,^{134,135,136} the time of deposition,¹³⁷ the number of deposited layers,¹³⁶ and the concentration of deposition solution.¹³⁴

Thanks to the advantages of LbL assembly, a large number of works has been reported and some reviewers described the diverse facts of LbL assembly. For example, Decher *et al.*¹¹⁵ compared LbL assembly with Langmuir-Blodgett technique and discussed the superlattice architectures of the resulting films of polyelectrolyte. Caruso *et al.*¹³⁸ reviewed the nano-engineering of particle surfaces; Hammond *et al.*¹³⁹ reviewed how to integrate form and function into multilayered films; Ariga and colleagues¹⁴⁰ reviewed the versatility of LbL assembly; Liu and co-workers¹¹⁰ reviewed different template materials and architectures; Quinn *et al.*¹⁴¹ reviewed the formation of multilayer thin films prepared through non-electrostatic interactions; Borges and Mano¹⁴² reviewed the molecular driving forces used for LbL assembly; Caruso's group reviewed how different assembly technologies affect the properties of the resulting multilayered films,¹⁴² and they also discussed the technological evolution of LbL assembly over time and how methods and equipment were repurposed from

other fields to LbL assembly.¹⁴³ Very recently, the progress in LbL assembled biogenic capsules and their applications was reviewed by Xuan and coworkers.¹²⁵ Obviously, LbL assembly approach has shown its great flexibility and versatility in preparing multilayer films involving in chemical and/or bio-materials. The driving force of LbL assembly is a key parameter to ensure the film growth.

1.3.2 Presentation of the different types of non-covalent interactions used for the LbL film construction

Many different significant approaches for prepare multilayer films on the basis of non-covalent interactions have been reported so far. Among these, electrostatic interactions and H-bonds are the most widely used driving forces to construct multilayer films.

1.3.2.1 Exploitation of conventional electrostatic interactions

As one of the most important driving forces in the development of LbL multilayer films, the electrostatic interaction driven LbL process occurs in aqueous solution where the building blocks are water-soluble and multi-charged species, such as polyelectrolytes,¹³⁴ and colloidal particles.¹¹⁴ Polyelectrolytes possess versatile structures in solution that are helpful to prepare polymer films with well-tailored structures and functionalities. Several examples of polyelectrolytes are existing in nature, such as polysaccharides,¹⁴⁴ proteins,^{145,146} deoxyribonucleic acid (DNA) and ribonucleic acid (RNA)^{147,148}. Moreover, synthetic polyelectrolytes have emerged to fabricate multilayer films by LbL assembly (Figure 1-18).

Polyelectrolytes can be divided into two groups according to their charge density along polymer chains and also according to their sensitivity to pH. One corresponds to strong polyelectrolytes which are wholly charged along the polymer chains in the solution, typical examples are poly(diallyldimethylammonium chloride) (PDADMAC) and poly(sodium styrene sulfonate) (PSS) (Figure 1-18).¹³⁴ The other group is associated to weak polyelectrolytes for which polymer chains are ionisable partly

charged in solution such as pH-sensitive poly(acrylic acid) (PAA) and poly(ethyleneimine) (PEI),¹⁴⁹ for which the charge density is dependent on the pH. Moreover, other external stimuli, such as ionic strength,¹⁵⁰ temperature,¹³³ the addition of specific biological moieties,¹⁵¹ or ionic surfactants¹⁵² would further affect the molecular organization, composition and surface properties of the obtained multilayer films.

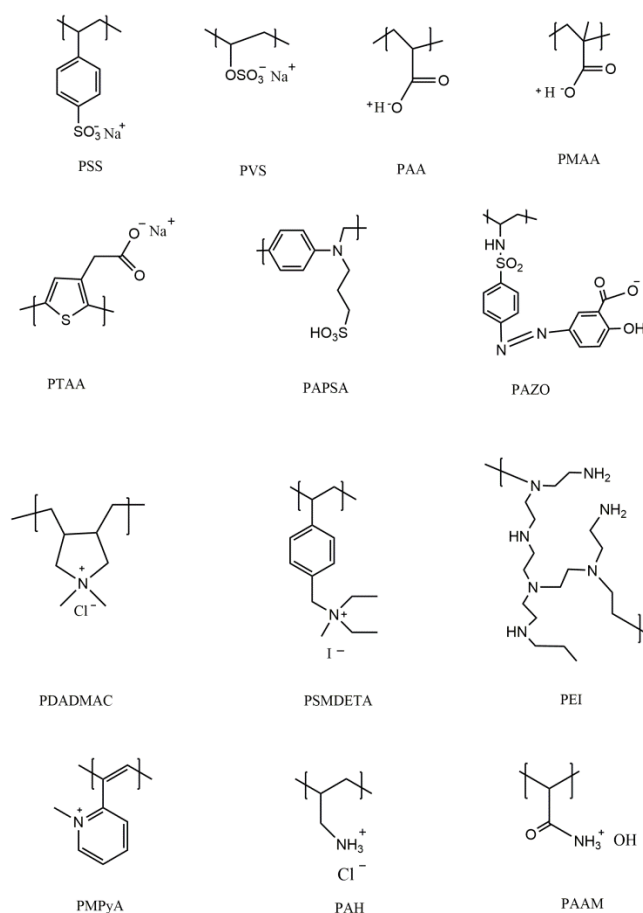


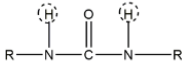
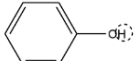
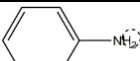
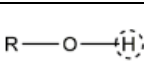
Figure 1-18 Examples of polyelectrolytes used in LbL self-assembly films.

1.3.2.2 Exploitation of H-bonds

In 2011, IUPAC defined hydrogen bonds (H-bonds) as an attractive interaction between a hydrogen atom from a molecule or a molecular fragment X–H in which X is more electronegative than H, and an atom or a group of atoms in the same or a different molecule.¹⁵³ H-bond with energies ranging from 4 to 170 kJ/mol is a directional attractive interaction between H-bond donor and acceptor, which have

been found in natural living organisms, determining the secondary structure of biological molecules such as proteins, nucleic acids, and the behavior of lipid membranes.¹⁵⁴ The most common proton donor and acceptor groups in synthetic polymers are shown in Table 1-11.

Table 1-11 Examples of proton donors and acceptors groups in polymeric structures.

Proton donor	Proton acceptor
	
	
	
	
	
	
	

The uniform distribution of electron density leads to the basicity and acidity of proton donor (Lewis base) and acceptor (Lewis acid), respectively.¹⁵⁵ The intrinsic structure and the external environment on acidity of proton donor and basicity of proton acceptor affect the strength of hydrogen bond, which would further impact the morphology, composition, thickness and property of LbL multilayer films. Any polymer exhibiting electron-deficient hydrogen atoms bonded with O, N, and F atoms can be regarded as H-bond donors. On the contrary, polymers contain non-hydrogenated O, N atoms which possessing one or more lone electron pairs, are known as H-bond acceptors. Some carboxylic acid or amide groups containing polymers can be used as both H-bond donors and acceptors depending on the partners to which they are associated. Figure 1-19 shows some examples of synthetic polymers

used in H-bonds mediated LbL self-assembly.

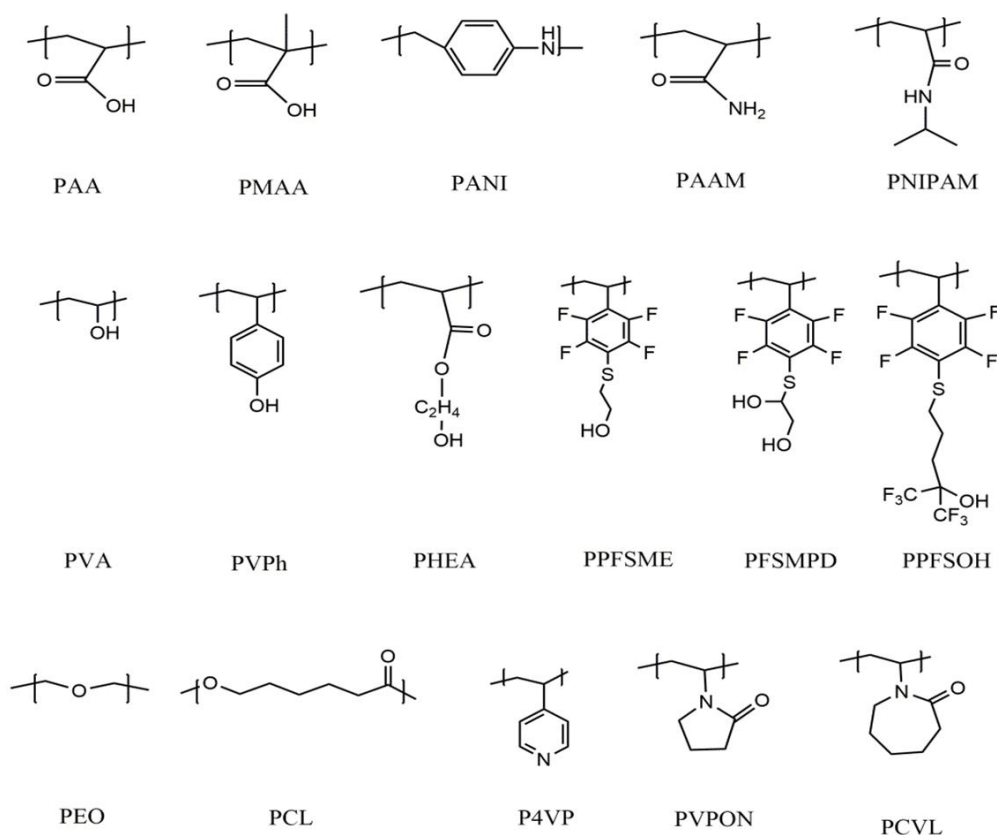


Figure 1-19 Examples of synthetic polymers used in H-bond driven LbL assembly.

As pioneers, Stockton and Rubner¹⁵⁶ reported on the H-bonds driven LbL assembly of polyaniline (PANI) as H-bond donor with different nonionic H-bond acceptor polymers such as poly(vinylpyrrolidone) (PVPON), poly(vinyl alcohol) (PVA), poly(acrylamide) (PAAM), and poly(ethylene oxide) (PEO). They described the basic H-bond self-assembly process as well as how parameters such as molecular weight, solution pH, and polymer type influence the bilayer thickness and the conductivity of the resulting multilayer thin films. H-bond acceptor polymers include polyesters, polyacrylates, pyridine derivatives, and polyether.¹⁵⁷ It is worth mentioning that by introducing hydroxyl groups in poly(2,3,4,5,6-pentafluorostyrene) (PPFS) backbones via *para*-fluoro substitution reaction, the formed hydroxylated PPFS copolymers (PPFSME, PFSMPD and PPF SOH, Figure 1-19) as H-bond donors were used in mediating the LbL self-assembly with P4VP.^{23,52,60} In addition, natural polymer materials, such as polysaccharides¹⁴⁴ and lignin¹⁵⁸ have been

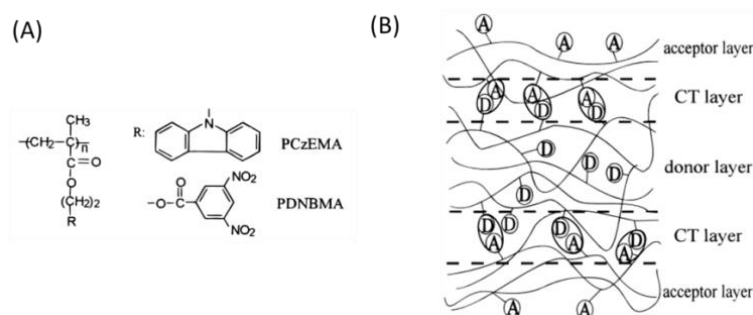
modified to prepare LbL multilayer films.

The use synthetic polymers allow for the incorporation of natural molecules into multilayer films not only in water but also in organic solvents, enlarging the scope of such LbL films. Thanks to this merit, significant progress has been made to tune the H-bonded film growth mechanism and many characterization methods have been used to monitor the process of assembly. Typically, the surface morphology is often studied by optical polarizing microscopy, scanning electron microscopy (SEM), or by atomic force microscopy (AFM) to achieve additional information on roughness; the thickness of the films is measured by surface profilometry, AFM or ellipsometry and the H-bonds are often highlighted by FT-IR or XPS; the alternately changing of the outermost layer is characterized by water contact angle (WCA) measurement; the mechanical properties are often studied by quartz crystal microbalance (QCM) or quartz crystal microbalance with dissipation monitoring (QCM-D).

1.3.2.3 Other kinds of physical interactions

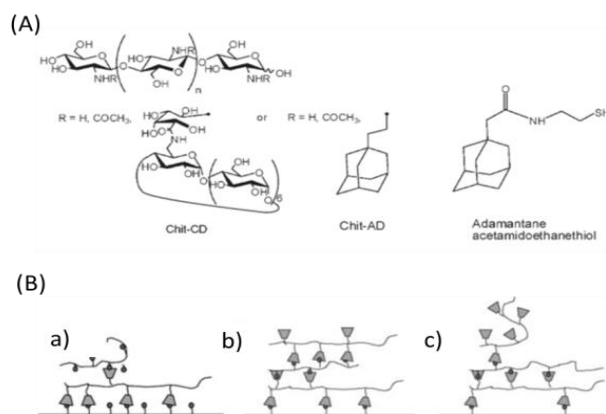
In addition to the frequently used electrostatic interactions or H-bonds, many other physical interactions have also been employed to create various multilayer architectures through the LbL assembly technique. Few examples are cited below:

(1) Charge-transfer interactions. For example, poly[2-(9-carbazolyl)ethyl methacrylate] (PCzEMA) and poly[2-[(3,5-dinitrobenzoyl)oxy]ethyl methacrylate] (PDNBAM) are bearing nonionic pendant groups in their side chains which have electron-donating and electron-accepting character, respectively. Multilayer films were obtained by alternate adsorption of these polymers onto gold and quartz substrates (Scheme 1-43).¹⁵⁹



Scheme 1-43 (A) Chemical structures of PCzEMA and PDNBMA; (B) Side-view illustration of the deposited film. For simplicity a carbazoyl group and a 3,5-dinitrobenzoyl group are represented as D and A, respectively. Pairs of D and A forming charge-transfer (CT) complexes are circled.¹⁵⁹

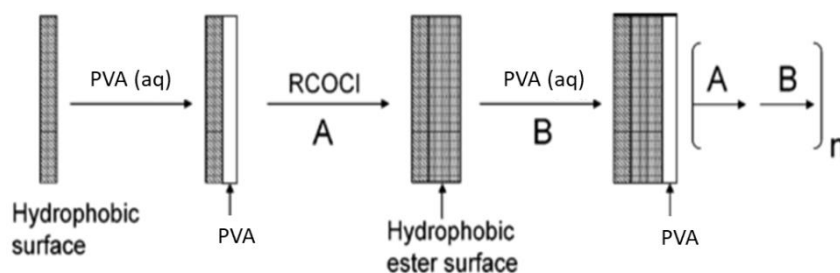
(2) Host-guest interactions. Heyden *et al.*¹⁶⁰ prepared multilayer films by using host-guest interactions between two modified chitosans: one with cyclodextrin cavities and the other with adamantyl moieties, on gold coated quartz crystal (Scheme 1-44-A). In particular, the authors observed an impact of the structure, namely the adamantane densities on the self-assembly growth and on the mass absorption (Scheme 1-44-B).



Scheme 1-44 (A) Chemical structures of adamantane- and cyclodextrin-grafted chitosan and the thiol-adamantane used to functionalize the gold-coated quartz crystal; (B) Cartoon representing the influence of the adamantyl densities on the self-assembly growth: (a) high, (b) medium and (c) low adamantyl ratio.¹⁶⁰

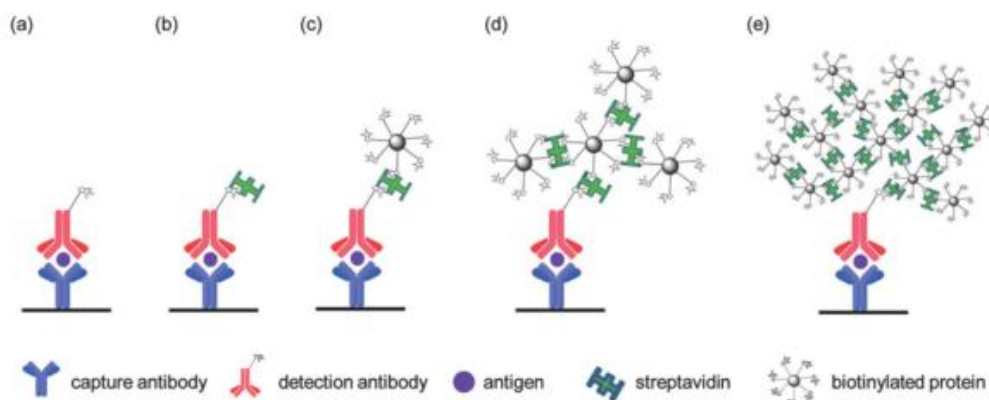
(3) Hydrophobic interactions. For example, poly(vinyl alcohol) (PVA) was adsorbed from aqueous solution to propyldimethylsilyl-modified silicon wafers. This thin semicrystalline coating was chemically modified using acid chlorides to form thicker, hydrophobic coatings.¹¹⁰ The products of the modification reactions allowed

for the adsorption of a subsequent layer of PVA that can subsequently be hydrophobized. This two-step process (adsorption/chemical modification) led to a LbL deposition to prepare coatings with controlled thickness, chemical structure, and wettability control (Scheme 1-45).



Scheme 1-45 Multilayer formation by the repetitive process of adsorption and chemical reaction of PVA.¹¹⁰

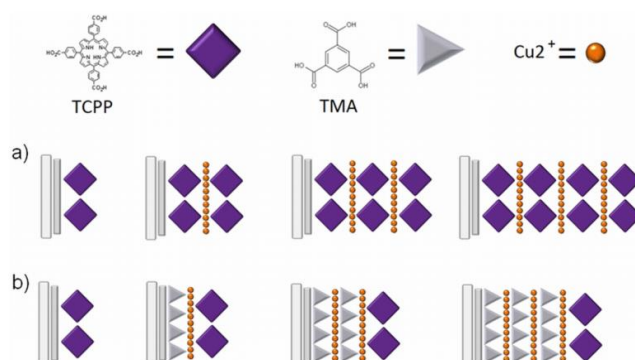
(4) Biospecific interactions, such as the well-known molecular recognition of avidin-biotin pair interactions,¹⁶¹ antibody-antigen interactions,¹⁶² lectin-carbohydrate interactions¹⁶³ and DNA hybridization.¹⁶⁴ Chu *et al.*¹⁶¹ demonstrated that the biotin-streptavidin recognition interactions driven LbL assembly allow for preparing streptavidin biotinylated protein networks (SBPN) (Scheme 1-46).



Scheme 1-46 Illustration of the preparation of biospecific interactions driven-streptavidin biotinylated protein networks via LbL assembly.¹⁶¹

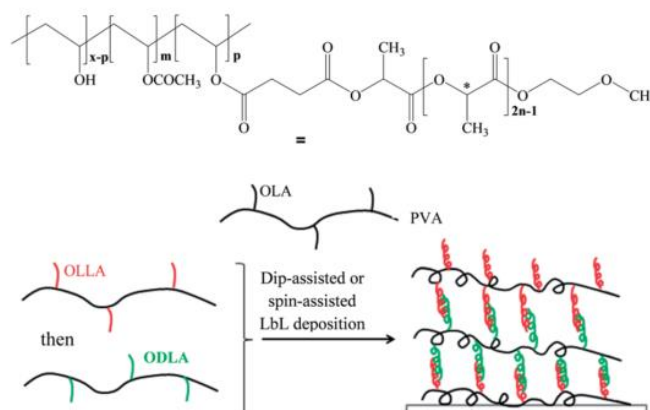
(5) Coordination chemistry interactions. Joyce *et al.*¹⁶⁵ prepared a series of metal-organic coordination films with tetra(4-carboxyphenyl)porphyrin (TCPP) and trimesic acid (TMA) ligands and Cu^{2+} ion linkers via LbL onto TiO_2 -modified indium

tin oxide electrodes (Scheme 1-47). The strong molecular interactions established between the metal ions and organic ligands mediate the formation of films.



Scheme 1-47 The growth of metal–organic coordination multilayer films: (a) $(\text{TCPP}/\text{Cu}^{2+})_n/\text{TCPP}/\text{TiO}_2/\text{ITO}$ with $n=0,1,2$, and 3, corresponding to films of 1, 2, 3, and 4 TCPP layers; (b) $\text{TCPP}/\text{TiO}_2/\text{ITO}$ and $(\text{TCPP}/\text{Cu}^{2+})/(\text{TMA}/\text{Cu}^{2+})_n/\text{TMA}/\text{TiO}_2/\text{ITO}$ with $n=0, 1$, and 2, corresponding to buffers of 0, 1, 2, and 3 TMA layers.¹⁶⁵

(6) Stereocomplexes interactions. Thin films stemming from the formation of stereocomplex between oligolactate of opposite chirality poly(lactide) (OLLA and ODLA) covalently anchored onto PVA chains was described by Bahloul,¹⁶⁶ who studied the feasibility to construct films by sequential adsorption of PVA-g-ODLA and PVA-g-OLLA graft copolymers by dip- and spin-assisted processes and concluded that co-crystallization involving the two homochiral copolymers is the main driving force for the step by step film build up (Scheme 1-48).



Scheme 1-48 Route to $[\text{PVA-g-OLLA}/\text{PVA-g-ODLA}]$ -based LbL film.¹⁶⁶

1.3.3 H-bonds mediated LbL films involving -COOH containing polymers

As one of the most commonly studied non-electrostatic interactions exploited for LbL assembly, H-bonds have been used to successfully incorporate many uncharged polymers into multilayer films. This benefits from many polymers contain moieties that can act as H-bond donors and/or acceptors, for example carboxylic acid containing polymers, which are popular building blocks in LbL assembly multilayer films thanks to their merits in used as either H-bond donor or acceptor depending on the partners to which they are associated. One can cite the most used weak polyacids, poly(acrylic acid) (PAA),¹⁶⁸ poly(methacrylic acid) (PMAA)^{143,169} and carboxylic acid modified natural lignin.¹⁵⁸ In this part, we mainly focus on -COOH containing polymers as H-bond donors to mediate the fabrication of multilayer films. The influence of the intrinsic properties (such as molecular structure, and molecular weight) and the external environment (for instance pH, concentration and solvent) on the growth of multilayer films will be discussed.

PAA/Poly(vinyl alcohol)(PVA) or PMAA/PVA film

Lee *et al.*¹⁷⁰ reported on H-bonds driven multilayer thin films which consist of poly(vinyl alcohol) (PVA) and weak polyacids such as PAA or PMAA via dip-coating in aqueous solutions (pH 2.0) onto glass substrates modified with poly(glycidyl methacrylate) (PGMA). The authors demonstrated that the multilayer growth was dramatically dependent on the molecular weight and the degree of hydrolysis of PVA (Figure 1-20).

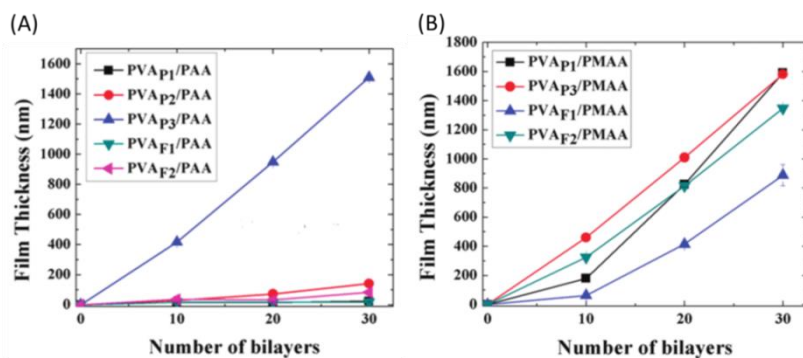


Figure 1-20 Growth behavior of: (A) PVA/PAA systems; (B) PVA/PMAA systems. Partly hydrolyzed (87-89%) PVA: PVA_{P1} (Mw = 24.5 kg/mol); PVA_{P2} (Mw = 88.4 kg/mol); PVA_{P3} (Mw = 131 kg/mol). Fully hydrolyzed (98-99%) PVA: PVA_{F1} (Mw = 21.4 kg/mol), PVA_{F2} (Mw = 144 kg/mol).¹⁷⁰

Figure 1-20-A shows that the fully hydrolyzed PVA_{F1} (21.4 kg/mol) and PVA_{F2} (144 kg/mol) used in the PVA/PAA systems led to very small thickness increments per deposition cycle even with the higher molecular weight PVA_{F2}. The multilayer growth of partly hydrolyzed PVA_{P1} (24.5 kg/mol), PVA_{P2} (88.4 kg/mol) and PVA_{P3} (131 kg/mol) with PAA systems was strongly dependent on the molecular weight of PVA. Only multilayers created from the highest molecular weight PVA_{P3} showed high thickness increments per bilayer (50 nm/bilayer).

In the PVA/PMAA multilayer systems (Figure 1-20-B), reasonable multilayer growth was obtained for all PVA samples. Since the degree of hydrolysis determines the density of hydroxyl groups along the PVA chain, it also affects the capability to develop hydrogen bonds. The partially hydrolyzed PVA_{P3} with the highest molecular weight yielded a thick film with a thickness of 1.6 μm after 30 bilayers. It can be concluded that the use of the more strongly interacting polyacid PMAA results in average thickness increments comparable to the best PVA/PAA system, regardless of the molecular weight and the degree of hydrolysis of the PVA utilized to fabricate the multilayer.

PAA/Poly(2-ethyl-2-oxazoline) (PEtOX) film

Li *et al.*¹⁷¹ reported an antifouling and self-healing polymeric film fabricated by LbL assembly of partially hydrolyzed PEtOX and PAA. They prepared PEtOX-EI-x%

($x=7-100$) with x being the degree of hydrolyzed monomers per polymer chain as hydrogen bond acceptors by controlling the degree of hydrolysis of PEtOX carried out in acidic conditions (Figure 1-21-A).

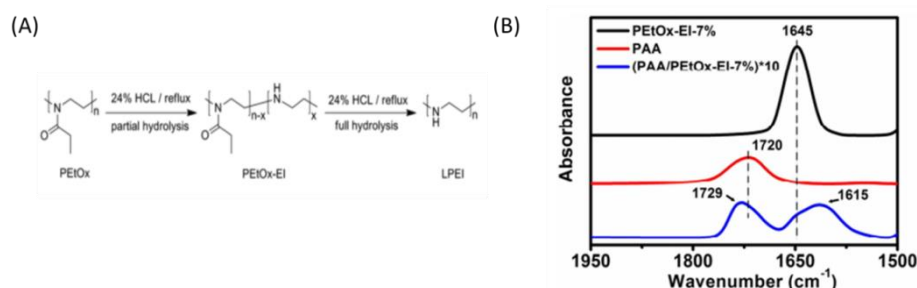


Figure 1-21 (A) Synthetic route of the partially (PEtOX-EI- $x\%$) and fully hydrolyzed LPEI; (B) FTIR spectrum of PAA, PETOX-EI-7% and (PAA/PETOX-EI-7%)*10 deposition cycles. ¹⁷¹

The fabrication of LbL-assembled PAA/PEtOX-EI- $x\%$ films was conducted automatically by a programmable dipping machine on freshly cleaned silicon and glass substrates. The driving force was investigated by FTIR and the corresponding spectrum is shown in Figure 1-21-B. The characteristic peak at 1720 cm^{-1} in the PAA film is attributed to the $-\text{C}=\text{O}$ stretching vibration of the carboxylic acid groups in PAA, whereas the corresponding peak in the (PAA/PEtOX-EI-7%)* n (with n represents the number of deposition cycles) film shifts to 1729 cm^{-1} when $n = 10$. The FTIR spectrum of the PEtOX-EI-7% film shows a characteristic peak of the amide groups at 1645 cm^{-1} . The peak of the amide groups in the (PAA/PEtOX-EI-7%)*10 film appears as a red shift from 1645 to 1615 cm^{-1} . The obvious peak shifts of the carbonyl and amide groups in the FTIR spectra indicate that the H-bonds between amide groups of PEtOX-EI-7% and carboxylic acid groups of PAA are the driving force for the formation of the PAA/PEtOX-EI-7% films. Then, the authors evaluated the film growth of the (PAA/PEtOX-EI- $x\%$)* n by measuring the thickness with a surface profilometer (Figure 1-22-A).

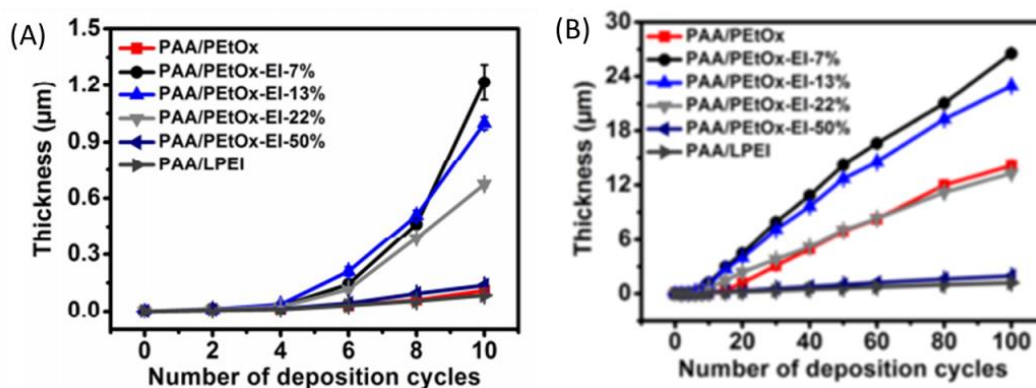


Figure 1-22 Thickness of PAA/PEtOx-EI-x%)*10 ($x=0,7,13,22,50$ and 100) films as a function of deposition cycles (A) the initial 10 deposition cycles; (B) From 0 to 100 cycles.¹⁷¹

It can be seen that the thickness of (PAA/PEtOX-EI-x%)*n ($x = 7, 13$ and 22) exhibited a typically exponential increase for the 10 first deposition cycles (Figure 1-22-A). Afterward, the thickness rapidly increases in a nearly linear manner (Figure 1-22-B), and the film with $x = 7$ is the thickest one. Based on these thickness variations without any other analysis, the authors concluded that as the hydrolysis degree of PEtOX increases, the amount of amide groups in the corresponding PEtOX-EI-x% polymers decreases and hence the H-bonds between PEtOX-EI-x% and PAA in (PAA/PEtOX-EI-x%)*100 films gradually become weaker. The decrease of H-bonds and the more extended configuration of PEtOX-EI-x% in solution explain the film thickness decrease of the (PAA/PEtOX-EI-x%)*100 films. Besides, the authors studied the antifouling properties of the thermally cross-linked (PAA/PEtOX-EI-7%)*100 films which shows strong resistance to adhesion of both Gram-negative *Escherichia coli* and Gram-positive *Bacillus subtilis* bacteria due to the high surface and bulk concentration of the antifouling polymer PEtOX-EI-7%.

PAA/Poly(ethylene oxide) (PEO) film

PEO is the most commonly employed polymer in lithium batteries due to its ability to solvate low lattice energy lithium salts. In Delongchamp and coworkers' work,¹⁷² highly ionic conductive H-bonded PEO/PAA LbL films were fabricated by alternate deposition of PEO and PAA layers from aqueous solutions onto

indium-doped tin oxide coated glass. The effect of the molecular weight and pH of the solutions on the thickness of multilayer films are shown in Figure 1-23.

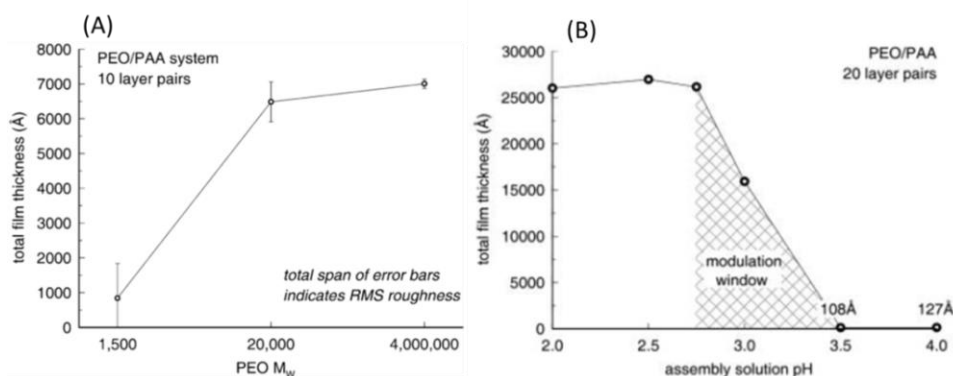


Figure 1-23 Variation of PEO/PAA film thickness (A) with PEO M_w (total span of error bars indicates surface roughness); (B) with assembly solution pH, the region marked “modulation window” indicates the pH range over which the polyacid is sufficiently ionized so that the growth of film is suppressed but assembly is still possible.¹⁷²

As PEO M_w increases, film thickness increases and roughness decreases (Figure 1-23-A). At very low M_w such as 1.5 kg/mol, the films exhibit roughness that is greater than the total film thickness, indicating no controlled film deposition but instead poor adhesion of globular agglomerates. With M_w increases, the films eventually become smoother and thicker, asymptotically approaching what appears to be a limit thickness value. The stronger influence of M_w is due to the low cross-link density of H-bonded LbL films. Very low M_w PEOs may not possess a sufficient polyvalency of interacting ether oxygens to fully satisfy the protic surface and uniformly reverse the surface chemical identity. A PEO M_w of 4000 kg/mol must be employed to achieve LbL assembly of thick, smooth, and uniform PEO/PAA films. The effect of deposition bath pH on PEO/PAA assembly is illustrated in Figure 1-23-B. It can be seen that assembly proceeds to a greater extent at lower pH. However, the thickness of PEO/PAA deposition begins to decrease at pH = 3.0 and declines towards zero at pH = 3.5. PAA would be 1% ionized in solution at pH = 3; apparently even such a small amount of uncompensated negative ionization is sufficient to prevent any deposition. PAA solution ionization of ~5% at pH = 3.5 results in negative charge repulsion which prohibits film formation. This result is quite consistent with the

critical pH value of 3.6 for PEO/PAA complex formation in solution.¹⁷³

PAA/Polyethylene glycol (PEG) film

LbL multilayer films provide opportunity to load functional compounds “embedded” within the film which would alter the property of films. Cui *et al.*¹²⁶ prepared a new kind of highly ionic conductive solid polymer electrolyte (Figure 1-24-A).

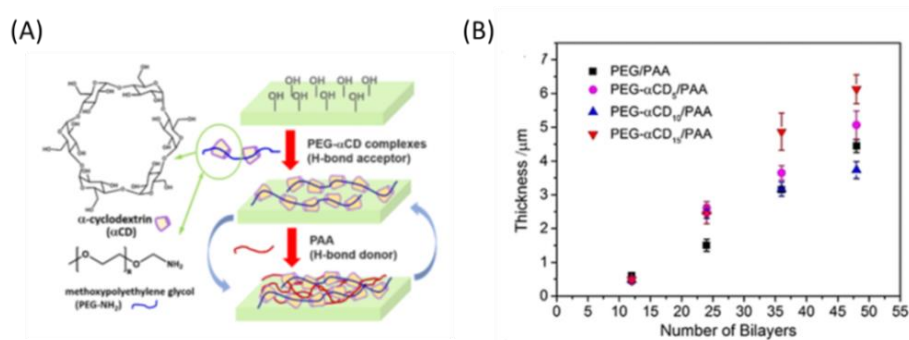


Figure 1-24 (A) The PEG- α CD complex structure and the LbL deposition process of PEG- α CD/PAA multilayer film; (B) Thickness of the LbL films versus deposition cycles, PEG- α CD₅, PEG- α CD₁₀, and PEG- α CD₁₅ stand for the different ratios of EG unit to α CD (5:1, 10:1, and 15:1).¹²⁶

In their work, (PEG)- α -cyclodextrin (α CD) (PEG- α CD) was obtained firstly by supramolecular interactions between amine groups modified PEG and α CD, used as H-bond acceptors. PEG- α CD complexes with three different ratios of EG unit to α CD (5:1, 10:1, and 15:1, which were denoted as PEG- α CD₅, PEG- α CD₁₀, and PEG- α CD₁₅, respectively) and were used to fabricate multilayer films with PAA driven by hydrogen bonding between carboxyl groups of protonated PAA and ether oxygen atoms of PEG backbone (Figure 1-24-A). Figure 1-24-B shows the evolution of the thickness as a function of the deposited bilayers. It can be seen that the thickness of the PEG- α CD₁₅ containing film exhibits a linear growth behavior as the deposition cycle increases, while both the PEG- α CD₅ and PEG- α CD₁₀ films show retarded growth. The presence of α CD may contribute to loopy packed films compared to the free PAA/PEG system which shows a low growth rate. The authors argued that α CD

are randomly distributed on PEG backbone, which can cause a strong steric effect between different layers and can result in unstable growth on film thickness as the deposition cycle increases.

Lignin derivatives/Poly(4-vinylpyridine) (P4VP) film

A lignin-based polymer (GCL1-JB) was prepared by graft sulfonation of alkali lignin from bamboo pulp black liquor.¹⁷⁴ This lignin-based polymer (GCL1-JB) has carboxylic and hydroxyl groups and can be used as H-bond donor in LbL assembly. The use of different solvent for each polymer partner was reported by Deng *et al.*¹⁵⁸ who prepared LbL self-assembled films of carboxylic acid containing lignin (GCL1-JB) and P4VP by dipping an amine-modified quartz slide alternately into water for H-bond donor (GCL1-JB) and methanol for H-bond acceptor (P4VP) (Figure 1-25-A).

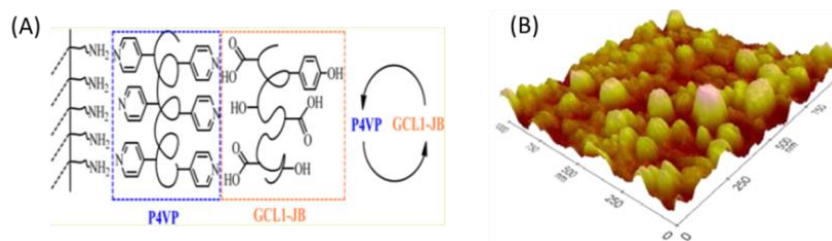


Figure 1-25 (A) Scheme of GCL1-JB/P4VP LbL self-assembled films based on hydrogen bonding interaction; (B) AFM image of GCL1-JB/P4VP-10 bilayers films.¹⁵⁸

The LbL process of GCL1-JB/P4VP films was monitored by UV-vis spectroscopy, some results are shown in Figure 1-26.

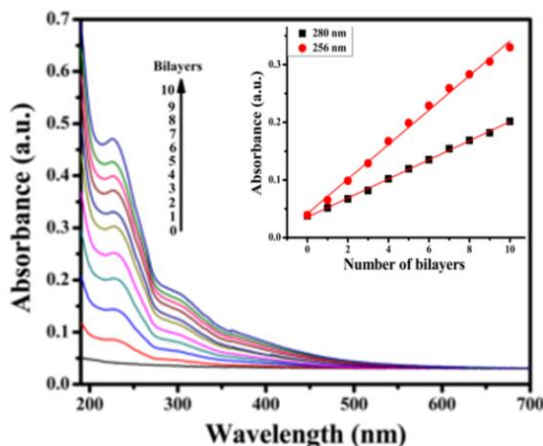


Figure 1-26 UV-vis spectra of GCL1-JB/P4VP self-assembled films as a function of bilayers. The dipping solutions were 1.0 g/L GCL1-JB in water and 1.0 g/L P4VP in methanol. Inset: The absorbance at λ 280 nm and λ 256 nm of GCL1-JB/P4VP self-assembled films versus number of bilayers. ¹⁵⁸

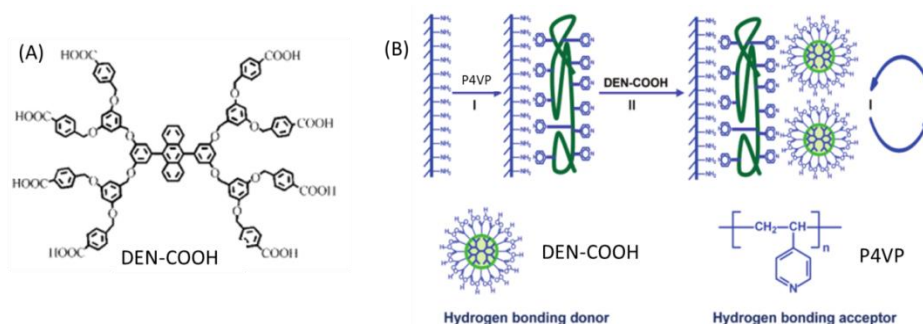
Globally, the absorbance of GCL1-JB/P4VP self-assembled films rises with the number of bilayers, indicating that the adsorption amount of GCL1-JB/P4VP self-assembled films increases. GCL1-JB and P4VP have characteristic absorbance at 280 nm and 256 nm, respectively. A linear increase of the absorbance at 280 nm and 256 nm (insert Figure 1-26) was observed, which means that the buildup of the film follows a regular thickness increase. The surface morphology was analyzed by AFM (Figure 1-25-B). Particles can be observed from the surface 3D image which indicates that the surface of GCL1-JB/P4VP self-assembled films after 10 bilayers is rough ($R_q = 4.03$ nm). Then, the authors prepared the GCL1-JB/PDMAC LbL self-assembled films based on electrostatic interaction by using 0.1 mmol/L PDMAC water solutions to replace the P4VP solution. Compared to the GCL1-JB self-assembled films based on electrostatic interactions, the authors demonstrated that the GCL1-JB self-assembled films with P4VP based on H-bonds have a larger adsorption amount due to the faster adsorption transfer rate from the dipping solution to the substrate surface.

DEN-COOH/P4VP film

The effect of organic solvent on the construction of multilayer films has been

explored by Zhang and co-workers.^{136,175,176} It was described the impact of the composition of ethanol/DMF on the stability of multilayer films of P4VP/poly(vinylphenol) (PVPh) and demonstrated that increasing the amount of DMF in the mixed solvents results in a marked decrease of the amount of polymers adsorbed on the substrate which is attributed to the increased polarity of the adsorption solutions.¹³⁶

As for $-\text{COOH}$ containing polymers, the authors¹⁷⁶ prepared multilayers of carboxylated dendrimers (DEN-COOH) with P4VP via LbL assembly (Scheme 1-49-A) from methanol solutions.



Scheme 1-49 (A) Chemical structure of DEN-COOH; (B) schematics of the LbL assembly of P4VP and DEN-COOH on a quartz substrate: (I) adsorption of P4VP and (II) adsorption of DEN-COOH.¹⁷⁶

The chemical structure of DEN-COOH used in their work is shown in Scheme 1-49-A. The quartz slide (for UV-vis analysis) and CaF_2 plate (for FTIR analysis) were modified with $-\text{NH}_2$ and poly(ethyleneimine) (PEI), respectively, before LbL deposition. Multilayer films were prepared by the alternate immersion of the substrates into methanol solutions. The UV-vis spectra of multilayer films are shown in Figure 1-27-A.

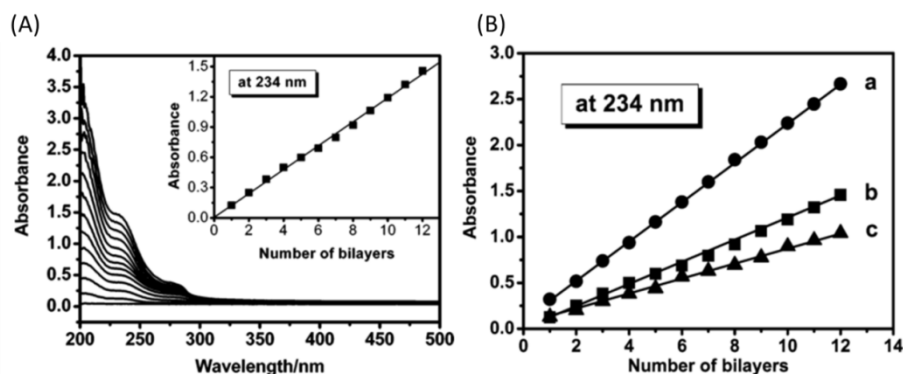


Figure 1-27 (A) UV-vis spectra of $(\text{P4VP/DEN-COOH})_n$ multilayer films with $n = 0-12$ on NH_2 -modified quartz substrates. Inset: absorbance at 234 nm versus the number of deposition cycles. (B) Influence of the concentration on the UV absorption (at 234 nm) against the number of deposition cycles. (a, $[\text{P4VP}] = 1 \text{ mg/mL}$, $[\text{DEN}] = 0.16 \text{ mg/mL}$); (b, $[\text{P4VP}] = 1 \text{ mg/mL}$, $[\text{DEN}] = 0.08 \text{ mg/mL}$); (c, $[\text{P4VP}] = 0.5 \text{ mg/mL}$, $[\text{DEN}] = 0.08 \text{ mg/mL}$).¹⁷⁶

The characteristic peaks at 234 and 281 nm are assigned to the π - π^* transition of the benzene ring of DEN-COOH, demonstrating the incorporation of DEN-COOH molecules into the multilayers. The authors cannot assign a unique absorption band solely to P4VP, due to the overlapping of the spectra. The inset of Figure 1-27-A shows that the absorbance at 234 nm increases proportionally with the number of deposition cycles which indicates that an approximately equal amount of DEN-COOH is deposited for each adsorption procedure, and that the P4VP/DEN-COOH LbL films grow uniformly along the deposition cycles. However, the observed growth at 281 nm is non linear which can account for the formation of DEN-COOH aggregates within the multilayer.

The authors also examined the dependence of the concentration of DEN-COOH and P4VP solutions on the adsorption behavior. The thickness versus concentration is shown in Figure 1-27-B. It is found that the amount of DEN-COOH adsorbed per bilayer increases with the concentration of DEN-COOH (Figure 1-27-B-a and b). When the concentration of P4VP rises 0.5 (Figure 1-27-B-c) to 1.0 mg/mL (Figure 1-27-B-b), the adsorbed amount of the DEN-COOH is also increases. The driving force for the construction of the P4VP/DEN-COOH multilayer film was identified by FT-IR spectroscopy (Figure 1-28-A).

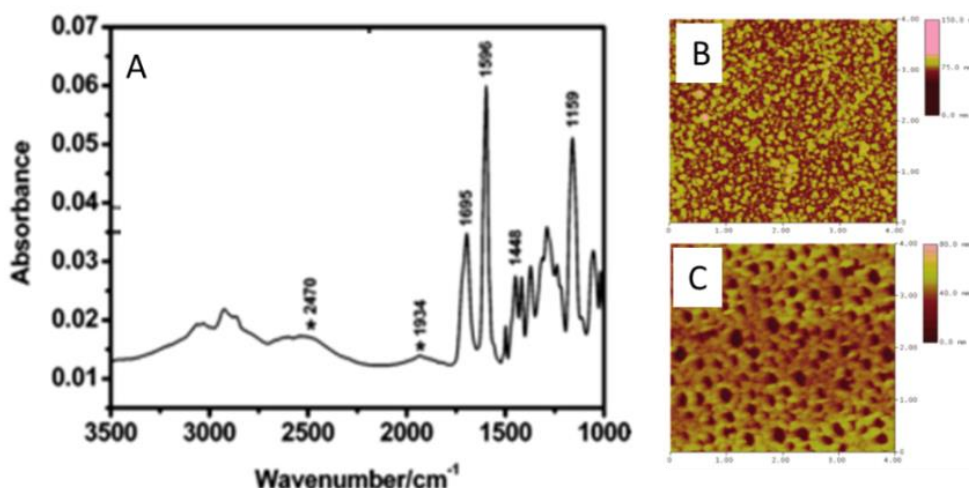


Figure 1-28 (A) FT-IR spectrum of a (P4VP/DEN-COOH)_{n=8} multilayer film on a PEI-modified CaF₂ plate; AFM height images of (P4VP/DEN-COOH)_{n=14} multilayer films on a quartz substrate after immersion in a pH = 12.5 NaOH aqueous solution at 25 °C for 10 (B) and 180 min (C).¹⁷⁶

It can be seen clearly that an O-H stretching vibration appears at 2470 and 1934 cm⁻¹, indicating H-bonds between the carboxylic acid of DEN-COOH and the pyridine groups of P4VP. The morphology variation of the P4VP/DEN-COOH multilayer film in a basic aqueous solution was explored by using AFM. After an immersion in basic solutions for 10 min, the surface of the multilayer film is rough and highly covered with granular structures (Figure 1-28-B). After immersing into basic solutions for 180 min, the micropores on the surface with the diameter of 380 nm and depth of 36 nm are observed (Figure 1-28-C). The authors suggested that DEN-COOH is removed rapidly by the basic solution and the morphology variation would thus be the result of the reconfiguration of P4VP at the surface.

PAA/P4VP film

With the same strategy as DEN-COOH/PAA film, the same group used methanol as solvent to fabricate H-bonded LbL films of PAA/P4VP.¹⁷⁵ As shown in Figure 1-29, both the UV-vis absorbance at 256 nm and the thickness of the film increase linearly with the number of layer pairs, which indicates that the LbL assembly process under the present conditions is uniform.

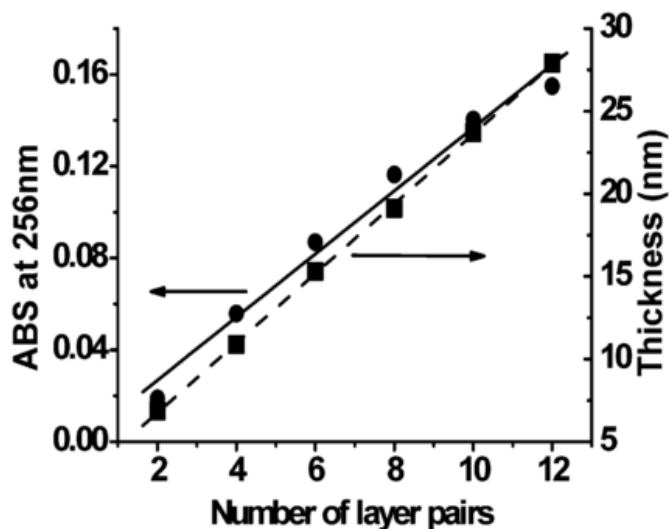


Figure 1-29 Growth of the UV-vis absorbance at 256 nm (donated by circle, fitted by solid line) and the thickness calculated from X-ray patterns (donated by square, fitted by dash line) of PAA/P4VP LbL films as a function of the number of layer pairs.¹⁷⁵

A small thickness around 26 nm for 12 deposited bilayers was obtained. Then the authors investigated the influence of a basic aqueous solution on the change of film composition. Microporous film can be produced by a prolonged immersion of the LbL film in a basic solution (Figure 1-30).

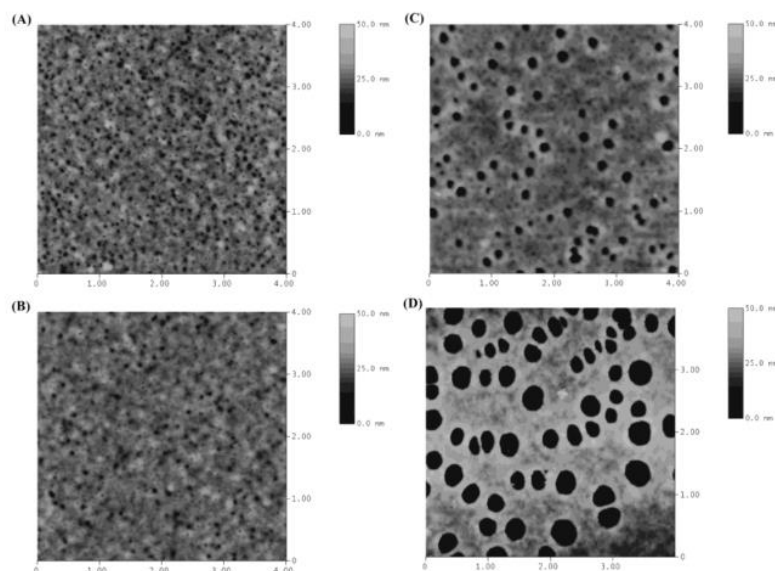


Figure 1-30 AFM height images ($4 \mu\text{m} \times 4 \mu\text{m}$) of 25-layer PAA/P4VP LbL films after immersion in pH = 12.5 NaOH aqueous solution at 25 °C for 10 (A), 40 (B), 140 (C), and 180 min (D).¹⁷⁵

The AFM images show a series of microporous films with different surface

coverage, depth, and shape of the holes. The spinodal holes, several hundred nanometers in diameter, grow with time. During immersion from 10 to 180 min, the coverage and depth of the holes increase from 10 to 30% and from approximately 12 to 35 nm, respectively. When the multilayer film is dipped into the basic aqueous solution, the carboxylic acid groups of PAA are ionized by the solution, which leads to a disruption of H-bond between the two polymers. Hence, PAA can be removed from the film because of its solubility in the basic solution, while P4VP remains due to its poor solubility in basic aqueous solution. The extended P4VP chains on the substrate are gradually folded, which induces a microporous ultrathin film.

PAA/poly(N-vinylpyrrolidone)(PVPON) film

Zhunuspayev *et al.*¹⁷⁷ studied the formation of multilayer film based on PAA and poly(N-vinylpyrrolidone)(PVPON) film prepared via LbL by using various deposition concentration and solvent (Figure 1-31).

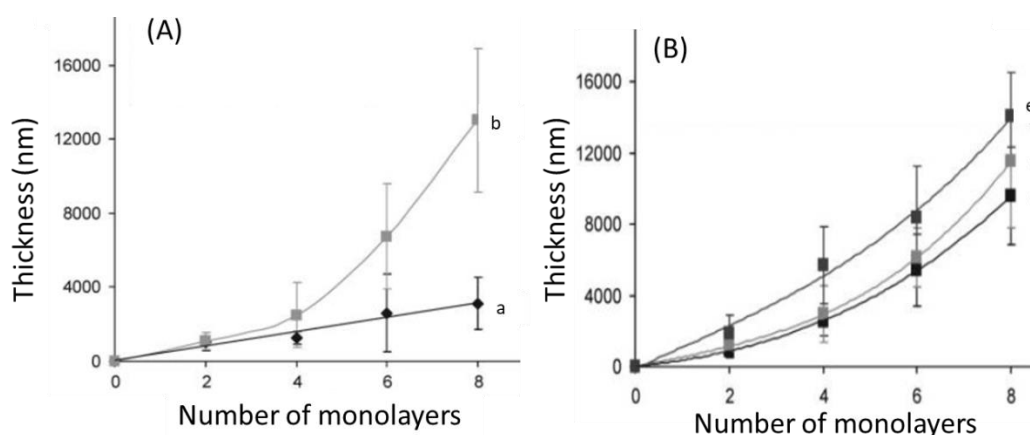


Figure 1-31 Thickness of H-bonded PAA/PVPON film formed from aqueous solution at pH 3.0 (A) at a concentration of 0.05 (a) or 0.1 (b) unit-base mol/L; from alcoholic solvent (B): methanol (c), ethanol (d) and isopropanol (e) at a concentration of 0.1 unit-base mol/L, as a function of the number of monolayers.¹⁷⁷

The authors used two different concentrations of polymers (0.05 and 0.1 unit-base mol/L) to study the impact on the resulting thickness evolution with the number of deposited monolayers (Figure 1-31-A) by using aqueous solution at pH 3.0. A linear growth thickness for the lower concentration is observed (0.05 unit-base

mol/L, Figure 1-31-A-a). At higher polymer concentrations (0.1 unit-base mol/L), this dependence is exponential (Figure 1-31-A-b). The authors suggested that a high concentration favors the aggregation of interpolymer complexes between PAA and PVPON on the glass surface. The formation of multilayered film on glass slides was also studied in methanol, ethanol and isopropanol. The growth thickness in these alcoholic solvent is exponential with the number of monolayers and the efficiency of deposition increases in the following order: methanol < ethanol < isopropanol which is agrees well with the intensity of complexation in solutions and coincides with a reduction in solvents dielectric constants: 33, 24.3 and 18, respectively.

Ma *et al.*¹⁷⁸ also studied the effect of solvent on the formation of the H-bonded PAA/PVPON film. It was demonstrated that the film can be produced in acidic water with a much quicker grow rate than that in alcohols, including methanol, ethanol and isopropanol. This is due to the fact that PAA and PVPON adopt much compact chain conformation in acidic water, compared with in alcoholic solvents. The formed thin films can be quickly disintegrated after immersion into high electric constant solvent, for example polar aprotic dimethylsulfoxide (DMSO). Moreover, it was reported that PAA/PVPON film cannot be fabricated in other polar aprotic solvents, such as dimethylacetamide (DMA), tetramethylurea (TMU) and N-methyl pyrrolidone (NMP) because of their strong interactions with polymers.

1.3.4 Conclusion

In summary, layer-by-layer (LbL) self-assembly is a powerful technique to fabricate multilayer films with controlled architecture and composition. Among the various driving forces for mediating LbL self-assembly, H-bonds mediated LbL self-assembly in aqueous solutions have undergone significant recent progress. However, there is still many fundamental features of H-bonded self-assembly that are left to be further explored, for example, the organic solvent effect on the growth mechanism and surface features of the water non-soluble polymers containing multilayer films.

1.4 References

- (1) Battioni, P.; Brigaud, O.; Desvaux, H.; Mansuy, D.; Traylor, T. G. Preparation of Functionalized Polyhalogenated Tetraaryl-Porphyrins by Selective Substitution of the P-Fluorines of Meso-Tetra-(Pentafluorophenyl)porphyrins. *Tetrahedron Lett.* **1991**, *32* (25), 2893–2896.
- (2) Kvičala, J.; Beneš, M.; Paleta, O.; Král, V. Regiospecific Nucleophilic Substitution in 2,3,4,5,6-Pentafluorobiphenyl as Model Compound for Supramolecular Systems. Theoretical Study of Transition States and Energy Profiles, Evidence for Tetrahedral SN2 Mechanism. *J. Fluor. Chem.* **2010**, *131* (12), 1327–1337.
- (3) Muir, M.; Baker, J. A Simple Computational Model for Predicting the Site for Nucleophilic Substitution in Aromatic Perfluorocarbons. *J. Fluor. Chem.* **2005**, *126* (5), 727–738.
- (4) Baker, J.; Muir, M. The Meisenheimer Model for Predicting the Principal Site for Nucleophilic Substitution in Aromatic Perfluorocarbons - Generalization to Include Ring-Nitrogen Atoms and Non-Fluorine Ring Substituents. *Can. J. Chem.* **2010**, *88* (7), 588–597.
- (5) Pitois, C.; Wiesmann, D.; Lindgren, M.; Hult, A. Functionalize Fluorinated Hyperbranched Polymers for Optical Waveguide Applications. *Adv. Mater.* **2001**, *13* (19), 1483–1487.
- (6) Coatings, A.; Imbesi, P. M.; Gohad, N. V.; Eller, M. J.; Orihuela, B.; Rittschof, D.; Schweikert, E. A.; Mount, A. S.; Wooley, K. L. Noradrenaline-Functionalized Hyperbranched Cross-Linked Networks As Dual-Fluoropolymer-Poly(ethylene Glycol) Mode, Anti-Biofouling Coatings. *ACS Nano* **2012**, *6* (2), 1503–1512.
- (7) Hvilsted, S.; Borkar, S.; Siesler, H. W.; Jankova, K. Novel Fluorinated Polymer Materials Based on 2,3,5,6-Tetrafluoro-4-Methoxystyrene. *ACS Symp. Ser.* **2003**, *854*, 236–249.
- (8) Borkar, S.; Jankova, K.; Siesler, H. W.; Hvilsted, S. New Highly Fluorinated

- Styrene-Based Materials with Low Surface Energy Prepared by ATRP. *Macromolecules* **2004**, *37* (3), 788–794.
- (9) Hvilsted, S.; Forcén, P.; Oriol, L.; Sánchez, C.; Alcalá, R.; Ramanujam, P. S. Novel Polymer Architectures for Optical Storage. In *Electroactive polymers : materials & devices*; 2007; Vol. II, pp 165–174.
- (10) Dimitrov, I.; Jankova, K.; Hvilsted, S. Synthesis and ATRP of Novel Fluorinated Aromatic Monomer with Pendant Sulfonate Group. *J. Fluor. Chem.* **2013**, *149*, 30–35.
- (11) Zhu, P.; Meng, W.; Huang, Y. Synthesis and Antibiofouling Properties of Crosslinkable Copolymers Grafted with Fluorinated Aromatic Side Chains. *RSC Adv.* **2017**, *7* (6), 3179–3189.
- (12) Valtola, L.; Koponen, A.; Karesoja, M.; Hietala, S.; Laukkanen, A.; Tenhu, H.; Denifl, P. Tailored Surface Properties of Semi-Fluorinated Block Copolymers by Electrospinning. *Polymer.* **2009**, *50* (14), 3103–3110.
- (13) Ma, J.; Cheng, C.; Wooley, K. L. Cycloalkenyl-Functionalized Polymers and Block Copolymers: Syntheses via Selective Raft Polymerizations and Demonstration of Their Versatile Reactivity. *Macromolecules* **2009**, *42* (5), 1565–1573.
- (14) Martinelli, E.; Hill, S. D.; Finlay, J. A.; Callow, M. E.; Callow, J. A.; Glisenti, A.; Galli, G. Amphiphilic Modified-Styrene Copolymer Films: Antifouling/fouling Release Properties against the Green Alga *Ulva Linza*. *Prog. Org. Coatings* **2016**, *90*, 235–242.
- (15) Jun, M.; Cheng, C.; Sun, G.; Wooley, K. L. Well-Defined Polymers Bearing Pendant Alkene Functionalities via Selective RAFT Polymerization. *Macromolecules* **2008**, *41* (23), 9080–9089.
- (16) Powell, K. T.; Cheng, C.; Wooley, K. L. Complex Amphiphilic Hyperbranched Fluoropolymers by Atom Transfer Radical Self-Condensing Vinyl (Co)polymerization. *Macromolecules* **2007**, *40* (13), 4509–4515.
- (17) Ott, C.; Hoogenboom, R.; Schubert, U. S. Post-Modification of Poly(pentafluorostyrene): A Versatile “click” method to Create Well-Defined

- Multifunctional Graft Copolymers. *Chem. Commun.* **2008**, No. 30, 3516–3518.
- (18) Hussain, H.; Tan, B. H.; Mya, K. Y.; Liu, Y.; He, C. B.; Davis, T. P. Synthesis, Micelle Formation and Bulk Properties of Poly(ethylene Glycol)-b-Poly(pentafluorostyrene)-G-Polyhedral Oligomeric Silsesquioxane Amphiphilic Hybrid Copolymers. *J. Polym. Sci. Part A Polym. Chem.* **2010**, *48* (1), 152–163.
- (19) Becer, C. R.; Kokado, K.; Weber, C.; Can, A.; Chujo, Y.; Schubert, U. S. Metal-Free Synthesis of Responsive Polymers: Cloud Point Tuning by Controlled “click” Reaction. *J. Polym. Sci. Part A Polym. Chem.* **2010**, *48* (6), 1278–1286.
- (20) Babiuch, K.; Becer, C. R.; Gottschaldt, M.; Delaney, J. T.; Beer, B.; Wyrwa, R.; Schnabelrauch, M.; Schubert, U. S. Adhesion of Preosteoblasts and Fibroblasts onto Poly(Pentafluorostyrene)-Based Glycopolymers and Their Biocompatibility. *Macromol. Biosci.* **2011**, *11* (4), 535–548.
- (21) Álvarez-Paino, M.; Muñoz-Bonilla, A.; Marcelo, G.; Rodríguez-Hernández, J.; Fernández-García, M. Synthesis and Lectin Recognition Studies of Glycosylated Polystyrene Microspheres Functionalized via Thiol-para-Fluorine “click” Reaction. *Polym. Chem.* **2012**, *3* (12), 3282.
- (22) Jin, Y.; Wong, K. H.; Granville, A. M. Enhancement of Localized Surface Plasmon Resonance Polymer Based Biosensor Chips Using Well-Defined Glycopolymers for Lectin Detection. *J. Colloid Interface Sci.* **2016**, *462*, 19–28.
- (23) Chen, J.; Dumas, L.; Duchet-Rumeau, J.; Fleury, E.; Charlot, A.; Portinha, D. Tuning H-Bond Capability of Hydroxylated-poly(2,3,4,5,6-Pentafluorostyrene) Grafted Copolymers Prepared by Chemoselective and Versatile Thiol-Para-Fluoro “click-Type” coupling with Mercaptoalcohols. *J. Polym. Sci. Part A Polym. Chem.* **2012**, *50* (16), 3452–3460.
- (24) Varadharajan, D.; Delaittre, G. Accessing Libraries of Bifunctional Block Copolymers Using Distinct Pentafluorophenyl Moieties. *Polym. Chem.* **2016**, *7* (48), 7488–7499.

- (25) Valtola, L.; Karesoja, M.; Tenhu, H.; Ihalainen, P.; Sarfraz, J.; Peltonen, J.; Malinen, M.; Urtti, A.; Hietala, S. Breath Figure Templated Semifluorinated Block Copolymers with Tunable Surface Properties and Binding Capabilities. *J. Appl. Polym. Sci.* **2014**, *132* (1), 1–9.
- (26) Cai, T.; Yang, W. J.; Neoh, K.-G.; Kang, E.-T. Preparation of Jellyfish-Shaped Amphiphilic Block-Graft Copolymers Consisting of a Poly(ϵ -Caprolactone)-Block-Poly(pentafluorostyrene) Ring and Poly(ethylene Glycol) Lateral Brushes. *Polym. Chem.* **2012**, *3* (4), 1061–1068.
- (27) Becer, C. R.; Babiuch, K.; Pilz, D.; Hornig, S.; Heinze, T.; Gottschaldt, M.; Schubert, U. S. Clicking Pentafluorostyrene Copolymers: Synthesis, Nanoprecipitation, and Glycosylation. *Macromolecules* **2009**, *42* (7), 2387–2394.
- (28) Babiuch, K.; Pretzel, D.; Tolstik, T.; Vollrath, A.; Stanca, S.; Foertsch, F.; Becer, C. R.; Gottschaldt, M.; Biskup, C.; Schubert, U. S. Uptake of Well-Defined, Highly Glycosylated, Pentafluorostyrene-Based Polymers and Nanoparticles by Human Hepatocellular Carcinoma Cells. *Macromol. Biosci.* **2012**, *12* (9), 1–10.
- (29) De León, A. S.; Del Campo, A.; Labrugère, C.; Fernández-García, M.; Muñoz-Bonilla, A.; Rodríguez-Hernández, J. Control of the Chemistry Outside the Pore in Honeycomb Patterned Films. *Polym. Chem.* **2013**, *4* (14), 4024–4032.
- (30) De León, A. S.; Del Campo, A.; Fernández-García, M.; Rodríguez-Hernández, J.; Muñoz-Bonilla, A. Fabrication of Structured Porous Films by Breath Figures and Phase Separation Processes: Tuning the Chemistry and Morphology Inside the Pores Using Click Chemistry. *ACS Appl. Mater. Interfaces* **2013**, *5* (9), 3943–3951.
- (31) Fan, K.; Granville, A. Surface Property Modification of Silver Nanoparticles with Dopamine-Functionalized Poly(pentafluorostyrene) via RAFT Polymerization. *Polymers (Basel)*. **2016**, *8* (3), 81–92.
- (32) Kim, K.; An, T. K.; Kim, J.; Jeong, Y. J.; Jang, J.; Kim, H.; Baek, J. Y.; Kim,

- Y. H.; Kim, S. H.; Park, C. E. Grafting Fluorinated Polymer Nanolayer for Advancing the Electrical Stability of Organic Field-Effect Transistors. *Chem. Mater.* **2014**, *26* (22), 6467–6476.
- (33) Nenov, S.; Hoffmann, M. S.; Steffen, W.; Klapper, M.; Müllen, K. Fluorous Miniemulsions: A Powerful Tool to Control Morphology in Metallocene-Catalyzed Propene Polymerization. *J. Polym. Sci. Part A Polym. Chem.* **2009**, *47* (6), 1724–1730.
- (34) Schuster, T.; Golling, F. E.; Krumpfer, J. W.; Wagner, M.; Graf, R.; Alsaygh, A. A.; Klapper, M.; Mullen, K. Poly(isobutylene) Nanoparticles via Cationic Polymerization in Nonaqueous Emulsions. *Macromol Rapid Commun* **2015**, *36* (2), 204–210.
- (35) Bhebhe, M. N.; De Eulate, E. A.; Pei, Y.; Arrigan, D. W. M.; Roth, P. J.; Lowe, A. B. Reactive Conjugated Polymers: Synthesis, Modification, and Electrochemical Properties of Polypentafluorophenylacetylene (Co)Polymers. *Macromol. Rapid Commun.* **2017**, *38* (2), 1600450–1600456.
- (36) Noy, J.-M.; Friedrich, A.; Batten, K.; Bhebhe, M. N.; Busatto, N.; Batchelor, R. R.; Kristanti, A.; Pei, Y.; Roth, P. J. Para-Fluoro Postpolymerization Chemistry of Poly(pentafluorobenzyl Methacrylate): Modification with Amines, Thiols, and Carbonylthiolates. *Macromolecules* **2017**, *50* (18), 7028–7040.
- (37) Noy, J.-M.; Koldevitz, M.; Roth, P. J. Thiol-Reactive Functional Poly(meth)acrylates: Multicomponent Monomer Synthesis, RAFT (Co)polymerization and Highly Efficient Thiol-Para-Fluoro Postpolymerization Modification. *Polym. Chem.* **2015**, *6* (3), 436–447.
- (38) Cakir, N.; Tunca, U.; Hizal, G.; Durmaz, H. Heterofunctionalized Multiarm Star Polymers via Sequential Thiol-Para-Fluoro and Thiol-Ene Double “click” Reactions. *Macromol. Chem. Phys.* **2016**, *217* (5), 636–645.
- (39) Boufflet, P.; Casey, A.; Xia, Y.; Stavrinou, P. N.; Heeney, M. Pentafluorobenzene End-Group as a Versatile Handle for Para Fluoro “click” Functionalization of Polythiophenes. *Chem. Sci.* **2017**, *8*, 2215–2225.
- (40) Giannopoulos, P.; Nikolakopoulou, A.; Andreopoulou, A. K.; Sygellou, L.;

- Kallitsis, J. K.; Lianos, P. An Alternative Methodology for Anchoring Organic Sensitizers onto TiO₂ Semiconductors for Photoelectrochemical Applications. *J. Mater. Chem. A* **2014**, 2 (48), 20748–20759.
- (41) Quast, M. J.; Mueller, A. Hyperbranched Polyfluorinated Benzyl Ether Polymers: Mechanism, Kinetics, and Optimization. *J. Polym. Sci. Part A Polym. Chem.* **2014**, 52 (7), 985–994.
- (42) Barner, L.; Cavalli, F.; Mutlu, H.; Steinmueller, S. O. The Para-Fluoro-Thiol Reaction as a Powerful Tool for Precision Network Synthesis. *Polym. Chem.* **2017**, 8 (25), 3778–3782.
- (43) Wild, A.; Winter, A.; Hager, M. D.; Görls, H.; Schubert, U. S. Perfluorophenyl-Terpyridine Ruthenium Complex as Monomer for Fast, Efficient, and Mild Metallopolymerizations. *Macromol. Rapid Commun.* **2012**, 33 (6–7), 517–521.
- (44) Gudipati, C. S.; Creenlief, C. M.; Johnson, J. A.; Prayoncpn, P.; Wooley, K. L. Hyperbranched Fluoropolymer and Linear Poly(ethylene Glycol) Based Amphiphilic Crosslinked Networks as Efficient Antifouling Coatings: An Insight into the Surface Compositions, Topographies, and Morphologies. *J. Polym. Sci. Part A Polym. Chem.* **2004**, 42 (24), 6193–6208.
- (45) Bartels, J. W.; Cheng, C.; Powell, K. T.; Xu, J.; Wooley, K. L. Hyperbranched Fluoropolymers and Their Hybridization into Complex Amphiphilic Crosslinked Copolymer Networks. *Macromol. Chem. Phys.* **2007**, 208 (15), 1676–1687.
- (46) Ober, K.; Douki, K.; Vohra, V. R.; Kwark, Y.; Conley, W.; Miller, D.; Zimmerman, P. New Strategies for High Resolution Photoresists. *J. Photopolym. Sci. Technol.* **2002**, 15 (4), 603–611.
- (47) Hvilsted, S. The Pentafluorostyrene Endeavours with Atom Transfer Radical Polymerization-Quo Vadis? *Polym. Int.* **2014**, 63 (5), 814–823.
- (48) Lu, W.; An, X.; Gao, F.; Zhu, J.; Zhou, N.; Zhang, Z.; Pan, X.; Zhu, X. Highly Efficient Chain End Derivatization of Selenol-Ended Polystyrenes by Nucleophilic Substitution Reactions. *Macromol. Chem. Phys.* **2017**, 218 (4), 1–

- 7.
- (49) Turgut, H.; Delaittre, G. On the Orthogonality of Two Thiol-Based Modular Ligations. *Chem. Eur.J.* **2016**, *22* (4), 1511–1521.
- (50) Turgut, H.; Schmidt, A. C.; Wadhvani, P.; Welle, A.; Müller, R.; Delaittre, G. The Para-Fluoro–Thiol Ligation in Water. *Polym. Chem.* **2017**, *8* (8), 1288–1293.
- (51) Dumas, L.; Fleury, E.; Portinha, D. Wettability Adjustment of PVDF Surfaces by Combining Radiation-Induced Grafting of (2,3,4,5,6)-Pentafluorostyrene and Subsequent Chemoselective “click-Type” Reaction. *Polymer.* **2014**, *55* (11), 2628–2634.
- (52) Chen, J.; Duchet, J.; Portinha, D.; Charlot, A. Layer by Layer H-Bonded Assembly of P4VP with Various Hydroxylated PPFS: Impact of the Donor Strength on Growth Mechanism and Surface Features. *Langmuir* **2014**, *30* (35), 10740–10750.
- (53) Atanasov, V.; Kerres, J. Highly Phosphonated Polypentafluorostyrene. *Macromolecules* **2011**, *44* (16), 6416–6423.
- (54) Atanasov, V.; Kerres, J. ETFE-G-Pentafluorostyrene: Functionalization and Proton Conductivity. *Eur. Polym. J.* **2015**, *63*, 168–176.
- (55) Atanasov, V.; Bürger, M.; Lyonnard, S.; Porcar, L.; Kerres, J. Sulfonated Poly(pentafluorostyrene): Synthesis & Characterization. *Solid State Ionics* **2013**, *252*, 75–83.
- (56) Jisr, R. M.; Rmaile, H. H.; Schlenoff, J. B. 7- Hydrophobic and Ultrahydrophobic Multilayer Thin Films from Perfluorinated Polyelectrolytes. *Angew. Chemie - Int. Ed.* **2005**, *44* (5), 782–785.
- (57) Babiuch, K.; Wyrwa, R.; Wagner, K.; Seemann, T.; Hoepfner, S.; Becer, C. R.; Linke, R.; Gottschaldt, M.; Weisser, J.; Schnabelrauch, M.. Functionalized, Biocompatible Coating for Superparamagnetic Nanoparticles by Controlled Polymerization of a Thioglycosidic Monomer. *Biomacromolecules* **2011**, *12* (3), 681–691.
- (58) Martinelli, E.; Pelusio, G.; Yasani, B. R.; Glisenti, A. Surface Chemistry of

- Amphiphilic Polysiloxane/Triethyleneglycol-Modified Poly (Pentafluorostyrene) Block Copolymer Films Before and After Water Immersion. *Macromol. Chem. Phys.* **2015**, No. 216, 2086–2094.
- (59) THEATO, P.; KLOK, H.-A. Functional Polymers by Post-Polymerization Modification: Concepts, Guidelines and Applications. In *John Wiley & Sons*; 2013.
- (60) Chen, J.; Vuluga, D.; Crousse, B.; Legros, J.; Duchet-Rumeau, J.; Charlot, A.; Portinha, D. Polyfluorinated Mercaptoalcohol as a H-Bond Modifier of poly(2,3,4,5,6-Pentafluorostyrene) (PPFS) Enhancing Miscibility of Hydroxylated-PPFS with Various Acceptor Polymers. *Polymer*. **2013**, *54* (15), 3757–3766.
- (61) Ting, S. R. S.; Chen, G.; Stenzel, M. H. Synthesis of Glycopolymers and Their Multivalent Recognitions with Lectins. *Polym. Chem.* **2010**, *1* (9), 1392.
- (62) Dimitrov, I.; Takamuku, S.; Jankova, K.; Jannasch, P.; Hvilsted, S. Proton Conducting Graft Copolymers with Tunable Length and Density of Phosphonated Side Chains for Fuel Cell Membranes. *J. Memb. Sci.* **2014**, *450*, 362–368.
- (63) Dimitrov, I.; Takamuku, S.; Jankova, K.; Jannasch, P.; Hvilsted, S. Polysulfone Functionalized with Phosphonated Poly(pentafluorostyrene) Grafts for Potential Fuel Cell Applications. *Macromol. Rapid Commun.* **2012**, *33* (16), 1368–1374.
- (64) Shao, Z.; Sannigrahi, A.; Jannasch, P. Poly(tetrafluorostyrenephosphonic Acid)-Polysulfone Block Copolymers and Membranes. *J. Polym. Sci. Part A Polym. Chem.* **2013**, *51* (21), 4657–4666.
- (65) Atanasov, V.; Oleynikov, A.; Xia, J.; Lyonnard, S.; Kerres, J. Phosphonic Acid Functionalized Poly(pentafluorostyrene) as Polyelectrolyte Membrane for Fuel Cell Application. *J. Power Sources* **2017**, *343*, 364–372.
- (66) Young, T. An Essay on the Cohesion of Fluids. Thomas Young Source: Philosophical Transactions of the Royal Society of London, Vol. 95 (1805), Pp. 65-87 Published By: *Philos. Trans. R. Soc. London* **1805**, *95* (1805), 65–87.

- (67) Neinhuis, C.; Barthlott, W. Characterization and Distribution of Water-Repellent, Self-Cleaning Plant Surfaces. *Ann. Bot.* **1997**, *79* (6), 667–677.
- (68) Barthlott, W.; Neinhuis, C. Purity of the Sacred Lotus, or Escape from Contamination in Biological Surfaces. *Planta* **1997**, *202* (1), 1–8.
- (69) McHale, G.; Shirtcliffe, N. J.; Newton, M. I. Contact-Angle Hysteresis on Super-Hydrophobic Surfaces. *Langmuir* **2004**, *20* (23), 10146–10149.
- (70) Kiuru, M.; Alakoski, E. Low Sliding Angles in Hydrophobic and Oleophobic Coatings Prepared with Plasma Discharge Method. *Mater. Lett.* **2004**, *58* (16), 2213–2216.
- (71) Miwa, M.; Nakajima, A.; Fujishima, A.; Hashimoto, K.; Watanabe, T. Effects of the Surface Roughness on Sliding Angles of Water Droplets on Superhydrophobic Surfaces. *Langmuir* **2000**, *16* (13), 5754–5760.
- (72) Bhushan, B.; Her, E. K. Fabrication of Superhydrophobic Surfaces with High and Low Adhesion Inspired from Rose Petal. *Langmuir* **2010**, *26* (11), 8207–8217.
- (73) Nine, M. J.; Tung, T. T.; Alotaibi, F.; Tran, D. N. H.; Losic, D. Facile Adhesion-Tuning of Superhydrophobic Surfaces between “Lotus” and “Petal” Effect and Their Influence on Icing and Deicing Properties. *ACS Appl. Mater. Interfaces* **2017**, *9* (9), 8393–8402.
- (74) Nosonovsky, M.; Bhushan, B. Green Tribology: Biomimetics, Energy Conservation and Sustainability. *Green Energy Technol.* **2012**, *49*, 25–40.
- (75) Wenzel, R. N. Resistance of Solid Surfaces to Wetting by Water. *J. Ind. Eng. Chem. (Washington, D. C.)* **1936**, *28*, 988–994.
- (76) Cassie, A. B. D.; Baxter, S. Wettability of Porous Surfaces. *Trans. Faraday Soc.* **1944**, *40*, 546–551.
- (77) Li, X.-M.; Reinhoudt, D.; Crego-Calama, M. What Do We Need for a Superhydrophobic Surface? A Review on the Recent Progress in the Preparation of Superhydrophobic Surfaces. *Chem. Soc. Rev.* **2007**, *36* (8), 1350–1368.

- (78) Feng, X.; Jiang, L. Design and Creation of Superwetting/antiwetting Surfaces. *Adv. Mater.* **2006**, *18* (23), 3063–3078.
- (79) Su, B.; Tian, Y.; Jiang, L. Bioinspired Interfaces with Superwettability: From Materials to Chemistry. *J. Am. Chem. Soc.* **2016**, *138* (6), 1727–1748.
- (80) Patankar, N. A. Mimicking the Lotus Effect: Influence of Double Roughness Structures and Slender Pillars. *Langmuir* **2004**, *20* (19), 8209–8213.
- (81) Roach, P.; Shirtcliffe, N. J.; Newton, M. I. Progress in Superhydrophobic Surface Development. *Soft Matter* **2008**, *4* (2), 224–240.
- (82) Wen, Q.; Guo, Z. Recent Advances in the Fabrication of Superhydrophobic Surfaces. *Chem. Lett.* **2016**, *45* (10), 1134–1149.
- (83) Scarratt, L. R. J.; Steiner, U.; Neto, C. A Review on the Mechanical and Thermodynamic Robustness of Superhydrophobic Surfaces. *Adv. Colloid Interface Sci.* **2017**, *246*, 133–152.
- (84) Sun, M.; Luo, C.; Xu, L.; Ji, H.; Ouyang, Q.; Yu, D.; Chen, Y. Artificial Lotus Leaf by Nanocasting. *Langmuir* **2005**, *21* (19), 8978–8981.
- (85) Gang Zhang, Dayang Wang, Zhong-Ze Gu, and H. M. Fabrication of Superhydrophobic Surfaces from Binary Colloidal Assembly. *Langmuir* **2005**, *21* (20), 9143–9148.
- (86) Xie, Q.; Fan, G.; Zhao, N.; Guo, X.; Xu, J.; Dong, J.; Zhang, L.; Zhang, Y.; Han, C. C. Facile Creation of a Bionic Super-Hydrophobic Block Copolymer Surface. *Adv. Mater.* **2004**, *16* (20), 1830–1833.
- (87) Agarwal, S.; Horst, S.; Bognitzki, M. Electrospinning of Fluorinated Polymers: Formation of Superhydrophobic Surfaces. *Macromol. Mater. Eng.* **2006**, *291* (6), 592–601.
- (88) Kothary, P.; Dou, X.; Fang, Y.; Gu, Z.; Leo, S. Y.; Jiang, P. Superhydrophobic Hierarchical Arrays Fabricated by a Scalable Colloidal Lithography Approach. *J. Colloid Interface Sci.* **2017**, *487*, 484–492.
- (89) Teshima, K.; Sugimura, H.; Inoue, Y.; Takai, O.; Takano, A. 4-Wettability of Poly(ethylene Terephthalate) Substrates Modified by a Two-Step Plasma Process: Ultra Water-Repellent Surface Fabrication. *Chem. Vap. Depos.* **2004**,

- 10 (6), 295–297.
- (90) Fresnais, J.; Benyahia, L.; Poncin-Epaillard, F. Dynamic (De)wetting Properties of Superhydrophobic Plasma-Treated Polyethylene Surfaces. *Surf. Interface Anal.* **2006**, *38* (c), 1380–1385.
- (91) Cao, M.; Guo, D.; Yu, C.; Li, K.; Liu, M.; Jiang, L. Water-Repellent Properties of Superhydrophobic and Lubricant-Infused “slippery” Surfaces: A Brief Study on the Functions and Applications. *ACS Appl. Mater. Interfaces* **2016**, *8* (6), 3615–3623.
- (92) Basu, B. J.; Dinesh Kumar, V.; Anandan, C. Surface Studies on Superhydrophobic and Oleophobic Polydimethylsiloxane-Silica Nanocomposite Coating System. *Appl. Surf. Sci.* **2012**, *261*, 807–814.
- (93) Yilgor, I.; Bilgin, S.; Isik, M.; Yilgor, E. Facile Preparation of Superhydrophobic Polymer Surfaces. *Polymer* **2012**, *53* (6), 1180–1188.
- (94) Lau, K. K. S.; Bico, J.; Teo, K. B. K.; Chhowalla, M.; Amaratunga, G. A. J.; Milne, W. I.; McKinley, G. H.; Gleason, K. K. Superhydrophobic Carbon Nanotube Forests. *Nano Lett.* **2003**, *3* (12), 1701–1705.
- (95) Basu, B. B. J.; Paranthaman, A. K. A Simple Method for the Preparation of Superhydrophobic PVDF-HMFS Hybrid Composite Coatings. *Appl. Surf. Sci.* **2009**, *255* (8), 4479–4483.
- (96) Zhou, H.; Wang, H.; Niu, H.; Gestos, A.; Lin, T. Robust, Self-Healing Superamphiphobic Fabrics Prepared by Two-Step Coating of Fluoro-Containing Polymer, Fluoroalkyl Silane, and Modified Silica Nanoparticles. *Adv. Funct. Mater.* **2013**, *23* (13), 1664–1670.
- (97) Honda, K.; Morita, M.; Takahara, A. Surface Molecular Aggregation Structure and Surface Properties of Poly(Fluoroalkyl Acrylate) Thin Films. *Macromolecules* **2005**, *38* (13), 5699–5705.
- (98) Wang, K.; Hu, N. X.; Xu, G.; Qi, Y. Stable Superhydrophobic Composite Coatings Made from an Aqueous Dispersion of Carbon Nanotubes and a Fluoropolymer. *Carbon N. Y.* **2011**, *49* (5), 1769–1774.
- (99) Bayer, I. S.; Steele, A.; Loth, E. Superhydrophobic and Electroconductive

- Carbon Nanotube-Fluorinated Acrylic Copolymer Nanocomposites from Emulsions. *Chem. Eng. J.* **2013**, *221*, 522–530.
- (100) Razmjou, A.; Arifin, E.; Dong, G.; Mansouri, J.; Chen, V. Superhydrophobic Modification of TiO₂ Nanocomposite PVDF Membranes for Applications in Membrane Distillation. *J. Memb. Sci.* **2012**, *415–416*, 850–863.
- (101) Kim, D.-Y.; Lee, J.-G.; Joshi, B. N.; Lathe, S. S.; Al-Deyab, S. S.; Yoon, S. S. Self-Cleaning Superhydrophobic Films by Supersonic-Spraying Polytetrafluoroethylene–titania Nanoparticles. *J. Mater. Chem. A* **2015**, *3* (7), 3975–3983.
- (102) Kamegawa, T.; Shimizu, Y.; Yamashita, H. Superhydrophobic Surfaces with Photocatalytic Self-Cleaning Properties by Nanocomposite Coating of TiO₂ and Polytetrafluoroethylene. *Adv. Mater.* **2012**, *24* (27), 3697–3700.
- (103) Qing, Y.; Yang, C.; Hu, C.; Zheng, Y.; Liu, C. A Facile Method to Prepare Superhydrophobic Fluorinated polysiloxane/ZnO Nanocomposite Coatings with Corrosion Resistance. *Appl. Surf. Sci.* **2015**, *326*, 48–54.
- (104) Prince, J. A.; Singh, G.; Rana, D.; Matsuura, T.; Anbharasi, V.; Shanmugasundaram, T. S. Preparation and Characterization of Highly Hydrophobic Poly(vinylidene Fluoride)-Clay Nanocomposite Nanofiber Membranes (PVDF-Clay NNMs) for Desalination Using Direct Contact Membrane Distillation. *J. Memb. Sci.* **2012**, *397–398*, 80–86.
- (105) Ganesh, V. A.; Nair, A. S.; Raut, H. K.; Yuan Tan, T. T.; He, C.; Ramakrishna, S.; Xu, J. Superhydrophobic Fluorinated POSS–PVDF–HFP Nanocomposite Coating on Glass by Electrospinning. *J. Mater. Chem.* **2012**, *22* (35), 18479.
- (106) Wang, L.; Liang, J.; He, L. Superhydrophobic and Oleophobic Surface from Fluoropolymer-SiO₂ Hybrid Nanocomposites. *J. Colloid Interface Sci.* **2014**, *435*, 75–82.
- (107) Li, K.; Zeng, X.; Lai, X.; Chai, S. Study on the Anti-Abrasion Resistance of Superhydrophobic Coatings Based on Fluorine-Containing Acrylates with Different T_g and SiO₂. *RSC Adv.* **2017**, *7* (75), 47738–47745.
- (108) Jana, S. C.; Jain, S. Dispersion of Nanofillers in High Performance Polymers

- Using Reactive Solvents as Processing Aids. *Polymer*. **2001**, *42* (16), 6897–6905.
- (109) Ozbay, S.; Erbil, H. Y. Superhydrophobic and Oleophobic Surfaces Obtained by Graft Copolymerization of Perfluoroalkyl Ethyl Acrylate onto SBR Rubber. *Colloids Surfaces A Physicochem. Eng. Asp.* **2015**, *481*, 537–546.
- (110) Xiao, F.-X.; Pagliaro, M.; Xu, Y.-J.; Liu, B. Layer-by-Layer Assembly of Versatile Nanoarchitectures with Diverse Dimensionality: A New Perspective for Rational Construction of Multilayer Assemblies. *Chem. Soc. Rev.* **2016**, *45* (11), 3019–3304.
- (111) Such, G. K.; Tjipto, E.; Postma, A.; Johnston, A. P. R.; Caruso, F. Ultrathin, Responsive Polymer Click Capsules. *Nano Lett.* **2007**, *7* (6), 1706–1710.
- (112) Such, G. K.; Quinn, J. F.; Quinn, A.; Tjipto, E.; Caruso, F. Assembly of Ultrathin Polymer Multilayer Films by Click Chemistry Assembly of Ultrathin Polymer Multilayer Films by Click Chemistry. *Polymer*. **2006**, *128* (29), 9318–9319.
- (113) Hobza, P.; Řezáč, J. Introduction: Noncovalent Interactions. *Chem. Rev.* **2016**, *116* (9), 4911–4912.
- (114) Ner, R. K. Multilayers of Colloidal Particles. *J. Colloid Interface Sci.* **1966**, *21*, 569–594.
- (115) Decher, G. Fuzzy Nanoassemblies: Toward Layered Polymeric Multicomposites. *Science* (80). **1997**, *277* (5330), 1232–1237.
- (116) Holder, K. M.; Smith, R. J.; Grunlan, J. C. A Review of Flame Retardant Nanocoatings Prepared Using Layer-by-Layer Assembly of Polyelectrolytes. *J. Mater. Sci.* **2017**, *52* (22), 12923–12959.
- (117) Seo, J.; Lutkenhaus, J. L.; Kim, J.; Hammond, P. T.; Char, K. Effect of the Layer-by-Layer (LbL) Deposition Method on the Surface Morphology and Wetting Behavior of Hydrophobically Modified PEO and PAA LbL Films. *Langmuir* **2008**, *24* (15), 7995–8000.
- (118) Tan, Y.; Yildiz, U. H.; Wei, W.; Waite, J. H.; Miserez, A. Layer-by-Layer Polyelectrolyte Deposition: A Mechanism for Forming Biocomposite Materials.

- Biomacromolecules* **2013**, *14* (6), 1715–1726.
- (119) Fernandes, D. M.; Teixeira, A.; Freire, C. Multielectrocatalysis by Layer-by-Layer Films Based on Pararosaniline and Vanadium-Substituted Phosphomolybdate. *Langmuir* **2015**, *31* (5), 1855–1865.
- (120) Shiratori, S. S.; Yamada, M. Nano-Scale Control of Composite Polymer Films by Mass-Controlled Layer-by-Layer Sequential Adsorption of Polyelectrolytes. *Polym. Adv. Technol.* **2000**, *11* (8–12), 810–814.
- (121) Vaterrodt, A.; Thallinger, B.; Daumann, K.; Koch, D.; Guebitz, G. M.; Ulbricht, M. Antifouling and Antibacterial Multifunctional Polyzwitterion/Enzyme Coating on Silicone Catheter Material Prepared by Electrostatic Layer-by-Layer Assembly. *Langmuir* **2016**, *32* (5), 1347–1359.
- (122) Malucelli, G. Surface-Engineered Fire Protective Coatings for Fabrics through Sol-Gel and Layer-by-Layer Methods: An Overview. *Coatings* **2016**, *6* (3), 33.
- (123) Kozlovskaya, V.; Zavgorodnya, O.; Chen, Y.; Ellis, K.; Tse, H. M.; Cui, W.; Thompson, J. A.; Kharlampieva, E. Ultrathin Polymeric Coatings Based on Hydrogen-Bonded Polyphenol for Protection of Pancreatic Islet Cells. *Adv. Funct. Mater.* **2012**, *22* (16), 3389–3398.
- (124) Takahashi, S.; Sato, K.; Anzai, J. Layer-by-Layer Construction of Protein Architectures through Avidin – Biotin and Lectin – Sugar Interactions for Biosensor Applications. *Anal Bioanal Chem* **2012**, *402*, 1749–1758.
- (125) Xuan, M.; Zhao, J.; Shao, J.; Du, C.; Cui, W.; Duan, L.; Qi, W.; Li, J. Recent Progresses in Layer-by-Layer Assembled Biogenic Capsules and Their Applications. *J. Colloid Interface Sci.* **2017**, *487*, 107–117.
- (126) Cui, M.; Lee, P. S. Solid Polymer Electrolyte with High Ionic Conductivity via Layer-by-Layer Deposition. *Chem. Mater.* **2016**, No. 28, 2934–2940.
- (127) Wang, W.; Xu, Y.; Backes, S.; Li, A.; Micciulla, S.; Kayitmazer, A. B.; Li, L.; Guo, X.; von Klitzing, R. Construction of Compact Polyelectrolyte Multilayers Inspired by Marine Mussel: Effects of Salt Concentration and pH As Observed by QCM-D and AFM. *Langmuir* **2016**, *32*, 3365–3374.
- (128) Voronin, D. V.; Grigoriev, D.; Möhwald, H.; Shchukin, D. G.; Gorin, D. A.

- Nonuniform Growth of Composite Layer-by-Layer Assembled Coatings via Three-Dimensional Expansion of Hydrophobic Magnetite Nanoparticles. *ACS Appl. Mater. Interfaces* **2015**, 7 (51), 28353–28360.
- (129) Lee, T.; Min, S. H.; Gu, M.; Jung, Y. K.; Lee, W.; Lee, J. U.; Seong, D. G.; Kim, B.-S. Layer-by-Layer Assembly for Graphene-Based Multilayer Nanocomposites: Synthesis and Applications. *Chem. Mater.* **2015**, 27 (11), 3785–3796.
- (130) Musameh, M.; Huynh, C. P.; Hickey, M.; Kyratzis, I. L. Surface Activation of CNT Webs towards Layer by Layer Assembly of Biosensors. *Analyst* **2016**, 141 (9), 2748–2755.
- (131) Sung, C.; Hearn, K.; Reid, D. K.; Vidyasagar, A.; Lutkenhaus, J. L. A Comparison of Thermal Transitions in Dip- and Spray-Assisted Layer-by-Layer Assemblies. *Langmuir* **2013**, 29 (28), 8907–8913.
- (132) Bahloul, M.; Pruvost, S.; Fleury, E.; Portinha, D.; Charlot, A. Dip- and Spin-Assisted Stereocomplexation-Driven LbL Self-Assembly Involving Homochiral PVA-G-OLLA and PVA-G-ODLA Copolymers. *RSC Adv.* **2015**, 5 (130), 107370–107377.
- (133) Tan, H. L.; McMurdo, M. J.; Pan, G.; Van Patten, P. G. Temperature Dependence of Polyelectrolyte Multilayer Assembly. *Langmuir* **2003**, 19 (22), 9311–9314.
- (134) Dubas, S. T.; Schlenoff, J. B. Factors Controlling the Growth of Polyelectrolyte Multilayers. *Macromolecules* **1999**, 32 (24), 8153–8160.
- (135) Poptoshev, E.; Schoeler, B.; Caruso, F. Influence of Solvent Quality on the Growth of Polyelectrolyte Multilayers. *Langmuir* **2004**, 20 (3), 829–834.
- (136) Zhang, H.; Wang, Z.; Zhang, Y.; Zhang, X. Hydrogen-Bonding-Directed Layer-by-Layer Assembly of Poly (4-Vinylpyridine) and Poly (4-Vinylphenol): Effect of Solvent Composition on Multilayer Buildup. *Langmuir* **2004**, 20 (20), 9366–9370.
- (137) Yang, Y. H.; Malek, F. A.; Grunlan, J. C. Influence of Deposition Time on Layer-by-Layer Growth of Clay-Based Thin Films. *Ind. Eng. Chem. Res.* **2010**,

- 49 (18), 8501–8509.
- (138) Caruso, F. Nanoengineering of Particle Surfaces. *Adv. Mater.* **2001**, *13* (1), 11–22.
- (139) Hammond, P. T. Form and Function in Multilayer Assembly: New Applications at the Nanoscale. *Adv. Mater.* **2004**, *16* (15 SPEC. ISS.), 1271–1293.
- (140) Ariga, K.; Hill, J. P.; Ji, Q. Layer-by-Layer Assembly as a Versatile Bottom-up Nanofabrication Technique for Exploratory Research and Realistic Application. *Phys. Chem. Chem. Phys.* **2007**, *9* (19), 2319.
- (141) Quinn, J. F.; Johnston, A. P. R.; Such, G. K.; Zelikin, A. N.; Caruso, F. Next Generation, Sequentially Assembled Ultrathin Films: Beyond Electrostatics. *Chem. Soc. Rev.* **2007**, *36* (5), 707–718.
- (142) Borges, J.; Mano, J-F. Molecular Interactions Driving the Layer-by-Layer Assembly of Multilayers. *Chem. Rev.* **2014**, *114*, 8883–8942.
- (143) Richardson, J. J.; Cui, J.; Björnmalm, M.; Braunger, J. A.; Ejima, H.; Caruso, F. Innovation in Layer-by-Layer Assembly. *Chem. Rev.* **2016**, *116* (23), 14828–14867.
- (144) Kaminski, G. A. T.; Sierakowski, M. R.; Pontarolo, R.; Santos, L. A. D.; Freitas, R. A. D. Layer-by-Layer Polysaccharide-Coated Liposomes for Sustained Delivery of Epidermal Growth Factor. *Carbohydr. Polym.* **2016**, *140*, 129–135.
- (145) Kong, W.; Zhang, X.; Gao, M. L.; Zhou, H.; Li, W.; Shen, J. C. A New Kind of Immobilized Enzyme Multilayer Based on Cationic and Anionic Interaction. *Macromol. Rapid Commun.* **1994**, *15* (10), 805–805.
- (146) Sun, Y.; Zhang, X.; Sun, C.; Wang, B.; Shen, J. Fabrication of Ultrathin Film Containing Bienenzyme of Glucose Oxidase and Glucoamylase Based on Electrostatic Interaction and Its Potential Application as a Maltose Sensor. *Macromol. Chem. Phys.* **1996**, *197*, 147–153.
- (147) Kakade, S.; Manickam, D. S.; Handa, H.; Mao, G.; Oupický, D. Transfection Activity of Layer-by-Layer Plasmid DNA/poly(ethylenimine) Films Deposited on PLGA Microparticles. *Int. J. Pharm.* **2009**, *365* (1–2), 44–52.

- (148) Jewell, C. M.; Lynn, D. M. Multilayered Polyelectrolyte Assemblies as Platforms for the Delivery of DNA and Other Nucleic Acid-Based Therapeutics. *Adv. Drug Deliv. Rev.* **2008**, *60* (9), 979–999.
- (149) Liu, X.; Dai, B.; Zhou, L.; Sun, J. Polymeric Complexes as Building Blocks for Rapid Fabrication of Layer-by-Layer Assembled Multilayer Films and Their Application as Superhydrophobic Coatings. *J. Mater. Chem.* **2009**, *19* (4), 497–504.
- (150) Nagaraja, A. T.; You, Y. H.; Choi, J. W.; Hwang, J. H.; Meissner, K. E.; McShane, M. J. Layer-by-Layer Modification of High Surface Curvature Nanoparticles with Weak Polyelectrolytes Using a Multiphase Solvent Precipitation Process. *J. Colloid Interface Sci.* **2016**, *466*, 432–441.
- (151) Abdelkebir, K.; Gaudière, F.; Morin-Grognet, S.; Coquerel, G.; Atmani, H.; Labat, B.; Ladam, G. Protein-Triggered Instant Disassembly of Biomimetic Layer-by-Layer Films. *Langmuir* **2011**, *27* (23), 14370–14379.
- (152) Rahim, M. A.; Choi, W. S.; Lee, H. J.; Jeon, I. C. Ionic Surfactant-Triggered Renewal of the Structures and Properties of Polyelectrolyte Multilayer Films. *Langmuir* **2010**, *26* (7), 4680–4686.
- (153) Arunan, E.; Desiraju, G. R.; Klein, R. A.; Sadlej, J.; Scheiner, S.; Alkorta, I.; Clary, D. C.; Crabtree, R. H.; Dannenberg, J. J.; Hobza, P. Definition of the Hydrogen Bond (IUPAC Recommendations 2011). *Pure Appl. Chem.* **2011**, *83* (8), 1637–1641.
- (154) Kharlampieva, E.; Kozlovskaya, V.; Sukhishvili, S. A. Layer-by-Layer Hydrogen-Bonded Polymer Films: From Fundamentals to Applications. *Adv. Mater.* **2009**, *21* (30), 3053–3065.
- (155) He, Y.; Zhu, B.; Inoue, Y. Hydrogen Bonds in Polymer Blends. *Prog. Polym. Sci.* **2004**, *29* (10), 1021–1051.
- (156) Cheung, J. H.; Stockton, W. B.; Rubner, M. F. Molecular-Level Processing of Conjugated Polymers. 4. Layer-by-Layer Manipulation of Polyaniline via Hydrogen-Bonding Interactions. *Macromolecules* **1997**, *30* (9), 2712–2716.
- (157) Kuo, S.; Chan, S.; Chang, F. Effect of Hydrogen Bonding Strength on the

- Microstructure and Crystallization Behavior of Crystalline Polymer Blends. *Macromolecules* **2003**, *55*, 6653–6661.
- (158) Deng, Y.; Wang, T.; Guo, Y.; Qiu, X.; Qian, Y. Layer-by-Layer Self-Assembled Films of a Lignin-Based Polymer through Hydrogen Bonding. *ACS Sustain. Chem. Eng.* **2015**, *3* (6), 1215–1220.
- (159) Shimazaki, Y.; Mitsuishi, M.; Ito, S.; Yamamoto, M. Preparation of the Layer-by-Layer Deposited Ultrathin Film Based on the Charge-Transfer Interaction. *Langmuir* **1997**, *7463* (3), 1385–1387.
- (160) Heyden, V. Der; Wilczewski, M.; Labbe, P.; Auze, R. Multilayer Films Based on Host – Guest Interactions between Biocompatible Polymers. *Chem. Commun.* **2006**, 3220–3222.
- (161) Chu, Y. W.; Wang, B. Y.; Lin, H.-S.; Lin, T.-Y., Hung, Y.-J; Engebretson, D. A. W. L.; Carey, J. R. Layer by Layer Assembly of Biotinylated Protein Networks for Signal Amplification. *Chem. Commun.* **2013**, *49*, 2397–2399.
- (162) Bourdillon, C.; Demaille, C.; Moiroux, J.; Savéant, J. M. Catalysis and Mass Transport in Spatially Ordered Enzyme Assemblies on Electrodes. *J. Am. Chem. Soc.* **1995**, *117* (46), 11499–11506.
- (163) Yao, H.; Hu, N. PH-Controllable on-off Bioelectrocatalysis of Bienzyme Layer-by-Layer Films Assembled by Concanavalin a and Glucoenzymes with an Electroactive Mediator. *J. Phys. Chem. B* **2010**, *114* (30), 9926–9933.
- (164) Kato, N.; Lee, L.; Chandrawati, R.; Johnston, A. P. R.; Caruso, F. Optically Characterized DNA Multilayered Assemblies and Phenomenological Modeling of Layer-by-Layer Hybridization. *J. Phys. Chem. C* **2009**, *113* (50), 21185–21195.
- (165) Joyce, J. T.; Laffir, F. R.; Silien, C. Layer-by-Layer Growth and Photocurrent Generation in Metal-Organic Coordination Films. *J. Phys. Chem. C* **2013**, *117* (24), 12502–12509.
- (166) Bahloul, M.; Chamignon, C.; Pruvost, S.; Fleury, E.; Charlot, A.; Portinha, D. Instantaneous Stereocomplex Driven Self-Assembly of Enantiomeric Poly(vinyl Alcohol)-Graft-Oligo(lactide) Copolymers in DMSO and Thin Film

- Formation Thereof. *Polymer*. **2015**, 79, 195–204.
- (167) Serizawa, T.; Yamashita, H.; Fujiwara, T.; Kimura, Y.; Akashi, M. Stepwise Assembly of Enantiomeric Poly(lactide)s on Surfaces. *Macromolecules* **2001**, 34 (6), 1996–2001.
- (168) Wang, L.; Wang, Z.; Zhang, X.; Shen, J.; Chi, L.; Fuchs, H. A New Approach for the Fabrication of an Alternating Multilayer Film of poly(4-Vinylpyridine) and Poly(acrylic Acid) Based on Hydrogen Bonding. *Macromol. Rapid Commun.* **1997**, 18, 509–514.
- (169) Zhang, X.; Chen, H.; Zhang, H. Layer-by-Layer Assembly: From Conventional to Unconventional Methods. *Chem. Commun.* **2007**, No. 14, 1395–1405.
- (170) Lee, H.; Mensire, R.; Cohen, R. E.; Rubner, M. F. Strategies for Hydrogen Bonding Based Layer-by-Layer Assembly of Poly(vinyl Alcohol) with Weak Polyacids. *Macromolecules* **2012**, 45 (1), 347–355.
- (171) Li, Y.; Pan, T.; Ma, B.; Liu, J.; Sun, J. Healable Antifouling Films Composed of Partially Hydrolyzed Poly(2-Ethyl-2-Oxazoline) and Poly(acrylic Acid). *ACS Appl. Mater. Interfaces* **2017**, 9 (16), 14429–14436.
- (172) Delongchamp, D. M.; Hammond, P. T. Highly Ion Conductive Poly (Ethylene Oxide) -Based Solid Polymer Electrolytes from Hydrogen Bonding Layer-by-Layer Assembly. *Langmuir* **2004**, 1 (8), 5403–5411.
- (173) Sukhishvili, S. A.; Granick, S. Layered, Erasable Polymer Multilayers Formed by Hydrogen-Bonded Sequential Self-Assembly. *Macromolecules* **2002**, 35 (1), 301–310.
- (174) Liu, Qing; Lou, Hongming; Qiu, X. Grafted-sulfonated Bamboo Pulping Liquor, Its Preparation and Property. *China Pulp Pap* **2009**, 28 (12), 22–26.
- (175) Fu, Y.; Bai, S.; Cui, S.; Qiu, D.; Wang, Z.; Zhang, X. Hydrogen-Bonding-Directed Layer-by-Layer Multilayer Assembly: Reformation Yielding Microporous Films. *Macromolecules* **2002**, 35 (25), 9451–9458.
- (176) Zhang, H.; Fu, Y.; Wang, D.; Wang, L.; Wang, Z.; Zhang, X. Hydrogen-Bonding-Directed Layer-by-Layer Assembly of Dendrimer and

- poly(4-Vinylpyridine) and Micropore Formation by Post-Base Treatment. *Langmuir* **2003**, *19* (20), 8497–8502.
- (177) Zhunuspayev, D. E.; Mun, G. A.; Hole, P.; Khutoryanskiy, V. V. Solvent Effects on the Formation of Nanoparticles and Multilayered Coatings Based on Hydrogen-Bonded Interpolymer Complexes of Poly (Acrylic Acid) with Homo- and Copolymers of N -Vinyl Pyrrolidone. *Langmuir* **2008**, *24* (28), 13742–13747.
- (178) Ma, S.; Yuan, Q.; Zhang, X.; Yang, S.; Xu, J. Solvent Effect on Hydrogen-Bonded Thin Film of Poly(vinylpyrrolidone) and Poly(acrylic Acid) Prepared by Layer-by-Layer Assembly. *Colloids Surfaces A Physicochem. Eng. Asp.* **2015**, *471*, 11–18.

Chapter 2: Poly(2,3,4,5,6-pentafluorostyrene) modified fumed silica and its application in preparing self-cleaning nanocomposite films

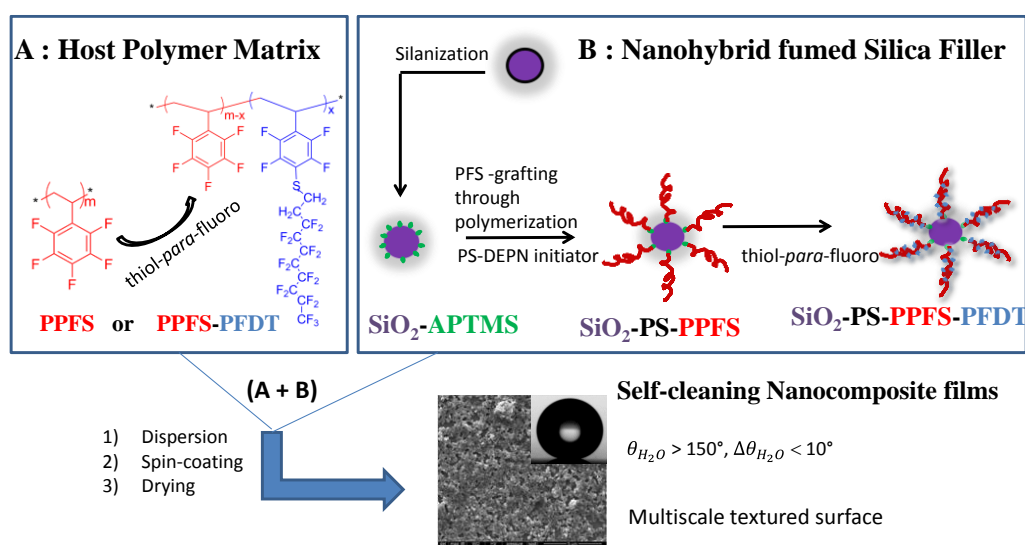
2.1 General introduction

Superhydrophobic surfaces are particularly important in fundamental research and practical applications. It has been reminded in Chapter 1.2 of the bibliographic part that such peculiar surface properties can be achieved with a hydrophobic polymer material endowed with a dual-roughened surface at nano/microscale.

In this context, fluorinated polymers are of special interest because of their inherent low surface energy provided by the fluorine atoms. Introducing preformed inorganic nanoparticles into such polymers has appeared as a powerful means to provide a multi-scale textured surface, taking advantage of the desirable properties of the two components in terms of processability, durability and/or mechanical properties of such resulting (nano)composite films. However, the dispersion of the inorganic particles especially nanoparticles in the polymer matrix is not an easy task if their surface chemistry is not carefully adjusted to favor the compatibilization degree between the filler and the polymer, which is the key parameter that controls the morphology and thus the surface topology.

As explained in detail in the general introduction of the manuscript, our initial motivation was to take advantage of the possible derivatization of PPFs to adjust the properties of the resulting polymer and then allows for preparing well-tailored materials, one example of which being (nano)composite thin polymer films. In this respect, PPFs appears as an interesting choice as a platform to synthesize both the polymer matrix and to act as a compatibilizer if chemically attached to the surface of the filler, in order to enhance the interfacial adhesion. We anticipated that chemical

derivation could act on both (chemical and morphological) criteria to achieve the appropriate dispersion of nanoparticles in the appropriate polymer matrix with the appropriate surface chemistry. Regarding the filler, our choice was towards fumed silica as it inherently presents a double scale of dimension (the one of the elementary nanoparticles that form aggregates up to hundreds of nanometers) that can provide the dual-roughened texture needed to achieve the surface property. Thus the general strategy is depicted in the following scheme:



Scheme 2-1 General strategy for the preparation of self-cleaning nanocomposite films envisaged with PPFS-based components

Hence this chapter describes the generation of nanocomposite films combining PPFS-modified fumed silica and various host-PPFS-based polymer matrices, either constituted of PPFS or PPFS chains bearing perfluoroalkyl segments as a result of a thiol-para-fluoro coupling reaction. This chapter is divided into two parts that actually correspond to two article manuscripts.

The first part was accepted for publication in *RSC Advances* (2016, 6, 58260-58267) and is entitled “**Nitroxide-mediated polymerization of pentafluorostyrene initiated by PS-DEPN through the surface of APTMS modified fumed silica: towards functional nanohybrids**”.

In particular, it deals with the synthesis of organic/inorganic hybrid fumed silica

particles to which PPFS are chemically anchored at the surface. They were prepared by NMP of PFS with PS-DEPN as a macroinitiator and (acryloxypropyl)trimethoxysilane-treated fumed SiO₂ (SiO₂-APTMS) using a “grafting through” strategy. Both the effect of solvent on the PFS polymerization kinetics (in presence or not of modified fumed silica particles) and the quantitative determination of the PS-b-PPFS grafting weight were emphasized. Moreover, the corresponding surface properties are discussed in terms of water wettability.

The second part was submitted for publication in European Polymer Journal by the time this manuscript was sent to the PhD reviewers, and is entitled “**Controlled perfluorination of fluorinated polymer and functionalized fumed silica: towards the design of self-cleaning (nano)composite films**”. This manuscript describes the modification of PPFS by semiperfluorinated alkyl thiol (PFDT) via *para*-fluoro substitution reaction in a controlled manner resulting in PPFS-PFDT derivatives with adjustable DS. Then the pre-synthesized hybrid fumed silica particles (SiO₂-PS-PPFS) were also modified by PFDT (SiO₂-PS-PPFS-PFDT). The preparation of a large panel of (nano)composite films from the different possible host matrix/silica particles combinations is described. Their wettability and morphological properties are discussed as a function of the structure of both host matrix and silica, as well as the silica content.

2.2 Nitroxide-mediated polymerization of pentafluorostyrene initiated by PS–DEPN through the surface of APTMS modified fumed silica: towards functional nanohybrids

2.2.1 Abstract

Poly(pentafluorostyrene) (PPFS) chains were anchored on the surface of silica nanoparticles (Aerosil A200 fumed silica) by nitroxide-mediated polymerization (NMP) with PS–DEPN as macroinitiator using a “grafting through” strategy with (acryloxypropyl)trimethoxysilane (APTMS)-modified silica. First, NMP of PFS was evaluated with and without silica in various solvents (namely N-methyl-2-pyrrolidone – MP, N,N-dimethylformamide – DMF, and toluene) that favor the dispersion of APTMS-silica in reaction medium. In both situations, polymerization presents all the features of a controlled process whatever the solvent is, with a marked impact of the solvent polarity on the kinetics. Moreover, NMP of PFS is faster in polar solvents when conducted in presence of APTMS-modified silica. By tuning polymerization time and/or solvent polarity, the weight ratio of organic matter to silica can be tuned from 5 to 32 wt%. The impact of such modification rate is demonstrated on the surface properties of SiO₂-PS-b-PPFS deposited on a silicon wafer: indeed, introduction of fluorinated segments in combination with dual roughness (due to inherent dimensions of fumed silica) lead to relevant hydrophobic surface properties with water contact angle as high as (132 ± 1.7)°.

2.2.2 Introduction

The grafting of polymers onto inorganic substrates has gathered attention due to their potential applications in the field of colloidal stabilization, surface property tailoring and micro-lithographic patterning.^{1–6} Surface modification of inorganic particles is generally undertaken by physisorption or chemical bonding of chains. Typically, three main routes are usually reported to chemically attach a polymer chain

to a surface: (i) the “grafting onto” method, where end functionalized polymers react with appropriate surface sites^{7,8} (ii) the “grafting from”, where chains grow in situ from preformed surface-grafted initiators^{9,10} and (iii) surface copolymerization through a covalently linked monomer (“grafting through”).¹¹ Silica particles are usually used as inorganic substrates to prepare inorganic–organic hybrids due to their mechanical resistance, high specific surface area and low cost.^{12,13} In the literature, silica-based substrates coated with well-defined polymeric chains have been achieved by polymerization techniques such as controlled free radical polymerization (CRP) due to its simplicity and versatility permitting to build up highly dense polymer brushes from silicon wafer¹⁴ or silica gel.^{15–17,18} In our previous studies,^{19,20} well-defined polystyrene-coated silica nanoparticles were obtained using a “grafting from” procedure and the nitroxide mediated polymerization (NMP) technique. In addition, generation of low surface energy surfaces, solvent resistant coatings and ultra-low dielectric constant films can be obtained by the use of fluorine containing polymers.^{21–23} In this context, polypentafluorostyrene (PPFS) and its corresponding copolymers are of particular interest.²⁴ Indeed, as a styrenic derivative the latter can be synthesized by various polymerization techniques, including CRP that makes the synthesis of functional sophisticated materials possible.^{25–29,30–32,33–35} Recently, fabrication of superhydrophobic surfaces using raspberry like particles with immobilized PPFS was demonstrated using a multistep synthesis including an ATRP process.³⁵ In addition, the labile para-fluorine of the pentafluorophenyl group in PPFS-based materials, can undergo regioselective substitution by nucleophiles such as amines, thiols and alcohols.^{36–38} Herein, we report for the first time the synthesis of hydrophobic PPFS-b-PS grafted silica particles by combining nitroxide mediated polymerization and the “grafting through” procedure. Indeed, the use of conventional free radical polymerization for the graft copolymerization of vinyl monomers with immobilized monomers does not permit to control the layer thickness that reaches a plateau after only a few hours polymerization. Moreover, due to the constant molecular weight of the grafted chains with the polymerization time, the graft density shows a similar behavior, as discussed by Ruhe.³⁹ This paper emphasizes both the

effect of solvent on the PFS polymerization kinetics and the quantitative determination of the PS-b-PPFS grafting weight. Moreover, the corresponding surface properties are discussed in terms of water wettability.

2.2.3 Experimental section

2.2.3.1 Materials

Aerosil*200 fumed silica (Aldrich) is characterized by an average diameter of 13 nm for the elementary particle (aggregates sizes ranging from 500 nm to 1 μ m) and a specific surface area of 200 m²/g. Before use, it was dried at 150°C under vacuum for 4 h. 2,3,4,5,6-pentafluorostyrene (PFS, 99%, Aldrich) was distilled under vacuum and stored at -20°C. Styrene (S, 99%, Aldrich) was distilled. DEPN (N-tert-butyl-N-(1-diethylphosphono-2, 2-dimethyl) propyl nitroxide) was used as received from Polymer expert. Toluene (99.8%, Aldrich), N, N-Dimethylformamide (DMF, 99%, Aldrich) and N-Methyl pyrrolidone (MP, 99%, Aldrich) were distilled before used. (acryloxypropyl) trimethoxysilane (APTMS) and all other chemical products (Aldrich) were used as received. The DEPN-based alkoxyamine (Styryl-DEPN) was prepared using a procedure described in the literature.⁴⁰

2.2.3.2 Analytical technique

Fourier Transform infrared (FT-IR). FT-IR spectra were recorded on a Bruker IFS 66/S spectrometer using pressed KBr pellet. The resolution of the measurement was 4 cm⁻¹ within a range of 500-4000 cm⁻¹ and an average of 32 scans.

Size Exclusion Chromatography (SEC). SEC characterizations were performed using a 2690 Waters Alliance System with CHCl₃ (HPLC grade) or THF (HPLC grade) as eluent at a flow rate of 1mL/min. The chromatographic device was equipped with four Styragel columns HR 0.5, 2, 4 and 6 at 40°C in series with a 2410 Waters refractive index detector and a 996 Waters photodiode array detector. A calibration curve was established with low dispersity index polystyrene standards.

Nuclear Magnetic Resonance Spectroscopy (NMR). ^1H and ^{19}F NMR spectra were recorded on a Bruker Advanced AM400 spectrometer at 400 MHz. Samples were dissolved in CDCl_3 and chemical shifts were determined in ppm with 64 scans for each kind of analysis.

Thermo Gravimetric Analysis (TGA). TGA measurements were performed on a TA Q500 at a heating rate of $10\text{ }^\circ\text{C}/\text{min}$ between 50 and 750°C under a nitrogen flow ($40\text{ mL}/\text{min}$).

Transmission Electron Microscope (TEM). TEM images were taken with a Philips CM120 transmission electron microscope operating at an accelerating voltage 80 kV . Crude products were deposited onto carbon layer covered copper grid while pure products were dispersed into THF with a concentration of $1\text{ mg}/\text{mL}$ before deposition.

Cryo-Scanning Electron Microscope (Cryo-SEM). Cryo-SEM images were taken by using a NEON 40 (Zeiss) scanning electron microscope.

Water Contact Angle Analysis (WCA). Water contact angle (WCA) measurements were carried out using a Dataphysics Digidrop contact angle meter equipped with a CDD2/3 camera with the sessile drop method and by using Milli-Q quality water as probe liquid. The tabulated results are the average of at least five measurements on different parts of each sample.

Atomic Force microscopy (AFM). AFM images were acquired in intermittent contact mode (tapping mode), on a wafer of $1\text{ cm} \times 1\text{ cm}$, in air at room temperature using an AFM Bruker Multimode 8 apparatus equipped with Nanoscope V controller. The scanning speed for image acquisition is 0.5 Hz . The used tips are TAP 150 with a radius of curvature of 8 nm . The surface roughness R_q was obtained by processing images using the Nanoscope Analysis software (version 1.5).

2.2.3.3 Preparation of macroinitiator (PS-DEPN)

Styrene (13.5 g ; 0.13 mol), and Styryl-DEPN (260 mg ; 0.65 mmol) were introduced in a glass tube, degassed with freeze–pump–thaw cycles and heated at

110°C for 40 min in an oil bath. The polymer was recovered by precipitation in excess methanol and dried in a high vacuum oven. Styrene conversion=15%, $M_n = 4100$ g/mol, $D = 1.30$.

2.2.3.4 Polymerization of PFS using PS-DEPN as macroinitiator

PFS was polymerized by NMP using PS-DEPN as macroinitiator in different solvents (Toluene, DMF and MP). In a model reaction, PFS (5 mL, 36.22 mmol) was solubilized in 5 mL of solvent (Toluene, DMF or MP) (5 mL). PS-DEPN (742 mg, 0.18 mmol) was added to get a mixture solution with $[PFS]/[PS-DEPN] = 200$. Then, the mixture was divided into 5 vials with the same volume (2 mL). The five flasks were degassed four times by freeze-pump-thaw cycles, flame-sealed under vacuum and then heated in a preheated oil bath at 110°C for various reaction times (0.5 h, 1 h, 2 h, 4 h and 6 h). The polymerization was stopped by immersing the flask into liquid nitrogen before breaking it. An aliquot was withdrawn and further dedicated to conversion determination by ^{19}F NMR. The reaction mixture was precipitated into cold methanol and filtered. Purification of the polymer was achieved by dissolving in THF and precipitated in cold methanol again. The pure polymers were collected and dried at 50 °C under vacuum for overnight.

2.2.3.5 Synthesis of APTMS-modified silica (SiO₂-APTMS)

A certain amount of APTMS, with a concentration of 4 – 40 $\mu\text{mol}/\text{m}^2$, was added into a toluene dispersion of SiO₂ (25 mg/mL). The reaction mixture was stirred for 30 min at room temperature and then at 110 °C for 24 h. The free non-grafted APTMS was eliminated by successive centrifugation/redispersion cycles in toluene. The APTMS-functionalized silica particles were collected and dried at 50 °C under vacuum overnight, then further characterized by FTIR and TGA. The latter technique was used to determine the APTMS grafting density according to the Equation 2.2-1:

$$\text{Grafting density } \left(\frac{\text{molecule}}{\text{nm}^2} \right) = \frac{W_{(\text{SiO}_2-\text{APTMS})} \times 100 - W_{(\text{SiO}_2)}}{M_{\text{APTMS}} \times S_{\text{spec}} \times 100} \times \frac{N_A}{10^{18}}$$

(Equation 2.2-1)

where $W_{(\text{SiO}_2-\text{APTMS})}$ and $W_{(\text{SiO}_2)}$ are the weight loss (in %) of APTMS-modified silica and neat silica between 50 and 750 °C; M_{APTMS} (g/mol) is the molar mass of APTMS and S_{spec} is the specific surface area of silica; N_A is the Avogadro constant. The grafting yield, which corresponds to the fraction of APTMS effectively covalently attached to the silica surface, was determined using the Equation (2.2-2):

$$\text{APTMS grafting yield (\%)} = \frac{\text{grafting density} \times 100}{[\text{APTMS}]}$$

(Equation 2.2-2)

where $[\text{APTMS}]$ ($\mu\text{mol}/\text{m}^2$) is the initial concentration of APTMS.

2.2.3.6 Polymerization of PFS in presence of APTMS modified silica and PS-DEPN by “grafting through” approach

For a typical reaction, a given amount of SiO_2 -APTMS (0.3 g) with a grafting density of APTMS equal to 0.55 molecule/ nm^2 was dispersed in 5 mL of solvent (Toluene, DMF or MP). After sonication for 10 min and stirring for 30 min at room temperature, a solution of PFS (5 mL, 36.22 mmol) and PS-DEPN (742 mg, 0.18 mmol) ($[\text{PFS}]/[\text{PS-DEPN}] = 200$) was added. The reaction mixture was divided into five vials with the same volume (2 mL). The five flasks were degassed four times by freeze-pump-thaw cycles, flame-sealed under vacuum and then heated in a preheated oil bath at 110°C for various reaction times (0.5 h, 1 h, 2 h, 4 h and 6 h). The polymerization was stopped by immersing the flask into liquid nitrogen before breaking it. An aliquot was withdrawn and further dedicated to conversion determination by ^{19}F NMR. The reaction mixture (directly after polymerization and before purification) was dedicated to TEM and Cryo-SEM analyses. Then free PS-b-PPFS chains possibly physisorbed to silica surface were removed by extensive

centrifugation (11000 rpm, 30 min) / redispersion cleaning cycles in THF (five times). After each cycle, the supernatant was collected, concentrated and precipitated in cold methanol to recover free polymer. Blank experiment involving neat silica was performed with the same procedure to confirm that ungrafted polymer chains were completely removed using such work up. After purification, the final PS-PPFS-grafted silica (SiO₂-PS-b-PPFS) particles and free polymers (PS-b-PPFS) were recovered separately and dried at 50 °C under vacuum overnight then were characterized by ¹H-NMR, ¹⁹F-NMR, FT-IR, TGA, and TEM. The PS-b-PPFS grafting weight was calculated by Equation 2.2-3,

$$\text{g(polymer)/g(silica)} = \frac{W_{(\text{SiO}_2\text{-PS-PPFS})} - W_{(\text{SiO}_2\text{-APTMS})}}{100 - W_{(\text{SiO}_2\text{-APTMS})}}$$

(Equation 2.2-3)

where $W_{(\text{SiO}_2\text{-PS-PPFS})}$ is the weight loss (in %) of PS-PPFS grafted silica between 50 and 750 °C.

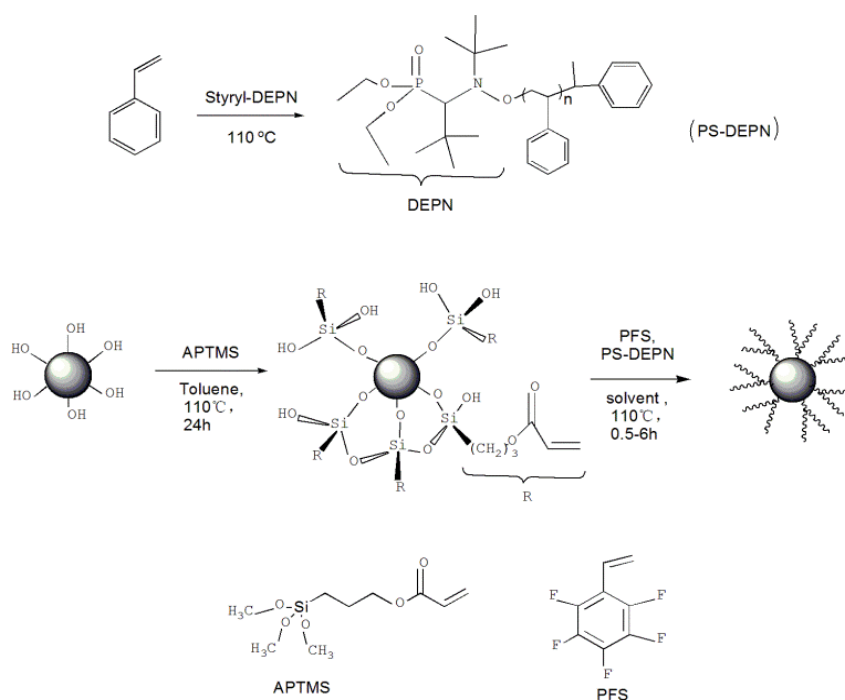
2.2.3.7 Deposition of the hybrid modified silica onto silicon wafer

Silicon wafers were purchased from Sil'tronix. They were cut into appropriate dimensions (typically 1 cm × 1 cm) before use, and activated by ozonolysis for 30 min prior to any deposition. Free PS-PPFS and hybrid SiO₂-PS-b-PPFS particles were dispersed into THF with a concentration of 30 mg/mL, and then 0.1 mL of such solutions was spin-coated onto the cleaned silicon wafer with a speed of 2000 rpm for 30s using a Polo Spin 150i / 200i spin-coater type from SPS-Europe. Then THF was evaporated at room temperature for two days before any analysis.

2.2.4 Results and discussion

In our synthetic strategy (Scheme 2.2-1), three steps were used to anchor PS-b-PPFS copolymer chains to the surface of silica particles. First, a

macroalkoxyamine based on DEPN and PS was prepared by nitroxide mediated polymerization, and APTMS-grafted silica particles were synthesized separately according to literature²¹ in order to introduce at the surface of the silica particles C=C double bonds that are reactive in radical (co)polymerization. Indeed, the thermal cleavage of PS-DEPN produces PS-based macroradicals that can react with both pentafluorostyrene and the vinyl group in grafted APTMS molecules leading to chemically bonded block copolymer chains at the silica surface (Scheme 2.2-1).



Scheme 2.2-1 Reaction Scheme for nitroxide polymerization of pentafluorostyrene initiated by PS-DEPN through the surface of APTMS functionalized fumed silica.

Then, PPFS chains with controlled molecular weights and narrow polydispersities were grown through the APTMS functionalized nanoparticles surface using a known amount of PS-DEPN macroinitiator (Scheme 2.2-1). The chain length of the grafted and the free PPFS-based copolymer is controlled by the pentafluorostyrene to PS-DEPN molar ratio, polymerization time and solvent that is used. It should be also mentioned that modified nanoparticles are multifunctional sites that may participate in crosslinking reactions.

2.2.4.1 Kinetic of the nitroxide mediated polymerization of PFS in presence of PS-DEPN and without silica

We have focused our study on the influence of the solvent on the kinetic of the nitroxide mediated polymerization of PFS employing a polystyrene macroinitiator (PS-DEPN). Indeed, it is well known that the homolysis of the C-ON bond in alkoxyamines at the initiation stage (k_d) plays a key role in the success of nitroxide polymerization.⁴¹ Moreover, it is of crucial importance to find the most suitable solvent for the forthcoming grafting reaction in presence of APTMS-grafted silica so the solvent effect was investigated in three solvent including Toluene, DMF and MP. The extension of PS-DEPN homopolymer ($M_n = 4100$ g/mol, $D=1,3$; see experimental part) with PFS in solution was carried out at 110 °C for different polymerization time and the monomer-to-macroinitiator ratio (200/1) was chosen such that the number-average molecular weight M_n at complete conversion of monomer would equal 40 000 g/mol. The structural characterization of the copolymers was achieved using both ^1H NMR and ^{19}F NMR spectroscopy. For example, Figure S2.2-1 illustrates the ^{19}F NMR spectrum of the crude PS-*b*-PPFS solution in MP after 4 hours. The conversion of PFS monomer in the withdrawn samples was calculated from the ^{19}F NMR spectrum (Figure S2.2-1) by use of the normalized area for the aromatic fluorines (*para* position at 156.5 ppm; I_p) for PFS as compared to the area of the aromatic fluorines (*para* position at 154.5 ppm; I_p') for PPFS according to the following equation: $\text{conversion} = I_p' / (I_p' + I_p)$.

In order to examine the controlled radical polymerization process, kinetics, molecular weight and dispersity were analyzed as a function of time. As it can be seen in Figure 2.2-1, a linear $\text{Ln}([M_0]/[M]t)$ vs. time plot was obtained for all the samples showing that radical concentration remains unchanged during the polymerization and therefore polymerization proceeds in a controlled manner.

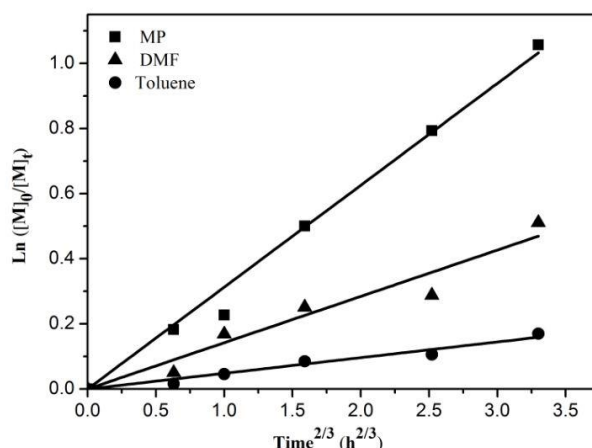


Figure 2.2-1 Kinetics of polymerization of PFS at 110°C; [PFS] = 3.6 mol/L; [PS-DEPN] = 0.018 mol/L in different solvents.

Assuming pseudo-first order kinetics for the steady-state stage of polymerization, the reaction rate equation can be stated as follows: $\text{Ln}([M]_0/[M]_t) = k_{app} t^{2/3}$ where, k_{app} is the slope of such linear variation and is known as apparent rate constant of polymerization. According to the results, k_{app} varied from $4.86 \times 10^{-5} \text{ s}^{-2/3}$ (MP as solvent) to $0.29 \times 10^{-5} \text{ s}^{-2/3}$ (Toluene as solvent). One can observe that the PFS polymerization rate is higher when using MP as solvent. As discussed by Marques⁴² and Billon,⁴³ the main factor that determines the decomposition rate of nitroxide adducts is a stabilization of radicals so one can suggest that the reason of the increase in k_{app} value in polar solvents is a stabilization of the liberated nitroxide due to its solvation by the polar molecules.

Moreover, SEC traces of PS-b-PPFS copolymers showed the increasing molecular weights of copolymers with increasing polymerization time and peaks with monomodal distribution, indicating the successful initiation of nitroxide mediated copolymerization by PS-DEPN, whatever the solvent is (Figure 2.2-2, MP as solvent).

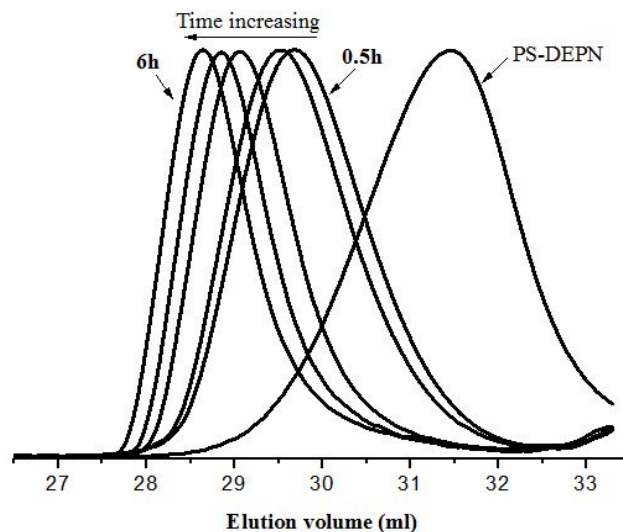


Figure 2.2-2 GPC traces of PS-*b*-PPFS copolymers versus polymerization time (MP as solvent).

For all the solvent (MP, DMF and Toluene), a linear correlation between number average molar mass M_n and conversion was obtained with polydispersity lower than 1.3. As an illustration, Figure 2.2-3 presents the results obtained for MP used as the solvent.

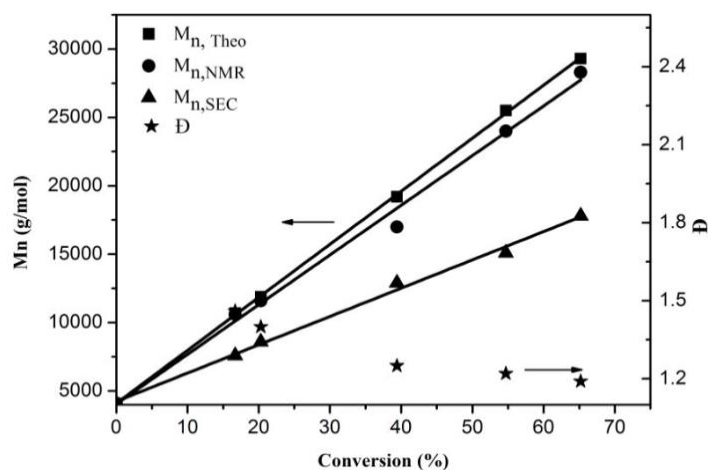


Figure 2.2-3 Linear dependence of M_n versus conversion and dispersity evolution during the polymerization of PFS at 110°C in MP.

One can observe that the molar masses determined by ^1H NMR are close to the theoretical ones. Considering Figure 2.2-3, we can conclude that the nitroxide mediated polymerization of PFS exhibits all the criteria of a controlled radical

polymerization.

2.2.4.2 Synthesis of the PS-*b*-PPFS-grafted silica

First, similarly to our previous results in this field,²¹ preliminary experiments were dedicated to the determination of the optimal conditions for grafting APTMS at the surface of silica. The corresponding APTMS grafting densities were determined by using thermogravimetric analysis and equation 1 (see experimental part). Indeed, it is well known that heating functionalized silica particles in an inert atmosphere removes the organic moieties and restores the silica structure. Figure S2.2-2 reports on the effect of the APTMS concentration on the grafting density. We can observe that the grafting density (determined by TGA) increases with increasing the APTMS content and reaches a plateau at high concentrations: a maximum grafting density of 0.55 molecule/nm² is achieved for a APTMS content of 18 μmol/m² and more. Then, the copolymerization of PFS with vinyl-grafted silica (4.3 wt.%) in presence of PS-DEPN with a [PFS] to [PS-DEPN] ratio of 200/1 was investigated according to a “grafting through” approach (Scheme 2.2-1). It results in the formation of polymer chains attached to the surface of silica and free chains dispersed in the solution. The polymerization of PFS was performed according to the same experimental procedure as in the absence of silica and similar conclusions were drawn: a linear Ln([M₀]/[M]) vs. time plot was obtained for all the samples (Figure S2.2-3) and MP permitted to obtain higher conversion than Toluene and DMF in presence of a silica content of 4.3 wt% (Table 2.2-1). Moreover, it should be noted that addition of silica nanoparticles (especially in DMF and MP) favorably affects the kinetics of PFS polymerization in polar solvents with apparent rate constants of polymerization increasing from to 4.86×10⁻⁵ s^{-2/3} to 8.41×10⁻⁵ s^{-2/3} for MP as solvent (Figure S2.2-3). As discussed by several authors,^{44,45} this phenomenon could be attributed to the partially polarizing effect of the silica nanoparticles on the reaction medium and thereby its acceleration effect on the polymerization rate. Herein, residual pendant hydroxyl groups on the surface of silica particles could possibly cause adsorption of DEPN radicals thus

prolonging the lifespan of the polymeric radicals and finally leading to a higher conversion.

Table 2.2-1 Effect of solvent on PFS conversion with and without APTMS-grafted silica.

time (h)	without silica			with 4.3 wt% silica-APTMS		
	PFS conversion (%)			PFS conversion (%)		
	Toluene	DMF	MP	Toluene	DMF	MP
0.5	2	5	17	1.7	17	17
1	5	16	20	2.2	19	31
2	8	22	39	4.3	34	48
4	10	25	55	7	47	74
6	16	40	65	12.2	62	76

After quantitative removal of the free block copolymer chains by extensive washings, analysis of the recovered silica powder by FTIR gave clear evidence of PPFS grafting (Figure 2.2-4).

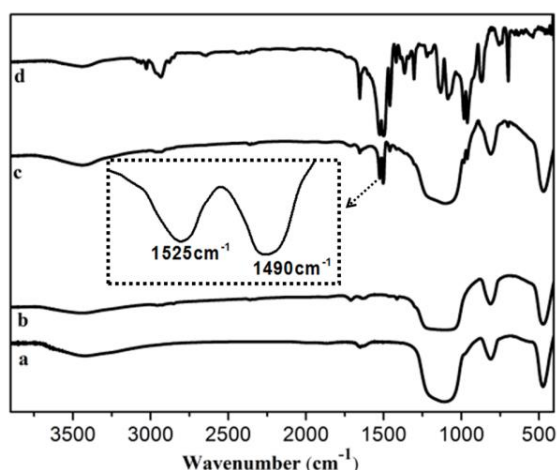


Figure 2.2-4 FT-IR spectra of a) SiO_2 , b) SiO_2 -APTMS, c) SiO_2 -PS-b-PPFS and d) free PS-b-PPFS copolymer.

Compared with silica, PS-b-PPFS-grafted silica exhibits a FTIR peak at 1740 cm^{-1} indicative of a carbonyl group from APTMS and a double band in the range of $1450\text{-}1550\text{ cm}^{-1}$ that can be ascribed to both the hydrogenated and the fluorinated aromatic ring vibrations.³⁷ Indeed, it can be observed in Figure S2.2-4 that the band located at 1490 cm^{-1} can be attributed to the PS- and PPFS- based aromatic vibration while the 1525 cm^{-1} one corresponds to the PPFS-based aromatic vibration only.

Further insight into the grafting reaction was obtained by determining the amount of polymer chains grafted on silica particles. Figure 2.2-5d presents a typical thermogram for free PS-b-PPFS copolymer exhibiting a decomposition temperature close to 450°C. It should be also noted that the decomposition temperature of PS-b-PPFS copolymer slightly increases after grafting onto the silica particles, as expected (Figure 2.2-5c). TGA results show that free PS-b-PPFS copolymer can be completely decomposed at a temperature of 550°C; therefore, the weight amount of PS-b-PPFS copolymer that is covalently attached to the silica surface is estimated by the weight loss of PS-b-PPFS-grafted silica sample between 200°C and 550°C after subtracting the contribution of APTMS groups (Figure 2.2-5b). From Figure 2.2-5, the PS-b-PPFS weight grafting is around 32% when polymerization proceeded in MP for 6 h.

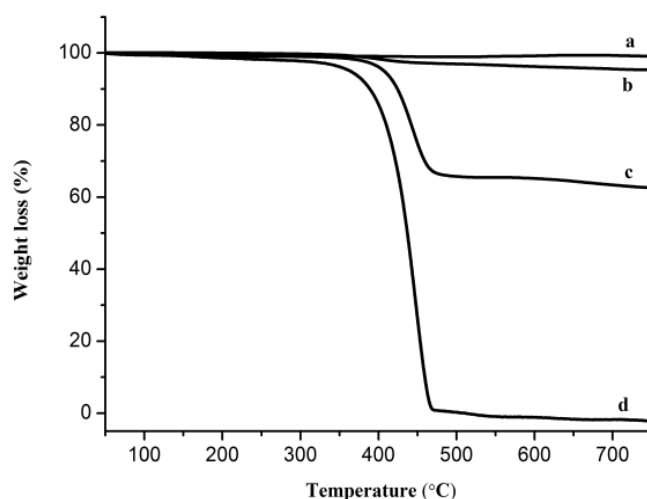


Figure 2.2-5 TGA of a) SiO₂, b) SiO₂-APTMS, c) SiO₂-PS-b-PPFS and d) free PS₃₆-b-PPFS₁₄₂.

Figure 2.2-6 reports on the effect of the PFS polymerization time on the polymer grafting weight on silica as a function of the solvent.

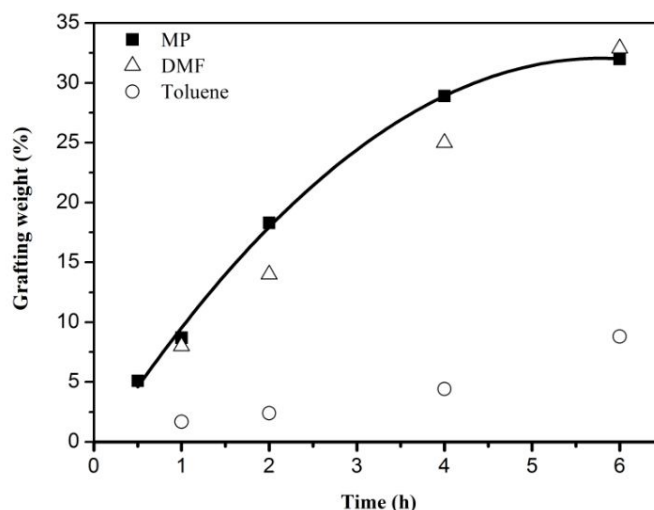


Figure 2.2-6 Amount of polymer grafting weight as a function of PFS polymerization time ([PFS]/[PS-DEPN] = 200/1, 4.3 wt.% of SiO₂-APTMS particles, 110°C). The line is a guide for the eye.

It is well known that the use of a “grafting onto” approach in order to functionalize a substrate by a reactive end terminated polymer leads to a decrease of the molar coverage by increasing the polymer molecular weight due to the corresponding reduction in the entropy effect.⁴⁵ Herein, by using the “grafting through” approach, it is observed the reversed situation so the PS-*b*-PPFS grafting weight increases with increasing PFS polymerization time (i.e. the PS-*b*-PPFS molar mass) whatever the solvent is. This behavior is probably due to the chemical affinity of APTMS-grafted silica particles for the PFS polymerization medium by increasing the chain length of the grafted PPFS block. However, the use of Toluene as solvent does not permit to obtain high polymer weight content even after 6h regarding the low PFS conversion when studying the effect of solvent on PFS conversion (Table 2.2-1). Interestingly, by using MP as solvent, the PPFS content on the silica surface varies from 5 wt% to 32 wt% and levels off after a polymerization time of 4h (Figure 2.2-6).

The characteristics of free PS-*b*-PPFS block copolymers synthesized in presence of APTMS-grafted silica are listed in Table S2.2-1. As shown in the latter Table S2.2-1, the well-defined PS-*b*-PPFS copolymers with different content of PPFS segments were successfully obtained whatever the solvent is.

Insight into morphology was provided by both cryo-SEM and TEM coupled with

EDX analysis. First, the evolution of the morphologies occurring with time during the polymerization of PFS was analysed. Cryo-fracture SEM image of the crude product prepared in MP at low conversion (17%, Table 2.2-1) shows the presence of PS-b-PPFS based nodules surrounded by silica nanoparticles suggesting a phase separation (Figure 2.2-7a). By increasing the PFS conversion to 31%, one can observe that the nodules have disappeared and the silica particles are homogeneously dispersed within the organic matrix due to favoured chemical affinity of the PS-b-PPFS grafted silica for the organic matrix, as discussed earlier (Figure 2.2-7b).

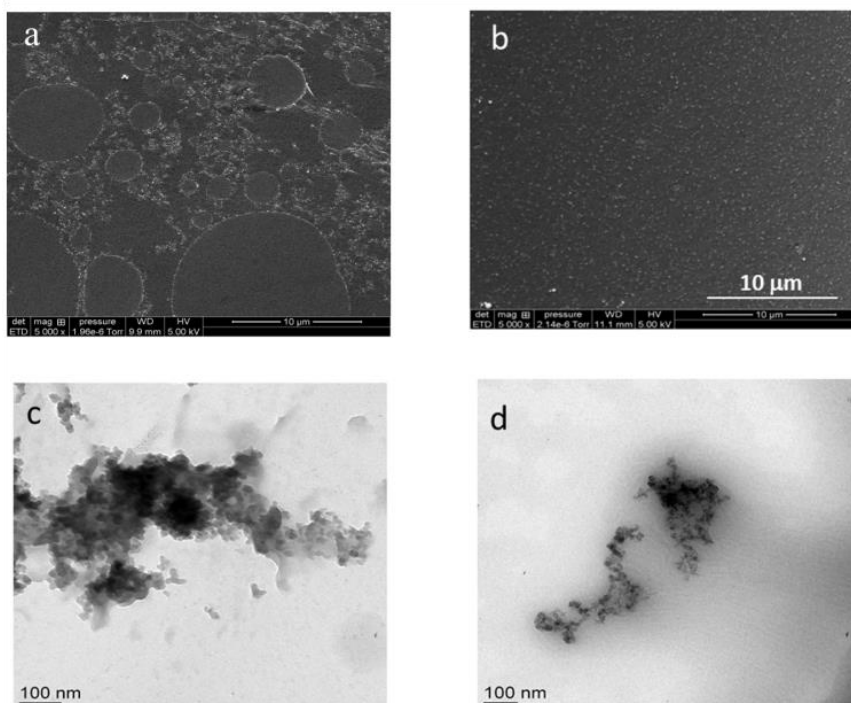


Figure 2.2-7 Cryo-fracture SEM images (a, b) and TEM images (c, d) of SiO₂-PS-b-PPFS crude product in MP (samples a,c- conversion =17%, samples b,d-conversion = 31%, see Table 2.2-1).

Moreover, TEM images of PS-b-PPFS grafted silica crude product in MP suggest that silica agglomerates are partly destroyed upon polymerization (Figure 2.2-7c and d). Indeed, Figure 2.2-7c shows micrometer-sized domains of stringy shaped aggregated particles for a PFS conversion of 17% while the silica particles appear into domains with a size close to 300 nm for a PFS conversion of 31% (Figure 2.2-7d). In addition, the TEM image of pure PS-b-PPFS grafted silica shows that majority of

particles are spherical shaped with diameter about 10 nm and that they are surrounded at the surface by a fuzzy polymer layer (Figure 2.2-8).

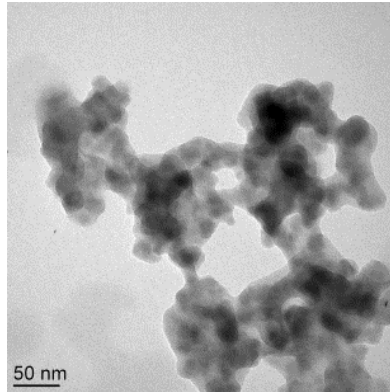


Figure 2.2-8 TEM image of pure SiO₂-PS-b-PPFS nanoparticles (t = 6h; MP) cast from THF suspension (c = 1mg/mL).

The EDX spectra of PS-b-PPFS-grafted silica nanoparticles evidences that the particles observed by TEM (dark regions in Figure 2.2-8) are homogeneously composed of carbon, of oxygen, silicon and fluorine elements, arguing that silica particles are modified with the aforementioned block copolymer (Figure S2.2-5).

Silica particles modified with fluorinated polymers such as PPFS chains constitute relevant candidates to impart hydrophobic surface properties to a given substrate. Thus, dispersions of SiO₂-APTMS and SiO₂-PS-b-PPFS in THF were spin-coated onto activated silicon wafers and the surfaces of the resulting thin films were analyzed by atomic force microscopy (AFM) and through water contact angle (WCA) measurements (Figure 2.2-9).

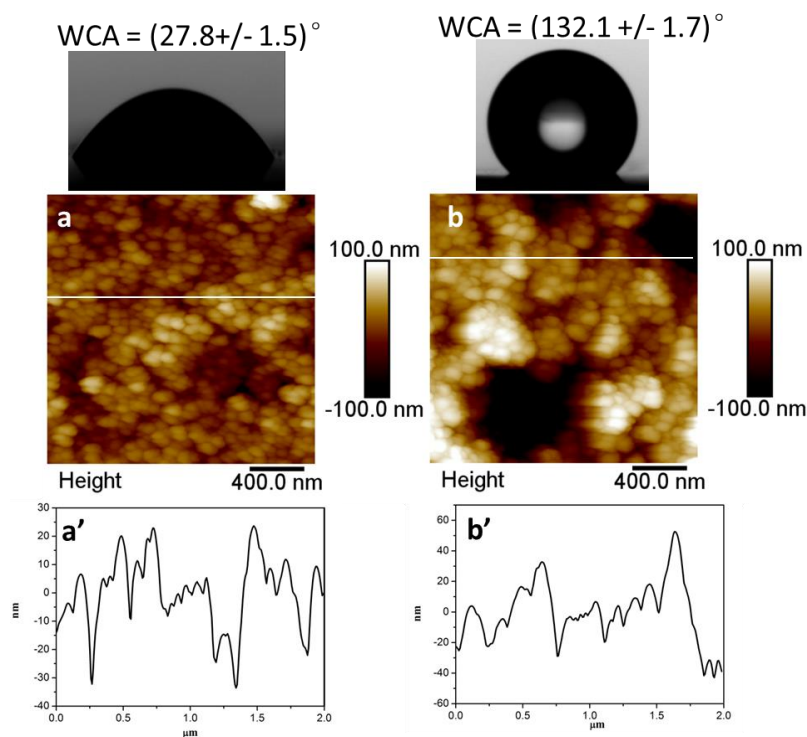


Figure 2.2-9 AFM topographic images of deposition resulting from a) SiO₂-APTMS; b) SiO₂-PS-b-PPFS (grafting weight = 32%, Figure 2.2-6) with the corresponding height profile and wettability properties.

First, compared to neat silicon wafer (Rq value of 0.25 nm, AFM image in Figure S2.2-6), AFM images of both SiO₂-APTMS and SiO₂-PS-b-PPFS enable to ascertain the presence of modified silica at the surface of the silicon wafer (Figure 2.2-9). Indeed, the height profiles of AFM images reveal a dual surface structuration with two main range sizes in lateral dimension (from few tens to few hundreds nm) as the signature of fumed silica particles which can be considered as elementary particles self-assembled in aggregates. This topology corroborates the two-level morphology of SiO₂-PS-b-PPFS evidenced by TEM analysis (Figure 2.2-8). The roughness (Rq) of SiO₂-APTMS is close to 23 nm while the one of SiO₂-PS-b-PPFS increases from 32.5 nm to 55.8 nm when the polymer grafting weight ranges from 5 wt% to 32 wt% (Figure 2.2-6).

Table 2.2-2 Water contact angles for APTMS grafted silica and PS-b-PPFS grafted silica based samples (^aSiO₂-APTMS)

Polymer grafting weight (%)	Water contact Angle (°)	Rq (nm)
0 ^a	27.8±1.5	23.2
5	85.2±2.0	32.5
18	126.5±1.1	42.4
32	132.1±1.7	55.8

Moreover, when water is deposited onto APTMS grafted silica and PS-b-PPFS grafted silica, SiO₂-APTMS exhibits a WCA of 27.8° while SiO₂-PS-b-PPFS displays a WCA in the range 85.2°-132.1° depending on the polymer grafting weight (Table 2.2-2). It is admitted that water contact angles of hydrophobic surfaces are higher than 90° while hydrophilic surfaces have smaller water contact angles (0-30°).⁴⁵ Herein, the presence of polar acrylate groups in SiO₂-APTMS mainly explains its low WCA. Hydrophobicity for SiO₂-PS-b-PPFS samples may be attributed to the nano-scale silica phase well mixed and strongly adhered to the PS-b-PPFS chains. Indeed, both the presence of low surface energy fluorinated groups and the corresponding undulating topology for SiO₂-PS-b-PPFS provide hydrophobic features to the surface, as shown in Figure 2.2-9b. It should also be noted that the WCA determined on a PS-b-PPFS film without silica equals (100.2 ± 1.0)° so the latter result confirms that the large WCA increase observed for SiO₂-PS-b-PPFS containing film is due to both the surface chemistry emanating from the polar character of long PPFS chains (M_n = 31600 g/mol) and the peculiar roughness stemming from the inherent dimensions of fumed silica particles.

2.2.5 Conclusions

Well-defined polystyrene-block-poly(pentafluorostyrene)-coated silica nanoparticles were prepared by nitroxide-mediated polymerization using a “grafting through” approach. The composition structure, chain length, and the polymer grafting weight were precisely controlled and the growth process exhibited all criteria of controlled radical polymerization. It was shown that addition of silica nanoparticles

affects the kinetics of PFS polymerization favorably in polar solvents with apparent rate constants of polymerization increasing by a factor two which may be due to adsorption of DEPN radicals. Moreover, contrary to the use of a “grafting onto” approach, it was observed that the PS-b-PPFS grafting weight increases with increasing PFS conversion probably due to the much favourable chemical affinity of APTMS-grafted silica particles for the PFS polymerization medium by increasing the chain length of the grafted PPFS block. Cryo-fracture SEM and TEM observations confirmed that the dispersability of silica in MP/PFS solution was improved when the PFS conversion was higher than 17% and the silica particles appear into domains with a size varying from 1 μ m to 300 nm by increasing the PFS conversion from 17% to 31%. Finally, it was shown that the hydrophobicity of PS-b-PPFS grafted silica hybrid films can be tailored by the PS-b-PPFS grafting weight.

Future work will examine the influence of the regioselective substitution of para-fluorine atoms of the pentafluorophenyl groups on the interactions between both the grafted polymer chains and silica particles. It is expected that this results will open the route to the elaboration of nanocomposite with potential applications in materials science.

2.2.6 References

- (1) Rybak, A.; Warde, M.; Beyou, E.; Chaumont, P.; Bechelany, M.; Brioude, A.; Toury, B.; Cornu, D.; Miele, P.; Guiffard, B.; et al. Synthesis of Polystyrene Coated SiC Nanowires as Fillers in a Polyurethane Matrix for Electromechanical Conversion. *Nanotechnology* **2010**, *21* (14), 145610.
- (2) Mayes, A. M.; Kumar, S. K. Tailored Polymer Surfaces. *MRS Bull.* **1997**, No. January, 43–47.
- (3) Boyes, S. G.; Brittain, W. J.; Weng, X.; Cheng, S. Z. D. Synthesis, Characterization, and Properties of ABA Type Triblock Copolymer Brushes of Styrene and Methyl Acrylate Prepared by Atom Transfer Radical Polymerization. *Macromolecules* **2002**, *35* (13), 4960–4967.

- (4) Randrianantoandro, H.; Nicolai, T.; Durand, D.; Prochazka, F. Viscoelastic Relaxation of Polyurethane at Different Stages of the Gel Formation. 1. Glass Transition Dynamics. *Macromolecules* **1997**, *30* (19), 5893–5896.
- (5) Kong, X. X.; Kawai, T.; Abe, J.; Iyoda, T. Amphiphilic Polymer Brushes Grown from the Silicon Surface by Atom Transfer Radical Polymerization. *Macromolecules* **2001**, *34* (6), 1837–1844.
- (6) Osborne, V. L.; Jones, D. M.; Huck, W. T. S. Controlled Growth of Triblock Polyelectrolyte Brushes. *Chem. Commun.* **2002**, *1* (17), 1838–1839.
- (7) Auroy, P.; Auvray, L.; Léger, L. Silica Particles Stabilized by Long Grafted Polymer Chains. From Electrostatic to Steric Repulsion. *J. Colloid Interface Sci.* **1992**, *150* (1), 187–194.
- (8) Prucker, O.; Rühle, J. Synthesis of Poly(styrene) Monolayers Attached to High Surface Area Silica Gels through Self-Assembled Monolayers of Azo Initiators. *Macromolecules* **1998**, *31* (3), 592–601.
- (9) Prucker, O.; Rühle, J. Mechanism of Radical Chain Polymerizations Initiated by Azo Compounds Covalently Bound to the Surface of Spherical Particles. *Macromolecules* **1998**, *31* (3), 602–613.
- (10) Laurent, P.; Souharce, G.; Duchet-Rumeau, J.; Portinha, D.; Charlot, A. “Pancake” vs. Brush-like Regime of Quaternizable Polymer Grafts: An Efficient Tool for Nano-Templating Polyelectrolyte Self-Assembly. *Soft Matter* **2012**, *8* (3), 715–725.
- (11) Bourgeat-Lami, E.; Lang, J. Encapsulation of Inorganic Particles by Dispersion Polymerization in Polar Media: 1. Silica Nanoparticles Encapsulated by Polystyrene. *J. Colloid Interface Sci.* **1999**, *197* (197), 293–308.
- (12) Tsujii, Y.; Ohno, K.; Yamamoto, S.; Goto, A.; Fukuda, T. Structure and Properties of High-Density Polymer Brushes Prepared by Surface-Initiated Living Radical Polymerization. *Adv. Polym Sci* **2006**, No. 197, 1–45.
- (13) KICKELBICK, G. *Concepts for the Incorporation of Inorganic Building Blocks into Organic Polymers on a Nanoscale*; 2003; Vol. 28.
- (14) Ruckenstein, E.; Li, Z. F. Surface Modification and Functionalization

through the Self-Assembled Monolayer and Graft Polymerization. *Adv. Colloid Interface Sci.* **2005**, *113* (1), 43–63.

(15) Hui, C. M.; Pietrasik, J.; Schmitt, M.; Mahoney, C.; Choi, J.; Bockstaller, M. R.; Matyjaszewski, K. Surface-Initiated Polymerization as an Enabling Tool for Multifunctional (Nano-)Engineered Hybrid Materials. *Chem. Mater.* **2014**, *26* (1), 745–762.

(16) Matyjaszewski, K.; Xia, J. Atom Transfer Radical Polymerization. *Chem. Rev.* **2001**, *101* (9), 2921–2990.

(17) Hawker, C. J.; Bosman, A. W.; Harth, E. New Polymer Synthesis by Nitroxide Mediated Living Radical Polymerizations. *Chem. Rev.* **2001**, *101* (12), 3661–3688.

(18) Chiefari, J.; Chong, Y. K. B.; Ercole, F.; Krstina, J.; Jeffery, J.; Le, T. P. T.; Mayadunne, R. T. A.; Meijs, G. F.; Moad, C. L.; Moad, G.; et al. Living Free-Radical Polymerization by Reversible Addition - Fragmentation Chain Transfer : The RAFT Process. *Macromolecules* **1998**, *31* (16), 5559–5562.

(19) Bartholome, C.; Beyou, E.; Bourgeat-Lami, E.; Chaumont, P.; Lefebvre, F.; Zydowicz, N. Nitroxide-Mediated Polymerization of Styrene Initiated from the Surface of Silica Nanoparticles. In Situ Generation and Grafting of Alkoxyamine Initiators. *Macromolecules* **2005**, *38* (4), 1099–1106.

(20) Bartholome, C.; Beyou, E.; Bourgeat-Lami, E.; Chaumont, P.; Zydowicz, N. Nitroxide-Mediated Polymerizations from Silica Nanoparticle Surfaces: “Graft from” Polymerization of Styrene Using a Triethoxysilyl-Terminated Alkoxyamine Initiator. *Macromolecules* **2003**, *36* (21), 7946–7952.

(21) Hansen, N. M. L.; Jankova, K.; Hvilsted, S. Fluoropolymer Materials and Architectures Prepared by Controlled Radical Polymerizations. *Eur. Polym. J.* **2007**, *43* (2), 255–293.

(22) Fu, G. D.; Yuan, Z.; Kang, E. T.; Neoh, K. G.; Lai, D. M.; Huan, A. C. H. Nanoporous Ultra-Low-Dielectric-Constant Fluoropolymer Films via Selective UV Decomposition of Poly(pentafluorostyrene)-Block-Poly(methyl Methacrylate) Copolymers Prepared Using Atom Transfer Radical Polymerization. *Adv. Funct.*

Mater. **2005**, *15* (2), 315–322.

(23) Souzy, R.; Ameduri, B. Functional Fluoropolymers for Fuel Cell Membranes. *Fluorinated Mater. Energy Convers.* **2005**, *30*, 469–511.

(24) Hvilsted, S. The Pentafluorostyrene Endeavours with Atom Transfer Radical Polymerization-Quo Vadis? *Polym. Int.* **2014**, *63* (5), 814–823.

(25) Jankova, K.; Hvilsted, S. Preparation of Poly(2,3,4,5,6-Pentafluorostyrene) and Block Copolymers with Styrene by ATRP. *Macromolecules* **2003**, *36* (5), 1753–1758.

(26) Borkar, S.; Jankova, K.; Siesler, H. W.; Hvilsted, S. New Highly Fluorinated Styrene-Based Materials with Low Surface Energy Prepared by ATRP. *Macromolecules* **2004**, *37* (3), 788–794.

(27) Bucholz, T. L.; Loo, Y.-L. Phase Behavior of Near-Monodisperse Semifluorinated Diblock Copolymers by Atom Transfer Radical Polymerization. *Macromolecules* **2006**, *39* (18), 6075–6080.

(28) Paz-Pazos, M.; Pugh, C. Synthesis, Isolation, and Thermal Behavior of Polybutadiene Grafted with poly(2,3,4,5,6-Pentafluorostyrene). *J. Polym. Sci. Part A Polym. Chem.* **2005**, *43* (13), 2874–2891.

(29) Powell, K. T.; Cheng, C.; Wooley, K. L. Complex Amphiphilic Hyperbranched Fluoropolymers by Atom Transfer Radical Self-Condensing Vinyl (Co)polymerization. *Macromolecules* **2007**, *40* (13), 4509–4515.

(30) Becer, C. R.; Babiuch, K.; Pilz, D.; Hornig, S.; Heinze, T.; Gottschaldt, M.; Schubert, U. S. Clicking Pentafluorostyrene Copolymers: Synthesis, Nanoprecipitation, and Glycosylation. *Macromolecules* **2009**, *42* (7), 2387–2394.

(31) Ott, C.; Hoogenboom, R.; Schubert, U. S. Post-Modification of Poly(pentafluorostyrene): A Versatile “click” method to Create Well-Defined Multifunctional Graft Copolymers. *Chem. Commun.* **2008**, *30* (30), 3516–3518.

(32) Gudipati, C. S.; Tan, M. B. H.; Hussain, H.; Liu, Y.; He, C.; Davis, T. P. Synthesis of Poly(glycidyl Methacrylate)-Block-Poly(pentafluorostyrene) by RAFT: Precursor to Novel Amphiphilic Poly(glyceryl Methacrylate)-Block-Poly(pentafluorostyrene). *Macromol. Rapid Commun.* **2008**, *29* (23), 1902–1907.

- (33) Irita, T.; Chen, D.; Li, X.; Wang, J.; Russell, T. P. Thin Films of Semifluorinated Block Copolymers Prepared by ATRP. *Macromol. Chem. Phys.* **2011**, *212* (22), 2399–2405.
- (34) Cai, T.; Yang, W. J.; Neoh, K.-G.; Kang, E.-T. Preparation of Jellyfish-Shaped Amphiphilic Block-Graft Copolymers Consisting of a Poly(ϵ -Caprolactone)-Block-Poly(pentafluorostyrene) Ring and Poly(ethylene Glycol) Lateral Brushes. *Polym. Chem.* **2012**, *3* (4), 1061–1068.
- (35) Puretskiy, N.; Ionov, L. Synthesis of Robust Raspberry-like Particles Using Polymer Brushes. *Langmuir* **2011**, *27* (6), 3006–3011.
- (36) Chen, J.; Dumas, L.; Duchet-Rumeau, J.; Fleury, E.; Charlot, A.; Portinha, D. Tuning H-Bond Capability of Hydroxylated-poly(2,3,4,5,6-Pentafluorostyrene) Grafted Copolymers Prepared by Chemoselective and Versatile Thiol-Para-Fluoro “click-Type” coupling with Mercaptoalcohols. *J. Polym. Sci. Part A Polym. Chem.* **2012**, *50* (16), 3452–3460.
- (37) Chen, J.; Duchet, J.; Portinha, D.; Charlot, A. Layer by Layer H-Bonded Assembly of P4VP with Various Hydroxylated PPFS: Impact of the Donor Strength on Growth Mechanism and Surface Features. *Langmuir* **2014**, *30* (35), 10740–10750.
- (38) Dumas, L.; Fleury, E.; Portinha, D. Wettability Adjustment of PVDF Surfaces by Combining Radiation-Induced Grafting of (2,3,4,5,6)-Pentafluorostyrene and Subsequent Chemoselective “click-Type” Reaction. *Polymer (Guildf)*. **2014**, *55* (11), 2628–2634.
- (39) Bialk, M.; Prucker, O.; Ruhe, J. Grafting of Polymers to Solid Surfaces by Using Immobilized Methacrylates. *Colloids Surfaces A Physicochem. Eng. Asp.* **2002**, *198–200*, 543–549.
- (40) Jean-Luc Couturier, O. G. WO2002012149A8, 2002.
- (41) Nicolas, J.; Guillaneuf, Y.; Lefay, C.; Bertin, D.; Gigmes, D.; Charleux, B. Nitroxide-Mediated Polymerization. *Prog. Polym. Sci.* **2013**, *38* (1), 63–235.
- (42) Audran, G.; Brémond, P.; Marque, S. R. A.; Obame, G. Chemically Triggered C–ON Bond Homolysis of Alkoxyamines. Part 4: Solvent Effect. *Polym. Chem.* **2012**, *3* (10), 2901.

- (43) Zaremski, M.; Borisova, O.; Xin, C.; Golubev, V. B.; Billon, L. Influence of Media Polarity on the Rate of Activation Of “dormant” chains in Nitroxide-Mediated Radical Polymerization. *J. Polym. Sci. Part A Polym. Chem.* **2012**, *50* (16), 3437–3443.
- (44) Guo, C.; Zhou, L.; Lv, J. Effects of Expandable Graphite and Modified Ammonium Polyphosphate on the Flame-Retardant and Mechanical Properties of Wood Flour-Polypropylene Composites. *Polym. Polym. Compos.* **2013**, *21* (7), 449–456.
- (45) Salami-Kalajahi, M.; Haddadi-Asl, V.; Behboodi-Sadabad, F.; Rahimi-Razin, S.; Roghani-Mamaqani, H. Effect of Silica Nanoparticle Loading and Surface Modification on the Kinetics of RAFT Polymerization. *J. Polym. Eng.* **2012**, *32* (1), 13–22.

2.2.7 Supporting information

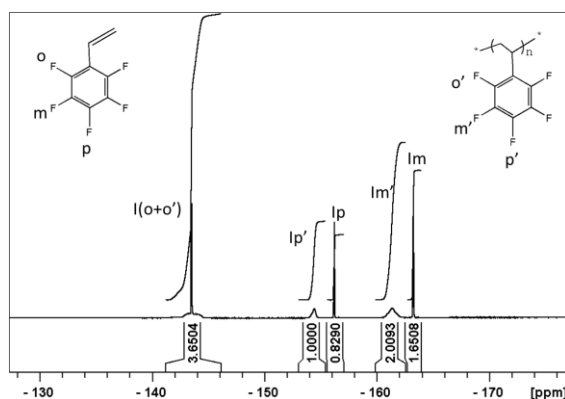


Figure S2.2-1 ^{19}F NMR of spectrum of the reaction mixture for calculation of the conversion PFS (presented spectrum corresponds to 55% conversion in MP after 4 hours).

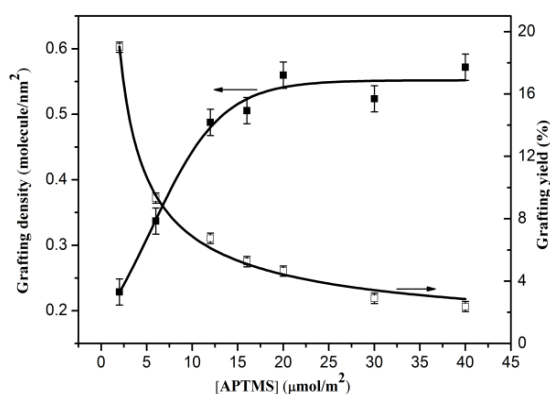


Figure S2.2-2 Grafting density (filled symbols) and grafting yield (hollow symbols) of APTMS as a function of the concentration of APTMS. Silica concentration 3.8 wt % in Toluene. Temperature 110 °C. Reaction time 24 h.

Table S2.2-1 Characteristics of free PS-PPFS block copolymers synthesized in presence of APTMS-grafted silica as a function of solvent.

Solvent	Time (h)	Conversion (%)	Mn (theo) (g/mol)	Mn (NMR) (g/mol)	Mn (SEC) (g/mol)	\bar{D}
MP	0.5	17	10700	10500	8900	1.29
	1	31	16100	17800	12600	1.18
	2	48	22700	24300	15100	1.15
	4	74	32800	30900	18000	1.14
	6	76	33600	31600	18900	1.15
DMF	0.5	17	9900	10500	11000	1.28
	1	19	10700	11100	12200	1.23
	2	34	16300	18200	16800	1.17
	4	47	21500	22500	19900	1.13
	6	62	27300	28500	23000	1.11
TOLUENE	1	2.2	5300	5400	4600	1.57
	2	4.3	6100	6500	5300	1.5
	4	7	7100	7300	5800	1.48
	6	12.2	9100	8700	7700	1.36

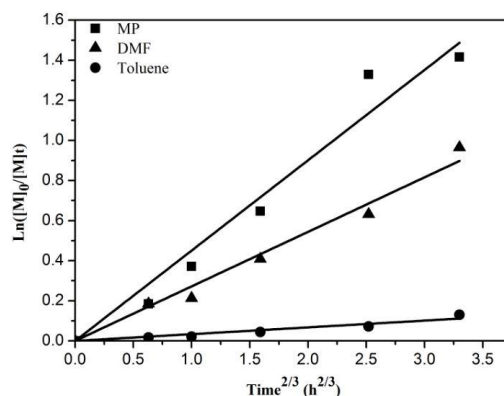


Figure S2.2-3 Kinetic plot for the polymerization of PFS in the presence of APTMS modified silica (4.3 wt.%).

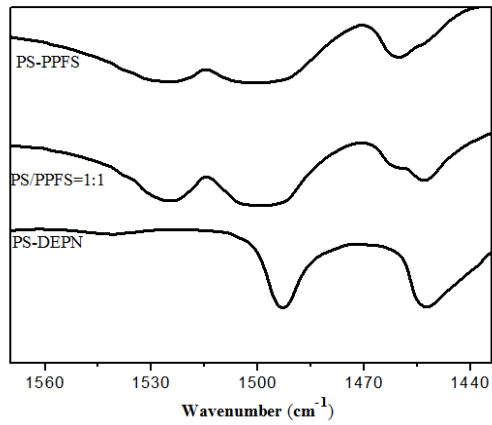


Figure S2.2-4 FT-IR spectra of free PS-*b*-PPFS copolymer, PS/PPFS homopolymers mixture ((1/1, w/w) and PS-DEPN macroinitiator

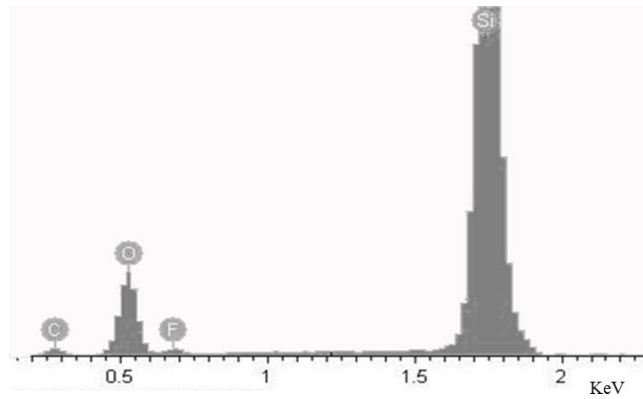


Figure S2.2-5 EDX analysis from TEM image for PS-*b*-PPFS grafted silica.

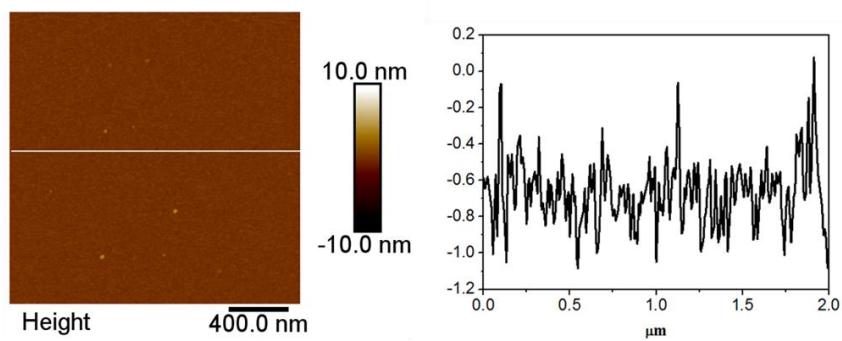


Figure S2.2-6 AFM topographic images of deposition resulting from neat silicon wafer.

2.3 Controlled perfluorination of fluorinated polymer and functionalized fumed silica: towards the design of self-cleaning (nano)composite films

2.3.1 Abstract

Synthesis of low surface energy perfluorinated poly(2,3,4,5,6-pentafluorostyrene) (PPFS) derivatives as well as the surface morphology and wetting properties of organic/inorganic (nano)composite films prepared by combining such polymers with functionalized silica (nano)particles is presented. The post-polymerization modification of PPFS with perfluorinated decane thiol (PFDT) via a versatile thiol-*para*-fluoro coupling was optimized to synthesize soluble fluoropolymer PPFS-PFDT with randomly distributed perfluorinated groups, which hydrophobicity is tuned by the degree of substitution (DS). Then, the coupling reaction was successfully applied to the perfluorination of fumed silica that was priority modified at the surface with PPFS-containing polymers. A library of fluorinated polymers (pristine PPFS or PPFS-PFDT with different DS), and 3 kinds of silica that differ in their surface chemistry (modified with a silane, with PPFS or with perfluorinated PPFS) were thus prepared and finally combined to elaborate nanocomposite films. DS of PPFS derivatives and silica content were both varied to obtain films with the appropriate surface chemistry and multiscale textured surface that endow the films with self-cleaning properties.

Keywords

pentafluorostyrene, thiol-*para*-fluoro coupling, superhydrophobic surfaces, fumed silica-based (nano)composite films

2.3.2 Introduction

Design of polymer materials with dedicated and tailored wetting surface properties is of high interest in various fields, from medicine and biotechnology to housing or microelectronics.¹ In particular, surfaces with superhydrophobic properties are of great interest due to endless potential technological applications, such as anti-fouling surfaces, anti-fogging and anti-icing coatings, drag reduction, etc.²⁻⁴ Superhydrophobicity relies on the difficult wetting of a surface by water, which is characterized by an apparent water contact angle θ_{H_2O} greater than 150° . Moreover, when the water hysteresis is low (typically $< 10^\circ$), self-cleaning and easily roll-off properties are achieved, as exhibited by the natural “Lotus” effect.^{5,6} It is well-known that hydrophobic polymer material endowed with a dual-roughened surfaces in nano/microscale can manifest such super water-repellency. Numerous down-top and bottom-up strategies have been reported to engineer superhydrophobic polymer films, including for instance the selective etching or the patterning of surface with lithography,^{7,8} the templating by breath figures,⁹ the Layer-by-layer deposition,^{10,11} the structuration of polymer films *via* a phase separation mechanism,¹² the control of the polymer crystallization,¹³ the electrospinning of fibers that inherently present characteristic length at different scales,^{14,15} among many others. Furthermore, the introduction of preformed inorganic particles within well-suited polymer matrices has appeared as a powerful means to provide a multi-scale surface texturing, taking advantage of the desirable properties of the two components in terms of processability, durability and/or mechanical properties.¹⁶⁻¹⁹ To that extent, in many reports, silica particles, that present versatile and outstanding properties (availability of a large panel of sizes and morphologies and tunability of the surface chemistry, high mechanical properties) have been embedded into polymer matrices^{16,20-22} and, in this context, fluorinated polymers are of special interest because of their inherent low surface energy provided by the fluorine atoms. Polymers containing *n* perfluoro- $-(CF_2)_{n-1}-CF_3$ or semifluoro- $-(CH_2)_m(CF_2)_{n-1}-CF_3$ alkyl groups (with $n \geq 8$) as side

chains are particularly interesting due to their high θ_{H_2O} (above 120°).²³ However, these polymers are usually not soluble in most organic solvents, and thus copolymers, containing for instance methyl, butyl, stearyl, 2-hydroxyethyl (meth)acrylate, acrylic acid or styrene, synthesized by conventional radical polymerization (in emulsion or not) are preferred.²⁴⁻²⁹ Polyvinylidene fluoride and its copolymers, such as poly(vinylidene fluoride-co-hexafluoropropylene) have also been used.^{30,31} These various fluorinated polymers were utilized as host matrices and were mixed with commercially available hydrophobic silica particles, usually chemically modified with short hydrophobic silane agents (alkyl, vinyl, dimethyl siloxane). The silica fillers migration to the surface combined to the apolar character of the host polymer lead to straightforwardly prepared superhydrophobic films ($\theta_{H_2O} > 150^\circ$, and multiscale roughness for well suited silica content).²⁴⁻³¹ However, these conventional fluorinated (co)polymers and modified silica particles do not allow finely tailoring neither the surface chemistry nor the compatibilization degree between the filler and the polymer, which is yet well-known as being the key parameter controlling the morphology³² and thus the surface topology.

Other interesting fluorinated polymers that can be used for obtaining superhydrophobic properties are pentafluorostyrene (PFS)-based polymers. Indeed, PPFS shares the common properties of the C-F bonds and fluorine atoms with θ_{H_2O} around 110° , and tend to be more soluble than other fluorinated polymers in common organic solvents.³³ PPFS can be synthesized by controlled radical polymerization techniques³³⁻⁴³ and recently we described the synthesis of hydrophobic fumed PPFS-b-PS grafted silica particles by combining nitroxide mediated polymerization and the “grafting through” procedure.⁴³ Moreover, as reported by our group and others, the labile fluorine atom in *para* position can interestingly undergo substitution reactions with a number of nucleophiles including amines,³⁹ alcohols⁴⁴ and thiols^{41,45-49}. Some authors have thus reported the modification of the PFS monomer with semifluoroalkyl alcohols of different lengths, monomers that were then polymerized to end up with various polymer architectures.^{33,50,51} For homopolymers,

introducing fluorinated side chain increases the water contact angle ($\theta_{H_2O} \sim 122^\circ$) for a long side chain (8 carbons), as expected. However, the corresponding homopolymers turned out to be insoluble in common organic solvents used for fluorinated polymers (THF, DMF etc). Introducing shorter side chain (3 carbons) ensures solubility but the water contact angle was lower ($\theta_{H_2O} \sim 117^\circ$). Some other groups circumvent this issue by using PPFS-b-PS block copolymers containing a (short) PPFS sequence (degree of polymerization DP = 4) modified with a long semifluorinated side chain, and a long polystyrene block (DP = 89) that was here to ensure solubility.^{50,51} Sophisticated techniques (such as electrospinning⁵⁰ and breath figures⁵¹) that counterbalance the reduction of the water contact angle were then used to prepare superhydrophobic surfaces from this PPFS-based copolymer. Moreover, we can cite the elegant work of Pureskiy and Ionov who developed superhydrophobic coatings constituted of polymer-brush-based raspberry-like particles with grafted chains of PPFS.⁵² However, this multi-step strategy appears much tedious and difficult to scale up, when compared with the use of previously described (nano)composites.

In the continuing challenge to prepare surfaces with superhydrophobic features, we developed non-conventional (nano)composites by taking benefit of all attributes offered by both modifiable PPFS and fumed silica (Figure 2.3-1). Indeed, *i*) PPFS displays a very low surface energy with a good solubility in common organic and its apolar character can be adjusted by its degree of substitution (DS) and *ii*) fumed silica inherently presents a double scale of roughness (the one of the elementary nanoparticles that form aggregates up to hundreds of nanometers) and its surface can be modified in order to ensure an appropriate dispersion in the matrix. Thus PPFS was synthesized and further modified with a perfluorinated thiol (PFDT) in a controlled manner resulting in PPFS-PFDT derivatives. Then, acryloxytrimethoxysilane-grafted fumed silica (SiO₂-APTMS) was chemically modified by PS-b-PPFS block copolymers (SiO₂-PS-PPFS) followed by their substitution with PFDT (SiO₂-PS-PPFS-PFDT). Finally, these two components were combined in various

compositions, to end up with nanocomposite films and their wettability and morphological properties are discussed as a function of the composition and the silica content.

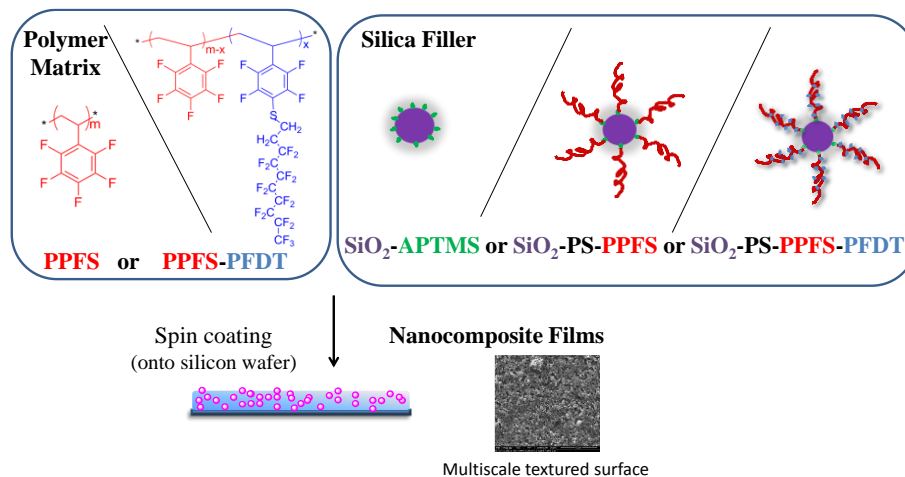


Figure 2.3-1 Route to the (nano)composite films

2.3.3 Experimental part

2.3.3.1 Materials

2,3,4,5,6-pentafluorostyrene (PFS, 99%, Aldrich) was distilled under vacuum and stored at -20°C . N-Methyl pyrrolidone (MP, 99%, Aldrich) was distilled before used. DEPN (N-tert-butyl-N-(1-diethylphosphono-2, 2-dimethyl) propyl nitroxide) was used as received from Polymer expert. The DEPN-based alkoxyamine (Styryl-DEPN) was prepared using a procedure described in the literature.⁵³ All other products, Methyl ethyl ketone (MEK, 99%); 1H,1H,2H,2H-Perfluorodecanethiol (PFDT, 97%); 1,8-Diazabicyclo[5.4.0]undec-7-ene (DBU, 98%); N,N-Diisopropylethylamine (DiPEA, 99.5%); N,N-Dimethylpyridin-4-amine (DMAP, 99%); Triethylamine (Et_3N , 99%) and Diiodomethane (99%) were purchased from Sigma-Aldrich and used as received. Milli-Q-quality water was used as probe liquid for wettability experiments. Silicon wafers were purchased from SIL'TRONIX. Nanohybrid particles (SiO_2 -APTMS and SiO_2 -PS-PPFS) were synthesized in our previous work.⁴³ The grafting density of APTMS is 0.55 molecule/ nm^2 , and the

grafting weight of PS-b-PPFS (composition is 87.9 wt% of PPFS) is 32 wt%.

2.3.3.2 Polymerization of 2,3,4,5,6-pentafluorostyrene (PFS)

PPFS was obtained by nitroxide mediated polymerization (NMP) conducted in MP using Styryl-DEPN as initiator. In a model reaction, PFS (5 mL, 36 mmol) was dissolved in MP (5 mL). Styryl-DEPN (72 mg, 0.18 mmol) was added to get a solution with $[PFS]/[Styryl-DEPN] = 200$. Then, the mixture was divided into 5 vials (2 mL each), each of them was degassed four times by freeze-pump-thaw cycles, flame-sealed under vacuum and then heated in a preheated oil bath at 110°C for various reaction times (0.5 h, 1 h, 2 h, 4 h and 6 h). Then polymerization was stopped by immersing the flask into liquid nitrogen. An aliquot was withdrawn and further dedicated to conversion determination by ^{19}F NMR. The polymer was recovered by precipitation conducted in cold methanol, then dissolved in THF and then precipitated again. The polymers were collected by filtration and then dried at 50 °C under vacuum overnight with a yield = 97% after 6 h.

2.3.3.3 Modification of PPFS by thiol-*para*-fluoro substitution reaction

PPFS was modified by nucleophilic substitution with PFDT using various bases (DBU, DiPEA, DMAP and Et₃N). In a typical procedure, PPFS (14 000 g·mol⁻¹, $D=1.2$, 1 equiv. of PFS units) was dissolved in MEK (concentration 100 g/L), then PFDT (0.5 equiv. of -SH) and DBU (0.1 equiv.) were sequentially added. The mixture was stirred for 10 min at room temperature. Polymers were purified by precipitation into cold methanol, rinsed twice with ethanol until no residual PFDT or base was revealed by 1H NMR. The collected polymers were dried at 40°C under vacuum overnight. Yield = 76%; degree of substitution (noted DS) was determined by ^{19}F NMR and/or by FTIR (27% in the given example). Specimens are then designated as PPFS-PFDT with their respective DS in the text. Comparatively, SiO₂-PS-PPFS were dispersed in MEK and modified with PFDT using only DBU as a base, at room temperature for 6h. DS was then determined by FTIR and TGA.

2.3.3.4 Film preparation.

Silicon wafers were cut into appropriate dimensions (typically 1 cm×1 cm) before used, and activated by ozonolysis for 30 min prior to any deposition. Polymer (PPFS or PPFS-PFDT) was dissolved in THF (30 mg/mL). A separate dispersion of hybrid SiO₂ particles (SiO₂-APTMS or SiO₂-PS-PPFS or SiO₂-PS-PPFS-PFDT) in THF (30 mg/mL) were added to the polymer solution with adjusting the volume ratio of the two solutions, such that dispersions with different silica content in weight percent (23 wt%, 35 wt%, 46 wt%,) were obtained. After sonication for 30 min, the mixture was magnetically stirred for 2 hours and then, 0.1 mL of such suspension was spin-coated onto the activated silicon wafer with a speed of 2000 rpm for 30 s using a Polo Spin 150i/200i spin-coater type from SPS-Europe. The sample was then dried at room temperature for two days before any analysis. The (nano)composite film is identified by the type of silica SiO₂-APTMS or SiO₂-PPFS or SiO₂-PS-PPFS-PFDT (DS = x %) with the associated silica content (23 wt%, 35 wt%, 46 wt%) and the type of the host matrix : PPFS or PPFS-PFDT (DS = y %).

2.3.3.5 Characterization Methods

Attenuated total reflection Fourier transform infrared (ATR-FTIR). ATR-FTIR spectra were recorded using a Nicolet iS10 apparatus (diamond crystal) with a resolution of 4 cm⁻¹ and a 32 scans accumulation within a range of 500–4000 cm⁻¹.

Size exclusion chromatography (SEC). SEC characterizations were performed using a 2690 Waters Alliance System with THF (HPLC grade) as eluent at a flow rate of 1 mL/min. The chromatographic device was equipped with four Styragel columns HR 0.5, 2, 4 and 6 at 40 °C in series with a 2410 Waters refractive index detector and a 996 Waters photodiode array detector. A calibration curve was established with low dispersity index Polystyrene standards.

Nuclear magnetic resonance spectroscopy (NMR). ¹H and ¹⁹F NMR spectra were recorded on a Bruker Advanced AM400 spectrometer at 400 MHz. Analytes

were dissolved in CDCl₃ or THF-d₈, chemical shifts were determined in ppm with 64 scans for each kind of analysis (at 25°C for DS ≤ 33%, 50°C otherwise). ¹H spectra were calibrated thanks to Tetramethylsilane at 0 ppm, while ¹⁹F spectra were calibrated thanks to the signal at -143 ppm that corresponds to the fluorine in {*ortho* + *ortho*'} positions (see Figure 2.3-2A).

Thermogravimetric analysis (TGA). TGA measurements were performed on a TA Q500 under a helium flow (40 mL/min) at a heating rate of 10 °C/min from room temperature up to 600 °C for polymers, to 800°C for polymer-grafted silica.

Differential scanning calorimetry (DSC). DSC thermal analyses were performed with a differential scanning calorimeter, DSC Q1854 from TA Instruments, in a temperature range of 0°C to 200 °C at a heating rate of 10 °C/min under a helium flow (25 mL/min). Three scans (heat/cool/heat, separated by a 2 min isotherm) were realized for each sample. The glass transition temperature (T_g) is automatically determined by the instrument from the second heating trace and is reported as the midpoint of the thermal transition.

Wettability. Water contact angle ($\theta_{\text{H}_2\text{O}}$), water hysteresis (advancing contact angle – receding contact angle) ($\Delta\theta_{\text{H}_2\text{O}}$) and methylene iodide contact angle ($\theta_{\text{CH}_2\text{I}_2}$) were measured using a Dataphysics Digidrop contact angle meter equipped with a CDD2/3 camera with the sessile drop method. The tabulated results are the average of at least five measurements on different locations of each sample. The surface energy γ_s was calculated by using the Owens-Wendt model, that uses the contact angles with the two above probe liquids θ_i and their two components (the one related to dispersive interactions $\gamma_{L,i}^D$ and to polar interactions $\gamma_{L,i}^P$) which sum results in their surface tension $\gamma_{L,i}$. Indeed, by combining (a) the Young's equation that lies γ_s to the solid/liquid interfacial tension $\gamma_{SL,i}$ according to $\gamma_s = \gamma_{SL,i} + \gamma_{L,i} \cos \theta_i$, with (b) the expression of $\gamma_{SL,i}$ according to the geometrical mean method that states that : $\gamma_{SL,i} = \gamma_s + \gamma_{L,i} - 2\left(\sqrt{\gamma_s^D \cdot \gamma_{L,i}^D} + \sqrt{\gamma_s^P \cdot \gamma_{L,i}^P}\right)$ one can then compute the dispersive γ_s^D and polar γ_s^P contributions, the sum of which is γ_s .

Scanning electron microscopy (SEM) and Energy dispersive X-ray analysis (EDX). A FEI QUANTA 250 Scanning Electron Microscopy coupled with a SAMX Microanalysis X-Ray system was used to observe the morphology and chemical composition of samples. A thin layer of Carbon was coated to obtain a conductive surface and make easily to perform EDX analysis. The accelerating voltage of 5KV was chosen to optimize at the same time the observation and EDX spectrum realized (depth analyzed EDX : 250 nm simulated by casino software).

Atomic force microscopy (AFM). AFM images were acquired in intermittent contact mode (tapping mode), on a wafer of 1 cm × 1 cm, in air at room temperature using an AFM Bruker Multimode 8 apparatus equipped with Nanoscope V controller. The scanning speed for image acquisition is 0.5 Hz. The used tips are purchased from Bruker with the model of SCANASYST-AIR. The surface roughness Rq was obtained by processing images using the Nanoscope Analysis software (version 1.5).

X-ray photoelectron spectroscopy (XPS). XPS analysis of the surfaces was conducted on a PHI Quantera SXM Spectrometer using monochromatized AlK α X-RAY radiation source with a photon energy of 1486.6eV. The pressure in the chamber was below 10⁻⁹-10⁻¹⁰ torr before the data were taken, and the voltage and current of the anode were set at 15 kV and 3 mA, respectively. The pass energy was 40 eV. The binding energy scale was fixed with setting the C1s peak maximum at 285.0 eV.

Determination of degree of substitution (DS). DS was independently determined by different analytical means. One resides in ¹⁹F NMR spectrum, through the ratio of the integral at $\delta = -133$ ppm (*meta*' fluorine of modified PFS units) to the one at $\delta = -143$ ppm (*ortho*'- and *ortho*-fluorines of overall PFS units, see Figure 2.3-2A). Another technique consists in the use of FTIR, through the ratio of the peak absorbance of modified PFS units ($A_{\text{modified PFS}}$, at 1473 cm⁻¹) to the one of unmodified PFS units ($A_{\text{unmodified PFS}}$ at 1497 cm⁻¹, see Figure 2B) that is related to DS (in mol%) according to: $\frac{A_{\text{modified PFS}}}{A_{\text{unmodified PFS}}} = \frac{A_{1473}}{A_{1497}} = k \cdot \frac{\text{DS}}{\text{DS}-100}$.⁵⁴ For such purpose, a calibration

line was built with homopolymers which DS was independently determined by ^{19}F NMR. By using the results obtained by TGA, the DS (in mol%) for polymer-modified silica can be determined according to the following equation:

$$DS = \frac{(W_{\text{SiO}_2\text{-PS-PPFS-PFDT}} - W_{\text{SiO}_2\text{-PS-PPFS}}) \cdot Mn_{\text{PS-PPFS}}}{DPn_{\text{PPFS}} \cdot (W_{\text{SiO}_2\text{-PS-PPFS}} - W_{\text{SiO}_2\text{-APTMS}}) \cdot (M_{\text{PFDT}} - 19)} \times 100\%$$

where $W_{\text{SiO}_2\text{-APTMS}}$, $W_{\text{SiO}_2\text{-PS-PPFS-PFDT}}$, $W_{\text{SiO}_2\text{-PS-PPFS}}$ are the weight loss of $\text{SiO}_2\text{-APTMS}$, $\text{SiO}_2\text{-PS-PPFS}$ and $\text{SiO}_2\text{-PS-PPFS-PFDT}$, respectively; DPn_{PPFS} is the degree of polymerization of the PPFS block in the grafts, $Mn_{\text{PS-PPFS}}$ and M_{PFDT} are the molecular weight of the PS-b-PPFS grafts (determined by ^1H NMR) and PFDT, respectively.

2.3.4 Results and discussion

2.3.4.1 Synthesis of polymer matrices: PPFS and PPFS-PFDT samples

In order to prepare (nano)composite films including perfluorinated-PPFS components either as the matrix and/or as the surface modifier of the nanofiller, both PPFS homopolymer and PPFS-coated silica nanoparticles were targeted to be further subjected to *para*-fluoro thiol substitution reaction. To evaluate the impact of the introduction of the perfluorinated side chain on the properties of the films, it appeared relevant to control the post-polymerization step, in particular regarding the adjustment of the extent of the modification; this optimization was performed on the homopolymers, and then applied to the modification of the PPFS-modified silica. Homopolymerization of PFS was achieved by NMP conducted at 110°C in MP using styryl-DEPN as initiator ($[\text{PFS}]_0/[\text{Styryl-DEPN}]_0$ ratio of 200) (Scheme 2.3-1).

perfluorinated chain, in conjunction with the band at 1473 cm^{-1} that we previously assigned to the fluorinated aromatic ring vibrations of the modified PFS (Figure 2.3-2B).⁵⁴ The DS can be determined by comparing the intensity of the peak at 1473 cm^{-1} to the one of the non-modified PFS units (at 1497 cm^{-1}) with the help of a calibration line established using samples which DS was independently determined by ^{19}F NMR.⁵⁴

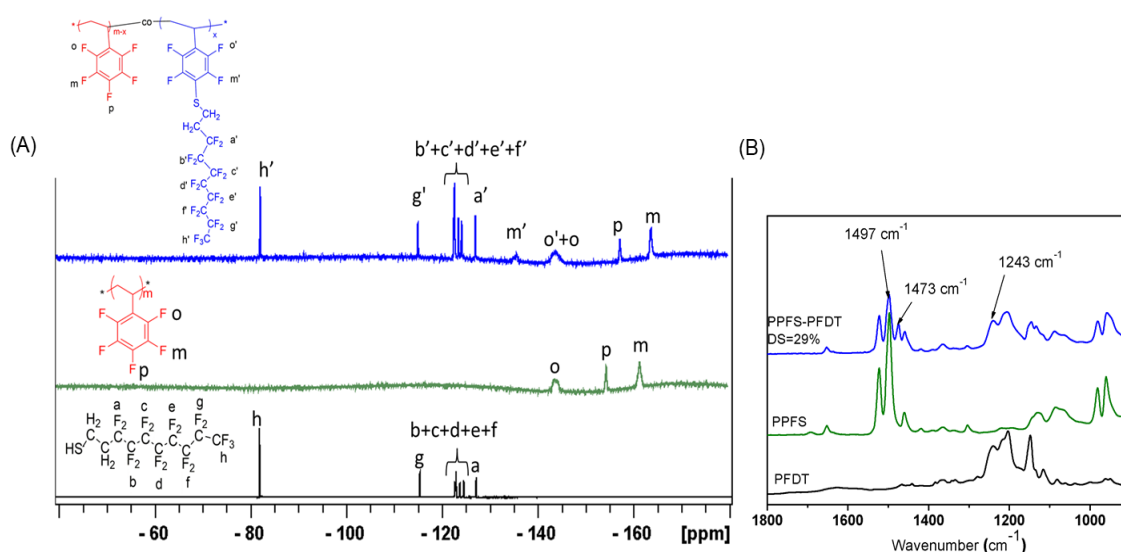


Figure 2.3-2 A] ^{19}F NMR in CDCl_3 and B] FTIR spectra of PFDT, PPFS and PPFS-PFDT (DS = 29%)

First, experiments were conducted at room temperature with a [PFS]:[PFDT]:[Base] ratio of 1:1:1 with various bases (Table 2.3-1, entries 1-4); the results are expressed as the DS attained at t time. By using amines with a rather strong (NEt_3 or DMAP) or null (DiPEA) nucleophilic character, it was observed that the DS values were in the 28-39% after a reaction time in the 180-210 min range (Table 2.3-1, entries 1-3). On the contrary, an almost instantaneous reaction was observed by using the non-nucleophilic strongest base DBU such that a DS of 84% was attained in 2 minutes (Table 2.3-1, entry 4). Such exceptional acceleration of thiol-*para*-fluoro substitution in presence of DBU has been recently reported on (pentafluorophenyl)acetamide⁵⁵ and PFS⁴⁵ containing copolymers.

Table 2.3-1 Effect of experimental conditions on the DS for the thiol-*para*-fluoro coupling on PPFS (entries 1-9) and SiO₂-PS-PPFS (entries 10-11).

Entry	PPFS-functional precursor	Base	[PFS]:[PFDT]:[Base]	Time (min)	DS (%)
1	PPFS (a)	DiPEA	1:1:1	210	28
2	/	DMAP	1:1:1	180	33
3	/	Et ₃ N	1:1:1	180	39
4	/	DBU	1:1:1	2	84
5	/	DBU	1:1:0.2	10	52
6	/	DBU	1:0.5:0.1	20	25
7	/	DBU	1:0.3:0.06	30	15
8	/	DBU	1:0.15:0.03	40	7
9	/	DBU	1:2:0.4	10	96
10	SiO ₂ -PS-PPFS (b)	DBU	1:0.3:0.06	360	13
11	/	DBU	1:1:0.2	360	47

(a) $M_n = 14\,000\text{ g.mol}^{-1}$ (SEC) (b) grafting weight = 32 w.%, $M_n = 31\,600\text{ g.mol}^{-1}$ (¹H NMR)

We were then interested in controlling the DS of PPFS in perfluorinated graft. Two strategies were envisioned: the first one consisted in adjusting the DS by kinetic control, the second one by tuning the [PFS]:[PFDT]:[DBU] ratio.

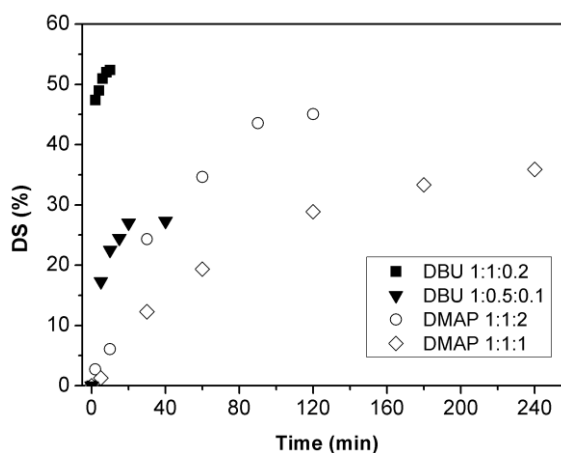


Figure 2.3-3 DS as a function of reaction time for thiol-*para*-fluoro coupling of PPFS with PFDT for various [PFS]:[PFDT]:[Base] ratios with DMAP (empty symbols) or DBU (filled symbols) as a base (see legend).

Figure 2.3-3 shows that the DS increases regularly with time when using DMAP as a base, tending to a plateau at a DS around 35% after 4 hours with using a [PFS]:[PFDT]:[Base] ratio of 1:1:1. By increasing the latter concentration ratio to 1:1:2, the reaction is rather accelerated and a higher DS of 45% is attained after 2h. It is thus rendered possible to adjust the DS for values up to 45% in a reasonable timescale. Because the reaction with DBU was much faster, it was needed to lower the DBU content to render the kinetic control possible. While modifying methacrylic-b-styrenic diblock copolymers containing a few PFS moieties in the styrenic block with an alkyl thiol, Delaittre *et al.*⁴⁵ demonstrated that the amount of DBU could be reduced to as low as 0.15 equiv. to achieve a DS of 48% in 4 hours when the [PFS]:[Thiol] ratio was set at 1:5. For our investigations, we chose to work with higher [PFS]:[PFDT] ratios to avoid excessive thiol content, and we fixed a [PFDT]:[DBU] ratio of 5:1 (Figure 2.3-3). By using a [PFS]:[Thiol]:[DBU] ratio of 1:1:0.2, a DS of 52% was obtained after 10 minutes and then leveled off. With lowering the ratio to 1:0.5:0.1, a DS of 25% was observed after 20 minutes and then kept globally constant until 40 minutes. While the kinetic control is difficult on the corresponding timescale, it is observed that the experimental DS tends to roughly half the value predicted from the [PFS]:[PFDT] ratio. The same conclusion arises from several experiments conducted with varying the [PFS]:[PFDT] ratio but keeping the [PFDT]:[DBU] ratio constant (Table 2.3-1, entries 5-9). The reasons explaining these results are not clear at this stage, but this second strategy makes it possible to prepare polymers with predicted DS by adjusting the initial [PFS]:[PFDT]:[DBU] ratio. Hence, by implementing all the synthetic conditions developed above, a library of homopolymers with any DS from 0 up to 100% was obtained. Then, the glass transition temperature of these functionalized polymers was determined by DSC. While the T_g found for pristine PPFS was 91°C, the one for PPFS-PFDT specimen with a DS of approximately 96% was around 28°C, which is very close to the one determined by Hvilsted *et al.* for homopolymers containing 15 Fluorine atoms in the side chain³³. These latter polymers were prepared by ATRP of a monomer priority substituted with the sodium alcoholates of the corresponding fluoroalcohol. As

expected, the presence of the long PFDT side group along the PFS backbone induces a plasticizing effect with a corresponding decrease of the T_g of around 70 °C. Figure 2.3-4 shows the evolution of the T_g of the PPFS-PFDT derivatives, irrespective of the base used during the synthesis step. Only one T_g was observed which value regularly decreases with the DS.

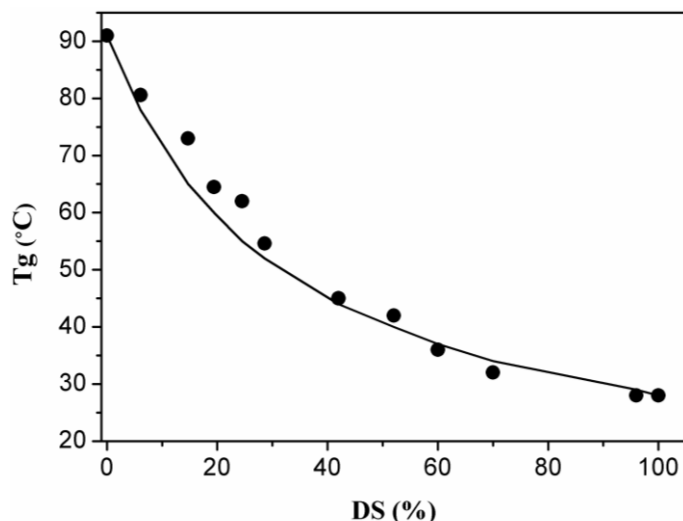


Figure 2.3-4 T_g of the PPFS-PFDT derivatives as a function of DS. The curve corresponds to the prediction of the T_g of a random copolymer by applying the Fox equation (equation 1).

We applied the Fox equation that predicts the T_g of a random copolymer from the T_g of each component weighed by their weight fraction according to:

$$\frac{1}{T_{g, \text{random copolymer}}} = \frac{W_{\text{PPFS}}}{T_{g, \text{PPFS}}} + \frac{W_{\text{PPFS-PFDT}}}{T_{g, \text{PPFS-PFDT}}} \quad (\text{equation 1})$$

A pretty well agreement was obtained with the experimental values, attesting that the copolymers display a rather random structure in both PPFS and PPFS-PFDT units. At this stage, it is worth noting that the solubility of the PPFS-PFDT specimens depends on their DS. It is actually well-known that the solubility of perfluoroalkyl-containing polymers depends on the number of fluorine atoms along the grafted chain; for example, Hvilsted *et al.*³³ showed that homopolymers containing 5 fluorine atoms are soluble in a common organic solvent such as THF even for very high molar mass (up to 140 000 g/mol) while homopolymers with 15 Fluorine atoms were insoluble. Back to the polymers presented herein, we evaluated

their solubility at a concentration of around 10 g/L, and for PPFS-PFDT specimens with DS up to 33%, their solubility was ensured in CHCl_3 and THF at room temperature and at 50 °C. For the PPFS-PFDT sample with a DS of 41%, it was necessary to heat it up to 50 °C in order to solubilize it in THF, while polymers with larger DS tend to be insoluble in CHCl_3 , THF and DMF even at 50°C. While these results may appear as a limitation in terms of the preparation of films by classical methods that generally imply the use of solvent, the wettability properties of PPFS-PFDT specimens showed that high DS are not needed to obtain low surface energy polymers. Indeed, preliminary investigations of the wettability properties of PPFS and PPFS-PFDT with DS ranging from 6 % to 41 %, were conducted by the determination of the water contact angle and the methylene iodide contact angle ($\theta_{\text{H}_2\text{O}}$ and $\theta_{\text{CH}_2\text{I}_2}$ respectively) on spin-coated PPFS-based polymers (Figure 2.3-5).

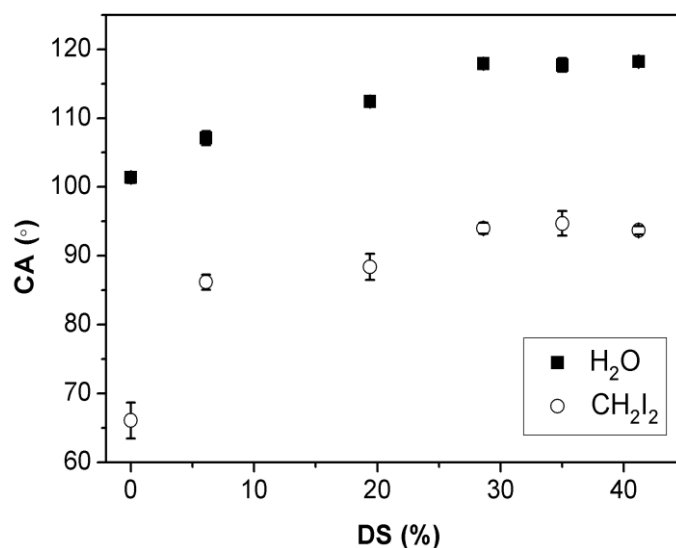


Figure 2.3-5 Evolution of the water contact angle (square) and the methylene iodide contact angle (circle) for PPFS-PFDT as a function of DS.

It appears that the introduction of perfluoroalkyl moieties along the PPFS backbone endows the resulting PPFS-PFDT polymers with enhanced hydrophobic and organophobic character. Indeed, $\theta_{\text{H}_2\text{O}}$ varies from 101° for PPFS up to a constant value around 118° for PPFS-PFDT having a DS of 29 %, while $\theta_{\text{CH}_2\text{I}_2}$ increases from 66.1° to 94°. The corresponding surface energy (determined from the Owens-Wendt model, see experimental part) significantly drops from 25 mJ/m² to

11.8 mJ/m².

These results that suggest a decrease of chemical affinities for the probing liquids are consistent with the presence of perfluorocarbon groups at the film surface. Moreover, $\theta_{\text{H}_2\text{O}}$, $\theta_{\text{CH}_2\text{I}_2}$ and thus surface energy, do not change anymore for larger DS attesting that DS values around 30% are high enough to benefit from the presence of long perfluorinated side chain.

2.3.4.2 Synthesis of nanohybrids: SiO₂-PS-PPFS-PFDT samples

The next part concerns the thiol-*para*-fluoro coupling of PPFS-coated silica nanoparticles, the synthesis of which was previously published.⁴³ Our strategy consisted in preparing acryloxy-modified silica (noted SiO₂-APTMS) that was subsequently involved in the nitroxide mediated polymerization of PFS initiated by PS-DEPN. The resulting silica decorated by a PS-*b*-PPFS corona is identified as SiO₂-PS-PPFS. While the organic content may be tuned by polymerization time,⁴³ a specimen made of 32 wt% of organic matter was used for further derivation step. Based on the results obtained on the homopolymers, DBU was chosen as base and and two [PFS]:[PFDT]:[DBU] ratios were envisioned (Table 2.3-1, entries 10-11), and the final DS was quantified using FTIR and TGA method (Figure SI3). The experimental DS was predicted by the initial [PFS]:[PFDT]:[DBU] ratio, even if the derivation step turned out to be slower in this case (6 hours) instead of a few tens of minutes for homopolymers. We obtained DS of respectively 13 and 47%, as determined by the FTIR-based method. TGA were then conducted on the two samples (Figure SI 3b) and it was observed that their weight loss were larger than the one of the pristine SiO₂-PS-PPFS, confirming the derivation. Moreover, this calculated DS from the thermograms (14% and 45%, respectively) were similar to the ones determined by FTIR. It is also worthnoting that the decomposition temperature of SiO₂-PS-PPFS-PFDT nanohybrids is slightly lower than the one of SiO₂-PS-PPFS specimens, attesting that the fluoro-based side groups are more thermally labile than the fluorine atom directly bonded to the phenyl ring. Comparable results were

obtained for the homopolymers modified with PFDT developed in this work (Figure SI4) and were previously reported in the literature for fluoroalkoxy modified PPFS samples.³³ Regarding the wettability properties, θ_{H_2O} resulting from the deposition of SiO₂-APTMS, SiO₂-PS-PPFS and SiO₂-PS-PPFS-PFDT (DS = 13%) dispersions onto silicon wafers by spin-coating without being embedded into any host polymer matrix, were measured as 27.8°, 132.1° and 154.8°, respectively (Table 2.3-2, entries 1-3). It can be observed that for a comparable DS, the introduction of PFDT impacts more both the water contact angle and the methylene iodide contact angle for the silica particles than for the homopolymers (Figure 2.3-5), highlighting the combined effect of the chemical and physical (roughness) aspect.

2.3.4.3 Preparation of (nano)composite films

At this stage, various hydrophobic fluorinated polymer matrices (PPFS and PPFS-PFDT derivatives with various DS) and functionalized fumed silica particles were available: one rather polar and modified with (acryloxypropyl)trimethoxysilane (SiO₂-APTMS) and the two hybrid hydrophobic silica : i) silica particles bearing PS-b-PPFS grafts up to 32 wt% (SiO₂-PS-PPFS) and ii) silica particles bearing PS-b-PPFS which PFS groups were partly modified by PFDT (SiO₂-PS-PPFS-PFDT, DS = 13%). The latter particles were preferred to the ones presenting a larger DS as they were more easily dispersible in the experimental conditions (THF) selected for the preparation of the (nano)composite film. Even if SiO₂-PS-PPFS-PFDT presents superhydrophobicity features, the deposition of silica-based hybrids not embedded in an organic matrix is expected to be less stable and durable than the association of modified silica particles with a well-suited polymer matrix.²⁴⁻²⁹ In that way, silica-based (nano)composite is preferred, and various films were prepared by spin-coating a SiO₂/polymer dispersion onto activated silicon wafer. The wettability measurements of the resulting films are gathered in Table 2.3-2. More specifically, we were interested in the value of θ_{H_2O} , water hysteresis ($\Delta\theta_{H_2O}$) and $\theta_{CH_2I_2}$.

First, one can observe the key role of the hydrophobic matrix on the wettability

measurements. Indeed, the combined association of PPFS or PPFS-PFDT with SiO₂-APTMS (entries 4 and 5) yields a noticeable θ_{H_2O} increase in regards with SiO₂-APTMS used solely (entry 1) and both pure PPFS and PPFS-PFDT (Figure 2.3-5). $\theta_{CH_2I_2}$ values are mainly influenced by the type of fluorinated polymer matrix (PPFS or PPFS-PFDT). The presence of fumed silica induces a peculiar surface morphology which favorably enhances the hydrophobic character of the (nano)composite film.

Table 2.3-2 Wettability measurements of the various SiO₂-containing samples spin-coated onto silicon wafers

Entry	Sample	Silica wt%	θ_{H_2O}	$\Delta\theta_{H_2O}(^\circ)$	$\theta_{CH_2I_2}(^\circ)$
1	SiO ₂ -APTMS	95	27.8 ± 1.5	----	0
2	SiO ₂ -PS-PPFS	68	132.0 ± 1.7	30.7 ± 2.0	65.9 ± 1.7
3	SiO ₂ -PS-PPFS-PFDT (DS = 13%)	60	154.8 ± 0.8	2.4 ± 0.5	123.9 ± 1.5
4	SiO ₂ -APTMS/PPFS	35	112.2 ± 0.5	33.0 ± 3.5	70.7 ± 4.0
5	SiO ₂ -APTMS/PPFS-PFDT (DS=29%)	35	129.4 ± 2.2	10.2 ± 1.3	95.9 ± 3.1
6	SiO ₂ -PS-PPFS/PPFS	35	135.7 ± 0.3	3.5 ± 1.4	90.7 ± 2.9
7	SiO ₂ -PS-PPFS/PPFS-PFDT (DS=6%)	35	135.1 ± 0.3	4.5 ± 2.3	96.5 ± 3.5
8	SiO ₂ -PS-PPFS/PPFS-PFDT (DS = 19%)	35	136.5 ± 3.5	13.0 ± 2.9	102.6 ± 5.0
9	SiO ₂ -PS-PPFS/PPFS-PFDT (DS = 29%)	35	142.8 ± 2.0	1.1 ± 0.5	114.1 ± 7.4
10	SiO ₂ -PS-PPFS/PPFS-PFDT (DS = 29%)	23	120.2 ± 0.9	17.0 ± 4.8	98.3 ± 6.5
11	SiO ₂ -PS-PPFS/PPFS-PFDT (DS = 29%)	46	154.5 ± 4.1	2.4 ± 0.7	119.8 ± 5.0
12	SiO ₂ -PS-PPFS-PFDT (DS = 13 %)/PPFS	46	147.7 ± 3.1	3.4 ± 1.2	127.7 ± 2.2
13	SiO ₂ -PS-PPFS-PFDT (DS = 13%)/PPFS-PFDT (DS = 29%)	46	152.3 ± 0.5	2 ± 0.5	118.8 ± 2.0

Based on SEM analyses (Figures 2.3-6, images A and B, and Figure SI6) that present their morphologies, the films composed of SiO₂-APTMS at 35 wt% incorporated in PPFS or PPFS-PFDT (DS = 29 %) exhibit a very irregularly dispersed morphology characterized by the presence of polymorphic and polydisperse agglomerates.

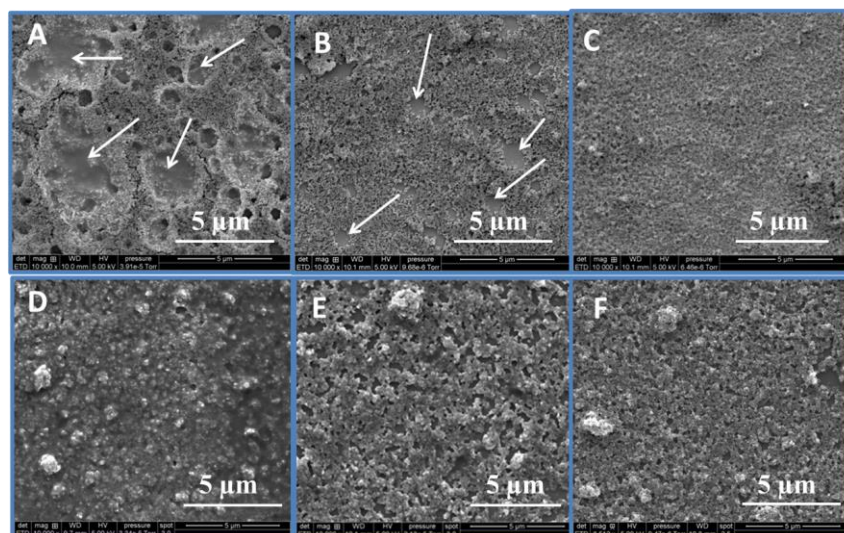


Figure 2.3-6 SEM images of SiO₂-APTMS (35 wt%) / PPFS (entry 4, image A), SiO₂-APTMS (35 wt%) / PPFS-PFDT (entry 5, image B), SiO₂-PS-PPFS (35 wt%) / PPFS (entry 6, image C), SiO₂-PS-PPFS (35 wt %) / PPFS-PFDT (DS = 29 %) (entry 9, image D), SiO₂-PS-PPFS (46 wt%) / PPFS-PFDT (DS = 29 %) (entry 11, image E) and SiO₂-PS-PPFS-PFDT (DS = 13 %) (46 wt%) / PPFS-PFDT (DS = 29 %) (entry 13, image F).

The size of the agglomerates can attain a diameter of around 40 μm (particularly for SiO₂-APTMS/PPFS, Figure SI5), value which does not match with the inherent dimensions of fumed silica (around 1 μm). Silica particles are not able to cover the whole surface leading to large roughness, which also explains the high $\Delta\theta_{\text{H}_2\text{O}}$ values. This pattern can be regarded as the consequence of the fairly bad dispersion state of SiO₂-APTMS in PPFS and PPFS-PFDT matrices, owing to the unfavored chemical affinities between polar silica and hydrophobic matrix. As explained in the literature, a too large agglomeration of silica particles combined with a scattered distribution on the surface are not well adapted to generate superhydrophobicity.¹⁶ In view of circumventing this weak interfacial adhesion, we turned to the use of hydrophobic SiO₂-PS-PPFS firstly introduced at the same content (35 wt%) in PPFS (Table 2.3-2, entry 6) and PPFS-PFDT (DS = 29 %) (Table 2.3-2, entry 9). Interestingly, the presence of PS-*b*-PPFS at the surface of the silica particle leads to a huge increase of $\theta_{\text{H}_2\text{O}}$ and to a decrease of $\Delta\theta_{\text{H}_2\text{O}}$, in comparison with their SiO₂-APTMS-based films analogs. Especially, the SiO₂-PS-PPFS /PPFS-PFDT (DS = 29 %) is particularly relevant since not only the $\theta_{\text{H}_2\text{O}}$ is very high (142.8°) and $\Delta\theta_{\text{H}_2\text{O}}$ is low (1.1°) but

also the contact angle with methylene iodide is significantly higher ($\theta_{CH_2I_2} = 114.1^\circ$), due to the presence of perfluoroalkyl moieties. However, these films do not exhibit superhydrophobic features. SEM analysis of PPFS (Figure 2.3-6, image C) and PPFS-PFDT (Figure 2.3-6, image D) containing chemically modified SiO₂-PS-PPFS particles, reveal a more fine bumpy morphology with smaller aggregates and a more homogeneous distribution of silica particles at the surface of the film, compared to the composite films including polar SiO₂-APTMS (Figure 2.3-6, images A and B, Figure SI5).

It is suggested that the enhanced compatibility between the hydrophobic PS-b-PPFS shell and the fluorinated matrix enables to disrupt most of silica agglomerates and thus to restore the natural dual size silica dimension (elementary particles and self-assembled aggregates), which is necessary to promote the hydrophobic character. The SiO₂ particles are tightly attached to each other by the adhesive action of PPFS-based corona. For the SiO₂-PS-PPFS (35 %) /PPFS-PFDT (DS = 29 %) film (Figure 2.3-6, image D), one can notice the presence of more numerous micrometric ill-defined silica aggregates (up to 2 μm in diameter), compared to the film obtained with PPFS as host matrix (Figure 2.3-6, image C) and this feature might probably contribute to the enhanced observed wettability measurements.

Moreover, X-ray photoelectron spectroscopy analysis were carried out on SiO₂-PS-PPFS (35 wt%)/PPFS and SiO₂-PS-PPFS (35 and 46 wt%)/PPFS-PFDT (DS = 29 %) samples in order to quantify their surface chemical composition (< 4 nm). The survey spectra (Figure SI6) clearly reveal the presence of Si, C, O, F and S elements (only for PPFS-PFDT-based films) and the surface compositions are summarized in Table 2.3-3.

Table 2.3-3 Atomic % of elements from XPS survey scans of SiO₂-PS-PPFS (35 %) /PPFS (entry 6), SiO₂-PS-PPFS (35 wt%) /PPFS-PFDT (DS = 29 %) (entry 9) and SiO₂-PS-PPFS (46 wt%) /PPFS-PFDT (DS = 29 %) (entry 11).

Entry	C (%)	O (%)	Si from oxide (%)*	F (%)	S (%)	F/C	Si/C
(6)	46.0	16.7	7.90	27.9	0	0.61	0.17
(9)	43.2	11.8	5.80	35.8	0.9	0.83	0.13
(11)	40.2	14.4	6.56	34.6	0.7	0.86	0.16

* obtained by taking into account the global Si atomic percent and the proportion of oxide form, obtained by deconvolution of the Si2p peak

The sulfur atoms detected for films with PPFS-PFDT as matrix argues the presence of -C-S- bonding resulting from the nucleophilic substitution of the fluorine atom of PFS by the perfluorodecanethiol derivative. This is also attested by the increase of F atomic percent (from 27.9 % (entry (6)) to around 35 % (entries 9 and 11)). Moreover, high-resolution core-level elemental scans of C1s of SiO₂-PS-PPFS /PPFS-PFDT films reveal the presence of -CF₂- bonds (at 291.6 eV) (see Figures SI7-SI9, Table S1), which is not detected for SiO₂-PS-PPFS /PPFS. These results enable to ascertain the presence of PFDT at the surface of the film,^{56,57} explaining the values of the contact angles. The key role of the PFDT moieties on the final surface properties can also be emphasized by the influence of modification extent of PPFS, quantified by the DS value. The comparison of the entries 7, 8 and 9 corresponding to SiO₂-PS-PPFS /PPFS-PFDT, with DS = 6, 19 and 29 %, respectively clearly underpins that the DS increase leads to a significant $\theta_{\text{H}_2\text{O}}$ and $\theta_{\text{CH}_2\text{I}_2}$ increase. However, it appeared not necessary to use a PPFS-PFDT with DS higher than 29 %, since a plateau in the $\theta_{\text{H}_2\text{O}}$ value was observed for larger DS (Figure 2.3-5). Thus, the high contact angles surge especially observed for SiO₂-PS-PPFS/PPFS-PFDT stems from both the surface chemistry emanating from the effect of apolar perfluorocarbon groups and the dually structured morphology induced by silica particles surrounded by the covalently anchored PS-b-PPFS chains. Nevertheless, as already mentioned, water contact angles did not reach 150°. As commonly reported in literature, the hydrophobicity can be tuned by varying the weight ratio of

silica/polymer and high silica amount are desired to endow a (nano)composite film with superhydrophobicity.³⁰ Therefore, the content of SiO₂-PS-PPFS into PPFS-PFDT (DS=29 %) was increased up to 46 wt% (entry 11). The rise of the Si/C ratio obtained from XPS analysis (Table 2.3-3) is consistent with the fact that more silica particles are present at the film surface. Very interestingly, the resulting (nano)composite film exhibits both superhydrophobic properties with a θ_{H_2O} value of 154.5° and a self-cleaning character, as revealed by the very low water hysteresis value ($\Delta\theta_{H_2O}$ = 2.4°). It thus presents the ‘Lotus effect’ named after the Lotus leaves that can remove dirt particles with the help of raindrops that do not adhere to the surface. Besides, the organophobic character is noticeably improved ($\theta_{CH_2I_2}$ = 119.8°). EDX analysis (Figure SI10) collected on various locations displays a high extent of surface coverage by silica particles and SEM images (Figure 2.3-6, images E and F) depict an interconnected binary structured morphology constituted of PPFS-surrounded silica particles continuously adhering to each other. Indeed, micrometric protrusions as well as SiO₂ in the state of nanoscale are visible. Moreover, it is worth mentioning that no crack is found at the surface of the film, meaning that even with 46 wt% of silica, good film-forming properties are maintained. The topography of this film was also both qualitatively and quantitatively evaluated by atomic force microscopy (AFM) analysis (Figure 2.3-7).

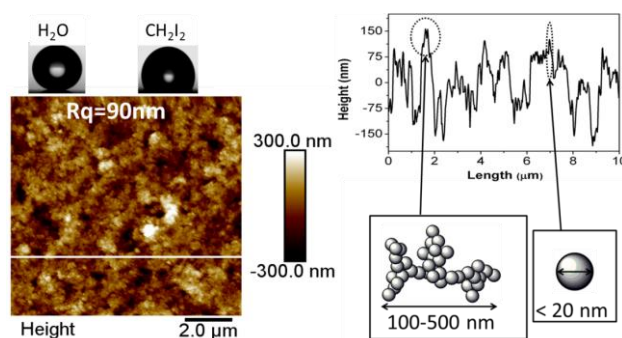


Figure 2.3-7 Topographic images of film resulting from SiO₂-PS-PPFS (46 wt%) /PPFS-PFDT (DS = 29 %) (entry 11), with the corresponding height profile and wettability properties.

The AFM image points out *i*) the presence of protrusions with a maximum height of around 225 nm and *ii*) a dual surface structuration with two main range sizes in

lateral dimension (from 200 to 500 nm and a second < 20 nm), as expected for fumed silica particles. This continuous micro/nano binary structure is also well illustrated by the corresponding 3D AFM image (Figure SI11). As explained earlier, perfluoroalkyl moieties were also introduced on the PPFS-based shell attached to silica particles (entry 10, Table 2.3-1). So, two additional (nano)composites were elaborated: SiO₂-PS-PPFS-PFDT (DS = 13%)/PPFS (entry 12, Table 2.3-2) and SiO₂-PS-PPFS-PFDT (DS = 13 %) /PPFS-PFDT (DS = 29 %) (entry 13), both containing 46 wt% in silica. It can be noted that the wettability features (θ_{H_2O} , $\Delta\theta_{H_2O}$ and $\theta_{CH_2I_2}$) for these two SiO₂-PS-PPFS-PFDT containing films are in the same order of magnitude that the ones of SiO₂-PS-PPFS/PPFS-PFDT (DS = 29 %), while their surface morphologies are also quite comparable (Figure 2.3-6, image F, Figure SI12).

Consequently, we can assume that the grafting of PFDT moieties on both SiO₂-PS-PPFS and PPFS host matrix is not needed to attain superhydrophobicity, while the presence of perfluoroalkyl groups either on silica (entry 12) or PPFS matrix (entry 11) and high functionalized silica content appear as key prerequisites. Thus, the probed dually-size packed morphology of these (nano)composite films (entry 11, 12 and 13) along with the ability of the surface to entrap air prevent water droplets from penetrating the nanopores of the film by reducing the effective contact area of water from the surface. These are the major reasons for the observed super water repellent surface, in accordance with the Cassie model.⁵⁸

2.3.5 Conclusion

(Nano)composite films with self-cleaning properties (θ_{H_2O} greater than 150° with water hysteresis lower than 10°) were prepared by combining polymers and fumed silica both containing poly(2,3,4,5,6-pentafluorostyrene) sequences that can be perfluorinated using a thiol-*para*-fluoro coupling in a controlled manner. Perfluorinated decane thiol was used as modifier, and the impact of operating conditions (base used as activator, [PFS]:[thiol]:[base] molar ratio, time) was first

evaluated on homopolymers in order to tune the degree of substitution that actually controls the surface energy of the derived polymers. The coupling reaction was then successfully applied to the perfluorination of fumed silica. From these results, it was concluded that the fabrication of (nano)composite films with self-cleaning properties requires i) the utilization of PFDT within host fluorinated matrix or immobilized on the silica corona in order to benefit from the presence of perfluoroalkyl groups, ii) the use of hydrophobic silica particles surrounded by a compatibilizing hydrophobic shell to obtain a well-suited dual roughness and a homogeneous topography surface and iii) a high enough silica content to generate an interconnected and well covering morphology. Thus, by carefully selecting the thiol used to modify the PPFS building block, considering that the extent of modification can be finely tuned and applied either to the derivation of the host polymer or at the surface of silica used as filler, we believe that the strategy that uses PPFS as a platform could be suitable to provide any specific property to a (nano)composite film.

2.3.6 References

- (1) Garbassi, F., Morra, M. & Occhiello, E. *Polymer Surfaces: From Physics to Technology*; Wiley: Chichester, 1998.
- (2) Bhushan, B.; Jung, Y. C. Natural and Biomimetic Artificial Surfaces for Superhydrophobicity, Self-Cleaning, Low Adhesion, and Drag Reduction. *Prog. Mater. Sci.* **2011**, *56* (1), 1–108.
- (3) Roach, P.; Shirtcliffe, N. J.; Newton, M. I. Progress in Superhydrophobic Surface Development. *Soft Matter* **2008**, *4* (2), 224–240.
- (4) Nosonovsky, M.; Bhushan, B. Superhydrophobic Surfaces and Emerging Applications: Non-Adhesion, Energy, Green Engineering. *Curr. Opin. Colloid Interface Sci.* **2009**, *14* (4), 270–280.
- (5) Yan, Y. Y.; Gao, N.; Barthlott, W. Mimicking Natural Superhydrophobic Surfaces and Grasping the Wetting Process: A Review on Recent Progress in Preparing Superhydrophobic Surfaces. *Adv. Colloid Interface Sci.* **2011**, *169* (2), 80–

105.

(6) Barthlott, W.; Neinhuis, C. Purity of the Sacred Lotus, or Escape from Contamination in Biological Surfaces. *Planta* **1997**, *202* (1), 1–8.

(7) Ou, J.; Pan, B.; Chen, Y.; Xie, C.; Xue, M.; Wang, F.; Li, W. Substrate-Independent Sequential Deposition Process to Obtain the Lotus Effect Based on Mussel-Inspired Polydopamine. *Appl. Surf. Sci.* **2015**, *327*, 149–153.

(8) Khorasani, M. T.; Mirzadeh, H.; Kermani, Z. Wettability of Porous Polydimethylsiloxane Surface: Morphology Study. *Appl. Surf. Sci.* **2005**, *242* (3–4), 339–345.

(9) Zhang, A.; Bai, H.; Li, L. Breath Figure: A Nature-Inspired Preparation Method for Ordered Porous Films. *Chem. Rev.* **2015**, *115* (18), 9801–9868.

(10) Bravo, J.; Zhai, L.; Wu, Z.; Cohen, R. E.; Rubner, M. F. Transparent Superhydrophobic Films Based on Silica Nanoparticles. *Langmuir* **2007**, *23* (13), 7293–7298.

(11) Wu, M.; An, N.; Li, Y.; Sun, J. Layer-by-Layer Assembly of Fluorine-Free Polyelectrolyte-Surfactant Complexes for the Fabrication of Self-Healing Superhydrophobic Films. *Langmuir* **2016**, *32* (47), 12361–12369.

(12) Xie, Q.; Fan, G.; Zhao, N.; Guo, X.; Xu, J.; Dong, J.; Zhang, L.; Zhang, Y.; Han, C. C. Facile Creation of a Bionic Super-Hydrophobic Block Copolymer Surface. *Adv. Mater.* **2004**, *16* (20), 1830–1833.

(13) Lu, X.; Zhang, C.; Han, Y. Low-Density Polyethylene Superhydrophobic Surface by Control of Its Crystallization Behavior. *Macromol. Rapid Commun.* **2004**, *25* (18), 1606–1610.

(14) Jiang, L.; Zhao, Y.; Zhai, J. A Lotus-Leaf-like Superhydrophobic Surface: A Porous Microsphere/nanofiber Composite Film Prepared by Electrohydrodynamics. *Angew. Chemie. Int. Ed.* **2004**, *43* (33), 4338–4341.

(15) Yu, J.; Han, S.; Hong, J. S.; Sanyal, O.; Lee, I. Synchronous Generation of Nano- and Microscaled Hierarchical Porous Polyelectrolyte Multilayers for Superwetable Surfaces. *Langmuir* **2016**, *32* (33), 8494–8500.

(16) Söz, C. K.; Yilgör, E.; Yilgör, I. Influence of the Coating Method on the

Formation of Superhydrophobic Silicone-Urea Surfaces Modified with Fumed Silica Nanoparticles. *Prog. Org. Coatings* **2015**, *84*, 143–152.

- (17) Zhang, J.; Pu, G.; Severtson, S. J. Fabrication of Zinc Oxide/polydimethylsiloxane Composite Surfaces Demonstrating Oil-Fouling-Resistant Superhydrophobicity. *ACS Appl. Mater. Interfaces* **2010**, *2* (10), 2880–2883.
- (18) Jung, Y. C.; Bhushan, B. Mechanically Durable Carbon Nanotube - Composite Hierarchical Structures with Superhydrophobicity, Self-Cleaning, and Low-Drag. *ACS Nano* **2009**, *3* (12), 4155–4163.
- (19) Tuteja, A.; Choi, W.; Ma, M.; Mabry, J. M.; Mazzella, S. A.; Rutledge, G. C.; McKinley, G. H.; Cohen, R. E. Designing Superoleophobic Surfaces. *Science* **2007**, *318* (5856), 1618–1622.
- (20) Sparks, B. J.; Hoff, E. F. T.; Xiong, L.; Goetz, J. T.; Patton, D. L. Superhydrophobic Hybrid Inorganic-Organic Thiol-Ene Surfaces Fabricated via Spray-Deposition and Photopolymerization. *ACS Appl. Mater. Interfaces* **2013**, *5* (5), 1811–1817.
- (21) Manoudis, Panagiotis N.; Karapanagiotis, Ioannis; Tsakalof, Andreas; Zuburtikudis, Ioannis; Panayiotou, C. Superhydrophobic Composite Films Produced on Various Substrates. *Langmuir* **2008**, *24* (19), 11225–11232.
- (22) Li, J. H.; Weng, R.; Di, X. Q.; Yao, Z. W. Gradient and Weather Resistant Hybrid Super-Hydrophobic Coating Based on Fluorinated Epoxy Resin. *J. Appl. Polym. Sci.* **2014**, *131* (20), 1–7.
- (23) Honda, K.; Morita, M.; Takahara, A. Surface Molecular Aggregation Structure and Surface Properties of Poly (Fluoroalkyl Acrylate) Thin Films. *Macromolecules* **2005**, *38* (13), 5699–5705.
- (24) Hsieh, C.T.; Wu, F.L.; Chen, W.Y. Super Water- and Oil-Repellencies from Silica-Based Nanocoatings. *Surf. Coat. Technol.* **2009**, *203* (22), 3377–3384.
- (25) Cengiz, U.; Elif Cansoy, C. Applicability of Cassie-Baxter Equation for Superhydrophobic Fluoropolymer-Silica Composite Films. *Appl. Surf. Sci.* **2015**, *335*, 99–106.

- (26) Yang, H.; Pi, P.; Yang, Z. ru; Lu, Z.; Chen, R. Design of a Superhydrophobic and Superoleophilic Film Using Cured Fluoropolymer@silica Hybrid. *Appl. Surf. Sci.* **2016**, *388*, 268–273.
- (27) Li, K.; Zeng, X.; Li, H.; Lai, X. Fabrication and Characterization of Stable Superhydrophobic Fluorinated-Polyacrylate/silica Hybrid Coating. *Appl. Surf. Sci.* **2014**, *298*, 214–220.
- (28) Chang, K.C.; Chen, H.; Huang, C.K.; Huang, S.I. Preparation of Super-Hydrophobic Film with Fluorinated-Copolymer. *J. Appl. Polym. Sci.* **2007**, *104* (3), 1646–1653.
- (29) Hsieh, C. Te; Chang, B. S.; Lin, J. Y. Improvement of Water and Oil Repellency on Wood Substrates by Using Fluorinated Silica Nanocoating. *Appl. Surf. Sci.* **2011**, *257* (18), 7997–8002.
- (30) Basu, B. B. J.; Paranthaman, A. K. A Simple Method for the Preparation of Superhydrophobic PVDF-HMFS Hybrid Composite Coatings. *Appl. Surf. Sci.* **2009**, *255* (8), 4479–4483.
- (31) Zhou, H.; Wang, H.; Niu, H.; Gestos, A.; Lin, T. Robust, Self-Healing Superamphiphobic Fabrics Prepared by Two-Step Coating of Fluoro-Containing Polymer, Fluoroalkyl Silane, and Modified Silica Nanoparticles. *Adv. Funct. Mater.* **2013**, *23* (13), 1664–1670.
- (32) Zou, H.; Wu, S.; Shen, J. Polymer/silica Nanocomposites: Preparation, Characterization, Properties and Applications. *Chem. Rev.* **2008**, *108* (9), 3893–3957.
- (33) Borkar, S.; Jankova, K.; Siesler, H. W.; Hvilsted, S. New Highly Fluorinated Styrene-Based Materials with Low Surface Energy Prepared by ATRP. *Macromolecules* **2004**, *37* (3), 788–794.
- (34) Jankova, K.; Hvilsted, S. Preparation of Poly(2,3,4,5,6-Pentafluorostyrene) and Block Copolymers with Styrene by ATRP. *Macromolecules* **2003**, *36* (5), 1753–1758.
- (35) Paz-Pazos, M.; Pugh, C. Synthesis, Isolation, and Thermal Behavior of Polybutadiene Grafted with poly(2,3,4,5,6-Pentafluorostyrene). *J. Polym. Sci. Part A: Polym. Chem.* **2005**, *43* (13), 2874–2891.

- (36) Bucholz, T. L.; Loo, Y.L. Phase Behavior of Near-Monodisperse Semifluorinated Diblock Copolymers by Atom Transfer Radical Polymerization. *Macromolecules* **2006**, *39* (18), 6075–6080.
- (37) Powell, K. T.; Cheng, C.; Wooley, K. L. Complex Amphiphilic Hyperbranched Fluoropolymers by Atom Transfer Radical Self-Condensing Vinyl (Co)polymerization. *Macromolecules* **2007**, *40* (13), 4509–4515.
- (38) Ott, C.; Hoogenboom, R.; Schubert, U. S. Post-Modification of Poly(pentafluorostyrene): A Versatile “click” method to Create Well-Defined Multifunctional Graft Copolymers. *Chem. Commun.* **2008**, *30* (30), 3516–3518.
- (39) Gudipati, C. S.; Tan, M. B. H.; Hussain, H.; Liu, Y.; He, C.; Davis, T. P. Synthesis of Poly(glycidyl Methacrylate)-Block-Poly(pentafluorostyrene) by RAFT: Precursor to Novel Amphiphilic Poly(glyceryl Methacrylate)-Block-Poly(pentafluorostyrene). *Macromol. Rapid Commun.* **2008**, *29* (23), 1902–1907.
- (40) Becer, C. R.; Babiuch, K.; Pilz, D.; Hornig, S.; Heinze, T.; Gottschaldt, M.; Schubert, U. S. Clicking Pentafluorostyrene Copolymers: Synthesis, Nanoprecipitation, and Glycosylation. *Macromolecules* **2009**, *42* (7), 2387–2394.
- (41) Irita, T.; Chen, D.; Li, X.; Wang, J.; Russell, T. P. Thin Films of Semifluorinated Block Copolymers Prepared by ATRP. *Macromol. Chem. Phys.* **2011**, *212* (22), 2399–2405.
- (42) Cai, T.; Yang, W. J.; Neoh, K.G.; Kang, E.T. Preparation of Jellyfish-Shaped Amphiphilic Block-Graft Copolymers Consisting of a Poly(ϵ -Caprolactone)-Block-Poly(pentafluorostyrene) Ring and Poly(ethylene Glycol) Lateral Brushes. *Polym. Chem.* **2012**, *3* (4), 1061-1068.
- (43) Yin, Q.; Aurelia, C.; Portinha, D.; Beyou, E. Nitroxide-Mediated Polymerization of Pentafluorostyrene Initiated by PS – DEPN through the Surface of APTMS Modified Fumed Silica : Towards Functional Nanohybrids. *Rsc Adv.* **2016**, *6* (63), 58260–58267.
- (44) Schuster, T.; Golling, F. E.; Krumpfer, J. W.; Wagner, M.; Graf, R.; Alsaygh, A. A.; Klapper, M.; Mullen, K. Poly(isobutylene) Nanoparticles via Cationic Polymerization in Nonaqueous Emulsions. *Macromol Rapid Commun* **2015**, *36* (2),

204–210.

(45) Turgut, H.; Delaittre, G. On the Orthogonality of Two Thiol-Based Modular Ligations. *Chem. Eur. J.* **2016**, *22* (4), 1511–1521.

(46) Turgut, H.; Schmidt, A. C.; Wadhvani, P.; Welle, A.; Müller, R.; Delaittre, G. The Para-Fluoro–Thiol Ligation in Water. *Polym. Chem.* **2017**, *8* (8), 1288–1293.

(47) Chen, J.; Dumas, L.; Duchet-Rumeau, J.; Fleury, E.; Charlot, A.; Portinha, D. Tuning H-Bond Capability of Hydroxylated-poly(2,3,4,5,6-Pentafluorostyrene) Grafted Copolymers Prepared by Chemoselective and Versatile Thiol-Para-Fluoro “click-Type” coupling with Mercaptoalcohols. *J. Polym. Sci. Part A: Polym. Chem.* **2012**, *50* (16), 3452–3460.

(48) Chen, J.; Vuluga, D.; Crousse, B.; Legros, J.; Duchet-Rumeau, J.; Charlot, A.; Portinha, D. Polyfluorinated Mercaptoalcohol as a H-Bond Modifier of poly(2,3,4,5,6-Pentafluorostyrene) (PPFS) Enhancing Miscibility of Hydroxylated-PPFS with Various Acceptor Polymers. *Polymer* **2013**, *54* (15), 3757–3766.

(49) Chen, J.; Duchet, J.; Portinha, D.; Charlot, A. Layer by Layer H-Bonded Assembly of P4VP with Various Hydroxylated PPFS: Impact of the Donor Strength on Growth Mechanism and Surface Features. *Langmuir* **2014**, *30* (35), 10740–10750.

(50) Valtola, L.; Koponen, A.; Karesoja, M.; Hietala, S.; Laukkanen, A.; Tenhu, H.; Denifl, P. Tailored Surface Properties of Semi-Fluorinated Block Copolymers by Electrospinning. *Polymer* **2009**, *50* (14), 3103–3110.

(51) Valtola, L.; Karesoja, M.; Tenhu, H.; Ihalainen, P.; Sarfraz, J.; Peltonen, J.; Malinen, M.; Urtti, A.; Hietala, S. Breath Figure Templated Semifluorinated Block Copolymers with Tunable Surface Properties and Binding Capabilities. *J. Appl. Polym. Sci.* **2014**, *132* (1), 1–9.

(52) Puretskiy, N.; Ionov, L. Synthesis of Robust Raspberry-like Particles Using Polymer Brushes. *Langmuir* **2011**, *27* (6), 3006–3011.

(53) Jean-Luc Couturier, O. G. WO2002012149A8, 2002.

(54) Dumas, L.; Fleury, E.; Portinha, D. Wettability Adjustment of PVDF Surfaces by Combining Radiation-Induced Grafting of (2,3,4,5,6)-Pentafluorostyrene

and Subsequent Chemoselective “click-Type” Reaction. *Polymer* **2014**, 55 (11), 2628–2634.

(55) Noy, J.M.; Koldevitz, M.; Roth, P. J. Thiol-Reactive Functional Poly(meth)acrylates: Multicomponent Monomer Synthesis, RAFT (Co)polymerization and Highly Efficient Thiol–para-Fluoro Postpolymerization Modification. *Polym. Chem.* **2015**, 6 (3), 436–447.

(56) Suzuki, S.; Whittaker, M. R.; Wentrup-Byrne, E.; Monteiro, M. J.; Grøndahl, L. Adsorption of Well-Defined Fluorine-Containing Polymers onto Poly(tetrafluoroethylene). *Langmuir* **2008**, 24 (22), 13075–13083.

(57) Weng, L. T.; Ng, K. M.; Cheung, Z. L.; Lei, Y. G.; Chan, C. M. Quantitative Analysis of Styrene-Pentafluorostyrene Random Copolymers by ToF-SIMS and XPS. *Surf. INTERFACE Anal.* **2006**, 38 (1), 32–43.

(58) Cassie, A. B. D.; Baxter, S. Wettability of Porous Surfaces. *Trans. Faraday Soc.* **1944**, 40, 546-551.

2.3.7 Supporting information

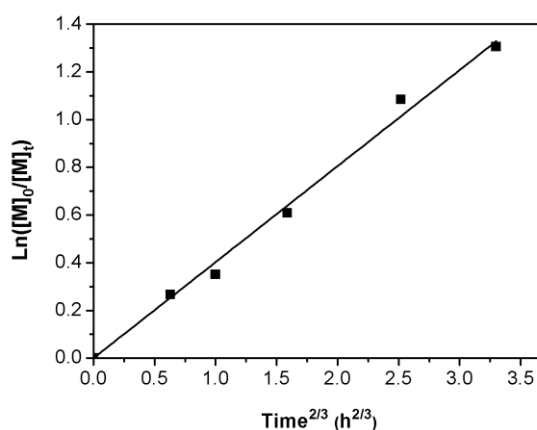


Figure SI1 Kinetics of polymerization of PFS at 110°C; [PFS] = 3.6 mol/L; [Styryl-DEPN] = 0.018 mol/L in the solvent of MP.

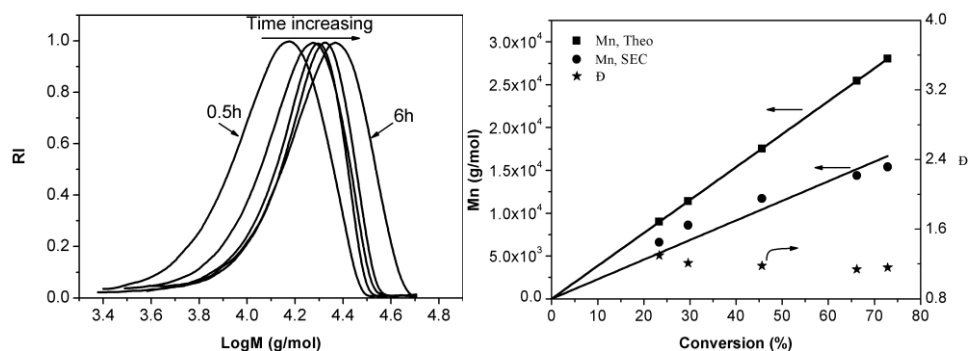


Figure SI2 SEC traces for different polymerization time (left) and Evolution of Mn and \bar{D} as a function of conversion (right) for the homopolymerization of PFS at 110°C; [PFS] = 3.6 mol/L; [Styryl-DEPN] = 0.018 mol/L in the solvent of MP.

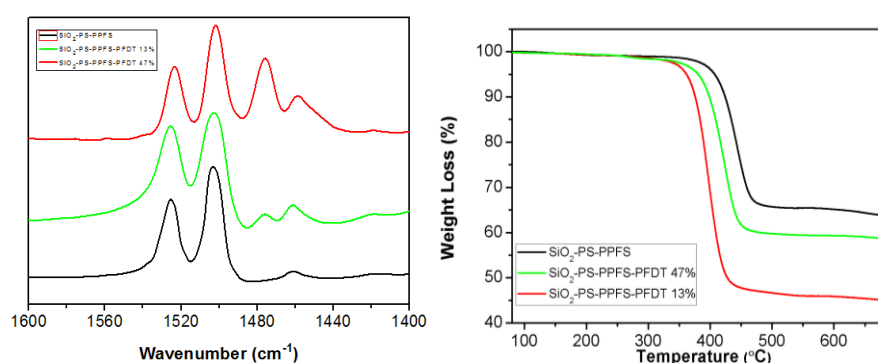


Figure SI3 FTIR spectra (left) and TGA thermograms (right) of SiO₂-PS-PPFS samples with DS = 0, 13 and 47%.

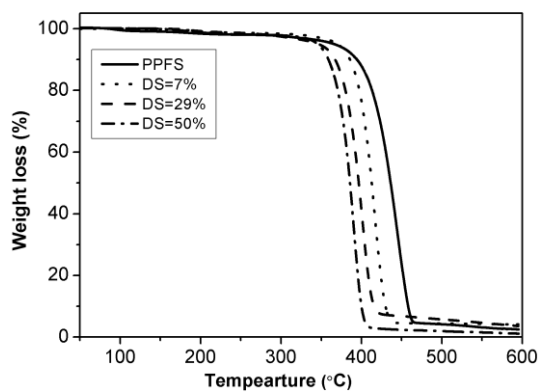


Figure SI4 TGA spectra for PPFS and PPFS-PFDT (7%, 29% and 50%).

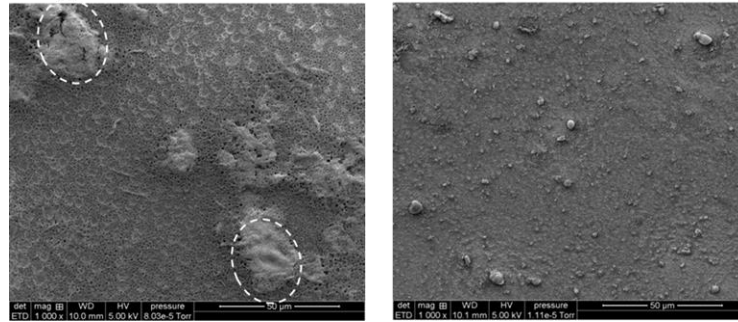


Figure SI5 SEM images of Si-APTMS (35 %) / PPFS (Table 2.3-2, entry 4, left) and Si-APTMS (35 %) / PPFS-PFDT (DS = 29 %) (Table 2.3-2, entry 5, right)

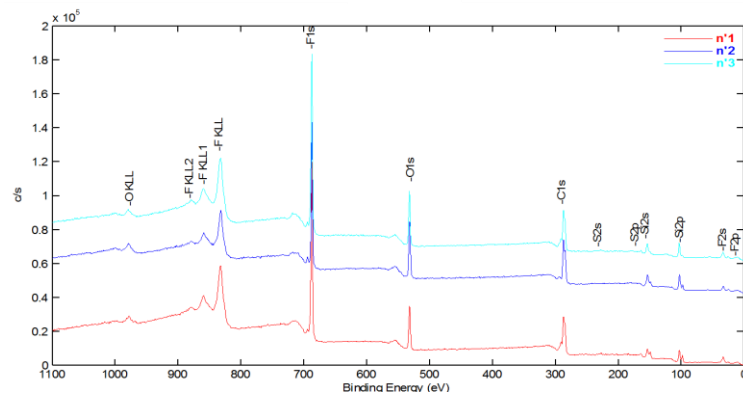


Figure SI6 XPS survey spectra of SiO₂-PS-PPFS (35 %) /PPFS (red, entry 3), SiO₂-PS-PPFS (35 %)/PPFS-PFDT (DS = 29 %) (dark blue, entry 9) and SiO₂-PS-PPFS (46 %) /PPFS-PFDT (DS = 29 %) (clear blue, entry 11).

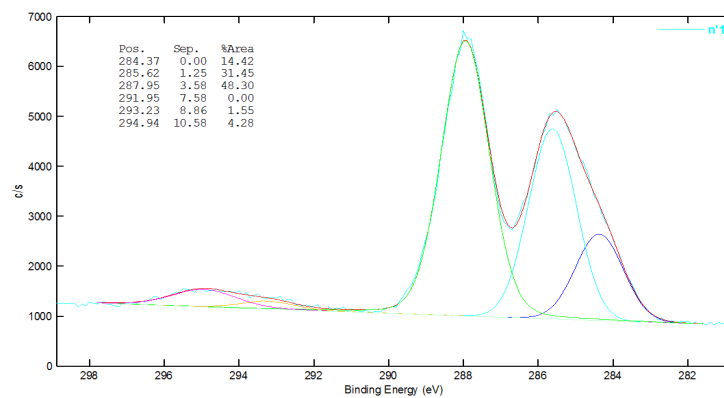


Figure SI7 C1s narrow scans of SiO₂-PS-b-PPFS (35 %) /PPFS (entry 4).

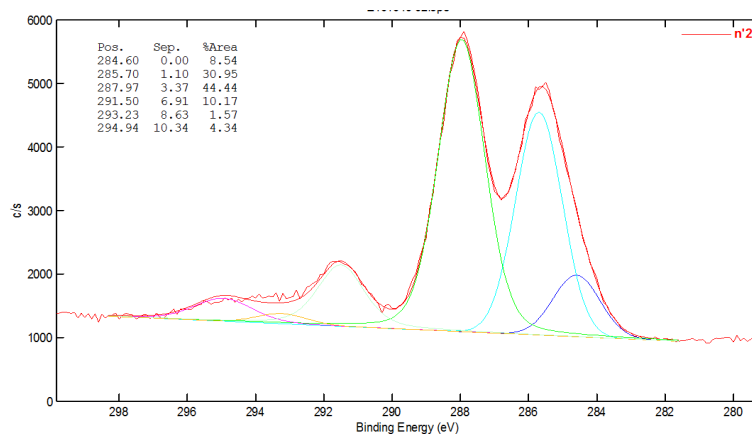


Figure SI8. C1s narrow scans of SiO₂-PS-PPFS (35 %) /PPFS-PFDT (DS = 29 %) (entry 9).

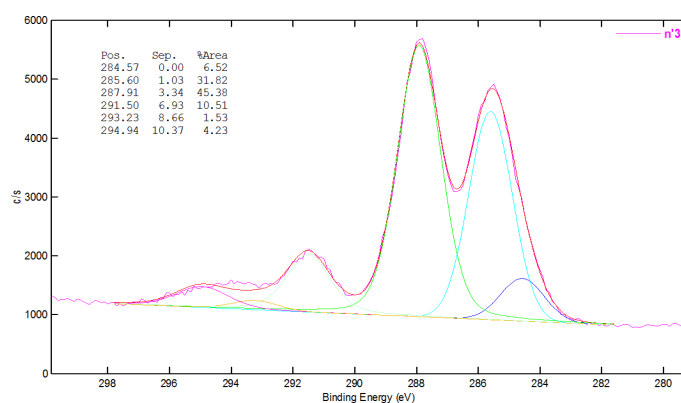


Figure SI9. C1s narrow scans of SiO₂-PS-PPFS (46 %) /PPFS-PFDT (DS = 29 %) (entry 11).

Table S1 Proportions in percent of the various chemical environments of carbon, obtained by the deconvolution of the C 1s peaks of SiO₂-PS-b-PPFS (35 %) /PPFS (entry 5), SiO₂-PS-b-PPFS (35 %) /PPFS-PFDT (DS = 29 %) (entry 8) and SiO₂-PS-b-PPFS (46 %) /PPFS-PFDT (DS = 29 %) (entry 10).

Entry	C-C/C-H (%)	CH-C/F (%)	C-F (%)	CF ₂ (%)
(5)	15	31	52	0
(8)	7	32	47	12
(10)	8	32	45	14

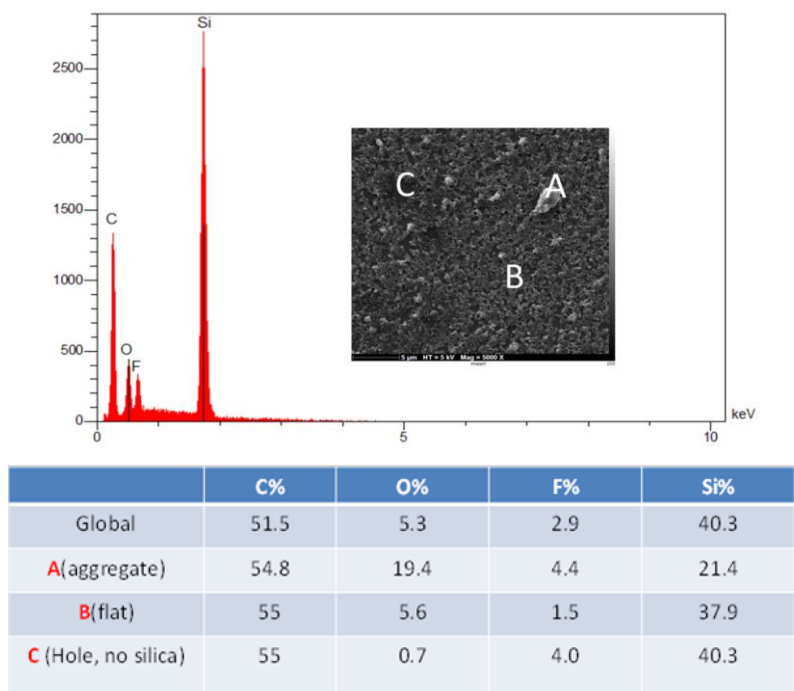


Figure SI10. EDX analysis of the SiO₂-PS-b-PPFS (46 %) /PPFS-PFDT (DS = 29 %) film (entry 11)

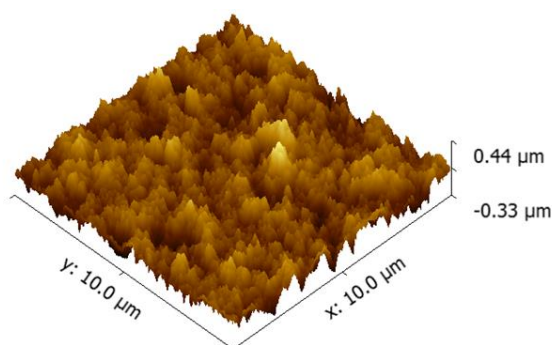


Figure SI11. 3D AFM image of SiO₂-PS-PPFS (46 %) /PPFS-PFDT (DS = 29 %) (entry 11).

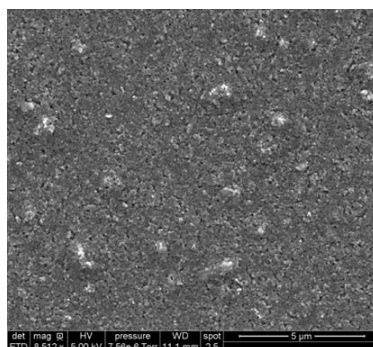


Figure SI12. SEM image of SiO₂-PS-PPFS-PFDT (DS 13 %) /PPFS (entry 12).

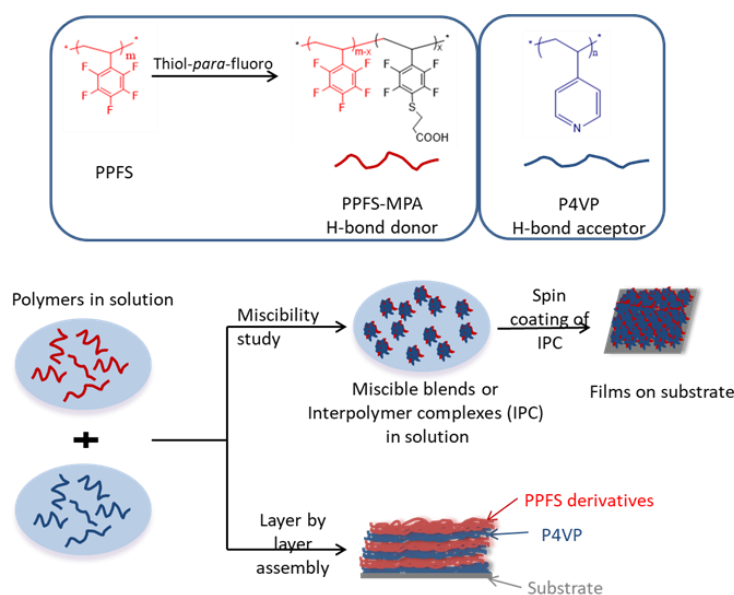
Chapter 3: Novel carboxylic acid modified poly(2,3,4,5,6-pentafluorostyrene) and their application in preparing H-bonds driven multilayer thin films

3.1 General introduction

PPFS has been extensively utilized in many important applicative fields due to its attractive properties including high thermal and chemical resistance, low refractive index, low dielectric constant, low wettability, anti-sticking properties and so on.¹⁻⁵ Furthermore, the carbon in *para* position of the benzenic ring is, in comparison with the other carbons, rather “positively charged” making the associated fluorine prone to be modified by various nucleophiles, such as thiols,⁶⁻⁹ amines^{10,11} and alcohols.^{3,5,12} The incorporation of these polymer derivatives into layer-by-layer (LbL) self-assembling thin films remains limited, to the best of our knowledge, only one work from our laboratory concerning hydroxylated PPFS was reported.¹³ This work concerned hydroxylated PPFS derivatives bearing either a (poly)fluorinated hydroxyl or one or two hydrogenated hydroxyl groups in conjunction with a strong H-bond acceptor partner (P4VP), and the role played by the chemical structure of the OH-based interacting moieties on the LbL self-assembly properties was investigated.^{14,15} As discussed in the bibliographic chapter, carboxylic acid containing polymers have become popular building blocks for the construction of multilayer films via LbL assembly thanks to their ability to develop non-covalent interactions, including electrostatic interactions and hydrogen bonds (H-bonds). One can cite the most used water-soluble weak polyacids, poly(acrylic acid) (PAA)¹⁶ and poly(methacrylic acid) (PMAA).^{17,18} However, scarce work reported the use of water-insoluble polyacids for LbL assembly process.

As explained in detail in the general introduction of this manuscript, one of the

objectives of this PhD project aims at using PPFS derivatives to construct thin films by LbL approach. Herein, PPFS is chemically modified in view to introduce carboxylic-acid moieties. These polar functions, able to be involved in H-bonds with well-chosen proton acceptor partner (P4VP in this work), are covalently tethered to the PPFS backbone through the thiol-*para*-fluoro substitution reaction with carboxylic acid-containing thiols as modifiers. The general strategy is depicted in the following scheme.



Scheme 3-1 General strategy for the preparation of LbL self-assembly polymer thin films.

First, this chapter describes the PPFS modification with carboxylic acid containing thiol. Then, the ability of PPFS derivatives to undergo H-bonds in solution with P4VP is studied. The effect of DS (namely the number of PFS repeating unit modified per polymer chain) and the nature of solvent on the H-bond propensity is discussed. In a second part, the elaboration of thin films via the successive spin-coating of PPFS-MPA/P4VP complexes preformed in solution onto a flat substrate is presented. Finally, the LbL self-assembly by using PPFS-MPA and P4VP, sequentially deposited onto flat substrates, is described and the resulting multilayer thin films are in-depth characterized in terms of growth mechanism, internal organization and surface features. In particular, the effect of the nature of solvent, the DS and the concentration of deposition solution are investigated.

3.2 Experimental part

3.2.1 Materials and characterization methods

Materials

Chloroform (CHCl₃, 99%), Methyl ethyl ketone (MEK, 99%), N, N-Dimethylformamide (DMF, 99%), 1,8-Diazabicyclo[5.4.0]undec-7-ene (DBU, 98%), Mercaptoacetic acid (MAA, 98%), 2-Mercaptopropionic acid (2MPA, 95%), Mercaptopropionic acid (MPA, 99%), Mercaptosuccinic acid (MSA, 97%) and Poly(4-vinylpyridine) (P4VP, 60 kg/mol) were purchased from Sigma-Aldrich and used as received. Microscope glass slides and silicon wafers were purchased from CARL-ROTH and SIL'TRONIX, respectively, and used as substrates onto which films were elaborated. Specimens with a size around 1 cm × 1 cm were cleaned by 15 min intervals of sonication in acetone, ethanol, and Milli-Q water. After dried under gentle nitrogen flow, they were activated by ozonolysis for 30 min and then readily used. Poly(2,3,4,5,6-pentafluorostyrene) (PPFS, 14 kg/mol, $\bar{M}_n = 1.2$) was synthesized, as described in the previous work (Chapter 2.3.3).

Characterization method

Nuclear magnetic resonance spectroscopy (NMR). ¹H- and ¹⁹F-NMR spectra were recorded on a Bruker Advanced AM400 spectrometer at 400 MHz with 64 scans each at room temperature. Analytes were dissolved in DMF-d₇. Chemical shifts were determined in ppm. ¹H-NMR spectra were calibrated thanks to tetramethylsilane at 0 ppm, while ¹⁹F-NMR spectra were calibrated thanks to the signal at -143 ppm that corresponds to the fluorine in (*ortho* + *ortho'*) positions (see Figure 3-1).

Attenuated total reflection Fourier transform infrared (ATR FT-IR). ATR FT-IR spectra were recorded using a Nicolet iS10 apparatus (diamond crystal) with a resolution of 4 cm⁻¹ and a 32 scans accumulation within a range of 500–4000 cm⁻¹.

Thermogravimetric analysis (TGA). TGA measurements were performed on a TA Q500 at a heating rate of 10 °C/min between 50 and 600 °C under a helium flow (40 mL/min).

Differential scanning calorimetry (DSC). DSC thermal analyses were performed with a differential scanning calorimeter, DSC Q1854 from TA Instruments, in a temperature range of 40 to 170 °C at a heating rate of 20 °C/min under the flow of helium (25 mL/min). Three scans (heat/cool/heat, separated by a 2 min isotherm) were realized for each sample.

Water contact angle (WCA) measurement. WCA and water hysteresis measurements were carried out by using a Dataphysics Digidrop contact angle meter equipped with a CDD2/3 camera with the sessile drop and by using milli-Q-quality water as probe liquid. The results are the average of at least five measurements on different part of each sample.

Intrinsic viscosity. The intrinsic viscosity $[\eta]$ of PPFS-MPA and P4VP in different solvents was measured with an Ubbelohd viscometer at 25 °C. PPFS-MPA and P4VP were dissolved in CHCl_3/MEK , DMF or EtOH at concentrations ranging from 1.25 to 6 mg/mL. The efflux time of the pure solvent flow through a thin capillary was recorded as t_0 firstly; then the efflux time (t) of the polymer solution with different concentration was recorded. The specific viscosity (η_{sp}) is expressed as

$\eta_{sp} = \frac{t}{t_0} - 1$. The relation between specific viscosity and intrinsic viscosity ($[\eta]$) is

demonstrated by the Huggins equation: $\frac{\eta_{sp}}{c} = [\eta] + k_H [\eta]c$, where c is the polymer

concentration and k_H is the Huggins coefficient. The intrinsic viscosity is the value of the corresponding graphic extrapolation when the polymer concentration is 0, by

using the equation of $[\eta] = \lim_{c \rightarrow 0} \frac{\eta_{sp}}{c}$.

Ultraviolet spectroscopy (UV). UV spectra of the films assembled on glass slides substrates (1.5 cm × 3.5 cm) were recorded on a Shimadzu UV-2550 spectrophotometer in transmission mode.

X-ray photoelectron spectroscopy (XPS). XPS analysis of the surfaces was

conducted on a PHI Quantera SXM Spectrometer using an aluminium $K\alpha$ X-ray radiation source with a photon energy of 1486.6 eV. The pressure in the chamber was below 10^{-9} - 10^{-10} torr before data were taken, and the voltage and current of the anode were set at 15 kV and 3 mA, respectively. The pass energy was 40 eV. The binding energy scale was fixed with setting the C1s peak maximum at 285.0 eV.

Atomic force microscopy (AFM). AFM images were acquired in intermittent contact mode (tapping mode), on silicon wafer with a size of 1 cm \times 1 cm, in air at room temperature using an AFM Bruker Multimode 8 apparatus equipped with Nanoscope V controller. The scanning speed for image acquisition is 0.5 Hz. The used tips were purchased from Bruker with the model of SCANASYST-AIR. The surface root mean square roughness (R_q) was obtained by processing images using the Nanoscope Analysis software (version 1.5). In order to access the film thickness, an indentation was delicately performed with a razor blade by ensuring a good access to the silicon substrate and the elimination of the removed polymer from the surface. The height difference created by the indentation can be probed by AFM topology, which provides the film thickness. At least 5 measurements were made on each sample to obtain an average dry film thickness.

3.2.2 Modification of PPFS by thiol-*para*-fluoro substitution reaction

PPFS was modified by -COOH containing thiols (MAA, 2MPA, MPA and MSA) under basic conditions (DBU as base) via thiol-*para*-fluoro substitution reaction. In a typical procedure, PPFS (0.5 g, 2.6 mmol PFS units) was dissolved in 2.8 mL of MEK, then MPA (2 mmol, 1.3 mL) and DBU (2 mmol, 0.9 mL) solutions in MEK were added into polymer solutions such that the final concentration of PPFS was 100 g/L and the molar ratio of (PFS):(-SH):(DBU) was 1:1:0.7. The mixture was stirred for 6 h at room temperature. After dilution with DMF, the resulting polymers were purified by precipitation into cold acidic water (pH < 3), rinsing twice with water until no residual thiol or base was revealed by $^1\text{H-NMR}$. The collected polymers were dried at

40 °C under vacuum for 12 hours with a yield of 81%; degree of substitution (DS) with a value of 32% was determined by ^{19}F -NMR in DMF- d_7 . Specimens are then designated as PPFS-MPA with their respective DS in the text (PPFS-MPA-DS).

3.2.3 Preparation of P4VP/PPFS-MPA blends

Blends were obtained by simply mixing appropriate amounts of PPFS-MPA with P4VP that were separately dissolved in a given solvent. Typically, 30 mg of PPFS-MPA-32% copolymer was dissolved in 5 mL of CHCl_3/MEK (v/v = 1/1), EtOH or DMF. An appropriate amount of H-bonds acceptor P4VP was separately dissolved in the same volume of the corresponding solvent CHCl_3/MEK , EtOH or DMF. A blend solution was prepared after mixing each other, such that a molar ratio of (-COOH):(4VP) is 1:6. The mixtures were stirred for 10 min and pictures were taken. After slow evaporation of the solvent (CHCl_3/MEK and EtOH) in glass vial at room temperature, the solid samples were dried at 25 °C under vacuum for two days. For the samples prepared in DMF, solvent was slowly evaporated at 50 °C and dried at 70 °C under vacuum for two days. The obtained solid polymer mixtures were analyzed by FT-IR in ATR mode, DSC and XPS.

3.2.4 Spin-assisted film buildup of preformed H-bonded interpolymer complexes

The PPFS-MPA-32% copolymer and P4VP were separately dissolved into CHCl_3/MEK (v/v = 1/1) with a concentration of 2 g/L then mixed, resulting in a turbid blend, revealing the formation of a so-called “Interpolymer complex” IPC (see text). The mixtures were stirred for 10 min at room temperature. Then 100 μL of this turbid solution was spin-coated onto freshly activated glass slides or silicon wafers, at a speed of 2000 rpm for 30 s by using a Polo Spin 150i/200i spin-coater type from SPS-Europe. After the deposition of one layer, the substrate was rinsed with pure CHCl_3/MEK by using the same spinning time and speed, and dried by a gentle stream of nitrogen. The procedure was repeated N times. The process of build-up was monitored by UV spectroscopy (when transparent glass slides were used) and the

topographic morphology was characterized by AFM. The interactions developed within the deposited mixture were confirmed by XPS.

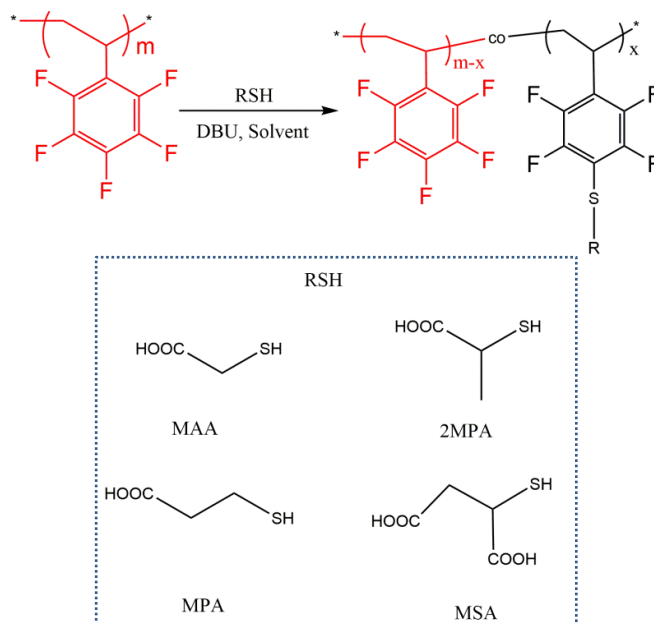
3.2.5 Preparation of H-bonded multilayer films

In a typical procedure, LbL assembly was started by immersing the freshly activated substrate into a P4VP solution (2 g/L) in EtOH for 5 min, followed by rinsing with the same solvent for 1 min statically and three back and forth movements to remove loosely bound P4VP from the substrate. After drying with gentle nitrogen flow, the substrate was transferred into PPFS-MPA (DS = 32%) solution (2 g/L) in EtOH for 5 min to add a PPFS-MPA layer and then rinsed with the corresponding solvent using the same procedure than the one used for P4VP layer, followed by drying process; the combination of such successive immersions corresponds to the deposition of a so-called one bilayer (BL). The procedure was repeated n times to deposit n (BL). Besides, other deposition solvents, including DMF for both P4VP and PPFS-MPA, CHCl_3/MEK for both P4VP and PPFS-MPA and CHCl_3 for P4VP combined to MEK for PPFS-MPA, were also employed to prepare multilayer films. The construction process was monitored by FT-IR in ATR mode or/and UV spectroscopy, the driving force was characterized by ATR FT-IR and XPS and the surface features were evaluated by WCA measurements and by AFM imaging.

3.3 Synthesis of carboxylated PPFS derivatives by thiol-*para*-fluoro substitution reaction

The incorporation of functional polar groups such as $-\text{COOH}$ into a polymer A is an efficient means to enhance the miscibility with another polymer B if the latter contains complementary functional groups to develop H-bonds. With the aim of preparing novel H-bond donor polymers and improving their miscibility with P4VP (qualified as strong H-bond acceptor polymer), PPFS homopolymers were modified with various $-\text{COOH}$ containing thiols by *para*-fluoro substitution reaction (PFSR)

(Scheme 3-2).



Scheme 3-2 Post-polymerization functionalization of PPFS by carboxylic acid-containing thiols RSH (MAA, 2MPA, MPA and MSA) via thiol PFSR.

PPFS with a molecular weight (M_n) of $\sim 14,000$ g/mol was synthesized, as described in the previous chapter (Chapter 2.3.3). Methyl ethyl ketone (MEK) or tetrahydrofuran (THF) were used as solvents in order to efficiently modify PPFS, according to the work of Chen and coworkers,¹⁴ who studied the PFSR of PPFS with various hydroxyl-containing thiols in various solvents. The authors demonstrated that MEK and THF accelerate the reaction, compared to the use of ethyl acetate. Various carboxylic acid-containing thiols (MAA, 2MPA, MPA and MSA) bearing one or two carboxylic acid moieties were used as modifiers, in the presence of a non-nucleophilic base (DBU), which has been recently reported a very efficient as coreactant in promoting PFSR with (pentafluorophenyl)acetamide¹⁹ and PFS-containing copolymers.²⁰ In the following sub-parts, we mainly focus on MPA and only a few trials concern modifications with MAA, 2MPA and MSA.

3.3.1 Chemoselective modification of PPFS

The chemical structures and the extent of the modification (quantified by the DS)

of the obtained polymers, for example concerning the PPFS-MPA copolymers, were qualitatively and quantitatively monitored by ^{19}F -NMR spectroscopy (Figure 3-1).

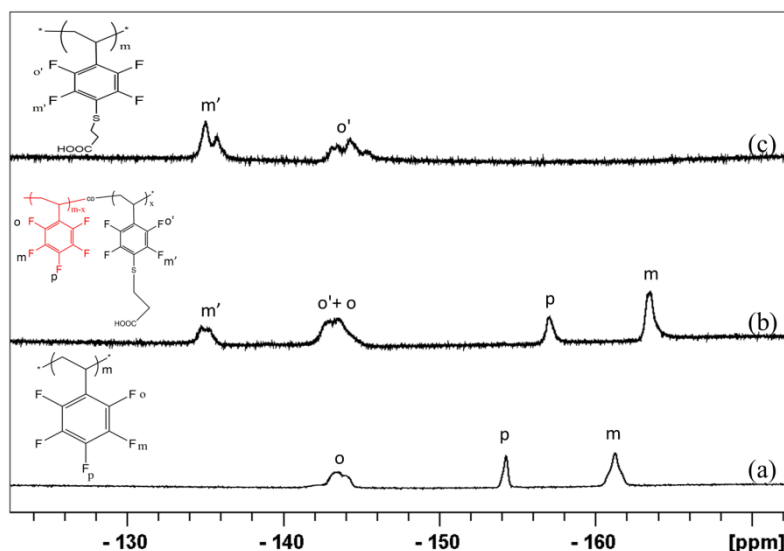


Figure 3-1 ^{19}F -NMR spectra of PPFS (a), PPFS-MPA-32% (b) and PPFS-MPA-100% (c).

As shown in Figure 3-1-a, the chemical shifts at -143 ppm, -154 ppm and -161 ppm are respectively attributed to the fluorine atoms in the *ortho*, *para* and *meta* positions of unmodified PFS units. After modification with MPA, in Figure 3-1-b, the chemical shifts of *para*-F and *meta*-F are shifted to downfield at -157 ppm and -164 ppm, respectively. Moreover, a new peak appears at -135 ppm which is ascribed to the *meta*'-F of modified PFS units; the *ortho*'-F of modified PFS is merged with the *ortho*-F at -143 ppm. In Figure 3-1-c, the two peaks corresponding to *ortho*' and *meta*'-F of modified PFS illustrate the total modification of PPFS. In particular, the DS of PPFS-MPA copolymers can be determined from the integrals (S) by using Equation 3-1.

$$DS = \frac{S(m')}{S(o'+o)} \times 100\% \quad (\text{Equation 3-1})$$

The successful modification of PPFS can be confirmed by FT-IR in ATR mode, the spectra of PPFS before and after modification is shown in Figure 3-2.

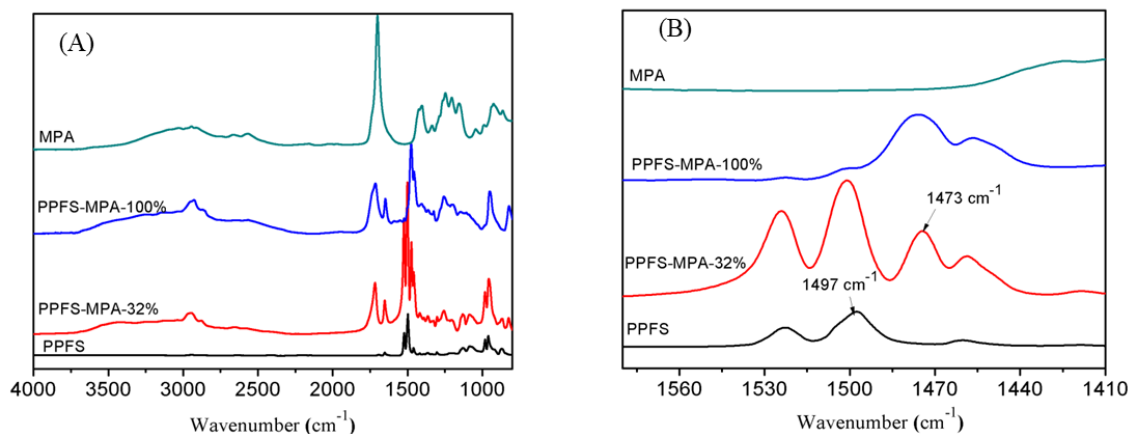


Figure 3-2 ATR FT-IR spectra of PPFS, MPA, PPFS-MPA-32% and PPFS-MPA-100%.

From Figure 3-2-A, compared with MPA and pristine PPFS, peaks in the range of 2250-3750 cm^{-1} can be ascribed to the hydroxyl-stretching vibration bands of $-\text{COOH}$. The peak at 1720 cm^{-1} is assigned to the $\text{C}=\text{O}$ stretching vibration of $-\text{COOH}$.²¹ Moreover, in Figure 3-2-B, we observe a band at 1497 cm^{-1} which is assigned to the fluorinated aromatic ring vibrations of the unmodified PFS and, after modification with MPA, a new band appears at 1473 cm^{-1} . All these features evidence that the carboxyl groups are anchored to PPFS polymer chains.

3.3.2 Kinetics of modification

As explained in the bibliographic part (Chapter 1.1.4.1), the presence of a base accelerates the reaction rate and improves the yield of conversion of *para*-fluoro substitution reaction (PFSR). In this work, DBU is used as base; it not only activates thiols to form thiolate as a nucleophile but also reacts with $-\text{COOH}$ groups. Based on this idea, the possibility of PFSR under basic experimental conditions (DBU as base) with various $-\text{COOH}$ containing thiols (MAA, $\text{pK}_a = 3.64$; 2MPA, $\text{pK}_a = 3.74$; MPA, $\text{pK}_a = 4.34$ and MSA, $\text{pK}_a = 3.49$) was studied (Table 3-1). As previously prevised, most of this PhD work has been dedicated to the use of MPA and only few trials were performed with MAA, 2MPA and MSA.

Table 3-1 Thiol-*para*-fluoro substitution reactions of PPFS with MAA, 2MPA, MPA and MSA.

Entry	Modifier	Time (min)	(PFS):(-SH):(DBU)	DS (%)
1	MAA	30	1:1:1	34
2	2MPA	45	1:1:1	33
3	MPA	360	1:1:0.4	0
4	MPA	360	1:1:0.6	15
5	MPA	360	1:1:0.7	32
6	MPA	30	1:1:0.8	37
7	MPA	30	1:1:1	45
8	MPA	10	1:2:1.6	56
9	MPA	5	1:2:2	100
10	MSA	10	1:2:2	60
11	MSA	10	1:2:3	100

Entry 1-9 : the reaction was performed in MEK at room temperature;

Entry 10-11 : the reaction was performed in DMF at 50 °C.

MAA (entry 1), 2MPA (entry 2), MPA (entry 7) with various pKa (3.64, 3.74, and 4.34, respectively) were employed to modify PPFS, the reactant molar ratio was kept at (PFS):(-SH):(DBU) = 1:1:1 and the reactions were stopped after the appearance of a precipitate resulting from the poor solubility of raw products in MEK. 2MPA needs longer reaction time (45 min, entry 2) than MAA (30 min, entry 1) to reach a conversion of 33% because of the steric hindrance of 2MPA. The weaker acid MPA (pKa = 4.34) results in an increased DS (45%) after 30 minutes (entry 7) for the same (PFS):(-SH):(DBU) = 1:1:1. As described in the previous work (Chapter 2.3.4.1), while performing PFSR with perfluorinated thiol as modifier, the DS could be tuned by adjusting the amount of DBU. Herein, various (PFS):(-SH):(DBU) ratios were applied to tune the DS, by increasing the DBU content for a constant (PFS:-SH) ratio (entries 3-7) or by increasing the (-SH and DBU) content (entry 8 and 9). DS from 0 up to 56% were obtained. With the dicarboxylic acid containing-thiol (MSA), reactions were carried out in DMF at 50 °C for solubility issues. We observe a large modification (DS = 60 %, entry 10) in a rather short time (10 min) with the ratio of 1:2:2; and a complete modification (DS = 100%, entry 11) in the same time scale (10

min) with the ratio of 1:2:3, due to the increased amount of DBU, which promotes the production of the nucleophilic thiolate.

In order to get more precise information on the control of the DS for low values (DS < 30 %), kinetics in THF and MEK with the ratio of 1:1:0.6 by using MPA as modifier were studied (Figure 3-3).

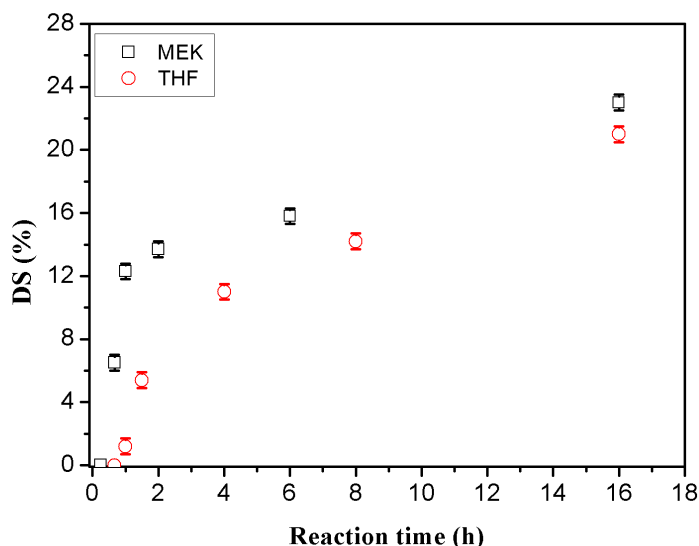


Figure 3-3 Kinetics of MPA modified PPFS with the molar ratio of (PFS):(-SH):(DBU) = 1:1:0.6 in THF (circle) and MEK (square).

We can observe that the reaction rate in MEK is faster than in THF in the early time of reaction, indicating a lower accessibility of the thiolate in THF compared to MEK, probably due to the possible occurrence of H-bonds between the given anion and the remaining hydroxyl groups of carboxylic acid.¹⁴ These H-bonds might be drastically reduced in a more polar solvent such as MEK due to stronger OH/solvent interactions. With consuming of thiol and DBU, less nucleophilic thiolate were produced. The difference of reaction becomes smaller; leading to a DS of 23% in MEK and 21% in THF after 16 h.

At this stage, two strategies to control the DS were developed. One consists in adjusting the reactant molar ratio, especially for DS higher than 30%, the other one consists in adjusting reaction time and polarity of solvent for DS less than 30%. Only the characterization related to PPFS-MPA with various DS (7%, 15%, 32% and 100%) are presented in the following parts.

3.3.3 Thermal properties of PPFS-MPA

The thermal properties of PPFS-MPA were studied by thermogravimetric analysis (TGA). The TGA curves and the corresponding derivative thermo-gravimetric (DTG) curves of PPFS and PPFS-MPA with various DS (7%, 15%, 32% and 100%) are shown in Figure 3-4.

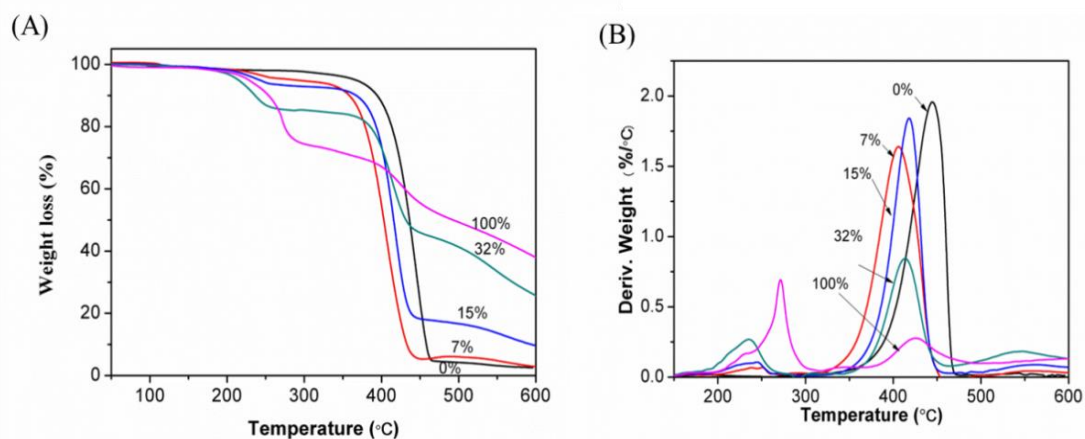


Figure 3-4 TGA and DTG curves of PPFS and PPFS-MPA (DS = 7%, 15%, 32% and 100%).

In Figure 3-4-A, compared with pristine PPFS, the mass loss of PPFS-MPA in the first stage starts from 200 °C to 300 °C due to the formation of anhydrides from carboxylic acid groups of PPFS-MPA, which was confirmed by ATR FT-IR with the appearance of a new band at 1852 cm^{-1} , corresponding to C=O groups of anhydride (Appendix, Figure AI 3-1).²² The higher the DS is, the more anhydrides were formed, as reflected by the increase of weight loss from 5 wt. % (DS = 7%) to 30 wt. % (DS = 100%). The second step corresponds to the degradation of the main chain and occurs in the range of 350 - 470 °C for both PPFS and PPFS-MPA. PPFS is completely degraded when temperature is higher than 470 °C, while PPFS-MPA is not completely degraded, especially for the more substituted derivatives (DS = 32% or 100%). One can notice a small bump centered at 550 °C that may correspond to a third step, indicating that the grafting of carboxylic acid lowers the initial decomposition temperature and the decomposition average rate.²³

3.3.4 Wettability properties of PPFS-MPA

PPFS-MPA copolymers with various DS were dissolved in DMF ($c = 30 \text{ g/L}$); thin films were prepared by spin-coating the solutions onto a pre-activated silicon wafer and the solvent was further evaporated. The surface wettability was evaluated by WCA measurements (Figure 3-5).

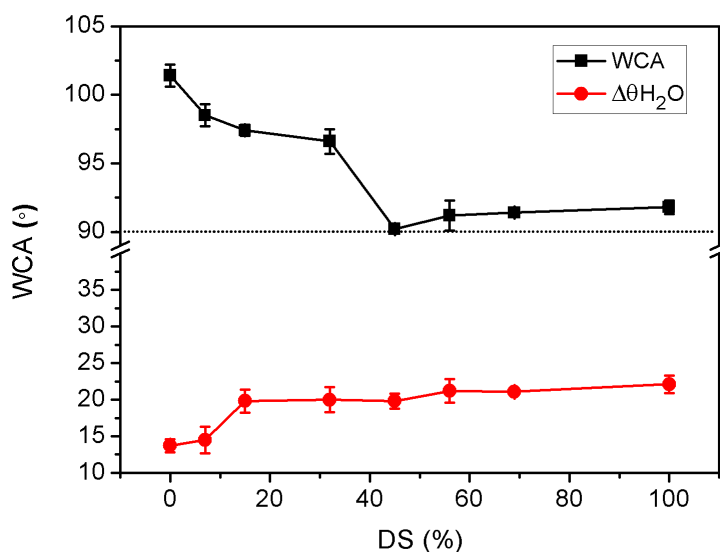


Figure 3-5 Water contact angle (WCA) and water hysteresis ($\Delta\theta_{H_2O}$) measurements as a function of DS for PPFS modified by MPA.

PPFS is well-known as a kind of hydrophobic polymer with a WCA around 101° ,⁴ the introduction of $-\text{COOH}$ onto the backbone of PPFS decreases its hydrophobicity, as evidenced by the decrease of WCA with the DS increase. A plateau with a WCA of 91° is obtained from DS higher than 45%. In spite of the introduction of polar $-\text{COOH}$ moieties, PPFS-MPA remains globally hydrophobic due to the fluorinated nature of the backbone. $\Delta\theta_{H_2O}$ of PPFS is 13° and reaches a plateau with a value of 20° with DS higher than 15%, indicating that the interfacial interactions between carboxylic acid groups from the polymer and water are enhanced, the polarity of carboxylated PPFS being promoted when the DS increases.¹⁴

3.3.5 Conclusion

As demonstrated by ^{19}F -NMR, especially in the case of MPA modified PPFS, the *para*-fluoro substitution reaction is chemoselective as the SH group solely reacts onto the *para*-fluorine of the fluorinated ring. The extent of nucleophilic substitution can be successfully adjusted especially in the case of MPA from relatively low (7%) up to a complete conversion (100%), by controlling the reaction time, the polarity of solvent and the molar ratio between reactants. Consequently, this chemical route leads to polymers with variable physico-chemical properties, as revealed by the study of the thermal properties and the water wettability measurements.

3.4 Study of the PPFS-MPA/P4VP blends

The association of polymers in solution through the formation of non-covalent forces, in particular, H-bonds, has received intensive attention because polymer blends can permit to access to novel polymer materials with improved properties.^{24,25,26,27} The compatibility degree between naturally incompatible polymers can be significantly changed by the interactions developed between the polymer chains. The so-called miscible blends can be obtained if the interactions of polymers in solution are weaker than the polymer/solvent interactions, resulting in a transparent solution; on the contrary, a turbid solution can be obtained when the interactions of polymers are stronger than the respective polymer/solvent interactions, the aggregates or precipitates in solution are defined as Interpolymer Complexes (IPC).^{25,26}

Our study is focused on the ability of carboxylated PPFS polymers (PPFS-MPA) to develop H-bonds in solution with a strong H-bond acceptor polymer: poly(4-vinylpyridine) (P4VP). In order to gain insight into the conformation of polymer chains and the interactions between polymer and solvent molecules, we will firstly discuss the intrinsic viscosity of polymer in various solvents. Then, the impact of the DS and the nature of the solvent used for the blend, on the formation of H-bonds between PPFS-MPA and P4VP are investigated.

3.4.1 Intrinsic viscosity measurements

The intrinsic viscosity $[\eta]$, a measure of a polymer's ability to increase the viscosity of a solvent, is one of the most fundamental properties of polymers in diluted solution.²⁸ It is widely used as a convenient means for determining the viscosimetric molecular weight or for reflecting polymer conformation and polymer chain size in solution. The conformation of a polymer in solution depends on three factors: flexibility of the chain, interactions between the repeating units of the chain, and interactions between the repeating units of the chain and the solvent molecules.²⁹ A high intrinsic viscosity means that interactions between solvent molecule and the polymer chains are favored, so that the polymer chains rather adopt an expanded conformation.³⁰ Hence, the $[\eta]$ measurement of P4VP and PPFS-MPA-32% in various solvents can be considered as a way to evaluate the quality of the solvent and to have an idea on the intrachain interactions existing between the polymers (Figure 3-6).

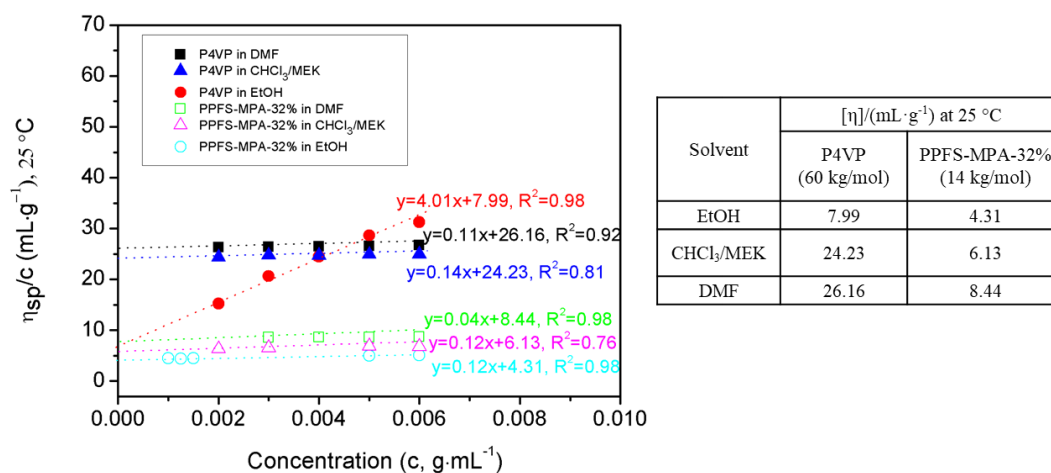


Figure 3-6 The evolution of intrinsic viscosity ($[\eta]$) of the polymer solutions in different solvents.

The intrinsic viscosity of P4VP varies as a function of the solvent (Figure 3-6). The $[\eta]$ of P4VP increases in the order of EtOH < CHCl₃/MEK < DMF means that the interactions between the solvent molecules and the polymer in DMF (and in CHCl₃/MEK) are stronger than in EtOH, probably leading to an extended conformation of P4VP chains in these two solvents. The $[\eta]$ value of PPFS-MPA-32%

follows the same order, as a function of the solvent. In EtOH, PPFS-MPA-32% chains seem to adopt a more compact chain conformation than in CHCl_3/MEK or in DMF, probably due to the presence of intrachain interactions and the poor solvation ability of fluorinated backbone in EtOH. Moreover, for a similar solvent, the $[\eta]$ of PPFS-MPA-32% is smaller than the one of P4VP, but it is important to keep in mind that the molar mass of PPFS-MPA-32% is much lower, compared to the one of P4VP (14 kg/mol against 60 kg/mol).

3.4.2 Influence of the DS of PPFS-MPA and the solvent on miscibility of PPFS-MPA with P4VP

The influence of the DS on the development of H-bonds between PPFS-MPA derivatives (DS = 7%, 15% or 32%) and P4VP in solutions was investigated in various solvents. First, CHCl_3 was used and the solubility of PPFS-MPA copolymers with low DS (7% and 15%) in CHCl_3 was examined at a concentration of 6 mg/mL. As shown in Figure 3-7, PPFS-MPA-7% in CHCl_3 leads to a transparent solution, while PPFS-MPA-15% gives a rather turbid solution.

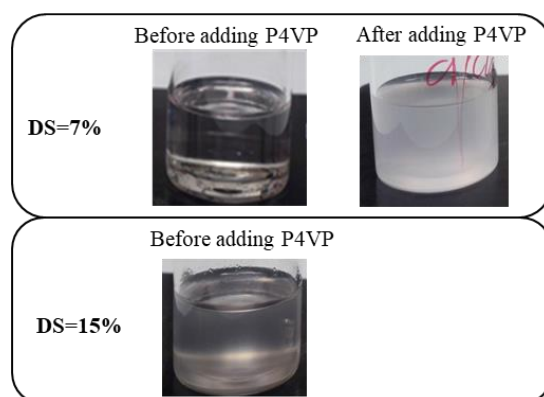


Figure 3-7 Images of PPFS-MPA (DS = 7% or 15%) solution in CHCl_3 before and after (only for DS = 7%) P4VP addition according to a molar ratio of $(-\text{COOH}):(\text{4VP}) = 1:6$.

The complexation behavior was studied by adding into PPFA-MPA-7% solution, the same volume of P4VP (which is well soluble in CHCl_3) with a molar ratio of $(-\text{COOH}):(\text{4VP}) = 1:6$. A turbid blend is then observed, indicating the formation of

an interpolymer complex (IPC). We postulated that H-bonds contribute to the formation of IPC, resulting in a solution with a milky aspect. To evaluate the impact of the DS on the formation of H-bonds, we utilized PPFS-MPA-15%, but it appears as insoluble in CHCl_3 . Hence, CHCl_3/MEK ($v/v = 1/1$) mixture, in which all PPFS-MPA (DS = 7%, 15%, 32%) derivatives and P4VP are completely soluble at a concentration of 6 mg/mL, was preferred. The resulting blends are shown in Figure 3-8.

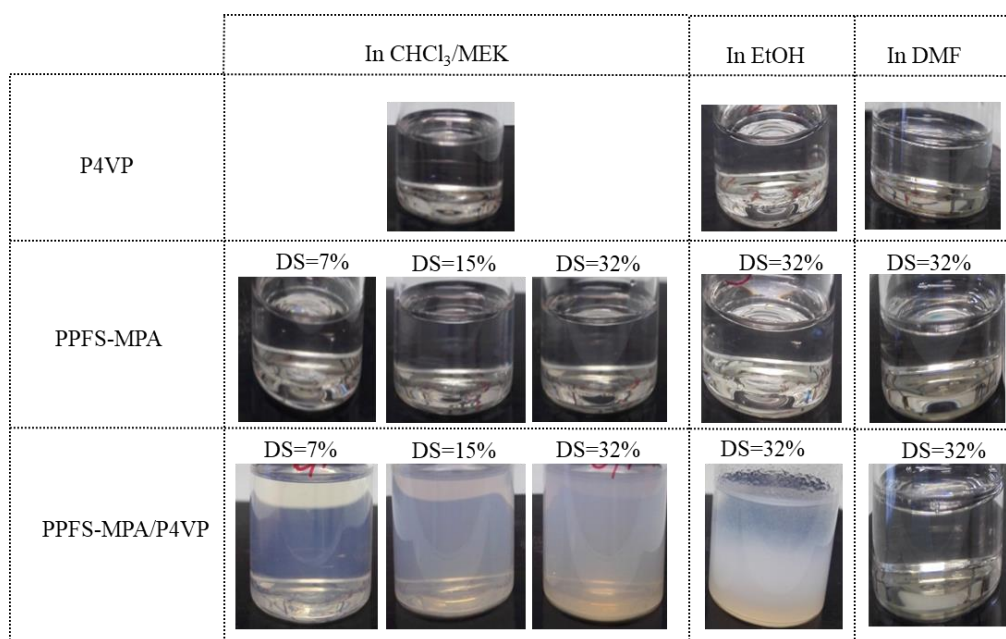


Figure 3-8 Images of P4VP, PPFS-MPA (DS = 7%, 15% and 32%) and their blends in various solvent (CHCl_3/MEK , EtOH and DMF) at room temperature. $(-\text{COOH}):(\text{4VP})$ molar ratio = 1:6.

As a blank, a transparent solution was obtained when blending PPFS and P4VP as no interaction occurs.¹⁴ When using CHCl_3/MEK as solvent, turbid solutions are instantaneously observed after the addition of P4VP into a PPFS-MPA, whatever the value of DS is. This turbidity reflects the formation of strong interactions between PPFS-MPA and P4VP, which overcome the natural repulsion between the two polymers when PPFS is not modified.¹⁵ With the increase of DS which directly affects the number of interacting sites per macromolecular chain, we can reasonably assume that more and more interactions are developed between the two partners, playing on the density and the size of IPC, which can be more spatially extended for higher DS,

as reflected by the enhanced turbidity. Moreover, for higher DS, we can think that the complexes are not solvated by the solvent, which contributes to promote the turbidity. This complexation induced turbid solution was reported in literature for other systems, such as PAA/PVA,³¹ PMMA/PVA,³¹ PAA/PEG³² and hydroxylated PPFS/P4VP.^{14,15} The researchers demonstrated that the formation of an IPC in a particular solvent depends on the balance between polymer-polymer interactions and polymer-solvent ones, and they evidenced that polymer-polymer interactions can be enhanced by increasing the number of interacting moieties, as revealed here in our work.

Then, we studied the effect of organic solvent, including EtOH and DMF, on the complexation ability for a given PPFS-MPA derivative with a DS = 32%. Indeed, complexes of poly(carboxylic acids) with H-bond acceptors can be formed in some organic solvents. For example, Ohno and co-workers³³ employed methanol and ethanol as solvent and observed the formation of PMAA/poly(N-vinyl pyrrolidone) (PVPON) complexes, which are induced by stronger polymer-polymer interactions than polymer-solvent interactions.

In our case, as shown in Figure 3-8, P4VP and PPFS-MPA-32% are well macroscopically soluble in EtOH and DMF at a concentration of 6 mg/mL. With EtOH as solvent, the mixing of PPFS-MPA-32% with P4VP instantaneously provides an IPC, as reflected by the turbidity and which indicates that the interactions of PPFS-MPA-32% with P4VP in EtOH are stronger than polymer-solvent interactions as also reflected by the low value of the intrinsic viscosity of the both polymers in ethanol. Besides, the formation of IPC seems to form a precipitate. We can think that the strong interactions yield non-solvated large aggregates undergoing a sedimentation in the solvent medium.³⁵

Furthermore, it has been reported that no complexation through H-bonds was observed between PMAA and PVPON in a polar aprotic solvent such as DMSO.³³ Indeed, DMSO acts as competitor and is a stronger H-bond acceptor than the carbonyl group of PVPON. By using a stronger H-bond acceptor polymer, poly(N,N-dimethyl-N',N',N'',N''-tetramethylenephosphoramidate) (PHMPA) than PVPON, the authors observed a complex of PMAA/PHMPA in DMSO and suggested

that the proton-accepting ability varies in the order of PHMPA > DMSO > PVPON.³⁴ In our case, we used another aprotic solvent DMF and a homogeneous transparent solution (Figure 3-8) is observed after mixing PPFS-MPA-32% with P4VP. It suggests that PPFS-MPA-32%/DMF and P4VP/DMF interactions are favored, as reflected by the high intrinsic viscosity values, at the expense of interchain interactions between PPFS-MPA-32% and P4VP. It thus appears that DMF acts as a competitive H-bond acceptor, as the strong polymer/solvent interactions prevent from the formation of IPC. A similar phenomenon describing a transparent solution in DMF was reported when mixing poly(p-vinylphenol) and pyridine-containing polymers.³⁶ Another example showing the detrimental impact of DMF onto polymer/polymer interactions is for PAA/PVPON blends: Ma *et al.*³⁰ observed a turbid solution when the blend was prepared in DMF, the turbidity of which was lower than in alcoholic solvents.

3.4.3 Evidence of the formation of H-bonds

FT-IR spectroscopy has proved to be a useful and facile technique to emphasize the formation of H-bonds when involving P4VP as the H-bond acceptor.¹⁵ Spectra of the raw polymers and of all the complexes arising from PPFS-MPA-32%/P4VP in solid state collected from CHCl₃/MEK, EtOH or DMF after a slow evaporation of the solvent are shown in Figure 3-9.

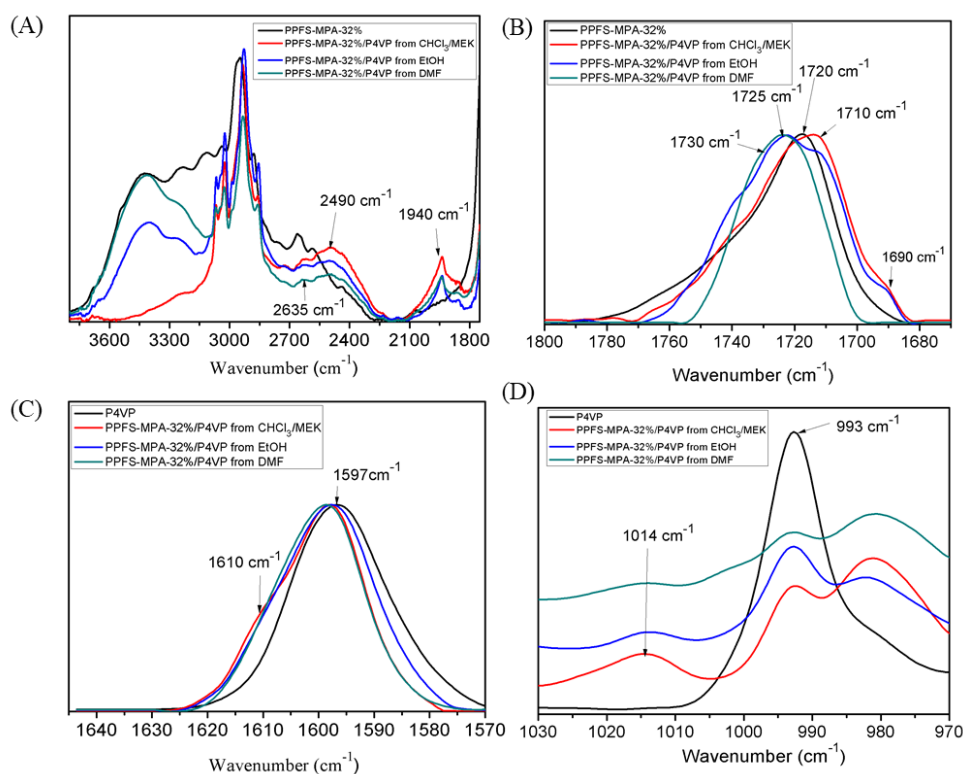


Figure 3-9 FT-IR spectra of PPFS-MPA-32%, P4VP and PPFS-MPA-32%/P4VP blends in solid state after solvent evaporation: carboxyl region (A) and (B); pyridine region (C) and (D).

In Figure 3-9-A, for PPFS-MPA-32%, the broad absorption bands at around 2665 and 2586 cm^{-1} are assigned to the O-H stretching vibration of carboxylic acid in COOH/COOH self-associated state, which shifts to 2635 and 2490 cm^{-1} with the appearance of a new broad peak at 1940 cm^{-1} after the IPC formation, as reported for poly(8-(4-carboxy-phenoxy)-octyl acrylate) (PCPOA) and poly(3-(4-pyridyl)-propyl acrylate) (PPyPA).³⁷ In Figure 3-9-B, the characteristic peak at 1720 cm^{-1} in the PPFS-MPA-32% is attributed to the -C=O stretching vibration of the carboxyl of PPFS-MPA, whereas the corresponding peak for blends of PPFS-MPA-32%/P4VP collected from CHCl_3/MEK or EtOH shifts to 1725-1730 cm^{-1} , with the appearance of new bands at around 1710 and 1690 cm^{-1} , corresponding to the self-associated COOH. Similar results were reported by Wang *et al.*,¹⁶ who studied H-bonds between PAA and P4VP. For the sample collected from DMF, H-bonded -COOH is observed at 1725 cm^{-1} , while no self-associated -COOH is observed, probably due to the fact that the polymer/DMF interactions promoted the expansion of the polymer chains in solution, which limits the self-associated interactions in the polymer when dried. In Figure

3-9-C and D, P4VP exhibits free pyridine ring bands at 1597 cm^{-1} and 993 cm^{-1} . After the mixing with PPFS-MPA-32%, two new shoulders appear: one at 1610 cm^{-1} and the other one centered around 1014 cm^{-1} , as demonstrated in other pyridine containing-polymer complexes, such as poly(monomethylitaconate) with poly(2-vinylpyridine) (P2VP) and P4VP,³⁸ poly(p-vinylphenol) with P2VP and P4VP,³⁶ and hydrolylated PPFS with P4VP.¹⁵ All of these features confirm that H-bonds exist for all PPFS-MPA-32%/P4VP blends collected from different solvents.

Moreover, X-ray photoelectron spectroscopy (XPS) is a powerful technique which allows for determining the type of supramolecular interactions for blends involving P4VP.³⁹ The XPS analyses of free P4VP and PPFS-MPA-32%/P4VP blends in solid state collected from different solvents (CHCl_3/MEK , EtOH or DMF) are shown in Figure 3-10.

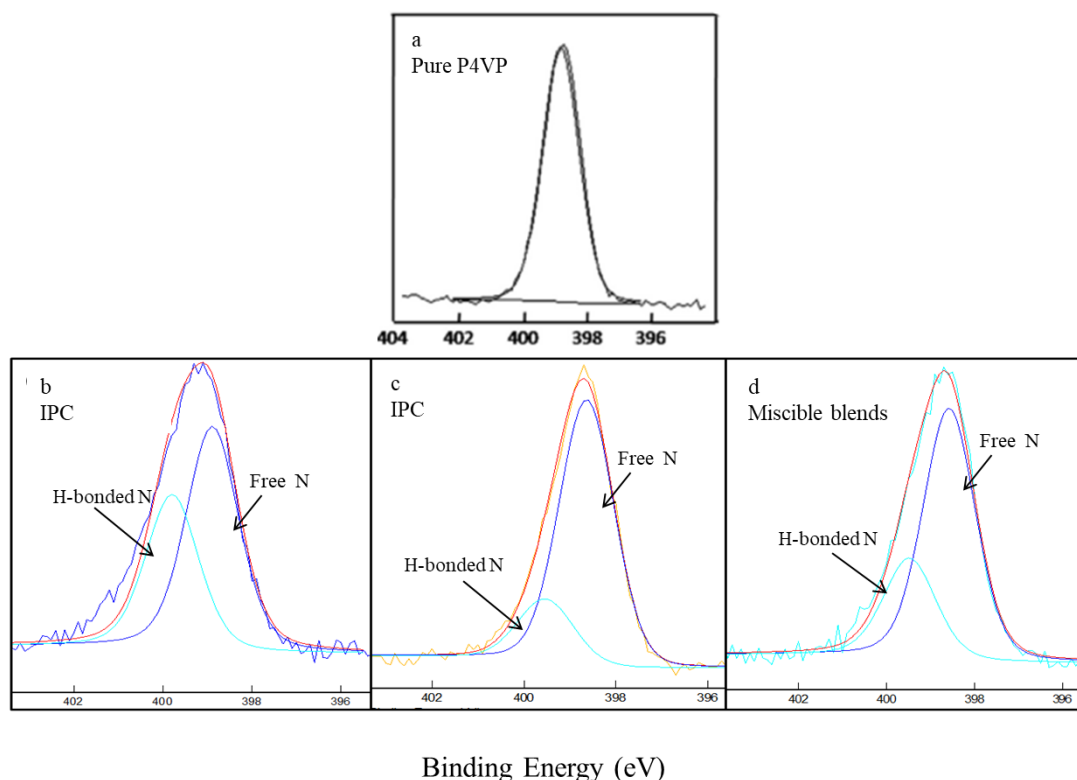


Figure 3-10 XPS N1s core-level spectra of P4VP (a)¹⁵; PPFS-MPA-32%/P4VP in solid state after solvent evaporation from CHCl_3/MEK (b), EtOH (c) and DMF (d).

For P4VP alone, one can observe only one symmetrical N1s peak at 398.8 eV, which corresponds to free nitrogen atoms of P4VP (Figure 3-10-a).¹⁵ For all the

blends, this peak is enlarged and it can reasonably be deconvoluted into two main responses (Figure 3-10-b, c and d). The major one centers at 398.8 eV is related to unassociated nitrogen atoms, while the minor one is associated to H-bonded nitrogen, which is rendered comparatively more electropositive than the free N atoms and thus appears at a binding energy of 399.9 eV.^{15,39,40} All these results confirm that PPFS-MPA derivatives are strong H-bond donors, and that they can develop specific interactions with the H-bond acceptor P4VP. It is also important to note that H-bonds are also visible in the blend recovered from DMF (Figure 3-10-d), while the mixture in solution led to a transparent solution. These two arguments permit to ascertain that PPFS-MPA/P4VP in DMF can be considered as a miscible blend. Even though XPS is a powerful technique to evidence the formation of H-bonds, it should be dubious and questionable to quantify the amount of pyridine rings involved in H-bonded domains.

3.4.4 Study of the interactions through the thermal properties

It is well known that the miscibility in polymer blends is mainly dictated by the chemical structure, the composition and the molecular weight of each component.⁴¹ H-bonded polymer blends are often miscible, and present a single glass transition temperature as a function of the composition within the blend.⁴² The PPFS-MPA/P4VP blends were cast from different solutions and analyzed by DSC (Figure 3-11).

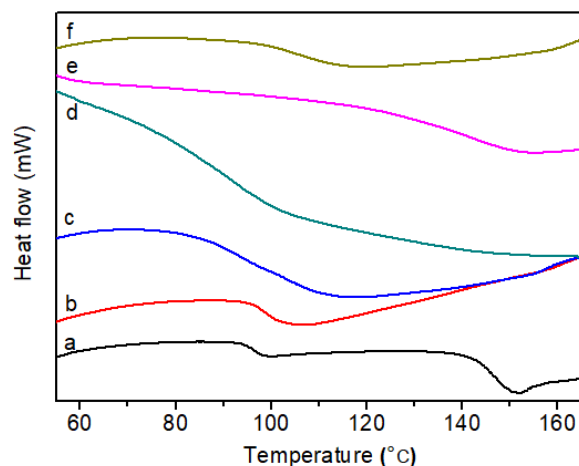


Figure 3-11 DSC curves of PPFS/P4VP (a); PPFS-MPA-7%/P4VP from CHCl_3/MEK (b); PPFS-MPA-15%/P4VP from CHCl_3/MEK (c); PPFS-MPA-32%/P4VP from CHCl_3/MEK (d); PPFS-MPA-32%/P4VP from EtOH (e) and PPFS-MPA-32%/P4VP from DMF (f).

In Figure 3-11-a, for neat PPFS mixed with P4VP, two T_g s which are close to the T_g of each pure polymer are observed, meaning that PPFS and P4VP are completely immiscible, which leads to two well separated phases. After the incorporation of carboxyl groups into PPFS chains with $DS = 7\%$, 15% or 32% , and after mixing with P4VP in CHCl_3/MEK , the blends exhibit only one T_g (Figure 3-11-b, c and d), which confirms the enhanced compatibility between the two polymers due to the formation of H-bonds. Similarly, only one T_g is observed for the blends of PPFS-MPA-32%/P4VP collected from EtOH and DMF (Figure 3-11-e and f), reflecting also the miscibility of PPFS-MPA-32% with P4VP.

3.4.5 Conclusion

Novel carboxylated-PPFS derivatives with various DS were successfully synthesized through the chemoselective thiol-*para* fluoro substitution reaction with carboxylic acid-containing thiols. Then, the ability of the PPFS derivatives modified with mercaptopropionic acid (MPA) (PPFS-MPA with $DS = 7\%$, 15% or 32%) to interact with P4VP through H-bonds was evaluated. For a given solvent CHCl_3/MEK , interpolymer complexes are spontaneously and instantaneously formed whatever the DS is, leading to turbid solutions. The highest DS gives a more turbid solution due to the strong interactions developed between the two polymers. For a given

PPFS-MPA-32%/P4VP blends, the effect of the solvent was analyzed (EtOH versus DMF). The solvent has an influence onto the H-bonds strength between the two partners. Indeed, the solvent affects the conformation adopted by the polymer chains, can act as a H-bond competitor and can more or less solvate the H-bonded aggregated domains. It results that EtOH largely favors the IPC formation made of PPFS-MPA-32%/P4VP, probably due to the increase of the density and the size of H-bonded aggregates which are not stable (non solvated) in EtOH. As reflected by the intrinsic viscosity values, interactions between the interacting polymers and ethanol are not favored, which enhance the miscibility between PPFS-MPA and P4VP. Miscible blends rather than IPC are formed when a polar aprotic solvent, such as DMF, is used. In this case, DMF much certainly acts as a competitor, yielding to a transparent blend in solution.

3.5 Construction of PPFS-MPA and P4VP based thin films

Polymer films play an increasingly important role in technological applications ranging from coatings, adhesives to various organic material based devices.^{43,44} Polymer films below a certain thickness range often exhibit physical properties that differ substantially from intrinsic bulk behavior.⁴⁵ Hence, we explore the ability of fabricating polymer thin films by using PPFS-MPA derivatives and P4VP. Firstly, the step-by-step film buildup by depositing H-bonded PPFS-MPA/P4VP interpolymer complexes is described. Then, we focus on the LbL self-assembly of P4VP and PPFS-MPA. In particular, the effect of the deposition solvent and the DS of PPFS-MPA is in-depth discussed.

3.5.1 Successive deposition of PPFS-MPA/P4VP interpolymer complexes

The step by step deposition of a turbid solution constituted of interpolymer complexes onto a flat substrate, or known as “2-in-1” method, was employed to prepare nanometric thin films, such as thin films of polyelectrolytes complexes⁴⁶ and stereocomplexation-driven complexes.⁴⁷ Here, we used this approach to construct thin

films by successive depositions of already formed H-bonded IPC *via* spin-coating.

PPFS-MPA-32% and P4VP were separately dissolved in a mixed solvent: CHCl_3/MEK , at a concentration of 2 g/L. As previously described, the mixing of the two polymers conducts to a turbid solution; this reflects the presence of large aggregates as a consequence of the IPC formation. This turbid solution was successively spin-coated up to 50 times onto priory activated silicon wafer with rinsing by CHCl_3/MEK between each deposition. To make sure that IPC were successfully deposited onto silicon wafer (50 deposition steps), XPS was used to analyze the surface chemical composition (Figure 3-12).

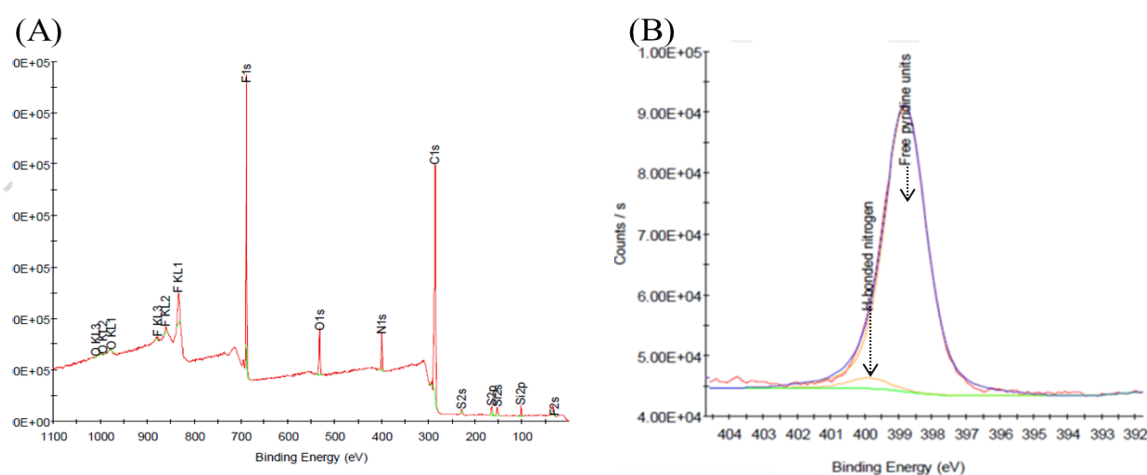


Figure 3-12 XPS survey spectrum (A) and N1s spectrum after 50 deposition steps of (PPFS-MPA-32%/P4VP) by spin-coating onto a silicon wafer.

In Figure 3-12-A, in addition to Si, other elements including C, O, N, F and S can be observed, indicating that polymer matter has been successfully deposited onto the substrate. The presence of the sulfur atom argues for the formation of -C-S- bonding, resulting from the nucleophilic substitution of the fluorine atom of PFS by the carboxylic acid containing thiol modifier. Moreover, in Figure 3-12-B, the presence of free pyridine units at 398.8 eV and also of H-bonded pyridine rings at 399.8 eV indicate the successful deposition of the H-bonds driven complexes. FT-IR technique in ATR mode was concomitantly used to analyze the surface chemical composition after 50 deposition steps. However, the signal intensities are quite weak (Figure AI 3-2-A). By performing a zoom in the region between 940 -1040 cm^{-1} , one

can observe an absorption band at 993 cm^{-1} of free pyridine and the other at 1014 cm^{-1} corresponding to H-bonded pyridine rings (Figure AI 3-2-B).

By taking benefit from the XPS analysis, it was found that the IPC of PPFS-MPA-32%/P4VP were well spin-coated after 50 steps (with a rinsing step between each deposition cycle) and we were interested in studying the growth mechanism of the deposited IPC during the whole process. Ultraviolet (UV) spectroscopy in transmission mode is a convenient method for monitoring the assembling process of polymer films onto a transparent substrate.^{31,48,49} Hence, the UV feature absorbance of the individual P4VP and PPFS-MPA in CHCl_3 solution at a concentration of 0.5 g/L was firstly investigated (Figure 3-13).

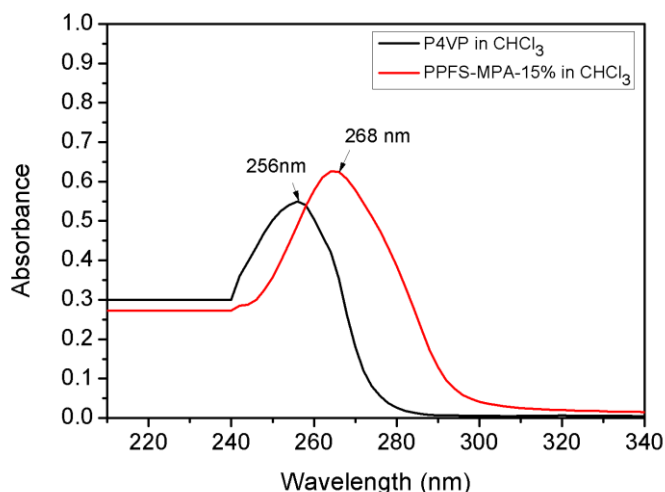


Figure 3-13 UV absorbance spectra of individual P4VP and PPFS-MPA-15% in CHCl_3 .

Two large absorbance peaks at around 256 nm and 268 nm are observed and can be assigned to $\pi\text{-}\pi^*$ transition of pyridine ring of P4VP and the benzene ring of PPFS-MPA, respectively.⁴⁸ These two absorbance signals allow for determining the deposited IPC when using “2 in 1” approach. Figure 3-14 presents the UV spectra of $(\text{PPFS-MPA-32\%/P4VP})_N$ onto a glass slide for different number of deposition steps ($N = 5, 10, 20, 30, 50$).

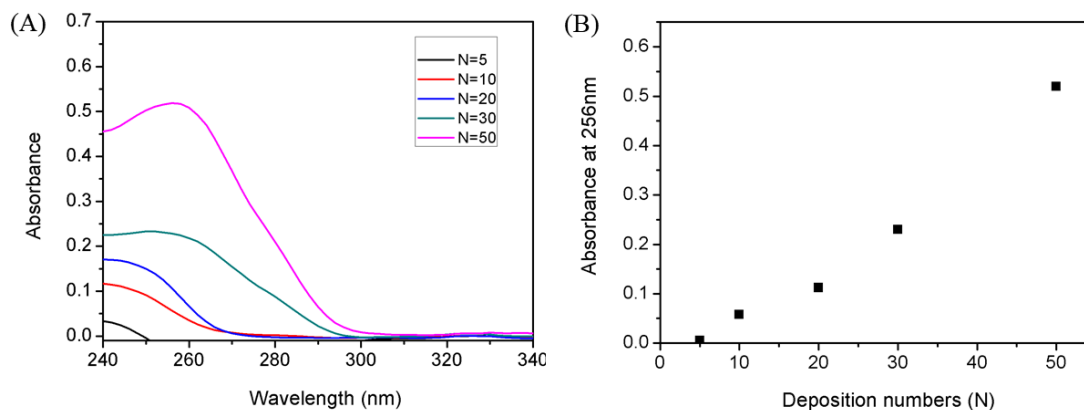


Figure 3-14 (A) UV spectra of (PPFS-MPA-32%/P4VP)_N after the deposition of the IPC formed in CHCl₃/MEK onto a glass slide; (B) Evolution of the absorbance at 256 nm as a function of the number of deposition (N).

The gradual increase in UV absorbance with the number of deposition steps indicates that the PPFS-MPA-32%/P4VP complexes were successfully deposited onto the substrates (Figure 3-14-A). After 5 depositions, the amount of IPC is certainly too low to be detected. The absorbance at 256 nm (Figure 3-14-A) and 268 nm (Figure AI 3-3) were plotted *versus* the number of deposition steps; they demonstrate an increase of the deposited amount all along the process, in spite of the washing step with CHCl₃/MEK after each deposition. Thus, it appears that PPFS-MPA-32%/P4VP complexes prefer to be located at the interface of the substrate, rather than to remain in solutions. Moreover, it is reasonable to think that not all –COOH groups are engaged in the H-bonded complexes. Thus, at each deposition step (N), one part of free –COOH can interact with a mixture deposited in the previous step (N-1) and also at the next one (N+1).

The growth of the film can be monitored by the measurement of the thickness by AFM (by performing a delicate scratch, see experimental part for the used procedure). Figure 3-15 shows the evolution of the thickness (determined by AFM), as a function of the number of the (PPFS-MPA-32%/P4VP) deposition steps (N).

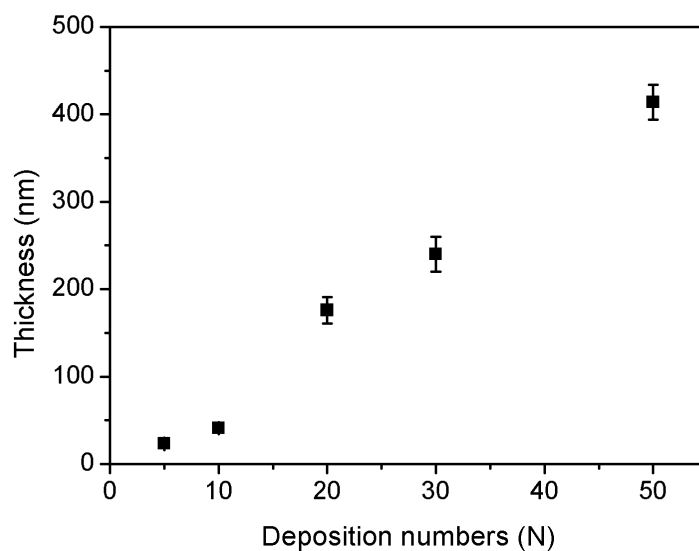


Figure 3-15 Evolution of the overall thickness of the film as a function of the number of deposition steps (N) of (PPFS-MPA-32%/P4VP).

The thickness steadily increases with the number of deposition steps, revealing a rise of the amount of IPC all along the deposition cycles. The thickness is around 20 nm after 5 deposition steps and increases up to around 420 nm after 50 steps.

The surface topology of spin-coated (PPFS-MPA-32%/P4VP)_N IPC onto the silicon wafer was characterized by AFM in tapping mode. Figure 3-16 gives the AFM images of (PPFS-MPA-32%/P4VP)_N after N= 5 and 50 depositions, respectively.

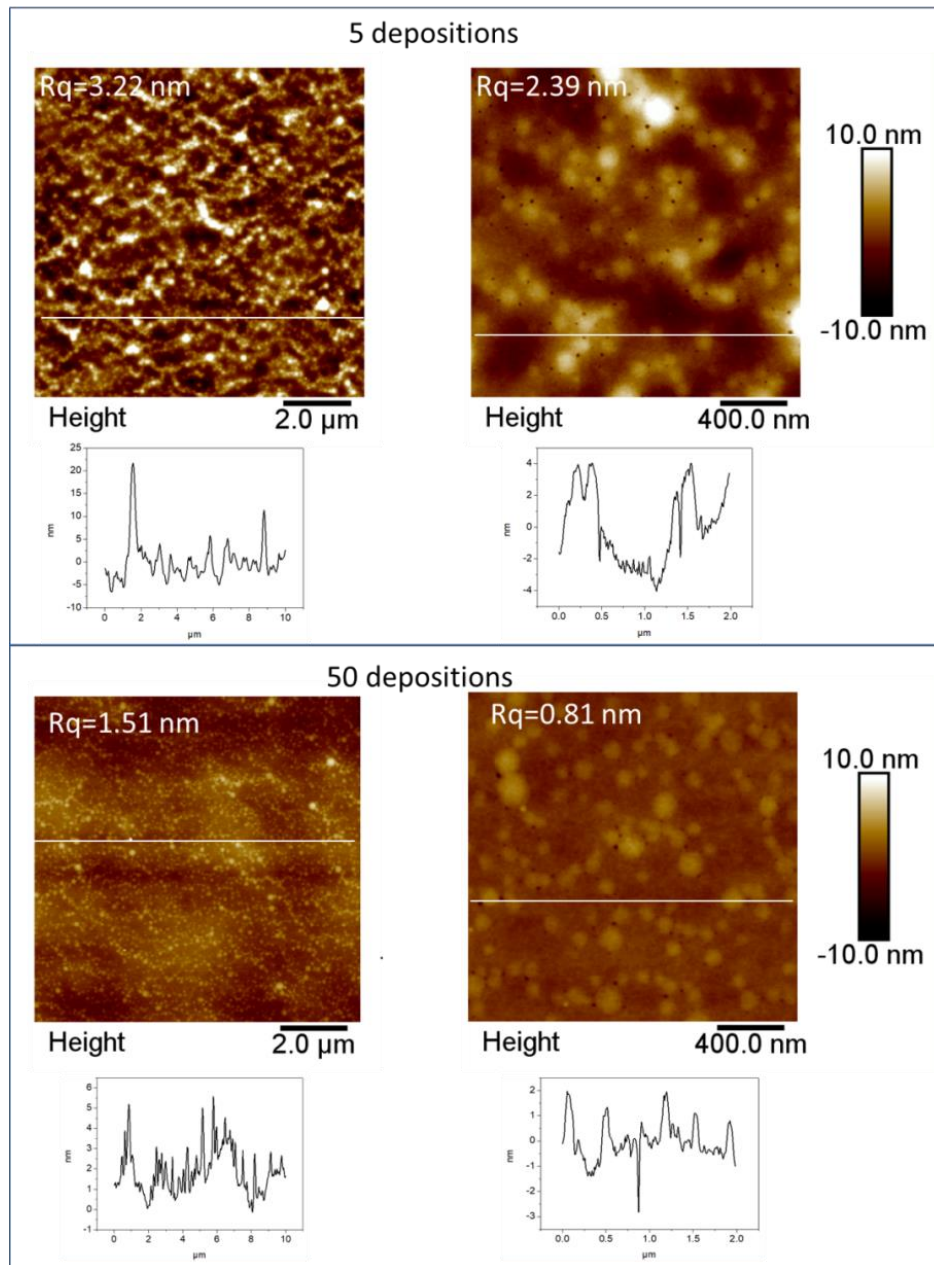


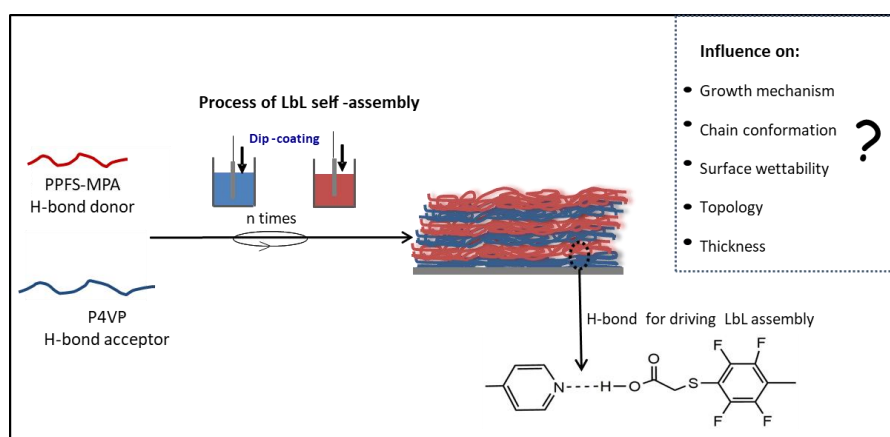
Figure 3-16 AFM topographic images with the corresponding height profiles of $(\text{PPFS-MPA-32\%/P4VP})_N$ ($N = 5$, up; $N = 50$, down) deposited by spin-coating onto a silicon wafer.

After 5 depositions, AFM imaging exhibits the presence of granular structures at the surface with a roughness (R_q) around 3.22 nm, at the scale $10 \mu\text{m} \times 10 \mu\text{m}$. At higher magnification ($2 \mu\text{m} \times 2 \mu\text{m}$), polydisperse nodules irregularly distributed on the surface are observed. It seems that the covering of the substrate by polymer matter is not totally uniform. However, if we compare the roughness value (3.22 nm) with the thickness value around 25 nm (Figure 3-15), we can assume that the deposition

leads to a polymer film. After the increase of the number deposition steps up to 50, AFM images reveal a well-covering, smooth and more homogenous film with a lower roughness (around 1.51 nm) at the scale of $10\ \mu\text{m} \times 10\ \mu\text{m}$. Thus, the successive deposition of a solution containing preformed H-bonded interpolymer complexes provides an alternative way in the fabrication of thin polymer films.

3.5.2 Construction of (P4VP/PPFS-MPA) $_n$ multilayer films through the LbL self-assembly approach

As explained in the bibliographic part (Chapter 1.3), the LbL self-assembly is a robust approach for surface functionalization, allowing for preparing thin polymer films with tailored features. Researchers have explored factors impacting the film growth mechanism and thus the structure and the properties of the resulting multilayer films. However, the growth mechanism and the internal structure of many films are far from being clear.^{18,50} With the aim of expanding the scope of LbL, we decided to use carboxylic acid-derived PPFS them as H-bond donors to prepare multilayer films with P4VP, as H-bond acceptor. The general strategy on which our work relies, is shown in Scheme 3-3.



Scheme 3-3 Schematic representation of (P4VP/PPFS-MPA) $_n$ multilayer films through LbL self-assembly approach.

H-bond PPFS-MPA donor copolymers differing in their DS (7%, 15% and 32%)

were designed, as described in Chapter 3.3. The LbL process was performed by the alternate immersion of the substrate (silicon wafer or glass slide) into the deposition solution. The construction of multilayer films is suspected to be driven by H-bonds between PPFS-MPA and P4VP. After showing the feasibility to use PPFS-MPA and P4VP to construct multilayer films through the LbL approach, we investigated the influence of different parameters on the film elaboration, such as the nature of the solvent, the extent of PPFS modification (quantified by DS), and the polymer concentration. In particular, the study of the growth mechanism by spectroscopic analysis and by thickness monitoring as well as the surface features elucidated by wettability measurements and AFM imaging, are discussed.

3.5.2.1 Evidence of the film feasibility

In previous work (Chapter 3.4.2), we have identified that EtOH favors the complexation ability between P4VP and PPFS-MPA-32% through H-bonds. IPC were formed and turbid solutions with precipitates were observed. Thus, we took benefit from these chemical affinities to elaborate novel H-bonded films by using EtOH as deposition solvent. Besides, in order to facilitate the formation of H-bonds, we firstly use the PPFS-MPA derivative with the highest DS (DS = 32 %).

Before analyzing the growth mechanism by UV spectroscopy, the UV absorbance spectrum of individual P4VP and PPFS-MPA-32% in EtOH was collected (Figure 3-17).

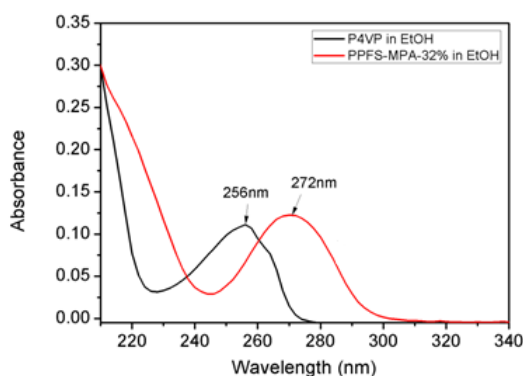


Figure 3-17 UV absorbance spectrum of P4VP and PPFS-MPA-32% in EtOH.

Figure 3-17 shows the UV transmission spectra of P4VP and PPFS-MPA-32% in EtOH at a concentration of 0.5 g/L. One can observe that both P4VP and PPFS-MPA-32% absorb at 256 nm, while solely PPFS-MPA-32% has a feature absorbance at 272 nm, which can consequently be used as a reference to follow the amount of deposited PPFS derivative after each deposition step.

The construction process consists in alternatively dipping a preactivated glass slide into a solution of P4VP and PPFS-MPA-32% in EtOH at a concentration of 2 g/L. A washing step was applied after each deposited layer. 30 monolayers, corresponding to 15 bilayers (BL) were deposited. During the LbL process, the deposition solution (P4VP and PPFS-MPA) remained clear and transparent and no cracks at the film surface were observed. UV analysis was performed after each deposition step and the corresponding UV spectra are shown in Figure 3-18.

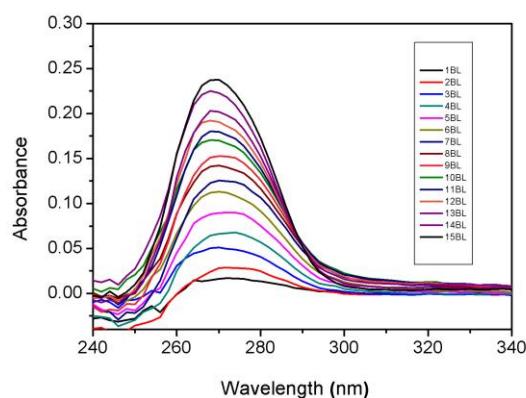


Figure 3-18 UV spectra of (P4VP/PPFS-MPA)_n (EtOH, DS = 32%, c = 2 g/L) deposited onto a glass slide.

The gradual increase of the characteristic absorbance of (P4VP/PPFS-MPA)_n with the number of deposited bilayers indicates that the successive dipping in EtOH solutions allows for the efficient deposition of polymers onto the substrate.

FT-IR spectroscopy in ATR mode was also employed in order to evidence the presence of polymers on the surface and to investigate the driving force for the film construction. However, in this case, no IR signals can be detected after 15 bilayers, much probably because of the very low amount of deposited polymer matter. XPS is more sensitive compared to ATR FT-IR and consequently was used to probe the

deposited (P4VP/PPFS-MPA-32%) with $n = 15$ BL (Figure 3-19).

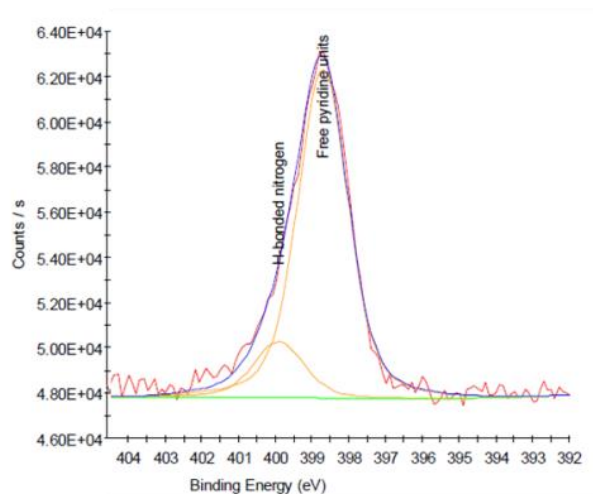


Figure 3-19 XPS N1s core-level spectrum of (P4VP/PPFS-MPA) $_n$ (EtOH, DS = 32%, $c = 2$ g/L) with $n = 15$ BL deposited onto a silicon wafer.

The XPS elemental analysis of the materials on the top surface (< 10 nm) shows the presence of C, O, N, S and F atoms at the film surface (Figure AI 3-4), arising from the successful deposition of P4VP and PPFS-MPA-32% onto the wafer substrate. Moreover, two N (1s) peaks at approximately 398.8 and 399.8 eV ascribed to free and H-bonded pyridine units, respectively, confirming that H-bonds are the driving forces for the LbL deposition (Figure 3-19). These results unambiguously prove the possibility to utilize PPFS-MPA and P4VP to construct multilayer thin films.

3.5.2.2 Influence of the nature of the deposition solvent

The solvent of the deposition solution plays an important role in the construction of thin films through LbL self-assembly. H-bonds driven multilayer films have been reported to be prepared in water, alcoholic solvents, dioxane, THF, DMF or mixed solvent.^{31,37,48,49,51} However, these solvents were used for different polymer partners,^{31,37,48} or used for the preparation of porous surface by post-treatment.^{49,51} Rare work described the influence of the solvent on the LbL assembly for one given system, especially for water-insoluble carboxylic acid containing polymers. Here, we studied the influence of the solvent, including EtOH (entry 1), DMF (entry 2), CHCl₃/MEK

(v/v = 1/1) mixture (entry 3) and CHCl₃ for P4VP combined to MEK for PPFS-MPA (entry 4), on the growth of (P4VP/PPFS-MPA-32%) multilayer films (Table 3-2).

Table 3-2 LbL self-assembly of (P4VP/PPFS-MPA) (DS = 32%) by using different deposition solvents

Polymer	Entry	Deposition Solvent	Resulting Solution*	Formation of film	Characterization method
P4VP/PPFS-MPA with DS = 32%	1	EtOH	Transparent	Yes	UV, XPS, AFM, WCA
	2	DMF	Transparent	No	UV
	3	CHCl ₃ /MEK	Turbid solution appear at 10 BL	Yes	ATR FT-IR, XPS, AFM, WCA
	4	CHCl ₃ for P4VP MEK for PPFS-MPA	Transparent	Yes	UV, ATR FT-IR, XPS, AFM, WCA
*The resulting solution refers to the macroscopic changes of P4VP solution					

The self-assembly process can be monitored by UV spectroscopy (when glass slide is used as substrate) or FT-IR spectroscopy in ATR mode (when silicon wafer is used as substrate). The formation of H-bonds was emphasized by XPS and the surface features were characterized by AFM or/and wettability measurements. The analysis was stopped after either the appearance of a turbid solution or the appearance of cracks at the surface.

3.5.2.2.1 General characterization of the depositions

1) By using DMF

The deposition of (P4VP/PPFS-MPA-32%) multilayer film by using DMF as solvent (Table 3-2, entry 2) was performed onto a glass slide. UV spectroscopy was used and Figure 3-20 depicts the corresponding UV spectra collected from 1 to 15 BL.

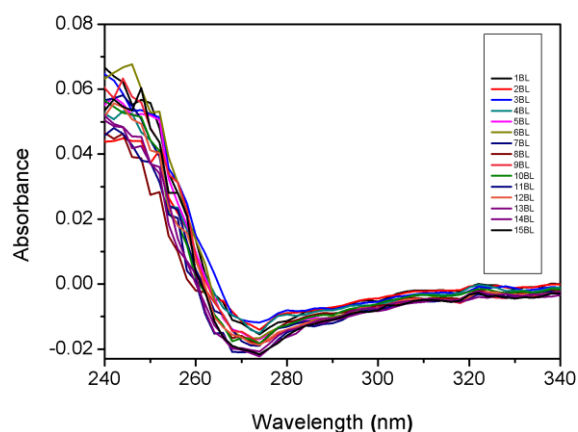


Figure 3-20 UV spectra of (P4VP/PPFS-MPA)*n* (DMF, DS = 32%, *c* = 2 g/L) deposited onto a glass slide.

The UV study shows that no film is formed onto the substrate when DMF is used as solvent (Figure 3-20). This result confirms the fact that DMF is detrimental for the formation of H-bonded IPC between P4VP and PPFS-MPA. As revealed by the high intrinsic viscosity value, interactions between each polymer and DMF are predominant, which prevent from the formation of the expected H-bonds between P4VP and PPFS-MPA-32%. As previously mentioned, DMF can act as a competitive H-bond acceptor able to interact with the carboxyl groups of PPFS-MPA-32%. Consequently, polymers prefer to remain in solution and no film is deposited. The same conclusion was reported for the combination of PVPON with PAA, deposited from DMF as solvent.³⁰ Moreover, we can ascertain that a miscible blend obtained in solution between two polymers does not allow for the construction of a film by LbL self-assembly. This link between the behavior in solution and the ability to obtain a film through LbL was already evidenced with hydroxylated-PPFS derivatives.¹³

2) By using a mixed solvent: CHCl₃/MEK

The deposition of (P4VP/PPFS-MPA)*n* (DS = 32%) multilayer films by using a mixed solvent CHCl₃/MEK (Table 3-2, entry 3) was carried out onto a silicon wafer. During the deposition cycles, the P4VP solution in CHCl₃/MEK in which the substrate is dipped remains transparent up to the deposition of 7 BL (Figure AI 3-5-a).

In the meantime, macroscopic cracks at the film surface are observed (Figure AI 3-5-c). By increasing the deposition to 10 BL, the P4VP solution becomes turbid (Figure AI 3-5-b), indicating that some matter initially present at the surface of the substrate, is transferred into the solution during the immersion step. Thus, from the deposition of 7 BL, the LbL deposition by using the mixed CHCl_3/MEK solvent does not permit to construct a stable self-assembled film. Consequently, only the deposition up to 7 BL is characterized.

FT-IR spectroscopy in ATR mode was used to monitor the assembly process and the corresponding FT-IR spectra of (P4VP/PPFS-MPA-32%) from $n = 1$ to 7 BL are shown in Figure 3-21.

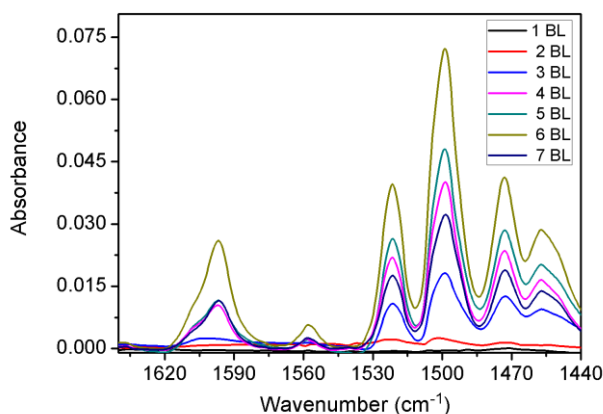


Figure 3-21 ATR FT-IR spectra of (P4VP/PPFS-MPA) $_n$ (CHCl_3/MEK , DS = 32%, $c = 2$ g/L) onto a silicon wafer.

The bands at 1597 cm^{-1} and 1522 cm^{-1} are assigned to P4VP ring vibration and to the C-F bond of aromatic ring of PPFS-MPA-32%, respectively. This evidences the presence of P4VP and PPFS-MPA-32% onto the surface of substrate. The IR intensity increases with the number of deposition steps, which means that more and more polymer is deposited all along the process ($n = 1 - 7$ BL).

3) By using CHCl_3 for P4VP combined to MEK for PPFS-MPA-32%

In order to avoid the desorption of polymers from the surface, we attempted to

use CHCl_3 for P4VP, combined to MEK for PPFS-MPA-32% (Table 3-2, entry 4). Indeed, contrary to the mixed solvent of CHCl_3/MEK , pure CHCl_3 is not a good solvent for PPFS-MPA-32%. Thus, we can expect that in these conditions, the desorption of PPFS-MPA should be limited or avoided. Interestingly, in this case, the P4VP containing solution remains clear during the whole deposition process, from 1 to 15 BL (entry 4). However, cracks (Figure AI 3-6) are observed after 8 deposition steps. UV and ATR FT-IR spectroscopy was exploited to analyze the depositions from $n = 1$ to 7 BL (Figure 3-22).

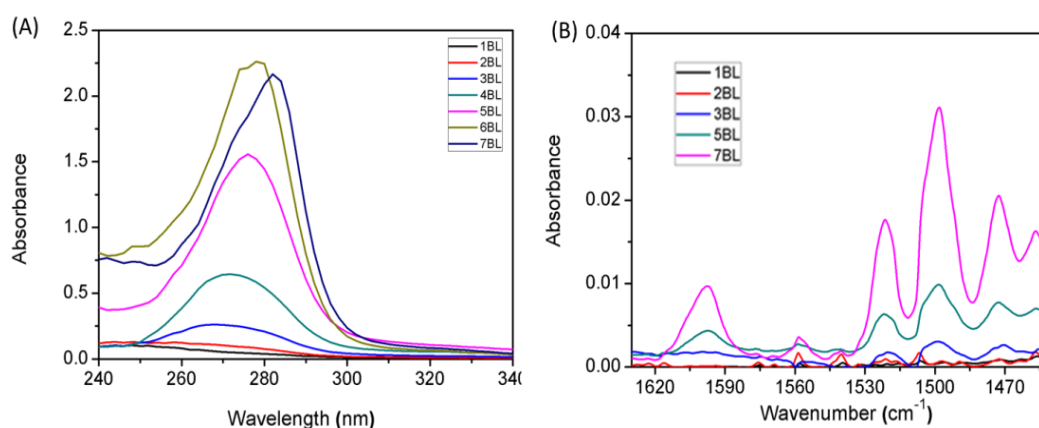


Figure 3-22 UV (A) and ATR FT-IR (B) spectra of $(\text{P4VP}/\text{PPFS-MPA})_n$ (CHCl_3 for P4VP and MEK for PPFS-MPA, DS = 32%, $c = 2$ g/L) onto a glass slide (A) and onto a silicon wafer (B).

Figure 3-22-A displays the UV absorbance spectra of the self-assembled film with from $n = 1$ to 7 BL. The increase of UV as well as IR absorbance (Figure 3-22-B) with the number of deposition steps underpins the successful deposition of polymers along the LbL process. The driving force for the construction of $(\text{P4VP}/\text{PPFS-MPA})_n$ multilayer films after 7 deposited bilayers was identified by XPS and ATR FT-IR spectroscopy (Figure 3-23).

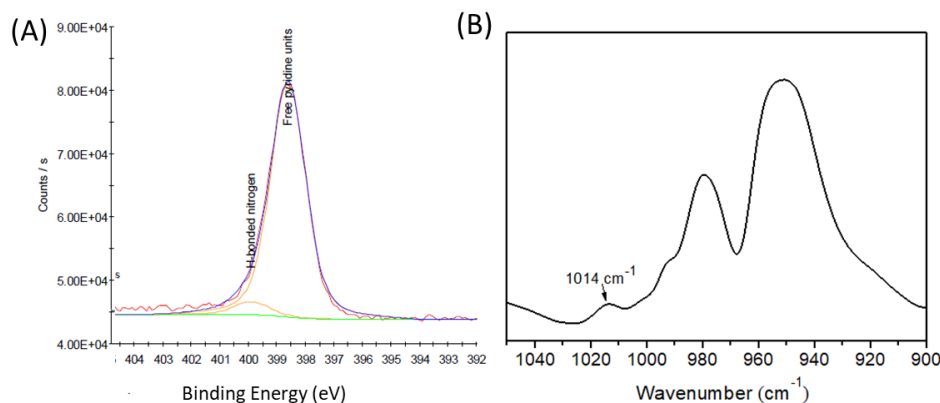


Figure 3-23 XPS N1s spectrum (A) and ATR FT-IR spectrum of (P4VP/PPFS-MPA)_n (CHCl₃ for P4VP and MEK for PPFS-MPA, DS = 32%, c = 2 g/L) (n = 7 BL).

In Figure 3-23-A, the peak at 399.8 eV corresponding to H-bonded nitrogen atoms proves the formation of H-bonds after the successive dipping steps. Figure 3-23-B shows a zoom on the range of 900-1040 cm⁻¹ of the IR spectrum and a novel peak appears at around 1014 cm⁻¹, which also confirms the presence of H-bonds within the multilayer film.

3.5.2.2.2 Study of the growth mechanism

1) By using EtOH

The evolution of the UV absorbance intensity ($\lambda = 272$ nm) and the evolution of the thickness (measured by AFM) as a function of the number of deposited bilayers *n* are shown in Figure 3-24.

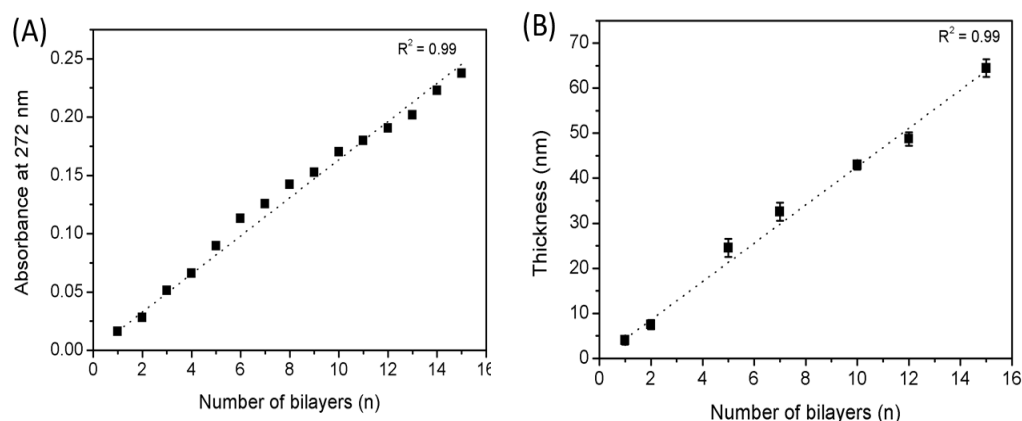


Figure 3-24 Evolution of UV absorbance at 272 nm and thickness of (P4VP/PPFS-MPA) $_n$ (EtOH, DS = 32%, $c = 2$ g/L) as a function of the number of deposited bilayers (up to 15 BL).

It can be seen that both the absorbance at 272 nm (Figure 3-24-A) and the thickness (Figure 3-24-B) follow a quasi linear increase with the number of deposition bilayers. This linear growth mechanism indicates that a constant increment of polymers is deposited at each deposition cycle. The total thickness is around 65 nm after 15 BL with an increment per assembling cycle around 4.3 nm. This relatively thin polymer films probably results from the quite compact conformation adopted by the polymer chains of PPFS-MPA-32% and P4VP in EtOH, as reflected by the low intrinsic viscosity. Thus, we can think that at each dipping cycle, few groups (-COOH or pyridine rings) deposited at a cycle n , efficiently interact with the layer deposited at $(n+1)$ deposition step, which can explain that the amount of polymer deposited at each cycle is relatively weak. Moreover, the fluorinated backbone of the PPFS derivatives is not well solvated by polar EtOH, since during the immersion step, it is reasonable to assume that the diffusion of PPFS-MPA within the film is limited, which also contributes to lower thickness. It is also for this reason, that no desorption of the PPFS-MPA from the deposited film is observed along the assembly process (contrary to the use of mixed CHCl_3/MEK , which is a better solvent for the carboxylated PPFS-derivatives).

2) By using CHCl₃/MEK

The FT-IR absorbance intensity recorded at 1597 cm⁻¹, assigned to the pyridine ring of P4VP, as well as the evolution of thickness (measured by AFM) were monitored as a function of the number of deposited bilayers (Figure 3-25). The evolution was followed up to 7 bilayers, since matter desorption occurs during the LbL process for higher n.

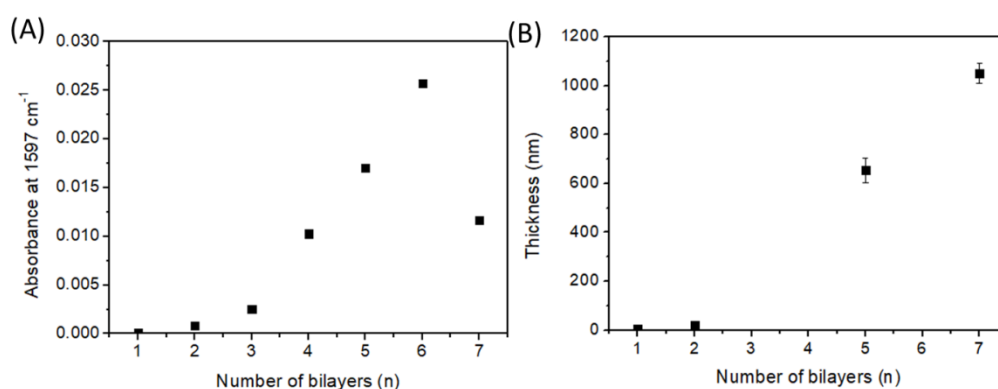


Figure 3-25 Evolution of the FT-IR absorbance at 1597 cm⁻¹ (A) and the thickness (B) of (P4VP/PPFS-MPA)_n (CHCl₃/MEK, DS = 32%, c = 2 g/L) as a function of the number of deposited bilayers (n) (up to 7 BL).

In Figure 3-25-A, the IR intensity of 1597 cm⁻¹ is quite weak for the first two bilayers, due to the very small amount of deposited polymers, as shown by the low measured thickness (Figure 3-25-B). Then, the IR response is enhanced with the increase of the deposition cycles, indicating that much polymer matter is deposited, which is consistent with the boost of the thickness up to around 1050 nm for n = 7 BL. A decrease of the IR intensity for n = 7 BL is observed as a result of the partial polymer desorption. Moreover, the appearance of macroscopic cracking on the surface can hamper the IR analysis. Concomitantly, we followed the evolution of the absorbance at 1522 cm⁻¹ (assigned to the response of PPFS-MPA), and a similar behavior was obtained (Figure AI 3-7).

It is important to mention, that up to 7 BL, much thicker film is constructed when using CHCl₃/MEK, compared to EtOH. The used solvent CHCl₃/MEK favors

the availability and accessibility of interacting sites at each deposition cycle, which certainly promotes the formation of H-bonds between the partner A deposited onto the surface and the partner B present in the dipping solution. However, the conformation of the polymer chain is different in the mixed solvent (more expanded), which also contributes to increase the thickness. Unfortunately, the film construction through LbL approach by using this mixed solvent seems to be jeopardized since a polymer desorption occurs after 7 BL. However, we can note that even it is impossible to deposit a large number of bilayers, the thickness is already particularly high for only 7 deposited bilayers.

3) By using CHCl₃ for P4VP and MEK for PPFS-MPA-32%

The UV feature absorbances of P4VP and PPFS-MPA derivative are overlapped (Figure 3-13), which did not permit to separately follow the deposition of P4VP or PPFS-MPA. Hence, we considered the absorbance at 286 nm, which can be attributed to only PPFS-MPA, to monitor the LbL self-assembled film on the glass slide. The film buildup process onto the silicon wafer was also monitored by the FT-IR absorbance at 1597 cm⁻¹. The thickness of the resulted film was measured by AFM (Figure 3-26).

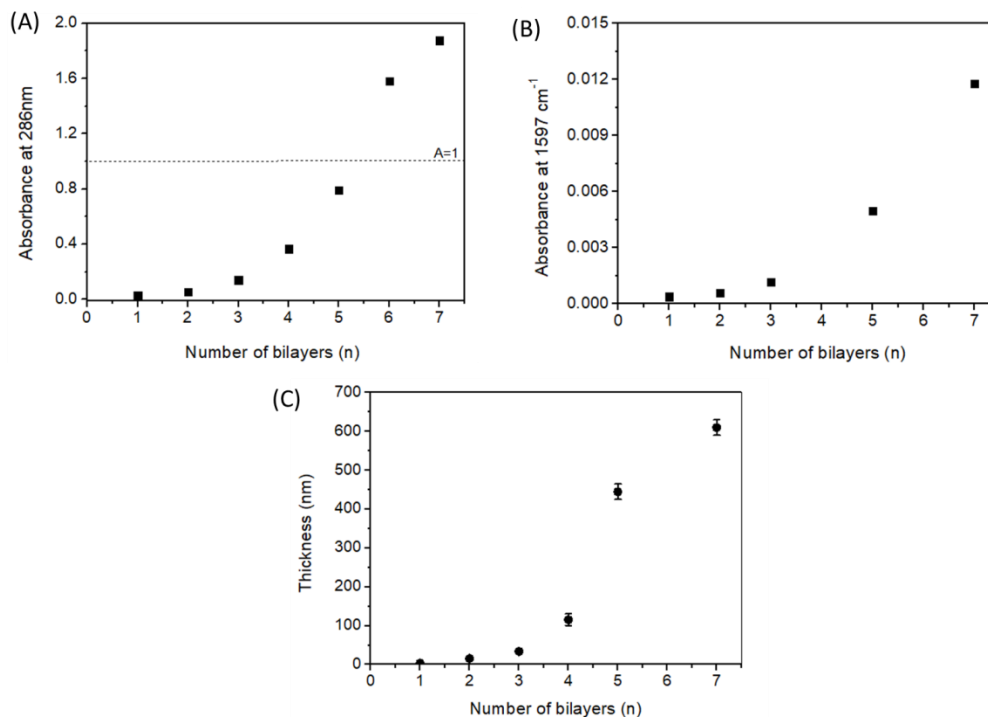


Figure 3-26 Evolution of UV absorbance at 286 nm (A), ATR FT-IR absorbance at 1597 cm^{-1} (B) and thickness (C) of (P4VP/PPFS-MPA) $_n$ (CHCl_3 for P4VP and MEK for PPFS-MPA, DS = 32%, $c = 2 \text{ g/L}$) as a function of the number of deposited bilayers (n).

Firstly, we can observe that the three evolutions, analyzed by different experimental techniques, are in agreement and follow the same profile, namely a slow increase up to 3 bilayers, a pronounced and sharp increase of the analyzed characteristic. This trend resembles the one obtained with using the mixed solvent: CHCl_3/MEK . As shown in Figure 3-26-A, the UV absorbance at 286 nm slightly increases from 1 to 3 BL, corresponding also to a very weak IR signal at 1597 cm^{-1} (Figure 3-26-B) (viewable also for IR at 1522 cm^{-1} , Figure AI 3-8). At the beginning of the deposition process, a small amount of polymer is deposited onto the substrate, resulting in a thickness around 35 nm for $n = 3$ BL (Figure 3-26-C). From the third bilayer, a steep increase of matter deposition leading to the formation of thicker films is observed. The thickness is somehow lower than the one measured from the use of the mixed solvent (CHCl_3/MEK). For instance, at a given number of deposited bilayers ($n = 5$ BL), the thickness is around 450 nm against 650 nm.

This thickness difference can be due to the chain conformation of each polymer, which is dependent on the nature of the solvent. A difference in the solvation ability

induces different modes of polymer adsorption and rearrangements. Indeed, as previously mentioned, P4VP is well soluble in CHCl_3 but insoluble in MEK, and on the contrary, PPFS-MPA-32% is well soluble in MEK but insoluble in CHCl_3 . We can suppose that the diffusion of PPFS-MPA-32% is quite limited during the immersion step in the solution of P4VP in CHCl_3 and similarly, the diffusion of P4VP is restricted in a MEK solution. This constrained diffusion can lead to an enhanced confinement, and certainly provides lower number of interacting sites available during the immersion steps (but still higher than for the use of EtOH).

3.5.2.2.3 Study of the surface features by AFM

The influence of the nature of the deposition solvent on the surface topology of (P4VP/PPFS-MPA) $_n$ multilayered film was investigated by AFM in tapping mode.

1) By using EtOH

Figure 3-27 shows the AFM height images of (P4VP/PPFS-MPA) $_n$ (DS = 32%, c = 2 g/L) obtained from EtOH with n = 1, 5, 7 and 15 BL deposited onto silicon wafer.

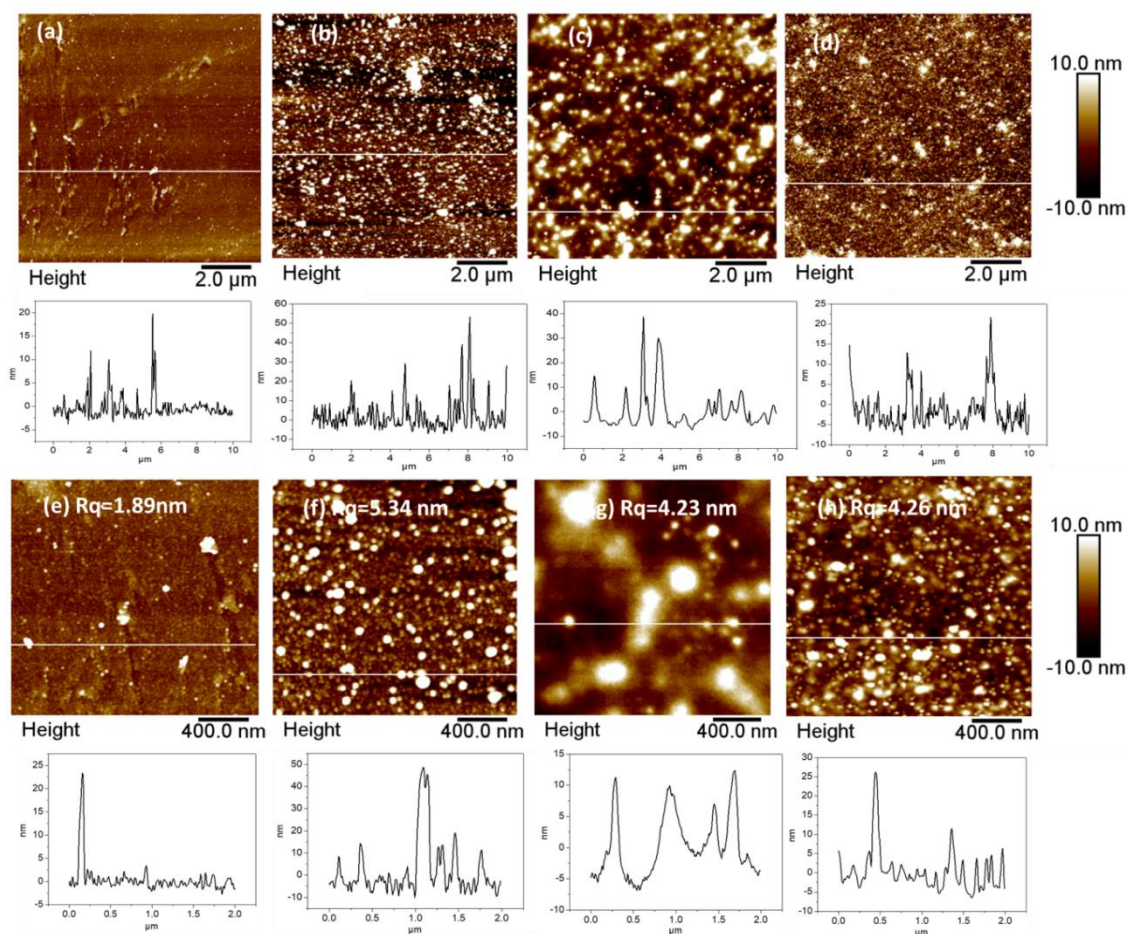


Figure 3-27 AFM topographic images with the corresponding height profiles of $(\text{P4VP/PPFS-MPA})_n$ (EtOH, DS = 32%, $c = 2$ g/L) with $n = 1$ (a, e), 5 (b, f), 7 (c, g), 15 (d, h) BL deposited onto the silicon wafer.

From the large scale image ($10 \mu\text{m} \times 10 \mu\text{m}$) (Figure 3-27-a, b, c and d), we can observe polymeric dots-protrusion or aggregates with a height of 5-50 nm that are irregularly distributed on the surface. The number of these aggregates rises with increasing the number of deposited bilayers from $n = 1$ to 15 BL. In the high magnification images corresponding to an area of $2 \mu\text{m} \times 2 \mu\text{m}$ (Figure 3-27-e, f, g and h), we observe that the size of the aggregates is enlarged when the number of deposited bilayers increases, due to the polymer accumulation on the substrate, leading to a roughness increase from 1.89 nm for $n = 1$ BL to 5.34 nm for $n = 5$ BL. This kind of morphology is consistent with the low amount of deposited P4VP and PPFS-MPA-32%, when solubilized in ethanol, as previously reflected by the thickness measurement and by the fact that we were not able to detect any signals by ATR

FT-IR. At this stage, we can anticipate that this uneven topography could affect the surface wettability.

2) By using CHCl_3/MEK

Figure 3-28 shows the AFM height images of $(\text{P4VP}/\text{PPFS-MPA})_n$ ($\text{DS} = 32\%$, $c = 2 \text{ g/L}$) obtained from the CHCl_3/MEK mixture, for $n = 1, 2$ and 5 BL deposited onto the silicon wafer.

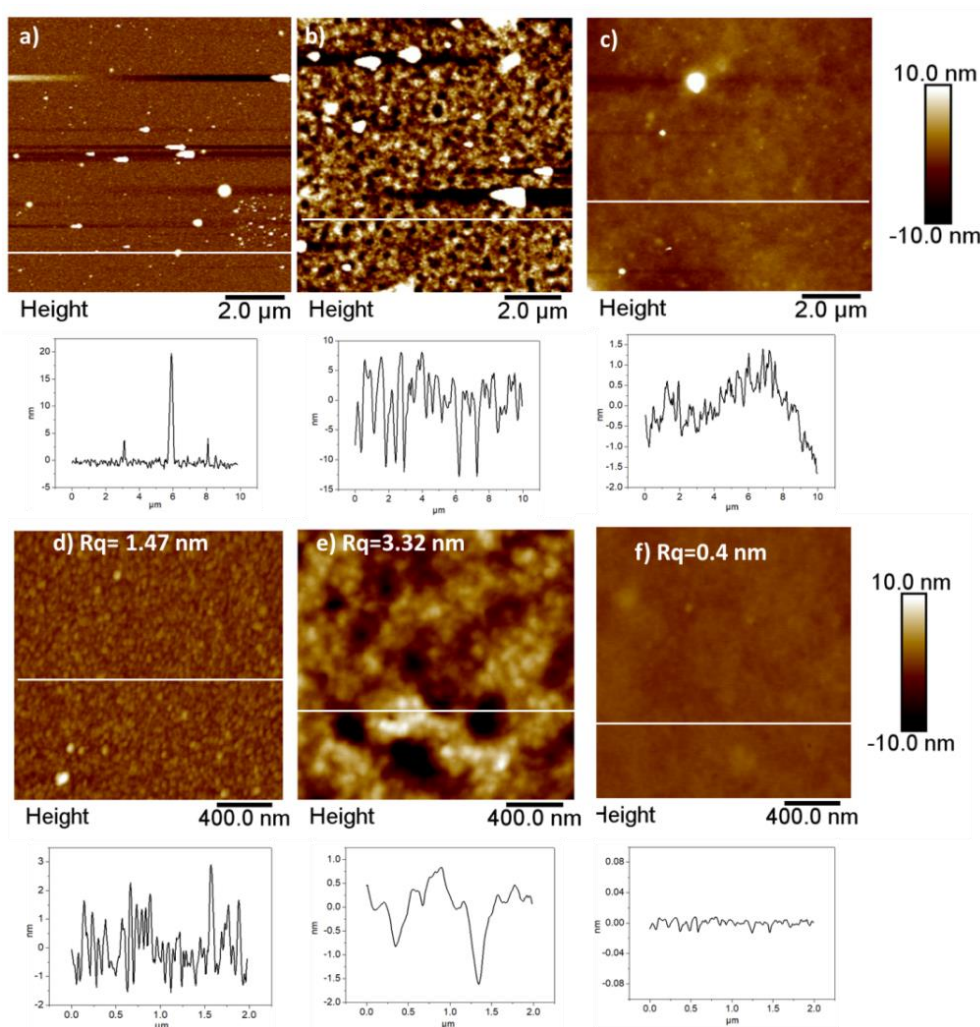


Figure 3-28 AFM topographic images with the corresponding height profiles of $(\text{P4VP}/\text{PPFS-MPA})_n$ (CHCl_3/MEK , $\text{DS} = 32\%$, $c = 2 \text{ g/L}$) with $n = 1$ (a); 2 (b) and 5 (c) BL deposited onto the silicon wafer.

The films, prepared from CHCl_3/MEK , displays totally different surface

morphologies, compared to the films constructed from EtOH, as revealed by AFM images ($10\ \mu\text{m} \times 10\ \mu\text{m}$) recorded for $n = 1$ (a), 2 (b) and 5 (c) deposited bilayers. After the first deposition cycles ($n = 1$ BL), one can observe from the high magnification image (Figure 3-28-d) polydisperse nodules or polymer aggregates with a small size around 5 nm. For $n = 2$ BL, the nodules become polydisperse and the surface is quiet rough ($R_q = 3.32$ nm). At this stage, as reflected by the previously presented measurements, the thickness is very low. For $n = 5$ BL, the film becomes smooth with a roughness of 0.4 nm, probably due to the increased amount of deposited polymers. No further AFM examination for $n = 7$ BL was performed, since macroscopic cracks are observed at the film surface.

3) By using CHCl_3 for P4VP and MEK for PPFS-MPA-32%

Figure 3-29 shows the AFM height images of $(\text{P4VP/PPFS-MPA})_n$ ($\text{DS} = 32\%$, $c = 2$ g/L) obtained from the use of CHCl_3 for P4VP and MEK for PPFS-MPA with $n = 1, 5$ and 7 BL deposited onto the silicon wafer.

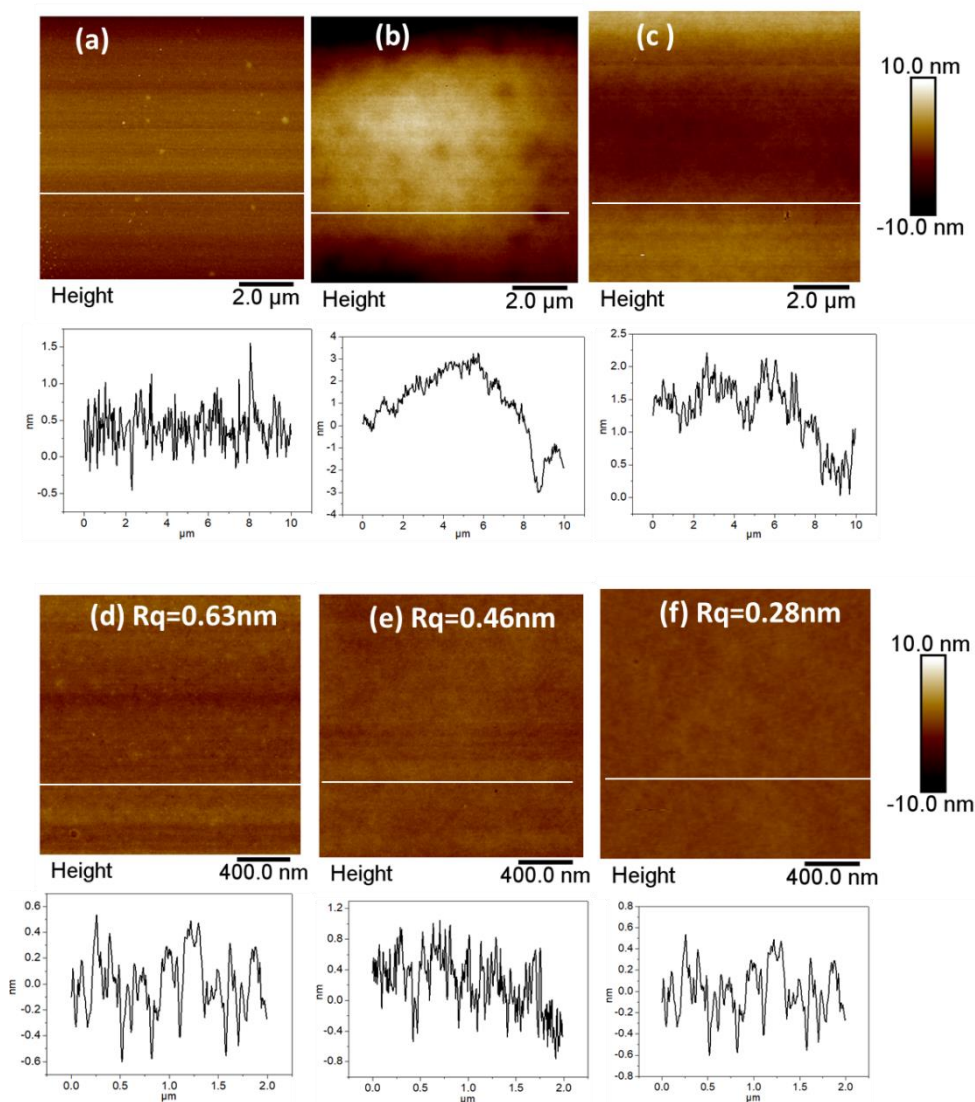


Figure 3-29 AFM topographic images with the corresponding height profiles of $(\text{P4VP/PPFS-MPA})_n$ (CHCl_3 for P4VP and MEK for PPFS-MPA, DS = 32%, $c = 2$ g/L) with $n = 1$ (a, d), 5 (b, e), 7 (c, f) BL deposited onto the silicon wafer.

All AFM images of the film constructed by using the CHCl_3 for P4VP and MEK for PPFS-MPA-32% evidence a homogeneous and particularly featureless surface morphology on a $10 \mu\text{m} \times 10 \mu\text{m}$ area (Figure 3-29-a, b and c), which is clearly different from the morphology, previously presented when other solvents were used. Moreover, the films are very smooth (Figure 3-29-d, e and f) with a R_q value lower than 0.5 nm after 7 bilayers.

3.5.2.2.4 Study of the surface features by wettability measurements

Surface wettability is quite sensitive to the chemical composition, surface roughness of the outermost layer in the range of 5-10 Å as well as the degree of interpenetration of the sequentially adsorbed polymers in LBL films.⁵² WCA and water contact angle hysteresis ($\Delta\theta$) measurements were collected after each deposited monolayer. The WCA and $\Delta\theta$ of pure P4VP and PPFS derivatives are indicated in the figure as reference. The evolution of WCA and $\Delta\theta$ of (P4VP/PPFS-MPA)_n (DS = 32%) by using different deposition solvents were compared to investigate the influence of the nature of the solvent on the internal organization (Figure 3-30).

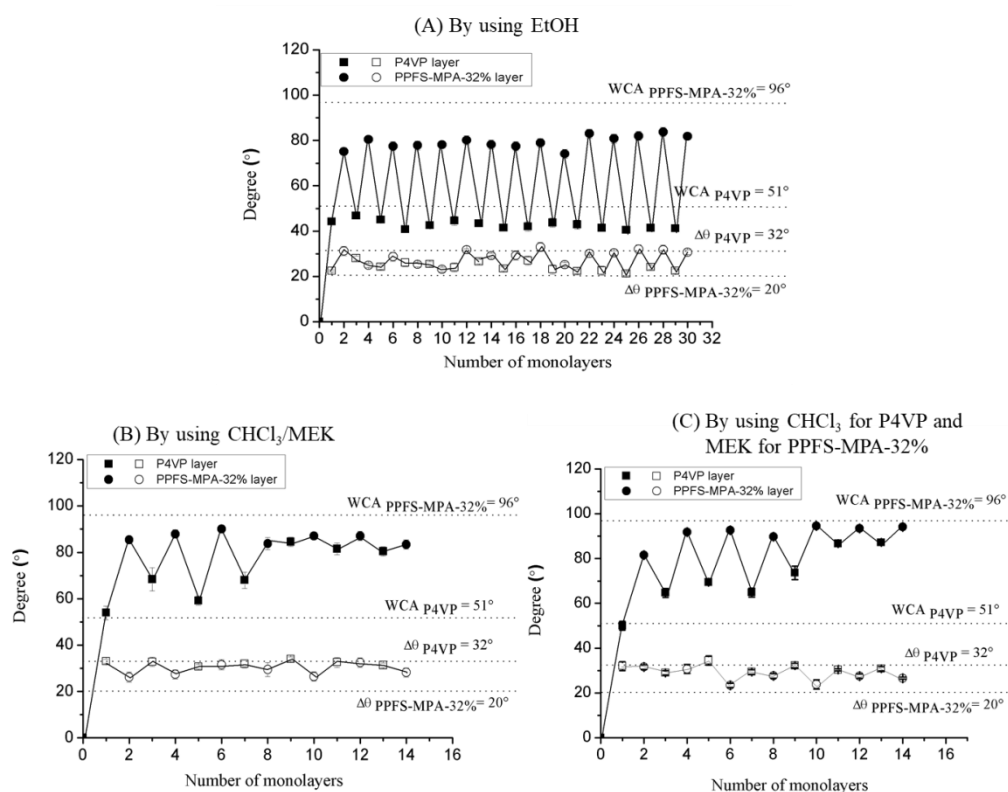


Figure 3-30 Evolution of WCA (filled symbol) and water hysteresis (open symbol) of (P4VP/PPFS-MPA)_n (DS = 32%, c = 2 g/L) by using different deposition solvents: EtOH (A), CHCl₃/MEK (B) and CHCl₃ for P4VP and MEK for PPFS-MPA (C), as a function of the number of deposited monolayers.

Firstly, we can observe that the WCA evolutions corresponding to the LbL

stepwise deposition by using the mixed solvent CHCl_3/MEK and the two separated solvents CHCl_3 and MEK present a quite similar behavior, which is clearly different from the one observed when EtOH was utilized.

More particularly, by using EtOH (Figure 3-30-A) as deposition solvent, the WCA increases up to 45° and 75° after the first deposition of P4VP and PPFS-MPA-32%, respectively. These values (lower than the one of pure P4VP and the one of PPFS-MPA-32%) reflects probably the impact of the substrate, all the more that the amount of deposited polymer is low.¹⁵ Note that from the first deposited monolayer, a WCA that differs from the one of the substrate is observed, while no IR signal was observed. Thus, we can ascertain that the lack of IR detection is solely due to a too limited amount of deposited polymer. From the deposition of the two first layers, we observe a clear periodic oscillation when the outermost layer is alternatively varied, with a WCA after the P4VP deposition of around 45° , and around 80° after the PPFS-MPA-32% deposition. The obtained multilayer films are quite hydrophilic and this can be the consequence of the peculiar surface topology, as previously underpinned by AFM imaging. Indeed, plenty of aggregates were observed on the surface (Figure 3-27), which leads to a rough surface which can play on the wettability features. Moreover, as afore explained, EtOH much certainly restricts the diffusion of polymer chains inside the films during the immersion steps, which contributes to yield very well stratified layers, almost compartmentalized and composed of individual interacting partner layer (as emphasized by the WCA evolution). This fact suggests that sequentially adsorbed layers can be used to systematically alter and control the wettability of substrate surface by simply changing the nature of the polymer adsorbed as the outermost layer.

By using CHCl_3/MEK (Figure 3-30-B), the WCA evolution is totally different. The WCA is 51° after the first deposition layer, indicating a complete coverage of the substrate by P4VP. Then, up to 7 monolayers, we can observe an alternation in WCA, the value of which is dictated by the nature of the last deposited polymer. As it was the case for the use of ethanol, this WCA variation reflects that favorable interactions

are developed at the interface between the polymer that is deposited and its partner that is already present on the substrate. However, the measured WCA do not correspond to the one of the corresponding pure polymer (higher than P4VP and lower than the one of PPFS-MPA). This means that the two polymers are detected at the surface. This can arise from *i*) a diffusion of polymers within the film during the dipping steps and/or *ii*) a not complete covering of the monolayer on the substrate by the further deposited partner. However, up to 7 monolayers, the thickness is small, which can be expected to limit the polymer diffusion and promote the polymer confinement within the film. After 7 monolayers, the oscillatory trend disappears and the WCA tends to a constant value (83°), whatever the deposited polymer. This suggests that at this stage, the diffusion might be much favored and the separated layers form rather disordered layers composed of interdigitated P4VP and PPFS-MPA-32% segments.

By using CHCl_3 for P4VP and MEK for PPFS-MPA-32% (Figure 3-30-C), as formerly precised, the pattern of WCA evolution follows a relatively similar trend. We observe an alternate variation of WCA up to 11 monolayers with a noticeable difference in WCA after each deposited monolayer, followed by a variation, in which the amplitude is much lower. This change of deposition regime is due to different modes of polymer adsorption during the LbL assembly. At the beginning of the process, quite stratified layers are formed, which then become rather disordered mixed polymer layers.

3.5.2.3 Influence of DS of PPFS-MPA by using CHCl_3 for P4VP and MEK for PPFS-MPA

It has been demonstrated that the control of the number of interacting sites of polymer involved in multilayered films is an important issue.^{15,53} For example, Li *et al.*⁵³ studied the LBL assembly of poly(2-ethyl-2-oxazoline) (PEtOx)/PAA and they varied the amount of H-bond acceptor moieties by adjusting the hydrolysis degree of PEtOx. Herein, we are interested in the effect of the amount of H-bond donors by

varying the extent of the modification of PPFS-MPA (various targeted DS), on the properties of the resulting LbL films (Table 3-3).

Table 3-3 LbL self-assembly of P4VP with PPFS-MPA (DS = 7%, 15% or 32%) in a given solvent (CHCl₃ for P4VP and MEK for PPFS-MPA).

Entry	Deposition Solvent	DS of PPFS-MPA	Resulting Solution*	Formation of film	Characterization method
4	CHCl ₃ for P4VP MEK for PPFS-MPA	32%	Transparent	Yes	UV, ATR FT-IR, XPS, AFM, WCA
5		15%	Transparent	Yes	UV, ATR FT-IR, XPS, AFM, WCA
6		7%	Transparent	No	UV
*The resulting solution refers to the macroscopic changes of P4VP solution					

The multilayer films were prepared by sequentially dipping a glass slide or a silicon wafer into a P4VP solution in CHCl₃ and a PPFS-MPA (DS = 32%, 15% or 7%) solution in MEK at $c = 2$ g/L. During the whole process, whatever the DS of PPFS-MPA is, the dipping solution remains transparent. However, as previously mentioned, cracks appear for DS = 32% from the deposition of 8 BL, while, macroscopically, no surface tears were observed for DS = 7% and 15%. The UV and FT-IR spectra of (P4VP/PPFS-MPA)_n with DS = 7% and 15% are shown in Figure 3-31.

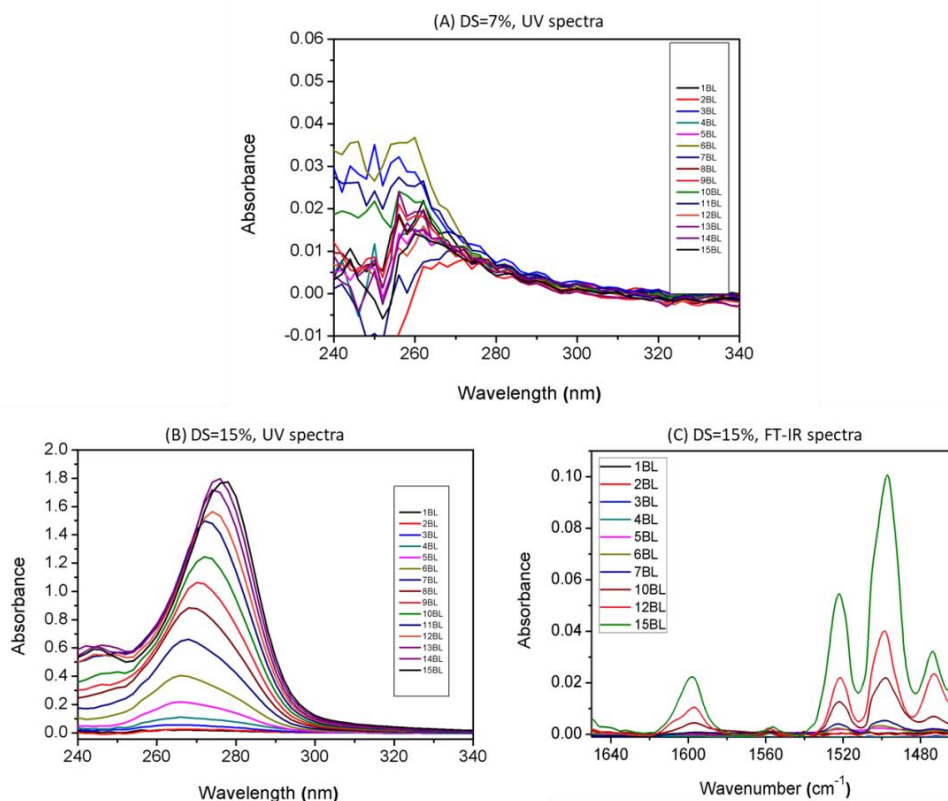


Figure 3-31 UV spectra (A, DS = 7%; B, DS = 15%) and ATR FT-IR spectra (C, DS = 15%) of (P4VP/PPFS-MPA)_n (CHCl₃ for P4VP and MEK for PPFS-MPA, c = 2 g/L).

By using PPFS-MPA with the lowest DS (7%) (Figure 3-31-A), no UV signal is detected, whatever the number of deposited bilayer. This is probably linked to limitation of the sensitivity of the technique, since in this case a too low amount of polymer is deposited. Thus, we can conclude that for a low DS, such as 7 %, no film is formed by the LbL approach. Once again, this result emphasizes the fact that the number of interacting groups per macromolecular chain is a key parameter, which controls the assembly process. Conversely, for the film with a DS = 15%, an UV response is detected and the absorbance increases with the number of deposited bilayers (Figure 3-31-B), as result of the progressive accumulation of the polymers onto the glass slide, during the stepwise assembly. The same behavior can be highlighted from the FT-IR spectra (Figure 3-31-C), for which the absorbance intensities increase as a function of the number of deposited layers.

3.5.2.3.1 Study of the growth mechanism

The UV absorbance (at $\lambda = 286$ nm) and the IR signal (at 1597 cm^{-1}), signatures of PPFS-MPA and P4VP embedded in the film, respectively, are plotted *versus* the number of deposited bilayers (n), for the system including a PPFS-MPA with a DS = 15%, and a DS of 32% (Figure 3-32-A, B). The corresponding thickness evolution is also depicted (Figure 3-32-C).

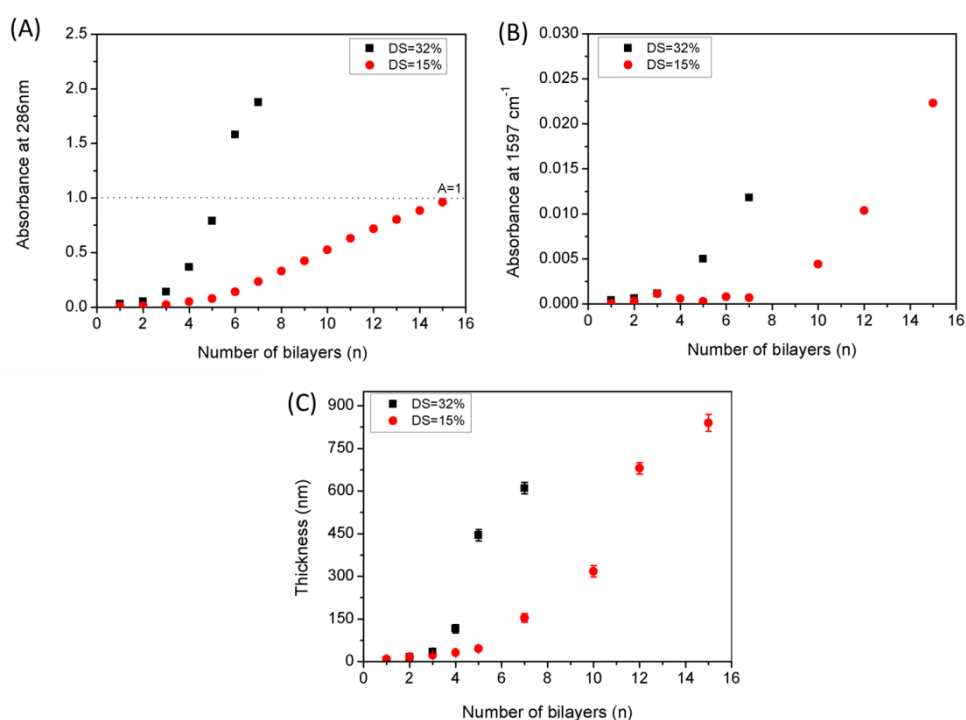


Figure 3-32 Evolution of the UV absorbance at 286 nm (A), ATR FT-IR absorbance at 1597 cm^{-1} (B) and thickness (C) of (P4VP/PPFS-MPA) $_n$ (CHCl_3 for P4VP and MEK for PPFS-MPA, DS = 15% or 32%, $c = 2$ g/L) as a function of the number of deposited bilayers (n).

Both UV and IR spectroscopic responses as well as the thickness evolution show that the film growth is highly dependent on the DS. In other words, the assembly is influenced by the number of $-\text{COOH}$ per PPFS-MPA chain, which directly influences the number of H-bond, developed between the two partners. Globally, from the Figure 3-32, we can underline two main features: i) for both DS, the assembly follows two modes of growth, a quite low deposition regime, followed by a much higher deposition rate, and ii) especially in the region for which the deposition is large, we

note that high DS contribute to form more thicker films. For the film with a DS = 15%, the UV absorbance (Figure 3-32-A) for $n = 0$ to 5 BL varies very few and a low amount of polymers is deposited, resulting in thin films with a thickness around 45 nm for $n = 5$ BL (Figure 3-32-C). Then from 6 BL, the thickness increases to reach a value of around 800 nm for 15 BL (Figure 3-32-C).

It appears that the UV response at 286 nm and the IR absorbance at 1597 cm^{-1} of the film are greater for higher DS. This suggests that a higher amount of polymer is deposited at each bilayer deposition, which can be ascribed to the increase of the H-bonds extent between PPFS-MPA and P4VP when a larger number of COOH groups per chain is involved. To illustrate this fact, we can see that, for $n = 7$ BL, the thickness of the film constructed from the use of PPFS-MPA-32 % is around 600 nm, against 150 nm for the film involving PPFSMPA-15 %.

3.5.2.3.2 Study of the surface features by AFM

Figure 3-33 shows the AFM images of $(\text{P4VP/PPFS-MPA})_n$ with DS = 15% ($c = 2\text{g/L}$) by using CHCl_3 for P4VP and MEK for PPFS-MPA. These images can be compared with the one presented in Figure 3-29 (obtained with PPFS-MPA with a DS = 32%).

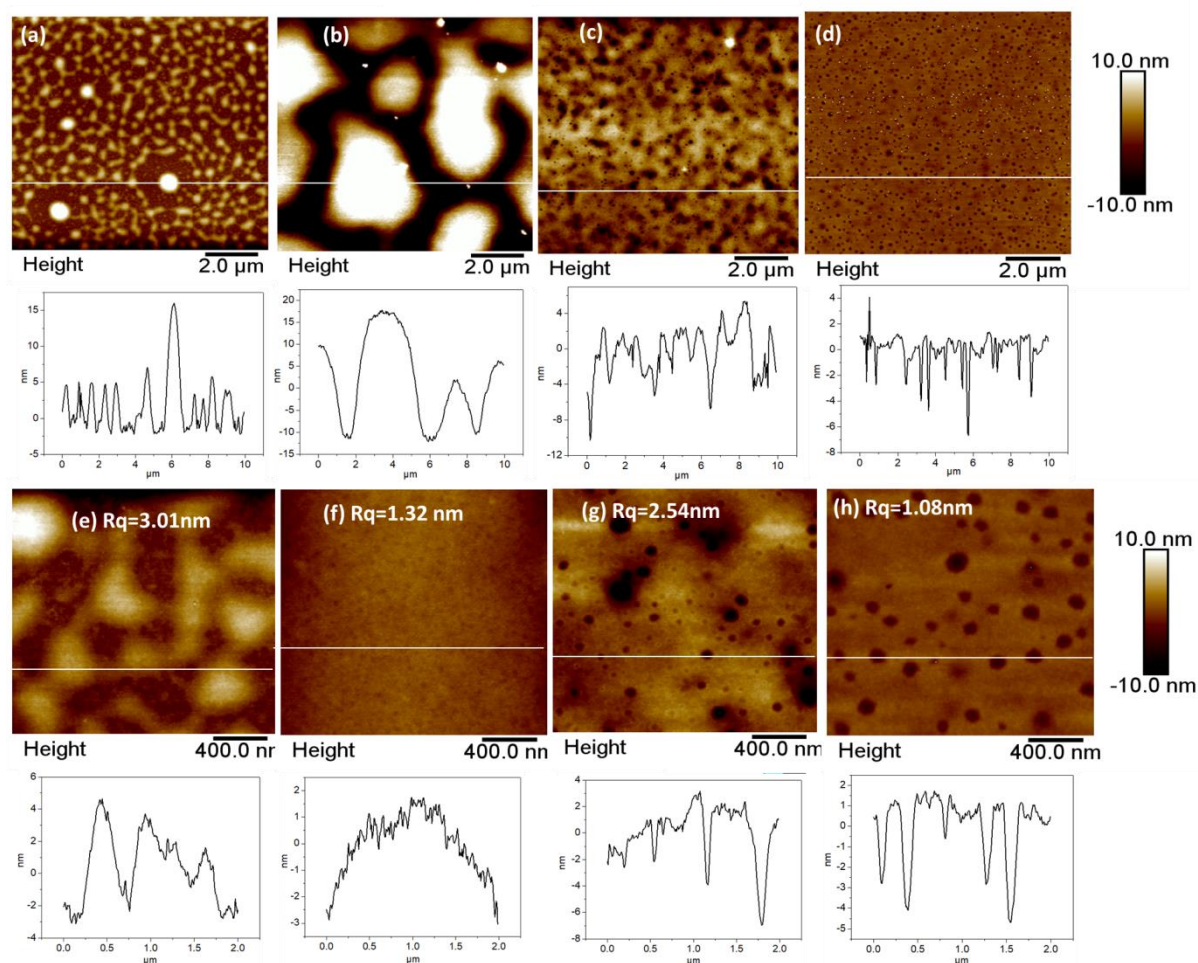


Figure 3-33 AFM topographic images with the corresponding height profiles of $(\text{P4VP/PPFS-MPA})_n$ (CHCl_3 for P4VP and MEK for PPFS-MPA, DS = 15%, $c = 2 \text{ g/L}$) for $n = 1$ (a, e), 5 (b, f), 7 (c, g), 15 (d, h) BL deposited onto the silicon wafer.

After one deposited bilayer, we can observe an original patchy topology with small protrusions and few bigger aggregates irregularly distributed on the surface (Figure 3-33-a), leading to a relatively high roughness of 3.01 nm (Figure 3-33-e). This special topology is totally different from the film constructed with the higher DS (32%) (Figure 3-29) and may arise from a different chain collapse to the surface and from a more spatially localized deposition, when a lower DS is used. This can be explained by the H-bonded zones, in which the extent is governed by the number of developed efficient interactions (which closely depend on the DS value). For $n = 2$ BL, an “island”-type structure is observed (Figure 3-33-b), which then steadily grow in lateral direction until a continuous film is formed (Figure 3-33-c and g). The width and the height of each “island” incrementally increase, leading to a decrease of the

distance between the neighboring nodules. However, it seems that the area between “islands” is not totally filled, so that regular holes with a depth around 5 nm are presented within the film (Figure 3-33-d). Moreover, the surface got smoother with an $R_q = 1.08$ nm for $n = 15$ BL (Figure 3-33-h), probably due to a decrease of the diameter of holes.

These AFM images show a totally different surface topology from the film elaborated from the derivative with $DS = 32\%$, for which homogenous and flat films without any pore were formed (Figure 3-29). This underpins that the film surface morphology can be tailored by the density of the H-bonds developed between the two partners.

3.5.2.3.3 Study of surface features by the wettability measurements

To gain information about the level of interlayer interpenetration present in sequentially adsorbed layers, the surface wettability evolution of (P4VP/PPFS-MPA) $_n$ (CHCl_3 for P4VP and MEK for PPFS-MPA, $DS = 15\%$ $c = 2$ g/L) was studied (Figure 3-34).

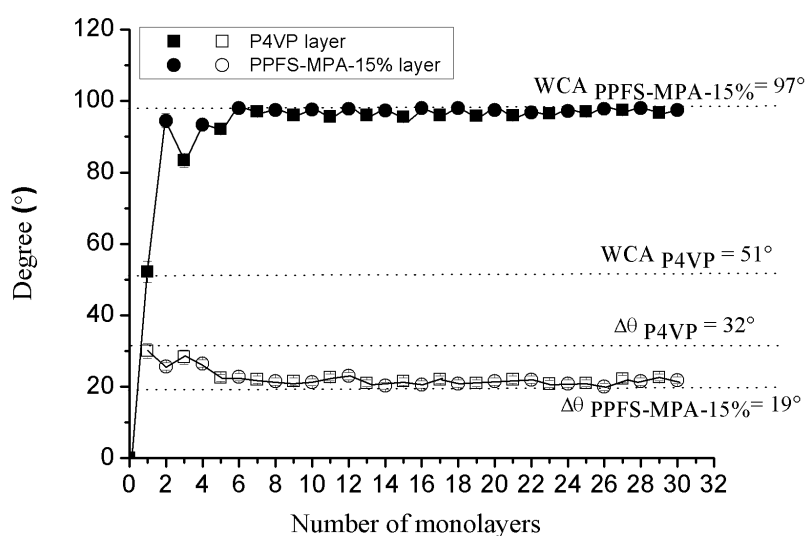


Figure 3-34 Evolution of WCA (filled symbol) and water hysteresis (open symbol) of (P4VP/PPFS-MPA) $_n$ (CHCl_3 for P4VP and MEK for PPFS-MPA, $DS = 15\%$, $c = 2$ g/L) as a function of the number of deposited monolayers.

After the first P4VP deposition, the WCA increases to 51° which confirms the successful deposition of P4VP layer. Then the WCA obtained after the PPFS-MPA-15% deposition is close to a value of 97° , reflecting the presence of carboxylated PPFS derivative at the surface. After the deposition of a second layer of P4VP, the WCA becomes 82° . This value is higher than the one of pure P4VP, which can result from the possible migration of PPFS-MPA-15% into the top layer. From the 7 deposited monolayers, the WCA remains constant around the WCA of the PPFS-MPA-15% whatever the nature of the deposited polymer is. The absence of WCA evolution indicates that P4VP is not probed at the surface; the layers are thus composed of interdigitated PPFS-MPA-15% and P4VP due to i) an insufficient coverage or/and ii) an intermixing, and only PPFS-MPA-15% is detected due to its migration on the surface. Also, we can note that these values of WCA are not only governed by the nature of the top layer but also by the surface topology, which is particularly uneven and textured, as emphasized by AFM imaging. In spite of the fact that no alternate WCA evolution is observed, a film can be progressively formed all along the deposition process, as revealed by the increase of the total thickness and by the UV and IR responses. The water hysteresis shows a similar behavior, with value of hysteresis that does not vary along the deposition process.

3.5.2.4 Other attempts by using CHCl_3/MEK mixture

In previous part (Chapter 3.5.2.2), we described the film buildup $((\text{P4VP}/\text{PPFS-MPA})_n$ with a DS = 32%) by using the mixed solvent CHCl_3/MEK as deposition solvent. However, a partial polymer desorption from $n = 7$ BL was evidenced. In order to limit this phenomenon, we were interested in lowering the DS at 15 %, and we decided to study the effect of both the DS in the mixed solvent (Table 3-4, entry 3 and 7), but also the influence of the concentration of the polymers on the features of the resulting films. Hence, we analyzed the LbL assembly of $((\text{P4VP}/\text{PPFS-MPA})_n$ with a DS = 15 %), for 2 different concentrations: 0.1 g/L and 2 g/L (Table 3-4, entry 7 and 8).

Table 3-4 LbL self-assembly of P4VP with PPFS-MPA (CHCl_3/MEK , DS = 15% or 32%) for two different concentrations

Entry	DS of PPFS-MPA	Deposition Solvent	Concentration (g/L)	Resulting Solution*	Formation of film	Characterization method
3	32%	CHCl_3/MEK	2	Turbid solution appear at 10 BL	Yes	ATR FT-IR, XPS, AFM, WCA
7	15%		2	Turbid solution appear at 5 BL	Yes	ATR FT-IR
8	15%		0.1	Transparent	Yes	AFM, WCA

*The resulting solution refers to the macroscopic changes of P4VP solution

3.5.2.4.1 Influence of the DS of PPFS-MPA

As previously reported for the construction of the film with DS = 32 %, from $n = 5$ BL, the dipping solution becomes turbid along the immersion steps, which is the signature of the desorption of polymers not sufficiently adhering to the substrate. Up to 5 BL, the assembly process was monitored by ATR FT-IR spectroscopy (Figure 3-35).

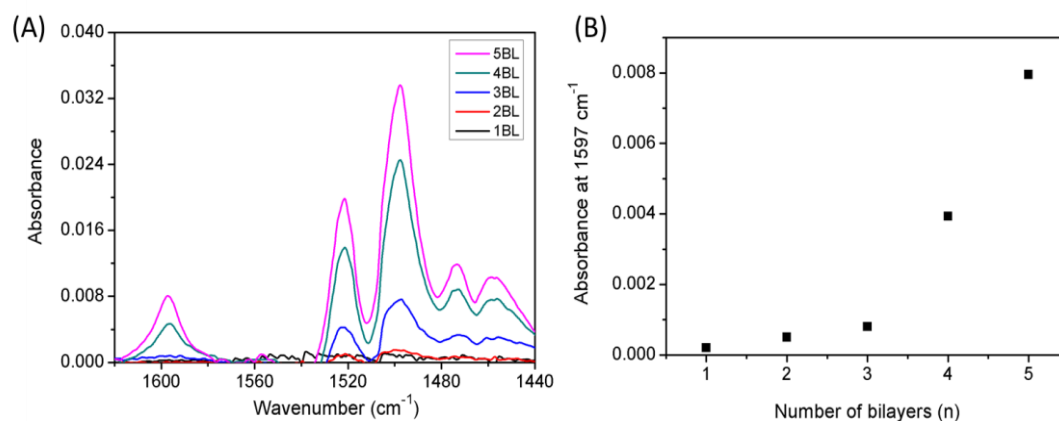


Figure 3-35 ATR FT-IR spectra of $(\text{P4VP}/\text{PPFS-MPA})_n$ (CHCl_3/MEK , DS = 15%, $c = 2$ g/L) and the corresponding evolution of the absorbance at 1597 cm^{-1} as a function of the number of deposited bilayers (n).

Similarly to the assembly including the PPFS-MPA derivative with DS = 32% (Figure 3-21), the IR response increases (Figure 3-35-A), meaning that polymers are successfully deposited onto the substrate. Two regimes can be observed, each being characterized by a completely different deposition rate. Indeed, as already reported,

we observe a limited evolution, followed by a sharp increase of the IR absorbance at 1522 cm^{-1} (Figure 3-35-B). The same tendency is observed when using the absorbance at 1522 cm^{-1} as reference (Figure AI 3-10). Moreover, the growth rate is lower than the one with higher DS (32%). Thus, as expected, high DS promotes the amount of deposited matter by favoring the interfacial interactions (as we afore discussed in the other solvent system).

3.5.2.4.2 Influence of the concentration of the deposition solution

It is well established that the deposited polymer concentration can affect the LbL deposition and the resulting properties of the film. Thus, a lower concentration ($c = 0.1\text{ g/L}$) was employed to prepare multilayer films. First, we can note that contrary to the $c = 2\text{ g/L}$, neither turbid solutions, nor cracked film were observed during the whole process from 1 BL to 15 BL. We intended to monitor the assembly process by using ATR FT-IR spectroscopy, however, no signal was detected even for $n = 15\text{ BL}$, probably due to a too low quantity of deposited polymer (as confirmed by the thickness measurement, *vide-infra*).

The film thickness is evaluated to gain insight of the film growth mechanism (Figure 3-36).

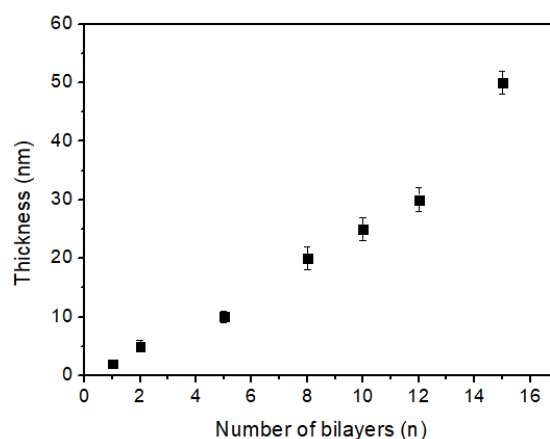


Figure 3-36 Evolution of the thickness measured by AFM of (P4VP/PPFS-MPA) $_n$ (CHCl_3/MEK , DS = 15%, $c = 0.1\text{ g/L}$) as a function of the number of deposited bilayers (n).

For $c = 0.1\text{ g/L}$, it appears that the thickness variation presents a linear evolution

with the number of deposited bilayers up to 12 BL, which indicates a constant amount of deposited polymer at each deposition cycle. A sharp increase seems occur after 15 BL, since the film thickness was shown to increase up to 50 nm. The very small thickness for $n = 15$ BL means that very limited polymers are deposited which cannot be detected by ATR FT-IR. If we compare with the one for $c = 2$ g/L, different modes of adsorption and rearrangements are observed, dependently of the polymer concentration. The growth mechanism is closely controlled by the concentration, which plays on the interactions developed within the film. Indeed, a high concentration affords a larger number of active H-bonds and additional chain entanglements, which change the conformation chains inside the film and contribute to increase the thickness.

Figure 3-37 shows the AFM images of self-assembled (P4VP/PPFS-MPA) $_n$ (CHCl₃/MEK, DS = 15%, $c = 0.1$ g/L) with $n = 2, 8$ and 15 BL.

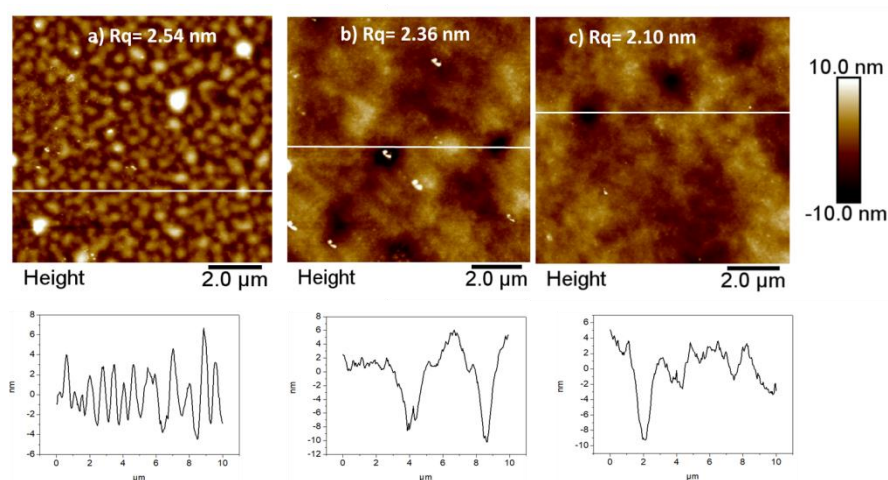


Figure 3-37 AFM topologic images with the corresponding height profiles of (P4VP/PPFS-MPA) $_n$ (CHCl₃/MEK, DS = 15%, $c = 0.1$ g/L) with $n = 2$ (a), 8 (b) and 15 (c) BL deposited onto the silicon wafer

All AFM images clearly show the successive deposition of polymer onto the substrate. The first two deposition bilayers at $c = 0.1$ g/L leads to the formation of nanoprotusions on the entire probed surface (Figure 3-37-a), such that the surface has a roughness of 2.54 nm. The size and the shape of aggregates change along the deposition process (Figure 3-37-b). The deposition seems to be quite stochastic and

heterogeneous and small areas with missing matter are visible (Figure 3-37-c).

The change of surface wettability of (P4VP/PPFS-MPA)_n (CHCl₃/MEK, DS = 15%, c = 0.1 g/L) film after each deposited monolayer was investigated by WCA measurements (Figure 3-38).

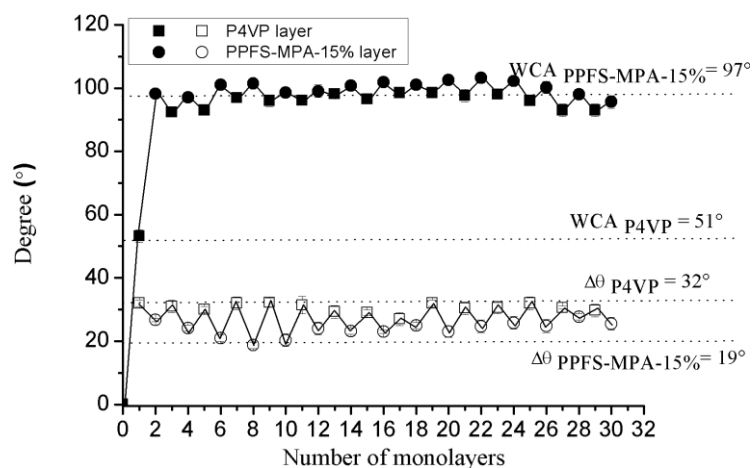


Figure 3-38 Evolution of WCA (filled symbol) and water hysteresis (open symbol) of (P4VP/PPFS-MPA) (CHCl₃/MEK, DS = 15%, c = 0.1 g/L) as a function of the number of deposited monolayers.

From the second deposition monolayer, the amplitude of the WCA evolution, after the deposition of each polymer, is very small. The WCA are particularly high, especially after the deposition of P4VP, which is known to be a more polar polymer. Such high WCA values show that P4VP is not detected at the top surface, and reflect the formation of interdigitated layers, with a more pronounced presence of PPFS-MPA at the surface. Even, we can note that the WCA becomes higher than the one of pure PPFS-MPA. We can assume that the surface topology, as evidenced by AFM, can contribute to enhance the hydrophobicity.

3.5.2.5 Conclusion

In summary, P4VP and PPFS-MPA based polymer films were prepared either by the successive deposition of H-bonded interpolymer complex (IPC) (composed of P4VP and PPFS-MPA-32%) preformed in solution, leading to a film with a thickness around 420 nm after 50 step depositions, or by H-bonds driven LbL assembly of

P4VP and PPFS-MPA derivatives. For LbL self-assembled film, two impact factors were emphasized. One is the nature of solvent which has a significant effect on the growth mechanism and surface features of multilayer films. At a given PPFS-MPA derivative with a DS = 32%, the H-bonded film cannot be prepared by using polar aprotic DMF; while a very thin film with a linear growth mechanism was observed by using EtOH. In this case, the resulting films are composed of quite well stratified layers and the films are rather hydrophilic and relatively rough. A faster and non-linear growth mechanism was found when using a mixed solvent CHCl₃/MEK or using CHCl₃ for P4VP and MEK for PPFS-MPA. The growth mechanisms provide much thicker films with disordered layers composed of interdigitated P4VP and PPFS-MPA segments. The desorption of film from the substrate was observed when using the mixed solvent CHCl₃/MEK.

The other parameter that we investigated is the DS value (i.e., the amount of carboxyl groups per chains of PPFS-MPA). At a given deposition solvent (CHCl₃ for P4VP and MEK for PPFS-MPA), no films was formed when a low DS (7 %) was used, contrary to DS = 15% or 32%. A high DS leads to a more pronounced growth and thicker films for a given n, suggesting that the number of H-bond donor moieties is a key parameter. Moreover, the concentration of the deposition solution can be used as an additional parameter to tune the film growth mechanism.

3.6 General Conclusion

In this last chapter of the manuscript, novel carboxyl groups containing PPFS were synthesized and employed as H-bond donors to build films with H-bond acceptor (P4VP). Firstly, carboxylated PPFS copolymers were synthesized by using carboxylic acid containing thiols as modifiers *via* the versatile thiol-*para*-fluoro substitution reaction. The reaction is chemoselective and the degree of substitution was successfully adjusted from relatively low (7%) up to complete (100%). The obtained mercaptopropionic acid (MPA) modified PPFS copolymers (PPFS-MPA) present variable physico-chemical properties. Then, blends between PPFS-MPA and

P4VP in solution were studied, in order to evaluate the propensity of PPFS-MPA to develop H-bonds. It was found that the miscibility of PPFS with P4VP was enhanced after modification with MPA, as reflected by the formation of strong H-bonded complexes. Interpolymer complexes, yielding turbid solutions, were formed in both CHCl_3/MEK and EtOH, while miscible blends were obtained in DMF. The advantage of this very fast complexation between PPFS-MPA and P4VP was exploited to build thin film (thickness ~ 420 nm) by successive spin-coating of a solution containing preformed (PPFS-MPA-32%/P4VP) interpolymer complexes. Furthermore, we exploited the self-assembly layer by layer (LbL) approach and we evidenced the feasibility to construct multilayer films by using P4VP and PPFS-MPA derivative. Moreover, we proved that the construction of the film was mediated by the formation of H-bond between the two chosen partners. We were interested in the effect of the nature of the deposition solvent, the extent of PPFS modification (DS = 7%, 15% and 32%) and the polymer concentration on the growth mechanism, on the amount of deposited polymer and on the surface features (surface topology and wettability behavior) of the resulting multilayer films. These investigations were performed through the use of rich and complementary surface analysis techniques, such as FT-IR in ATR mode, UV spectroscopy, AFM and wettability measurements.

We exploited the trend observed for the complexation in solution, and we showed that at a given DS value of PPFS-MPA (32%), the use of DMF does not afford any film, due to the competitor role of the solvent (which is consistent with the formation of miscible blends in DMF). Ethanol allows for the construction of very thin films, following a linear growth mechanism. The resulting films are relatively rough. WCA measurement revealed a hydrophilic character (WCA inferior to 90° after each deposited monolayer), with the alternative presence of the two polymers at the top surface, which reflects that the film is constituted of well stratified layers. A faster non-linear growth mechanism was emphasized for films constructed by using mixed solvent CHCl_3/MEK or separated solvents: CHCl_3 for P4VP and MEK for PPFS-MPA. In these cases, much thicker films were obtained (up to the micrometer scale), even for a low number of deposited bilayers, as a result of numerous effective

interactions developed between the two partners. AFM imaging demonstrated rather homogeneous films, compared to the use of ethanol. WCA measurements evidenced that disordered layers composed of interdigitated P4VP and PPFS-MPA were obtained. Increasing the DS contributed to boost the amount of deposited polymer and to increase the film thickness. In addition, it appeared that the DS variation allowed for changing the surface topology, since for lower DS, more uneven and textured films were formed. Decreasing the concentration leads to thinner films, but limits desorption of polymer during the process of assembly by immersion.

3.7 References

- (1) Pitois, C.; Wiesmann, D.; Mikael, L. and Hult, A. Functionalize Fluorinated Hyperbranched Polymers for Optical Waveguide Applications. *Adv. Mater.* **2001**, *13* (19), 1483–1487.
- (2) Hvilsted, S.; Forcén, P.; Oriol, L.; Sánchez, C.; Alcalá, R.; Ramanujam, P. S. Novel Polymer Architectures for Optical Storage. In *Electroactive polymers : materials & devices*; Hashmi, S. A., Chandra, A., Chandra, A., Eds.; Allied Publishers Ltd, 2007; Vol. II, pp 165–174.
- (3) Zhu, P.; Meng, W. and Huang, Y. Synthesis and Antibiofouling Properties of Crosslinkable Copolymers Grafted with Fluorinated Aromatic Side Chains. *RSC Adv.* **2017**, *7* (6), 3179–3189.
- (4) Borkar, S.; Jankova, K.; Siesler, H. W.; Hvilsted, S. New Highly Fluorinated Styrene-Based Materials with Low Surface Energy Prepared by ATRP. *Macromolecules* **2004**, *37* (3), 788–794.
- (5) Martinelli, E.; Hill, S. D.; Finlay, J. A.; Callow, M. E.; Callow, J. A.; Glisenti, A.; Galli, G. Amphiphilic Modified-Styrene Copolymer Films: Antifouling/fouling Release Properties against the Green Alga *Ulva Linza*. *Prog. Org. Coatings* **2016**, *90*, 235–242.
- (6) Bhebhe, M. N.; De Eulate, E. A.; Pei, Y.; Arrigan, D. W. M.; Roth, P. J.; Lowe, A. B. Reactive Conjugated Polymers: Synthesis, Modification, and

- Electrochemical Properties of Polypentafluorophenylacetylene (Co)Polymers. *Macromol. Rapid Commun.* **2017**, *38* (2), 1600450–1600456.
- (7) Barner, L.; Cavalli, F.; Mutlu, H.; Steinmueller, S. O. The Para-Fluoro-Thiol Reaction as a Powerful Tool for Precision Network Synthesis. *Polym. Chem.* **2017**, *8* (25), 3778–3782.
- (8) Boufflet, P.; Casey, A.; Xia, Y.; Stavrinou, P. N.; Heeney, M. Pentafluorobenzene End-Group as a Versatile Handle for Para Fluoro “click” Functionalization of Polythiophenes. *Chem. Sci.* **2017**, *8*, 2215–2225.
- (9) Turgut, H.; Schmidt, A. C.; Wadhvani, P.; Welle, A.; Müller, R.; Delaittre, G. The Para-Fluoro–Thiol Ligation in Water. *Polym. Chem.* **2017**, *8* (8), 1288–1293.
- (10) Gutsche, C. S.; Ortwerth, M.; Gräfe, S.; Flanagan, K. J.; Senge, M. O.; Reissig, H. U.; Kulak, N.; Wiehe, A. Nucleophilic Aromatic Substitution on Pentafluorophenyl-Substituted Dipyrans and Tetrapyrroles as a Route to Multifunctionalized Chromophores for Potential Application in Photodynamic Therapy. *Chem. - A Eur. J.* **2016**, *22* (39), 13953–13964.
- (11) Kong, X.; Zhang, H.; Xiao, Y.; Cao, C.; Shi, Y.; Pang, G. Effective, Transition Metal Free and Selective C–F Activation under Mild Conditions. *RSC Adv.* **2015**, *5* (10), 7035–7048.
- (12) Quast, M. J.; Mueller, A. Hyperbranched Polyfluorinated Benzyl Ether Polymers: Mechanism, Kinetics, and Optimization. *J. Polym. Sci. Part A Polym. Chem.* **2014**, *52* (7), 985–994.
- (13) Chen, J.; Duchet, J.; Portinha, D.; Charlot, A. Layer by Layer H-Bonded Assembly of P4VP with Various Hydroxylated PPFs: Impact of the Donor Strength on Growth Mechanism and Surface Features. *Langmuir* **2014**, *30* (35), 10740–10750.
- (14) Chen, J.; Dumas, L.; Duchet-Rumeau, J.; Fleury, E.; Charlot, A.; Portinha, D. Tuning H-Bond Capability of Hydroxylated-poly(2,3,4,5,6-Pentafluorostyrene) Grafted Copolymers Prepared by Chemoselective and Versatile Thiol-Para-Fluoro “click-Type” coupling with Mercaptoalcohols. *J. Polym. Sci.*

- Part A Polym. Chem.* **2012**, *50* (16), 3452–3460.
- (15) Chen, J.; Vuluga, D.; Crousse, B.; Legros, J.; Duchet-Rumeau, J.; Charlot, A.; Portinha, D. Polyfluorinated Mercaptoalcohol as a H-Bond Modifier of poly(2,3,4,5,6-Pentafluorostyrene) (PPFS) Enhancing Miscibility of Hydroxylated-PPFS with Various Acceptor Polymers. *Polymer (Guildf)*. **2013**, *54* (15), 3757–3766.
- (16) Wang, L.; Wang, Z.; Zhang, X.; Shen, J.; Chi, L.; Fuchs, H. A New Approach for the Fabrication of an Alternating Multilayer Film of poly(4-Vinylpyridine) and Poly(acrylic Acid) Based on Hydrogen Bonding. *Macromol. Rapid Commun.* **1997**, *18*, 509–514.
- (17) Zhang, X.; Chen, H.; Zhang, H. Layer-by-Layer Assembly: From Conventional to Unconventional Methods. *Chem. Commun.* **2007**, No. 14, 1395–1405.
- (18) Richardson, J. J.; Cui, J.; Björnmalm, M.; Braunger, J. A.; Ejima, H.; Caruso, F. Innovation in Layer-by-Layer Assembly. *Chem. Rev.* **2016**, *116* (23), 14828–14867.
- (19) Noy, J.-M.; Koldevitz, M.; Roth, P. J. Thiol-Reactive Functional Poly(meth)acrylates: Multicomponent Monomer Synthesis, RAFT (Co)polymerization and Highly Efficient Thiol-Para-Fluoro Postpolymerization Modification. *Polym. Chem.* **2015**, *6* (3), 436–447.
- (20) Turgut, H.; Delaittre, G. On the Orthogonality of Two Thiol-Based Modular Ligations. *Chem. Eur.J.* **2016**, *22* (4), 1511–1521.
- (21) Li, Y.; Pan, T.; Ma, B.; Liu, J.; Sun, J. Healable Antifouling Films Composed of Partially Hydrolyzed Poly(2-Ethyl-2-Oxazoline) and Poly(acrylic Acid). *ACS Appl. Mater. Interfaces* **2017**, *9* (16), 14429–14436.
- (22) Maurer, J. J.; Eustace, D. J.; Ratcliffe, C. T. Thermal Characterization of Poly(acrylic Acid). *Macromolecules* **1987**, *20* (1), 196–202.
- (23) Pandey, P. K.; Srivastava, A.; Tripathy, J.; Behari, K. Graft Copolymerization of Acrylic Acid onto Guar Gum Initiated by Vanadium (V)-Mercaptosuccinic Acid Redox Pair. *Carbohydr. Polym.* **2006**, *65* (4), 414–420.
- (24) Popescu, I.; Suflet, D. M.; Pelin, I. M. Investigation of Interpolymer

- Complexation Between Poly(Vinylcaprolactam) and Poly(Maleic Acid- *Alt*-Styrene). *J. Macromol. Sci. Part B* **2016**, *55* (7), 708–721.
- (25) Jiang, M.; Li, M.; Xiang, M.; Zhou, H. Interpolymer Complexation and Miscibility Enhancement by Hydrogen Bonding. *Adv. Polym. Sci.* **1999**, *146*, 121–196.
- (26) Bekturov, E. A.; Bimend, L. A. Interpolymer Complexes. *Adv. Polym. Sci* **1980**, *41*, 99–147.
- (27) Kuo, S.; Chan, S.; Chang, F. Effect of Hydrogen Bonding Strength on the Microstructure and Crystallization Behavior of Crystalline Polymer Blends. *Macromolecules* **2003**, *55*, 6653–6661.
- (28) Lu, Y.; An, L.; Wang, Z. G. Intrinsic Viscosity of Polymers: General Theory Based on a Partially Permeable Sphere Model. *Macromolecules* **2013**, *46* (14), 5731–5740.
- (29) M. Rubinstein; R.H. Colby. *Polymer Physics*; Oxford University Press, 2003.
- (30) Ma, S.; Yuan, Q.; Zhang, X.; Yang, S.; Xu, J. Solvent Effect on Hydrogen-Bonded Thin Film of Poly(vinylpyrrolidone) and Poly(acrylic Acid) Prepared by Layer-by-Layer Assembly. *Colloids Surfaces A Physicochem. Eng. Asp.* **2015**, *471*, 11–18.
- (31) Lee, H.; Mensire, R.; Cohen, R. E.; Rubner, M. F. Strategies for Hydrogen Bonding Based Layer-by-Layer Assembly of Poly(vinyl Alcohol) with Weak Polyacids. *Macromolecules* **2012**, *45* (1), 347–355.
- (32) Chen, Y.; Pang, Y.; Wu, J.; Su, Y.; Liu, J.; Wang, R.; Zhu, B.; Yao, Y.; Yan, D.; Zhu, X.; et al. Controlling the Particle Size of Interpolymer Complexes through Host-Guest Interaction for Drug Delivery. *Langmuir* **2010**, *26* (11), 9011–9016.
- (33) Ohno, H.; Abe, K.; Tsuchida, E. Solvent Effect on the Formation of Poly(methacrylic acid)- poly(N- vinyl- 2- pyrrolidone) Complex through Hydrogen Bonding. *Die Makromol. Chemie* **1978**, *179* (3), 755–763.
- (34) Ohno, H.; Nii, A.; Tsuchida, E. Solvent Effect on the Complex Formation of Poly(methacrylic Acid) with Proton-Accepting Polymers. *Makromol. Chemi.*

- 1980**, *181* (6), 1227–1235.
- (35) Zhunuspayev, D. E.; Mun, G. A.; Hole, P.; Khutoryanskiy, V. V. Solvent Effects on the Formation of Nanoparticles and Multilayered Coatings Based on Hydrogen-Bonded Interpolymer Complexes of Poly (Acrylic Acid) with Homo- and Copolymers of N -Vinyl Pyrrolidone. *Langmuir* **2008**, *24* (28), 13742–13747.
- (36) Dai, J; Goh, S. H.; Lee, S. Y. and Siow. K. S. Interpolymer Complexation between Poly(p-Vinylphenol) and Pyridine-Containing Polymers. *Polym. J.* **1994**, *26*, 905–911.
- (37) Chen, Q.; Ma, N.; Qian, H.; Wang, L.; Lu, Z. Layer-by-Layer Assembly of Two Polyacrylate Derivatives: Effect of Solvent Composition and Side-Chain Structure. *Polymer (Guildf)*. **2007**, *48* (9), 2659–2664.
- (38) Cesteros, L. C.; Velada, J. L. Polymer-Polymer Complexation Between Poly (monomethyl itaconate) and Poly (vinylpyridine)s. *Polymer (Guildf)*. **1995**, *36* (16), 3183–3189.
- (39) Goh, S. H.; Lee, S. Y.; Zhou, X.; Tan, K. L. X-Ray Photoelectron Spectroscopic Studies of Interactions between Poly (4-Vinylpyridine) and Poly (Styrenesulfonate) Salts. *Appl. Surf. Sci.* **1997**, *119* (1–2), 60–66.
- (40) Zhou, X.; Goh, S. H.; Lee, S. Y.; Tan, K. L. XPS and FTi.r. Studies of Interactions in Poly (Carboxylic Acid)/ Poly (Vinylpyridine). *Polymer (Guildf)*. **1998**, *39* (16), 3631–3640.
- (41) He, Y.; Zhu, B.; Inoue, Y. Hydrogen Bonds in Polymer Blends. *Prog. Polym. Sci.* **2004**, *29* (10), 1021–1051.
- (42) Kwei, T. K. The Effect of Hydrogen Bonding on the Glass Transition of Polymer Mixtures. *J. Polym. Sci.* **1984**, *22* (1), 307–313.
- (43) Tepper, R.; Bode, S.; Geitner, R.; Jäger, M.; Görls, H.; Vitz, J.; Dietzek, B.; Schmitt, M.; Popp, J.; Hager, M. D. and Schubert, U. S. Polymeric Halogen-Bond-Based Donor Systems Showing Self-Healing Behavior in Thin Films. *Angew. Chemie - Int. Ed.* **2017**, *56* (14), 4047–4051.
- (44) Kowel, S. T.; Selfridge, R.; Eldering, C.; Matloff, N.; Stroeve, P.; Higgins, B.

- G.; Srinivasan, M. P.; Coleman, L. B. Future Applications of Ordered Polymeric Thin Films. *Thin Solid Films* **1987**, *152* (1–2), 377–403.
- (45) HASHIM, A. A. *Polymer Thin Films*; 2010.
- (46) De Saint-Aubin, C.; Hemmerlé, J.; Boulmedais, F.; Vallat, M. F.; Nardin, M.; Schaaf, P. New 2-in-1 Polyelectrolyte Step-by-Step Film Buildup without Solution Alternation: From PEDOT-PSS to Polyelectrolyte Complexes. *Langmuir* **2012**, *28* (23), 8681–8691.
- (47) Bahloul, M.; Chamignon, C.; Pruvost, S.; Fleury, E.; Charlot, A.; Portinha, D. Instantaneous Stereocomplex Driven Self-Assembly of Enantiomeric Poly(vinyl Alcohol)-Graft-Oligo(lactide) Copolymers in DMSO and Thin Film Formation Thereof. *Polymer*. **2015**, *79*, 195–204.
- (48) Zhang, H.; Wang, Z.; Zhang, Y.; Zhang, X. Hydrogen-Bonding-Directed Layer-by-Layer Assembly of Poly (4-Vinylpyridine) and Poly (4-Vinylphenol): Effect of Solvent Composition on Multilayer Buildup. *Langmuir* **2004**, *20* (20), 9366–9370.
- (49) Fu, Y.; Bai, S.; Cui, S.; Qiu, D.; Wang, Z.; Zhang, X. Hydrogen-Bonding-Directed Layer-by-Layer Multilayer Assembly: Reformation Yielding Microporous Films. *Macromolecules* **2002**, *35* (25), 9451–9458.
- (50) Xiao, F.-X.; Pagliaro, M.; Xu, Y.-J.; Liu, B. Layer-by-Layer Assembly of Versatile Nanoarchitectures with Diverse Dimensionality: A New Perspective for Rational Construction of Multilayer Assemblies. *Chem. Soc. Rev.* **2016**, *45* (11), 3019–3304.
- (51) Zhang, H.; Fu, Y.; Wang, D.; Wang, L.; Wang, Z.; Zhang, X. Hydrogen-Bonding-Directed Layer-by-Layer Assembly of Dendrimer and poly(4-Vinylpyridine) and Micropore Formation by Post-Base Treatment. *Langmuir* **2003**, *19* (20), 8497–8502.
- (52) Quinn, A.; Tjipto, E.; Yu, A.; Gengenbach, T. R.; Caruso, F. Polyelectrolyte Blend Multilayer Films: Surface Morphology, Wettability, and Protein Adsorption Characteristics. *Langmuir* **2007**, *23* (9), 4944–4949.

- (53) He, T.; Jańczewski, D.; Guo, S.; Man, S. M.; Jiang, S.; Tan, W. S. Stable pH Responsive Layer-by-Layer Assemblies of Partially Hydrolysed poly(2-Ethyl-2-Oxazoline) and Poly(acrylic Acid) for Effective Prevention of Protein, Cell and Bacteria Surface Attachment. *Colloids Surfaces B Biointerfaces* **2018**, 161, 269-278.

3.8 Appendix Data

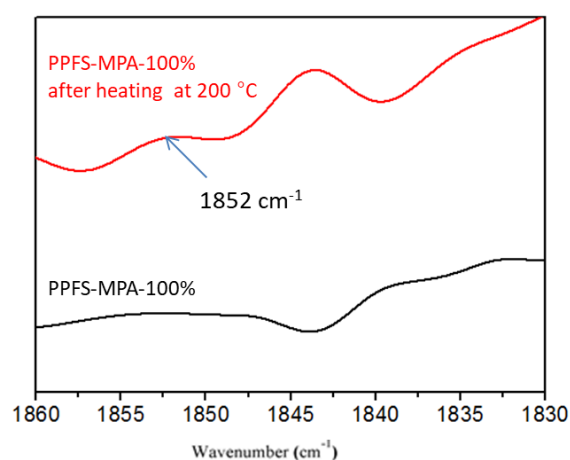


Figure AI 3-1 FT-IR spectra of PPFS-MPA-100% before (black line) and after (red line) heating at 200 °C.

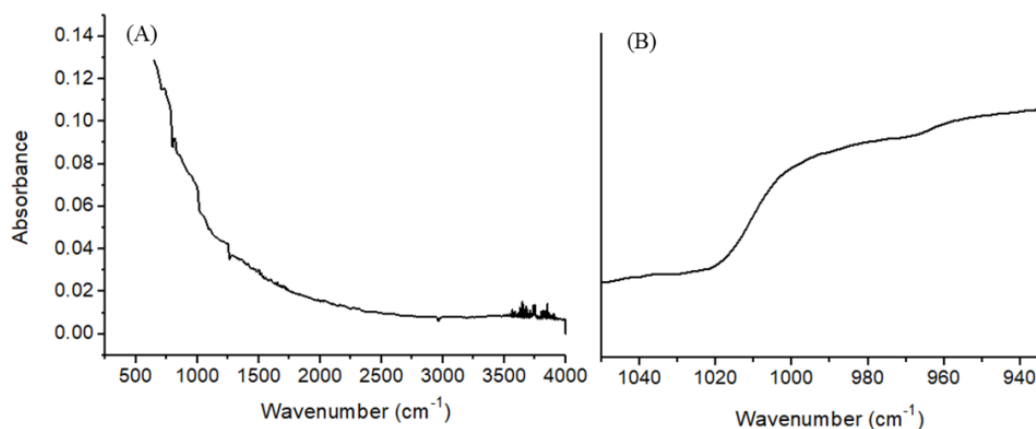


Figure AI 3-2 ATR FT-IR spectrum of (PPFS-MPA-32%/P4VP) after the solvent evaporation from CHCl_3/MEK after 50 deposition steps onto a silicon wafer (A); zoomed spectrum between 1050 cm^{-1} to 940 cm^{-1} (B).

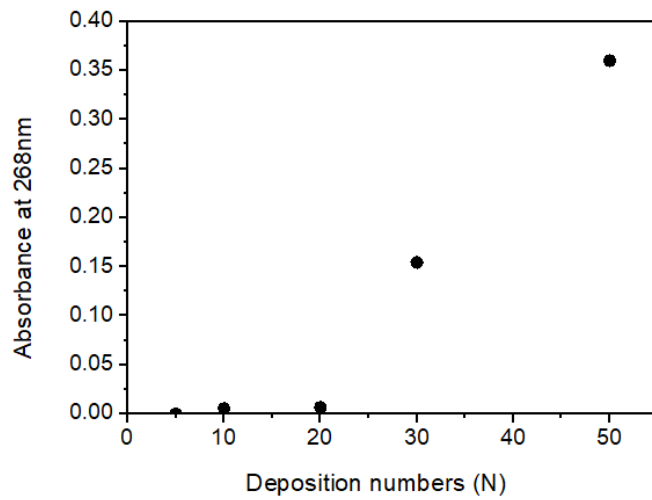


Figure AI 3-3 The evolution of UV absorbance at 268 nm of $(\text{PPFS-MPA-32\%/P4VP})_N$ after deposition of the IPC formed in CHCl_3/MEK , as a function of the number of deposition (N).

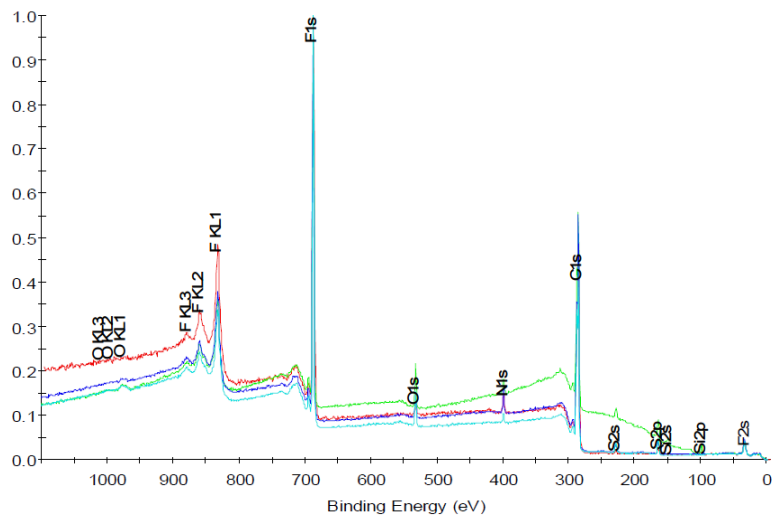


Figure AI 3-4 XPS elemental analysis of the self-assembled $(\text{P4VP/PPFS-MPA})_n$ film.

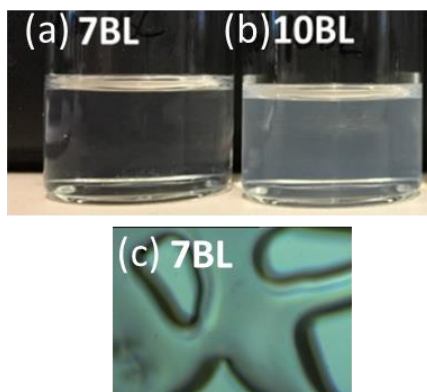


Figure AI 3-5 P4VP solutions used in the system of (P4VP/PPFS-MPA) $_n$ (CHCl_3/MEK , DS = 32%, 2 g/L) with $n = 7$ (a) and 10 BL (b); optical microscopy image of cracked film for $n = 7$ BL (c) onto a silicon wafer.

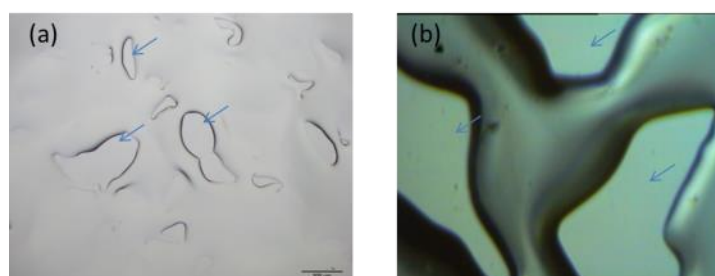


Figure AI 3-6 Optical microscopy image of cracked film (P4VP/PPFS-MPA) (CHCl_3 for P4VP and MEK for PPFS-MPA, DS = 32%, 2 g/L) onto a glass slide (a) and a silicon wafer (b).

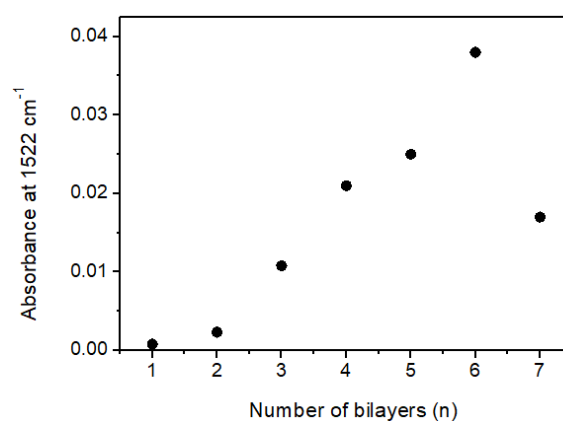


Figure AI 3-7 Evolution of the FT-IR absorbance at 1522 cm^{-1} of (P4VP/PPFS-MPA) $_n$ (CHCl_3/MEK , DS = 32%, $c = 2 \text{ g/L}$) as a function of the number of deposited bilayers (n) (up to 7 BL).

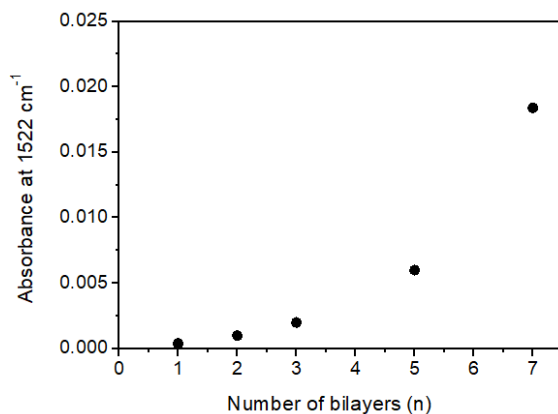


Figure AI 3-8 Evolution of the FT-IR absorbance at 1522 cm⁻¹ of (P4VP/PPFS-MPA)_n (CHCl₃ for P4VP and MEK for PPFs-MPA, DS = 32%, c = 2 g/L) as a function of the number of deposited bilayers (n) (up to 7 BL).

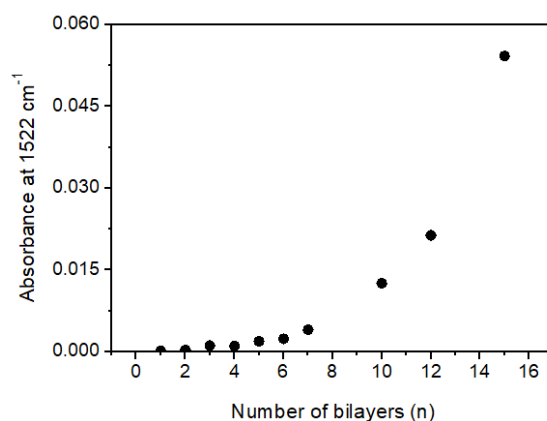


Figure AI 3-9 Evolution of the FT-IR absorbance at 1522 cm⁻¹ of (P4VP/PPFS-MPA)_n (CHCl₃ for P4VP and MEK for PPFs-MPA, DS = 15%, c = 2 g/L) as a function of the number of deposited bilayers (n) (up to 15 BL).

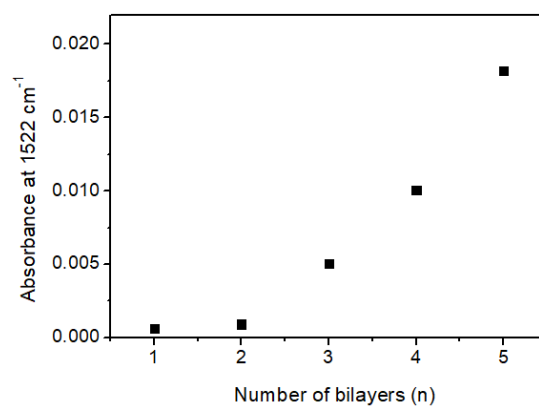


Figure AI 3-10 Evolution of the FT-IR absorbance at 1522 cm⁻¹ of (P4VP/PPFS-MPA)_n (CHCl₃/MEK, DS = 15%, c = 2 g/L) as a function of the number of deposited bilayers (n) (up to 5BL).

General Conclusions and Perspectives

The objective of this basic research project was to prepare different kinds of polymer thin films: i) self-cleaning silica-based (nano)composite films and ii) H-bonds driven layer by layer self-assembly films, both including poly(2,3,4,5,6-pentafluorostyrene) derivatives. Indeed, the chemical modification of preformed PPFS chains with judiciously chosen modifiers allows for designing interesting functional (co)polymers, which can be employed to develop novel polymer films.

The first chapter dedicated to bibliography focused on drawing the context of the PhD work. Hence, three distinct parts were presented. One has concerned *para*-fluoro substitution reactions (PFSR) of pentafluorophenyl containing polymers. This overview was declined according two directions: one dealt with the mechanism, substrates, nucleophiles and reaction conditions of PFSR; the other one was dedicated to strategies including pre- and post- polymerization modification, polymerization through PFSR as well as surface modification by PFSR. Then, main approaches of the preparation of superhydrophobic surfaces were described, in particular, a focus was allocated to super water-repellent (nano)composite films containing fillers embedded in fluorinated (co)polymers. The third and last section was assigned to a presentation of the LbL approach to construct films with a description of the non-covalent driving forces, which can be used for LbL self-assembly multilayer films. In particular, a large attention was devoted to multilayer films mediated by hydrogens bonds and including carboxylic acid containing polymers.

The second chapter described the preparation of superhydrophobic (nano)composite films based on hybrid modified silica particles and PPFS-based (co)polymers as host polymer matrix. Hence, the first section of the chapter 2, dealt with the preparation of hybrid silica particles. For this purpose, firstly, PPFS chains were anchored onto the surface of silica nanoparticles (Aerosil A200 fumed silica) by

nitroxide-mediated polymerization, by using PS-DEPN as macroinitiator, according to the “grafting through” strategy in presence of (acryloxypropyl)trimethoxysilane (APTMS)-modified silica. The composition structure, the chain length, and the polymer grafting weight were precisely controlled by tuning the polymerization time and/or solvent polarity. The growth process exhibited all criteria of a controlled radical polymerization and the weight ratio of organic matter to silica was tuned from 5 to 32 wt.%. It was shown that the addition of silica nanoparticles affects the kinetics of PFS polymerization and favorably in polar solvents with apparent rate constants of polymerization increasing by a factor two. This behavior was attributed to the adsorption of DEPN radicals onto the silica particles. Cryo-fracture SEM and TEM observations confirmed that the dispersability of silica and the size of the silica aggregates can be adjusted by the PFS conversion. Finally, it was shown that the hydrophobicity of PS-*b*-PPFS grafted silica hybrid films can be tailored by varying the PS-*b*-PPFS grafting weight. The introduction of fluorinated polymers (PPFS) in combination with dual roughness (induced by the aggregation of fumed silica nanoparticles) conducted to relevant hydrophobic surface properties with water contact angle as high as $(132 \pm 1.7)^\circ$. Subsequently, (nano)composite films with self-cleaning properties (water contact angle greater than 150° with water hysteresis lower than 10°) were prepared. PPFS and PPFS-modified hybrid fumed silica particles were perfluorinated by using the powerful and versatile thiol- PFSR in a controlled manner. Perfluorinated decane thiol (PFDT) was used as modifier, and the effect of experimental conditions (base used as activator, [PFS]:[thiol]:[base] molar ratio, time) was first evaluated on the PPFS modification in order to tune the degree of substitution that actually controls the surface energy of the derived polymers. The coupling reaction was then successfully applied to the perfluorination of fumed silica. From these results, it was concluded that the fabrication of (nano)composite films with self-cleaning properties requires i) the utilization of PFDT within host fluorinated matrix or immobilized on the silica corona in order to benefit from the presence of perfluoroalkyl groups, ii) the use of hydrophobic silica particles surrounded by a compatibilizing hydrophobic shell to obtain a well-suited dual

roughness and a homogeneous topography surface and iii) a high enough silica content to generate an interconnected and well covering morphology.

In the last chapter of the manuscript, novel carboxylated PPFS derivatives were synthesized and employed, as H-bond donor to construct LbL self-assembly films, with P4VP, as the H-bond acceptor. Firstly, carboxylated PPFS copolymers were synthesized by using carboxylic acid containing thiols as modifiers *via* the thiol-PFSR. The resulting reaction is chemoselective and the degree of substitution was successfully adjusted from relatively low (7%) up to a complete functionalization (100%). The obtained PPFS copolymers modified with mercaptopropionic acid (MPA) (PPFS-MPA) present tunable physico-chemical properties. Then, blends made of PPFS-MPA and P4VP in solution were studied, in order to evaluate the ability of PPFS-MPA to develop H-bonds. It was found that the miscibility of PPFS with P4VP is favored by the presence of carboxylic acid groups along the PPFS backbone, thanks to the formation of strong interchain H-bonds. Interpolymer complexes, leading to turbid solutions, were generated in both CHCl_3/MEK and EtOH medium, while miscible blends were obtained in DMF. This very fast complexation between PPFS-MPA and P4VP was exploited to build thin film (thickness ~ 420 nm) by successively spin-coating a solution containing preformed (PPFS-MPA-32%/P4VP) complexes. Furthermore, the self-assembly LbL approach was exploited to elaborate multilayer films based on P4VP and PPFS-MPA derivatives. Moreover, it has been demonstrated that the driving force for the film formation are H-bonds developed between the two deposited polymers. The influence of the nature of the deposition solvent, of the extent of PPFS modification (DS = 7%, 15% and 32%) and of the polymer concentration on the growth mechanism, the thickness and the surface properties (morphology and wettability behavior) were studied. In agreement with the investigation of complexation in solution, it appeared that at a given DS value of PPFS-MPA (32%), the use of DMF did not permit any film formation, probably due to the competitor role of the solvent. Conversely, ethanol allowed for the generation of quite thin and rough films, the growth mechanism of which is linear with the number of deposited layers. WCA measurement revealed the formation of polar films,

constituted of well stratified layers. Non-linear growth mechanism was underpinned for the films deposited from the mixed solvent CHCl_3/MEK or separated solvents: CHCl_3 for P4VP and MEK for PPFS-MPA. For these dipping solvents, much thicker films were formed (up to the micrometer scale). The resulting films are rather uniform and homogeneous, compared to the use of ethanol. WCA measurements showed that the LbL films are constituted of mixed layers of interpenetrated P4VP and PPFS-MPA. The increase of DS led to a significant increase of the film thickness. Indeed, high DS favors the amount of deposited polymer by enhancing the formation of H-bonds inside the films. Besides, the DS variation conducted to a change of the surface topology. As expected, lowering the concentration of the polymers yields thinner films.

It would be very interesting to continue and complete this thesis work in different directions.

Regarding thiol-PFSR applied on PPFS the control of the reaction with the carboxylic acid-containing thiols is still to be improved. Indeed, by lack of time, it has not been possible to thoroughly develop the conditions to precisely predict the DS, in particular for MAA, 2MPA and MSA modified PPFS, with setting the experimental parameters, the same way it has been possible when using perfluorinated thiol for example. Mastering the post-polymerization modification step is not the only way of controlling the distribution of function of interest along the backbone. Another chemical strategy relies on controlling (co)polymerization of PFS with a comonomer that would be inert with respect to PFSR (styrene for example); by determining the reactivity ratios, it would be possible to adjust both the composition and the microstructure of the copolymer that would finally be subjected to PFSR with the aim of modifying all the PFS units (the experimental conditions for such purpose have been found in our work).

Concerning the superhydrophobic nanocomposite films, it could be interesting to evaluate the durability of the films. In particular, the effect of external stresses, such as the thermal stability and the chemical resistance, as exposure to strong acid, base, ionic strength, solar UV could be investigated. These features are very important to be

considered, for any applicative field. Also, as the film contains high amount in inorganic particles, the abrasion and/or scratch resistance as well as the local surface mechanical properties (by AFM for instance) should be studied and quantified. Peak Force Quantitative Nanomechanical Mapping (QNM) AFM mode could be used to explore the mechanical properties at the interface polymer/fillers, in order to assess the quality of the interface. Also, it would have been beneficial to investigate the ability of this superhydrophobic surface to be self-cleaning by using, for instance, different kinds of dust compounds, as hydrophilic methylene blue and hydrophobic carbon black. In addition, as both superhydrophobicity and superoleophilicity can be simultaneously imparted by controlling the surface tension and the roughness of the substrate, the oil wettability of PPFS or PPFS-PFDT modified hybrid silica particles could be developed, which probably would find applications in the domain of the oil/water separation, which is greatly valuable in the oil and gas industry for gasoline production; or for the fabrication of anti-corrosive materials.

Concerning the LbL H-bonded films, a complementary study on the effect of other parameters, such as temperature, the presence of competitive reagents, the effect of the deposition mode, could be performed. The deposition of a much larger number of bilayers, by using an automatic deposition robot would have been relevant. The internal organization and the construction of the films (and also the diffusion of polymers in the multilayer films) should be analyzed by neutron reflectivity by incorporating deuterated moieties into the polymer backbone, by X-ray reflectivity, and by microscopic fluorescence after the incorporation of fluorescent tag. Moreover, when PPFS is completely modified by MPA (DS =100 %), the resulting polymer is soluble in water for well suited pH. Thus, it could be able to develop electrostatic interactions, exploitable to construct polyelectrolyte multilayer films. Moreover, we have focused our study here on the construction of LbL films with PPFS-MPA derivatives, but a comparable study with H-bond donors synthesized with using other thiols (the ones that have only been tested in our work, with various steric hindrance around the carboxylic acid group, with multiple carboxylic acids etc) would also be very interesting to evaluate the impact of structural factors on the feasibility, growth

mechanism and global features of such films.

Thus, by carefully selecting the thiol or other nucleophiles to modify the PPFS building block, considering that the extent of modification can be finely tuned and applied either to the derivation of polymers or of a polymer substrates, we believe that the strategy that uses PPFS as a platform could be suitable to provide any specific property to a film surface.



FOLIO ADMINISTRATIF

NOM : YIN

DATE de SOUTENANCE : 30/03/2018

Prénoms : Quanyi

TITRE : Thiol-para-fluoro modified PPFS as building blocks for the design of silica-based nanocomposite and layer by layer self-assembled thin films

NATURE : Doctorat

Numéro d'ordre : 2018LYSEI025

Ecole doctorale : Matériaux de LYON

Spécialité : Matériaux

RESUME : Ce travail de thèse décrit la préparation de deux types de films fins de polymères : i) des films nanocomposites à base de silice pyrogénée aux propriétés superhydrophobes et ii) des films LbL auto-assemblés, incluant tous deux des dérivés de poly(2,3,4,5,6-pentafluorostyrene) (PPFS), utilisés comme briques élémentaires de base. La stratégie utilisée ici consiste à exploiter les nombreux avantages que présente la réaction de substitution du fluor en position para du PPFS avec un thiol, pour générer de nouveaux dérivés aux propriétés ajustables à façon. Ainsi, le premier volet de la thèse a consisté à introduire des chaînes de PPFS de façon covalente à la surface de silice pyrogénée par une stratégie dite de «grafting through» en utilisant la polymérisation radicalaire contrôlée par les nitroxides, en présence de PS-DEPN comme macroamorceur. La cinétique de polymérisation du PFS en présence et sans silice a été étudiée dans divers solvants, et de ce travail résultent différentes particules hybrides de silices modifiées en surface par une couronne de PPFS. Ensuite, un thiol perfluoré (perfluorodecanethiol, PFDT) a été utilisé pour modifier le PPFS, considéré dans ce cadre comme matrice hôte pour la préparation des nanocomposites et pour modifier le PPFS présent à la surface des particules de silice. A partir de là, un large panel de films nanocomposite a été préparé à partir des différentes combinaisons possibles de polymère hôte (PPFS ou PPFS-PFDT) et de charges inorganiques de silice (modifiées par le PPFS ou le PPFS-PFDT). Les propriétés de mouillabilité ainsi que la morphologie de surface de chaque film ont été analysées et il en résulte que certains films présentent un caractère superhydrophobe. Le deuxième volet de la thèse a porté sur la modification du PPFS par des thiols porteurs de fonctions acide carboxylique, toujours par la réaction de substitution décrite précédemment. Différents dérivés de PPFS carboxylés de DS variés ont été synthétisés. Leur habilité à développer des liaisons hydrogène avec un polymère modèle accepteur de liaison H : la poly(4-vinyl pyridine) (P4VP) a été étudié. Il en ressort que dépendamment de la nature du solvant, des mélanges miscibles ou des complexes interpolymères ont été formés. Des solutions de complexes préformés ont été successivement déposées par spin-coating pour construire des films. De plus, des films multicouches LbL stabilisés par liaisons H entre le PPFS carboxylé et la P4VP ont été élaborés and il a été démontré que la nature du solvant de dépôt, ainsi que le taux de modification du PPFS, impactent fortement le mécanisme de croissance, l'épaisseur et les caractéristiques de surface, en termes de topologie et de mouillabilité.

MOTS-CLÉS : poly(2,3,4,5,6-pentafluorostyrene), substitution nucléophile avec un thiol, film nanocomposite, silice pyrogénée, surface superhydrophobe, interactions hydrogène miscibilité, auto-assemblage en couche par couche, films multicouches

Laboratoire (s) de recherche : Ingénierie des Matériaux Polymères (IMP) CNRS UMR 5223, Université Lyon1 et INSA de LYON

Directeur de thèse: Prof. BEYOU Emmanuel, Dr. CHARLOT Aurélia, Dr. PORTINHA Daniel



INSA

Président de jury :

Composition du jury :

DELAITE Christelle	Professeur (Université Haute-Alsace)	Rapporteuse
GROHENS Yves	Professeur (Université Bretagne-Sud)	Rapporteur
DUCHET-RUMEAU Jannick	Professeur (INSA de LYON)	Examinatrice
RIEGER Jutta	Chargé de Recherche CNRS (Université Paris 6)	Examinatrice
COLOMBANI Olivier	Maître de Conférences (Le Mans Université)	Examineur
BEYOU Emmanuel	Professeur (Université Lyon 1)	Directeur de thèse
CHARLOT Aurélia	Maître de Conférences (INSA de LYON)	Co-Directrice de thèse
PORTINHA Daniel	Maître de Conférences (INSA de LYON)	Co-Directeur de thèse